MASSACHUSETTS INSTITUTE OF TECHNOLOGY

LINCOLN LABORATORY

MILLSTONE HILL THOMSON SCATTER RESULTS FOR 1969

J. V. EVANS

Group 21

TECHNICAL REPORT 513

23 JULY 1974

Approved for public release; distribution unlimited.

LEXINGTON MASSACHUSETTS/

AIR FORCE (1) APRIL 4, 1975--37

ABSTRACT

This report summarizes the results for the electron-density distribution, electron and ion temperatures, and vertical ionization fluxes in the F-region obtained during 1969 using the Millstone Hill (42.6°N, 71.5°W) Thomson (incoherent) scatter radar system. These data, for the height interval approximately 200 to 900 km, were gathered over 24-hour observing periods, roughly twice per calendar month. The time resolution to obtain results over this entire height interval was either 30 or 45 minutes, depending upon which of two operating modes was employed.

The results for the diurnal variation of the electron density and temperature exhibit the characteristic summer and winter patterns discussed previously. The transition between the two takes place in April and October. Two cases of overhead auroral precipitation were observed during the year as a consequence of efforts to observe a stable red arc. Other instances of geomagnetically disturbed behavior were infrequent.

Vertical fluxes of ionization were measured, and the flux escaping to the magnetosphere near midday was found to have an average value of $\sim 5 \times 10^7$ $el/cm^2/sec$. Near midnight, the magnetosphere appears to supply the local ionosphere with a flux of about half this amount.

CONTENTS

I. INTRODUCTION

Since 1963, incoherent (Thomson) scatter radar measurements of F-region electron densities, and electron and ion temperatures have been measured at Millstone Hill, Westford, Massachusetts (42.6°N, 71.5°W).[1-6] This paper is the seventh in a series of annual reports, and presents the results gathered in this program during calendar year 1969. The observations reported were made for periods of 24 hours, approximately twice a month. The results obtained in earlier years have been published in the articles listed in Table I, and have been transmitted to the World Data Center A, Boulder, Colorado.

TABLE I

PUBLICATIONS CONCERNING THE MILLSTONE HILL UHF (68 cm Wavelength) THOMSON SCATTER RESULTS

Year	Months Covered	Publication
1963	February 1963 to January 1964	Ref. 1
	March, July, August, September	Ref. 7
	April, July, November	Ref. 8
1964	January through December	Ref. 2
	April, July, November	Ref. 9
1965	January through December	Ref. 3
	January, April, August	Ref. 10
	June	Ref. 11
	June, August, September	Ref. 12
1966	January through December	Ref. 4
	January, March, July, September	Ref. 13
1967	January through December	Ref. 5
	February, June, October, December	Ref. 13
1968	January through December	Ref. 6
	October	Ref. 14

During 1968 and 1969, the UHF incoherent scatter radar system was also employed to study a component of the reflected signals known as the "plasma-line." These reflections are produced by electrostatic waves in the electron gas impressed by fast photoelectrons. These results were gathered by students from the University of Illinois and the University of Michigan, and have been reported elsewhere.[15,16]

In addition to the measurements reported here of F-region observations made with the vertically directed UHF radar system, a number of measurements were conducted in 1969 of the

E-, F1-, and F2-regions employing the L-band radar with the beam directed obliquely. These measurements were aimed at determining the ion composition in the F1-region,[17,18] and the horizontal drift in the E- and F-regions.[14,19] Inasmuch as these results have also been reported, they are not included in this paper.

During the last quarter of 1969, work began on developing a new method of operating the UHF vertically pointing radar to extend the measurements to E- and F1-region heights. This required a solution of the ground-clutter problem that previously prevented observations in this height range,[5] as well as a means of improving the height resolution achievable. Both requirements were met by employing transmissions consisting of pairs of short pulses whose spacing could be varied. A digital computer was used to subtract out any echoes that appeared to be coherent from sweep, and to compute the echo autocorrelation function. However, this system was not brought into final operating form until 1970, and no further discussion of it will be presented here.

Section II provides a summary of the equipment, observing and data-processing procedures employed during 1969. These differed little from those employed in the latter part of 1968, and have previously been documented.[6,20] Sections III through V present the results of the synoptic studies of F-region densities, temperatures, and vertical ionization fluxes, while Sec. VI provides a summary. In the Appendix, a calculation is presented of the magnitude of the unwanted doppler shift introduced by the transmitter.

II. EQUIPMENT, OBSERVING AND DATA-PROCESSING PROCEDURES

A. Equipment

The UHF incoherent scatter radar equipment has been described previously.[1] During 1968, the spectrum analyzer portion of the receiver was replaced by one of newer design that was interfaced directly into the SDS 9300 computer. These changes are fully documented in Ref. 20, but require further comment here.

In the new spectrum analyzer, the integration of the echoes is carried out digitally by the SDS 9300 computer, thereby eliminating virtually all problems due to gain differences and drift. In addition, the signals are no longer gated from the timebase, but instead are continuously applied to a bank of 5-pole crystal filters each of which is matched to the length of the pulse employed (0.5 or 1.0 msec).

Each of the (two) filter banks available employs 24 filters spanning ±11.5 kHz about the radar frequency with 1-kHz spacing. The voltages at the filter outputs are sampled at 0.5-msec intervals so that a spectrum may be obtained every 75 km of altitude. Since the filters must be sampled sequentially (at intervals of 20 μsec), a tapped delay line is used to drive the filters in a manner that provides exact compensation for the delays between samples. Thus, although it takes 480 μsec to scan through all filters, the outputs correspond to the same real altitude.

Unfortunately, a few months after the 0.5-msec matched filters were placed in service (in 1968), the impulse response of several of them was found to have deteriorated. Accordingly, these were returned to the manufacturer for repair, and between November 1968 and February 1969 the 0.5-msec filter bank was operated with only half the filters in place. Owing to the frequency commutation scheme employed to position the filters, with respect to the signal spectrum, a double-sided spectrum was still obtained; however, only half as many echo samples were gathered per unit time.

No further difficulties were encountered with the spectrum analyzer during 1969, although a discrepancy between the results for the plasma temperature obtained with 0.5- and 1.0-msec pulses persisted. This error, which has been discussed in Ref. 20, was observable over the height interval 450 to 750 km where measurements were made with both pulse lengths. The disagreement was largest at night when it was manifest by lower estimates of the ion temperature T_i observed using the 0.5-msec pulses. The principal cause of this difficulty is believed to be the poor match provided by the 0.5-msec filters to the transmitted pulses, and an empirical correction scheme was eventually devised (see below).

In retrospect, it appears that a second source of error existed which compounded this problem. For the observations conducted with 1.0-msec pulses, the receiver suppression was removed exactly 1.0 msec prior to the first samples being taken from the filter bank. The sudden application of the signals to the filter bank produced transients which had not died out by the time of the first sample, thus rendering the 1.0-msec results at 450 km slightly in error. In October 1970, the time when the suppression is removed was advanced by 0.5 msec, thereby diminishing this effect.

The most serious difficulty encountered with the equipment during 1969 was a dramatic loss of antenna gain following a snow storm late in February. During this storm, the 1-inch mesh surface of the antenna iced over, and the dish filled with snow to a depth of $\geq$2 feet near the center. Gain measurements made by observing the radio star Cygnus showed that the loss in antenna gain was ~12 dB. During the course of the next few days, the snow was removed by hand, and the gain returned to within 2 dB of its earlier value. This residual loss was caused by the distortion of the mesh produced by the snow load. This loss gradually decreased as the surface returned to its original shape through being "worked" by daily cycling of the temperature. Thus, by the end of April, the gain was found to be 1.4 dB below its previous value. In June, when the rms surface tolerance was measured in a survey, it was found to be 1.05 inches, i.e., close to the original design value. A repetition of these events occurred in 1970, and during the summer of that year the surface was retensioned and provided with additional strength by means of a set of cables laid diagonally across the pipe supporting structure.

In December 1969, the last of a series of modifications to the antenna, designed to reduce unwanted ground-clutter echoes, was made. This was the addition of an extension to the conical horn feed that increased the directivity of the primary feed pattern. The taper of the intensity of the illumination over the reflector was increased from about 10 to about 20 dB. This had the effect of reducing the power scattered off the reflector edges and, more importantly, off the tripod feed support structure. The extension incorporated a quarter-wave choke, which raised the horn efficiency. The net effect of this modification appears to have been to broaden the beamwidth from about 0.7° to 0.8° without significantly altering the effective collecting area.

B. Observing Procedure

During 1969, we attempted to make observations twice per month for periods of 24 hours. Table II lists the dates and times for which measurements were successfully carried out and reduced; included is the mean of the planetary magnetic index K_p over each period of observation.

Following the introduction of the new spectrum analyzer in 1968, special efforts were made to detect the vertical drift of the ionization above $h_{max}F2$ (Ref. 20). For this reason, some observations were conducted in which the measurements made using the 1-msec pulses ("C-mode") were repeated four times in each cycle.[6,20] This raised the time to complete a cycle of measurement to 45 minutes.

TABLE II

INCOHERENT SCATTER OBSERVATIONS – 1969

Begin			End			Mean K_p	Obs†	Comments
Date	C*	EST	Date	C*	EST			
16 January		0930	17 January	D	0930	3–	Reg	
30 January		2000	31 January		0800	1_o	Drift	Incomplete
5 February		0930	6 February		0900	3–	Reg	
12 February		0920	13 February		0950	2+	Drift	
26 February		1030	27 February	D	1030	3_o	Reg	Antenna gain down 10 dB
21 March		1620	22 March		0510	3+	Reg	
23 March		2040	24 March	D	0500	7_o	Reg	Special auroral operation
25 March		1630	26 March		1630	3+	Drift	
9 April		0930	10 April	Q	0930	2_o	Reg	
23 April		2220	24 April		2210	2–	Drift	
6 May	q	0800	7 May	Q	0800	2–	Reg	Quiet
30 May		0800	31 May		0130	2+	Drift	Combined
1 June		2030	2 June		0630	1+	Drift	Combined
5 June	q	0930	6 June	Q	0900	1–	Reg	Quiet
23 June	Q	0820	24 June		0810	2_o	Drift	
1 July	D	0800	2 July		0815	3–	Reg	
9 July		0540	10 July		0440	2–	Drift	
29 July	Q	1800	30 July		1900	2_o	Drift	
14 August		0815	15 August	q	0845	1–	Reg	Quiet
26 August	D	1530	27 August	D	1530	3+	Drift	
9 September		0915	10 September		0900	2_o	Reg	
23 September		0800	24 September		0800	2+	Drift	
29 September	D	2200	1 October	D	0900	5_o	Reg	Special auroral operation
14 October	Q	1700	15 October	Q	1700	1_o	Drift	Quiet
3 November	D	1400	4 November		1700	2_o	Reg	
20 November	q	0830	21 November	Q	1000	1–	Drift	Quiet
8 December		1245	9 December	D	1245	2+	Reg	

* Condition:

Q One of five quietest days in month
q One of ten quietest days in month
D One of five most disturbed days in month

† Observations:

Data gathered and analyzed as described in Lincoln Laboratory Technical Report 477 (Ref. 20).
Reg = Regular; Drift = Drift Measurement.

In the normal operating mode, measurements were made using 0.1-, 0.5-, and 1.0-msec pulses in sequence, the complete cycle occupying 30 minutes. These runs are termed "regular" in Table II to distinguish them from those emphasizing the determination of "drift." Usually, 24 hours of each type of measurement were carried out in each calendar month.

The value of N_{max} to be employed in the data reduction was made available in the form of a measurement of the F-region critical frequency f_oF2 in megahertz at the start of each cycle.* This measurement was made by the radar operator, who then typed the value into the computer which stored it, along with all the other information, on magnetic tape. To make the measurement, the C-4 ionosonde was modified to permit it to be turned on and monitored remotely, as well as to have its frequency controlled by a remote frequency synthesizer. Thus, the operator would turn on the sounder and advance the frequency of the synthesizer until the F2 ordinary return was just perceived at great range. The synthesizer dials then gave the required value of f_oF2.

The intent of this procedure was to create a data tape that contained all the information required for processing, so that this could be carried out immediately upon completion of a run. However, the radar operators frequently encountered difficulty in reading f_oF2, especially at night. Thus, as a rule, these real-time estimates were not employed in the data analysis; instead, they were plotted as a function of time, together with those derived from the film records and values recorded at Ottawa, Canada; Maynard, Massachusetts (if available); and Wallops Island, West Virginia. A smooth curve was then drawn through this collection of points that followed the variation at Millstone, except when this was clearly at variance with the observations at all the other stations. Values were read from this curve at 30-minute intervals and punched onto IBM cards. The recorded data were then processed employing values of N_{max} for the electron-density profiles obtained by linear interpolation between the values available at half-hour intervals.

During 1969, the first attempts were made to conduct coordinated measurements with Dr. J. Noxon (Harvard University) who, at that time, was measuring the 5577-Å, 6300-Å, and other emission lines from the night sky, at the Blue Hills Observatory, Boston, Massachusetts. The principal objective of this joint effort was to observe a stable auroral red-arc, and determine if the 6300-Å emission could be accounted for in terms of impact excitation due to the high temperature of the electrons. In this the effort proved to be disappointing, as no overhead SAR-arcs were observed. However, on two occasions (Table II) Dr. Noxon alerted us to the presence of low-latitude auroral activity, and valuable optical and radar results were gathered simultaneously. Unfortunately, owing to the fact that the auroral luminosity is not detectable until after twilight, and it requires approximately two hours to commence operations at Millstone following notification of people at their homes, it was possible for the activity to have declined substantially by the time the radar measurements were under way. This appears to have been the case for the measurements on 29 September 1969.

In the past, efforts have been made to compare the observations gathered in the incoherent scatter observations with measurements gathered by various satellites. Usually, the comparisons were dependent on lucky coincidences between our operations and satellite passes over Millstone, although some early observations were scheduled to coincide with passes of the topside sounder, Alouette I.

---

* $N_{max} = 1.24 \times 10^4 (f_oF2)^2$ el/cm^3 when f_oF2 is expressed in megahertz.

Beginning in 1968, a number of observations were scheduled to coincide with passes of Alouette II at the request of scientists at the NASA Goddard Space Flight Center. During 1969, observations also were made during passes of the Explorer (AE-B), ISIS I, OGO VI and Alouette I satellites. Where possible, the regular monthly operations were scheduled to coincide with favorable passes, and Table III lists the satellite overflights of Millstone that occurred in routine operations scheduled with this in mind. Additional short periods of operation (typically 2 hours) were scheduled to coincide with other satellite passes as listed in Table IV. Results for these short observing periods are not included in this report, but may be made available on request.

The primary purpose of the measurements made during the passes of OGO VI was to permit comparisons of electron and ion temperatures deduced by remote sounding and in situ probe measurements, and most of the results of this exercise have been reported.[21] Comparisons with the records of the topside sounders in Alouette I, II or ISIS I have yet to be made.

C. Data Reduction

Beginning in July 1968, the results were gathered in a manner that placed together all the quantities of interest on a single data tape so that complete machine reduction became possible. The computer programs employed are described in Ref. 20. Basically, the electron-density profiles were obtained in a way that: (1) combined measurements made with the three pulse lengths, (2) removed spurious echoes due to satellites, (3) adjusted the absolute value to yield the correct value of $N_{max}F2$ as measured on the ionosonde, (4) removed the dependence on altitude variations of T_e/T_i, and on Debye length. This profile was available as a graph plotted by a Calcomp plotter, and on a printout as $\log_{10} N_e$ vs altitude.[20] Estimates of T_e and T_i were also provided on plots and on the printout. The values of T_e were corrected for the effects of the changing Debye length with altitude.[20] Table V contrasts the manner in which the measurements were made and reduced in each year since 1963.

It should be noted that the estimates of T_e and T_i were obtained by extracting two parameters from the measured spectra, viz., the half-peak-power width (proportional to T_e), and the ratio of the peak power in the wings to that at the center frequency (proportional to T_e/T_i). These values were inserted into analytical expressions that had been obtained to represent T_e and T_i, as functions of the ratio and width through scaling theoretical power spectra computed assuming only O^+ ions are present and that the Debye length is extremely small. In computing these theoretical power spectra, the effects of the transmitter pulse and the finite width of the filters in distorting the measurement were included.

To correct the estimate of the electron temperature $T_{e_{obs}}$ obtained in the above manner for the effect of the change in the Debye length on the spectrum, use was made of the expression[20]

$$T_e = T_{e_{obs}} \left(1 - \frac{1.62 \times T_{e_{obs}}}{N_e} \right)^{-1} . \qquad (1)$$

Unfortunately, this expression holds only so long as the second term in the parentheses remains ≤ 0.3. At high altitudes, $T_{e_{obs}}$ may be of the order of 2000 to 3000 K and the correction then becomes inaccurate as N_e approaches 10^4 el/cm^3. Thus, the electron temperatures obtained near or above this level are believed to be overestimates.

The existence of an error in the 0.5-msec (B-mode) results has been noted. Owing to the obviously better response of the 1.0-msec pulses to an applied RF pulse, it was assumed that

TABLE III

SATELLITE PASSES DURING REGULAR OPERATIONS IN 1969

Date	Time (EST)	Height (km)	Satellite
25 March	2041	910	Alouette II
10 April	0537	650	ISIS I
30 May	1904	1200	AE-B
23 June	1743		OGO VI
24 June	0407		OGO VI
1 July	1647		OGO VI
2 July	0312		OGO VI
9 July	1550		OGO VI
10 July	0215		OGO VI
23 September	1725	630	ISIS I
29 September	2149	974	Alouette I
30 September	2202	942	Alouette I

TABLE IV

SPECIAL OPERATIONS COINCIDING WITH SATELLITE PASSES IN 1969

Date	Time (EST)	Height (km)	Satellite
5 May	1541	584	Alouette I
18 June	1800	640	OGO VI
19 June	0420	430	OGO VI
27 June	1626		OGO VI
4 August	0849	650	ISIS I
29 September	1725	587	ISIS I
17 October	1453	730	ISIS I
17 October	1937	625	Alouette II
20 October	1538	785	ISIS I
27 October	1945	513	Alouette II
29 October	1809	512	Alouette II

TABLE V

OBSERVING PROGRAM AS A FUNCTION OF YEAR

Year	Length of Each Observing Period (hours)	Number of Observing Periods per Month	Time Taken to Measure One Profile (hours)	Number of Profiles Obtained per Month	Reduction Method Employed
1963	30	4	1.5	80	Mean hourly profiles constructed for each calendar month (Ref. 1)
1964	30	2	1.0	60	As in 1963
1965	48	1	0.5	96	As in 1963
1966	24	2	0.5	96	Each profile analyzed separately (Ref. 4)
1967	24	2	0.5	96	As in 1966
1968	24	2	0.5 or 0.75	96 or 64	As in 1965 until July when complete machine reduction began (Ref. 20)
1969	24	2	0.5 or 0.75	96 or 64	Machine reduction (Ref. 20)

the error stemmed from the fact that the B-mode filters appeared to be less well matched to 0.5-msec pulses. In order to remedy this, efforts were made to determine the proper spectrum response for the B-mode filters empirically by comparing spectra obtained in the two modes at the same height. This work was carried out by G. Lejeune.* Unfortunately, reliable and consistent results were not obtained, although a large number of spectra were compared. It seems possible that this approach failed, in part, because the comparison was made at 450 km (where the 1-msec results were also somewhat in error) and, in part, because the error appears to depend upon T_e/T_i. An empirical correction was obtained by J. E. Salah by comparing values of T_e/T_i obtained at 525 km with the two pulse lengths.[22] Figure 1 shows $(T_e/T_i)_{B\text{-mode}}$ as a function of $(T_e/T_i)_{C\text{-mode}}$. The distribution of points in this figure suggests that it is difficult to resolve temperature ratios below 1.4 using the shorter pulses. A plot of $(T_e/T_i)_{C\text{-mode}}$ vs T_i (B-mode) $- T_i$ (C-mode) is shown in Fig. 2, where a bias of up to 200 K can be seen at low values of T_e/T_i. The empirical corrections that have been devised for the B-mode results are based on the smooth linear curves in Figs. 1 and 2, i.e., they assume that $(T_e/T_i)_{C\text{-mode}}$ is correct. In a later version of the analysis program, corrections are applied to B-mode results at all heights if the temperature ratios measured by the two different pulses at 525 km differ by more

* On leave from the Centre National d'Etudes des Telecommunications, Issy-les-Moulineaux, Seine, France.

than 0.1, or if the ion temperatures derived from the two pulses differ by more than 100 K. These corrections are:

$$(T_e/T_i)' = 0.425(T_e/T_i) + 0.575 \qquad 1 \leq T_e/T_i < 1.47 \tag{2}$$

$$(T_e/T_i)' = 1.5(T_e/T_i) - 1 \qquad 1.47 \leq T_e/T_i \leq 2 \tag{3}$$

$$(T_e/T_i)' = T_e/T_i \qquad T_e/T_i > 2 \tag{4}$$

$$T_i' = T_i + 200 \qquad 1 \leq (T_e/T_i)' < 1.2 \tag{5}$$

$$T_i' = T_i - 333(T_e/T_i)' + 600 \qquad 1.2 \leq (T_e/T_i)' \leq 1.5 \tag{6}$$

$$T_i' = T_i - 200(T_e/T_i)' + 400 \qquad 1.5 < (T_e/T_i)' \leq 2.25 \tag{7}$$

$$T_i' = T_i - 50 \qquad 2.25 < (T_e/T_i)' < 3 \tag{8}$$

$$T_i' = T_i \qquad (T_e/T_i)' \geq 3 \tag{9}$$

$$T_e' = T_i'(T_e/T_i)' \tag{10}$$

where the primed quantities are the corrected parameters, and the unprimed quantities are the original measured values.

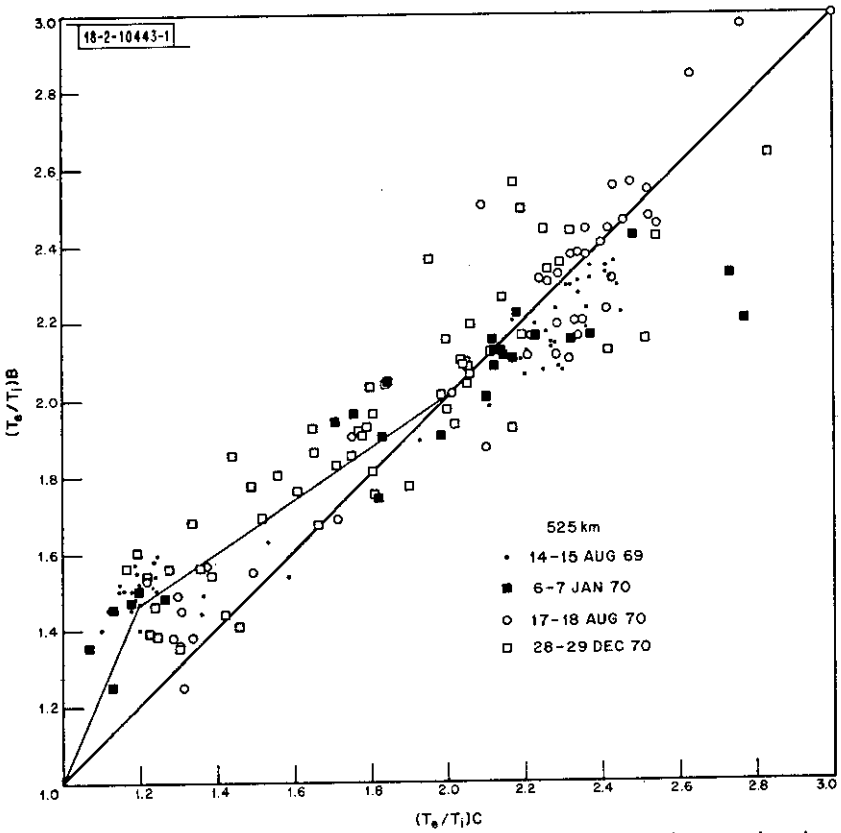

Fig. 1. T_e/T_i derived from 0.5-msec (B-mode) and 1.0-msec (C-mode) pulses.[22]

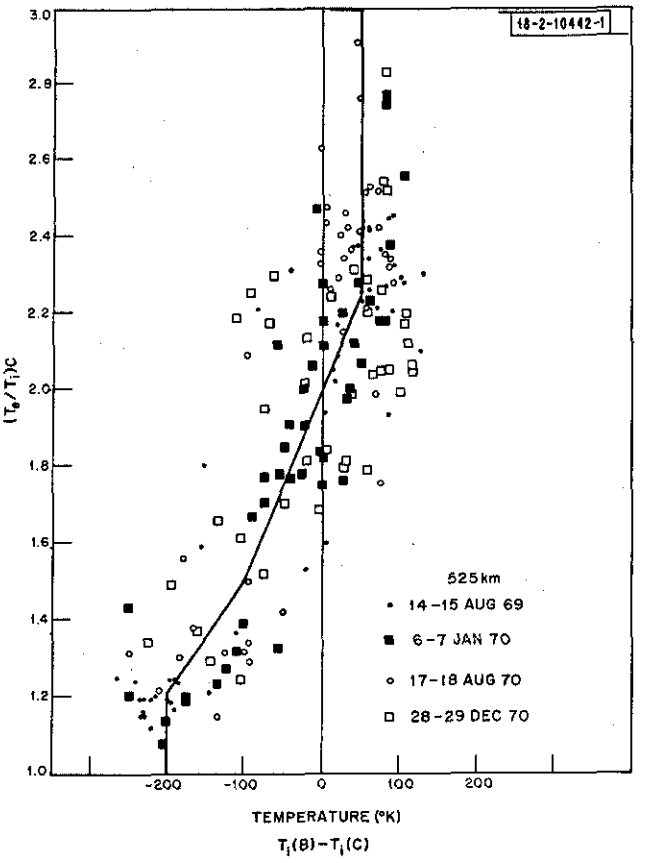

Fig. 2. Deviation between ion temperature derived using 0.5-msec (B-mode) and 1.0-msec (C-mode) pulses.[22]

Since, however, only the uncorrected results were available at the time the data in this report were examined, the influence of the poor B-mode results (chiefly at night in summer) was minimized by constructing temperature-vs-height profiles that largely depended on the C-mode (1-msec pulse) data.

The profiles of N_e, T_e, and T_i were used to construct contour diagrams showing the variation of these quantities over the height range 150 to 900 km (200 to 900 km at night). These were drawn by hand in the manner outlined earlier.[4]

As described in Ref. 20, a number of methods were developed to extract from the signal spectra estimates of the overall doppler shift, and hence of drift velocity. The theoretically optimum method and a simpler "least-mean-squares" method gave almost identical results. Owing to space limitations in the analysis program, this latter method was incorporated in the main program that reduces the data to obtain densities and temperatures. Initially, only the C-mode spectra were analyzed to obtain drift estimates. Later the program was modified to include the B-mode results which, though less accurate, proved to be valuable. To date, no method of presenting these data in a convenient graphical form has been devised, owing to their wide spread both with height and time. However, these data can be made available on request. This report does include results for F-region vertical fluxes obtained from these drift measurements (Sec. V).

III. ELECTRON-DENSITY RESULTS

A. General

Contours of the logarithm ($\log_{10} N_e$) of the electron density N_e (el/cm^3) are presented in Figs. 3(a) through (z). The contours are drawn at intervals of 0.2 over the range of altitudes for which $\log_{10} N_e > 3.2$. It is possible, however, that the results become unreliable when $\log_{10} N_e \leq 4.0$ (e.g., in the valley that forms between the E- and F-layers at night). Owing to malfunctions of the equipment, some days (e.g., 30-31 January) are incomplete. The observations for 30-31 May were marred by a failure in the spectrum analyzer, and additional measurements were made on 1-2 June. These two sets of data have been combined into a single contour plot [Fig. 3(l)].

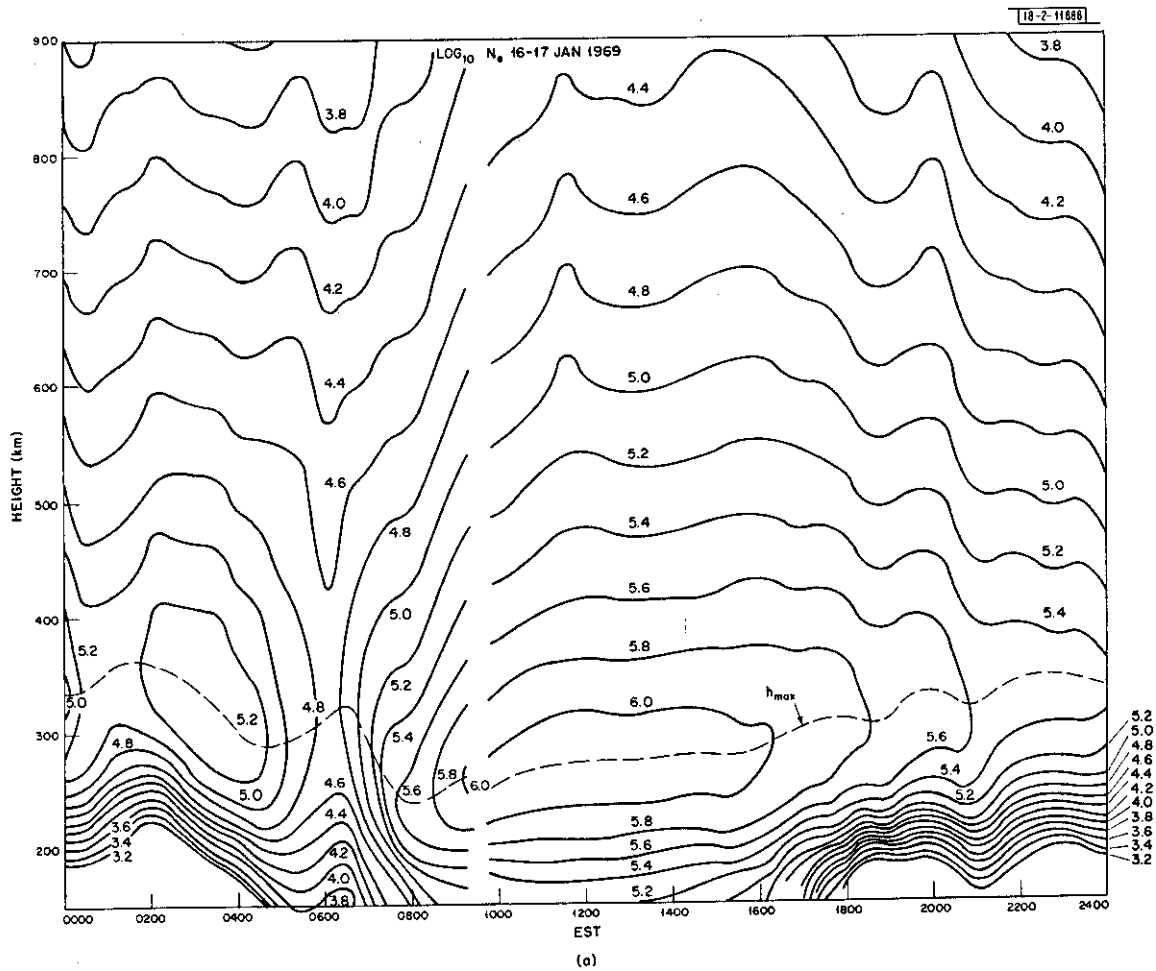

Fig. 3(a-z). Contours of $\log_{10} N_e$ observed on days listed in Table II.

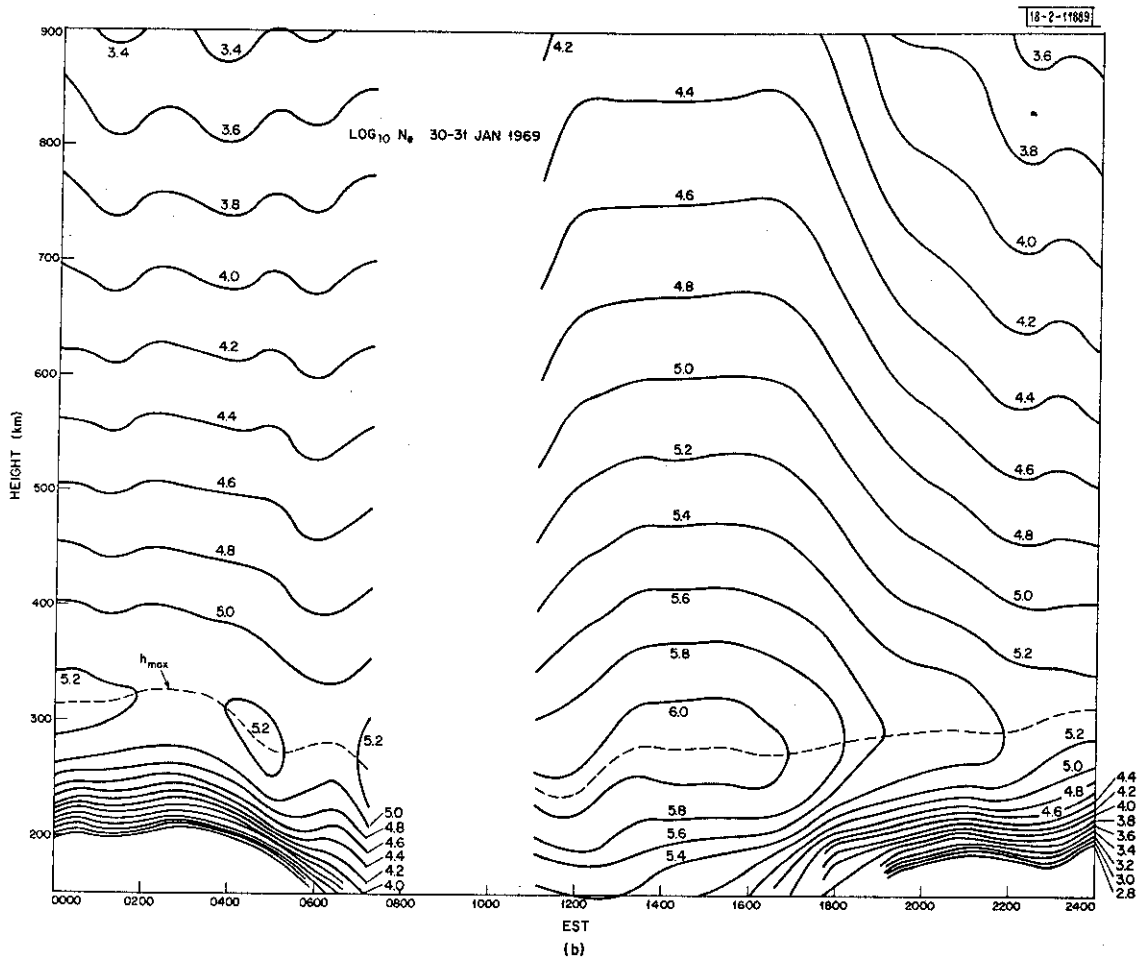

Fig. 3(a-z). Continued.

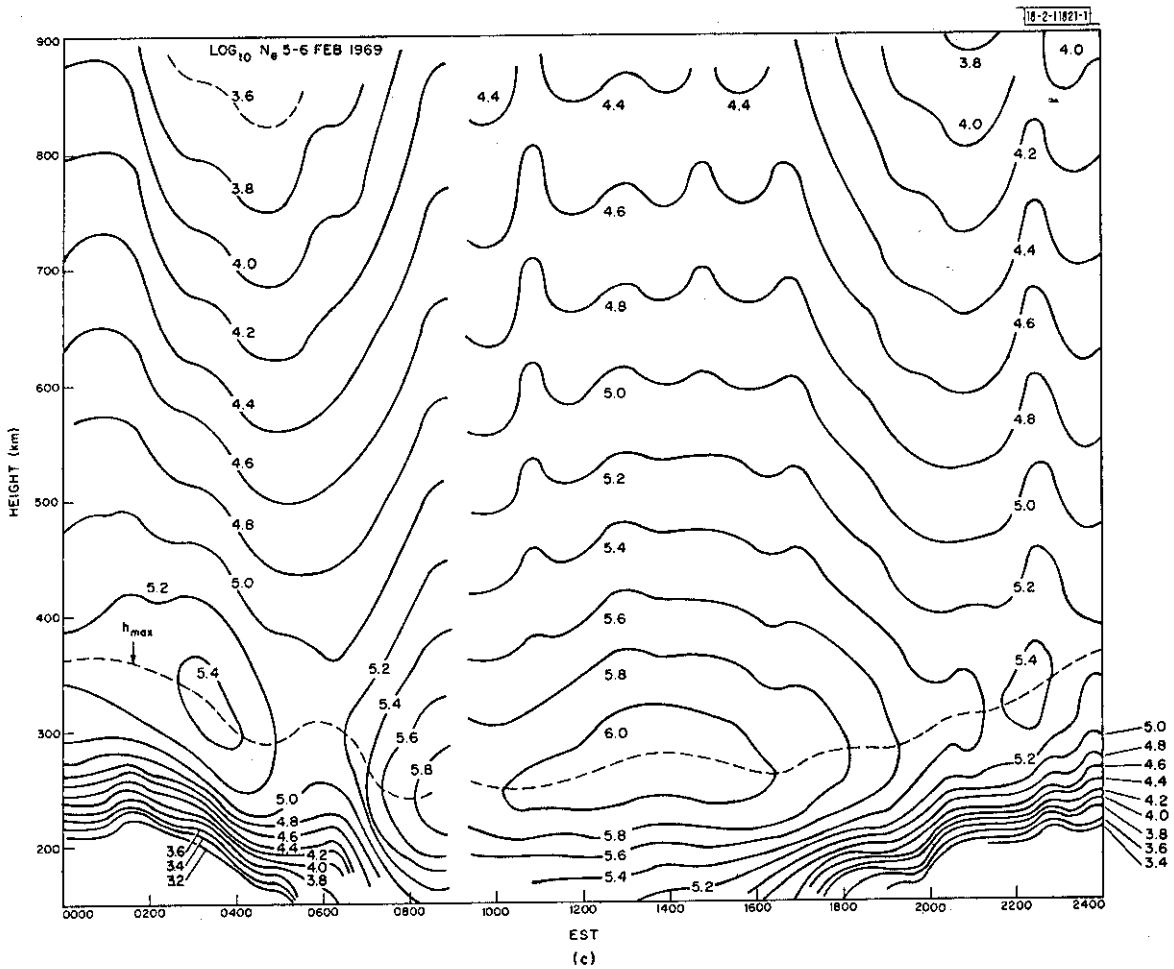

Fig. 3(a-z). Continued.

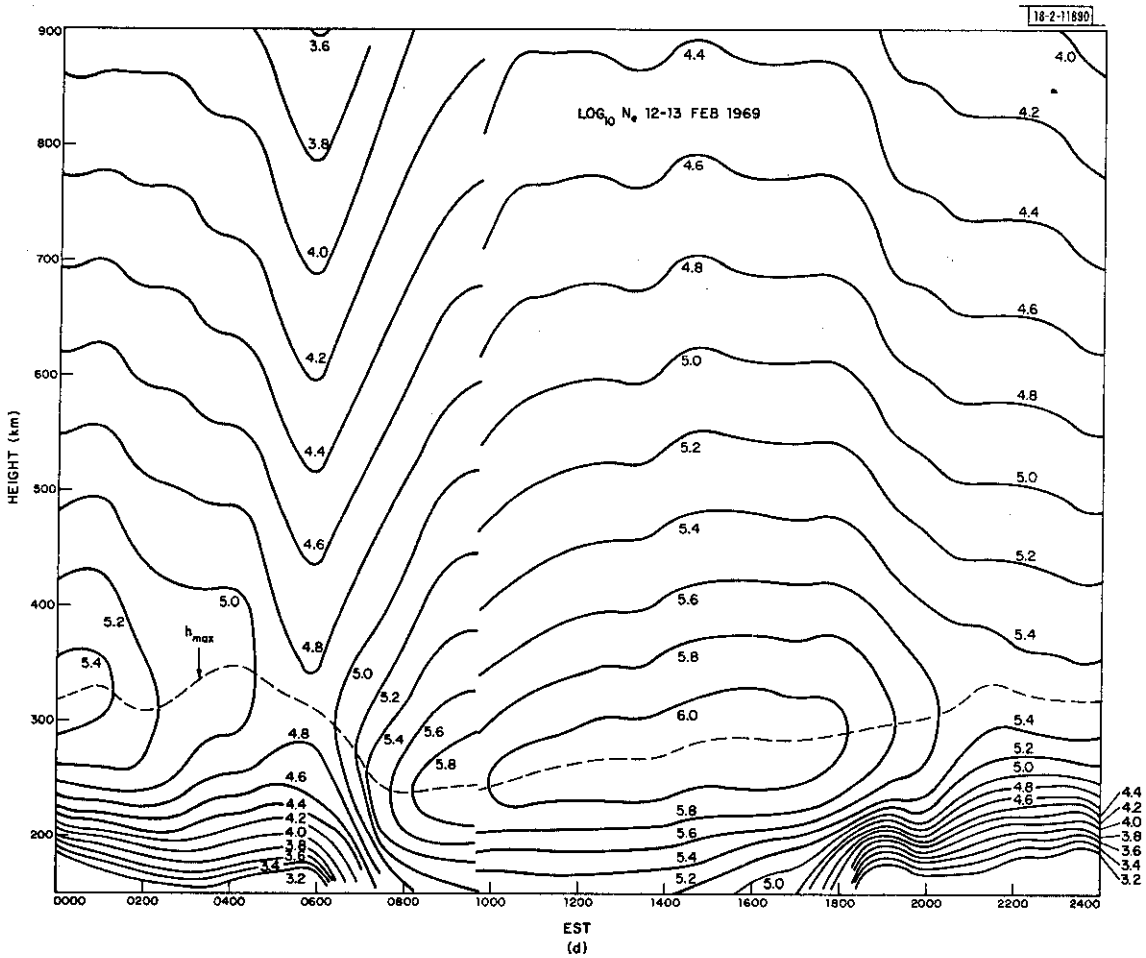

Fig. 3(a-z). Continued.

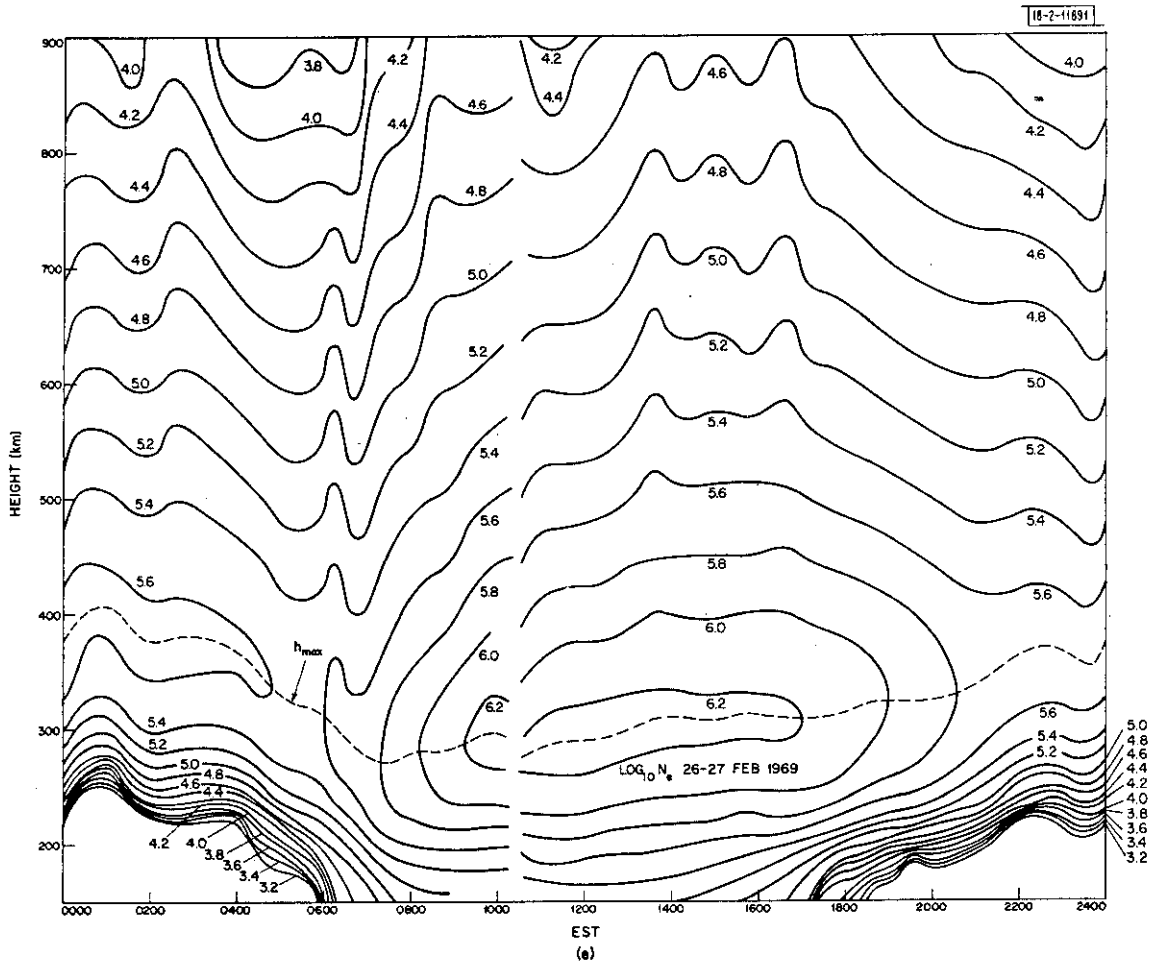

Fig. 3(a-z). Continued.

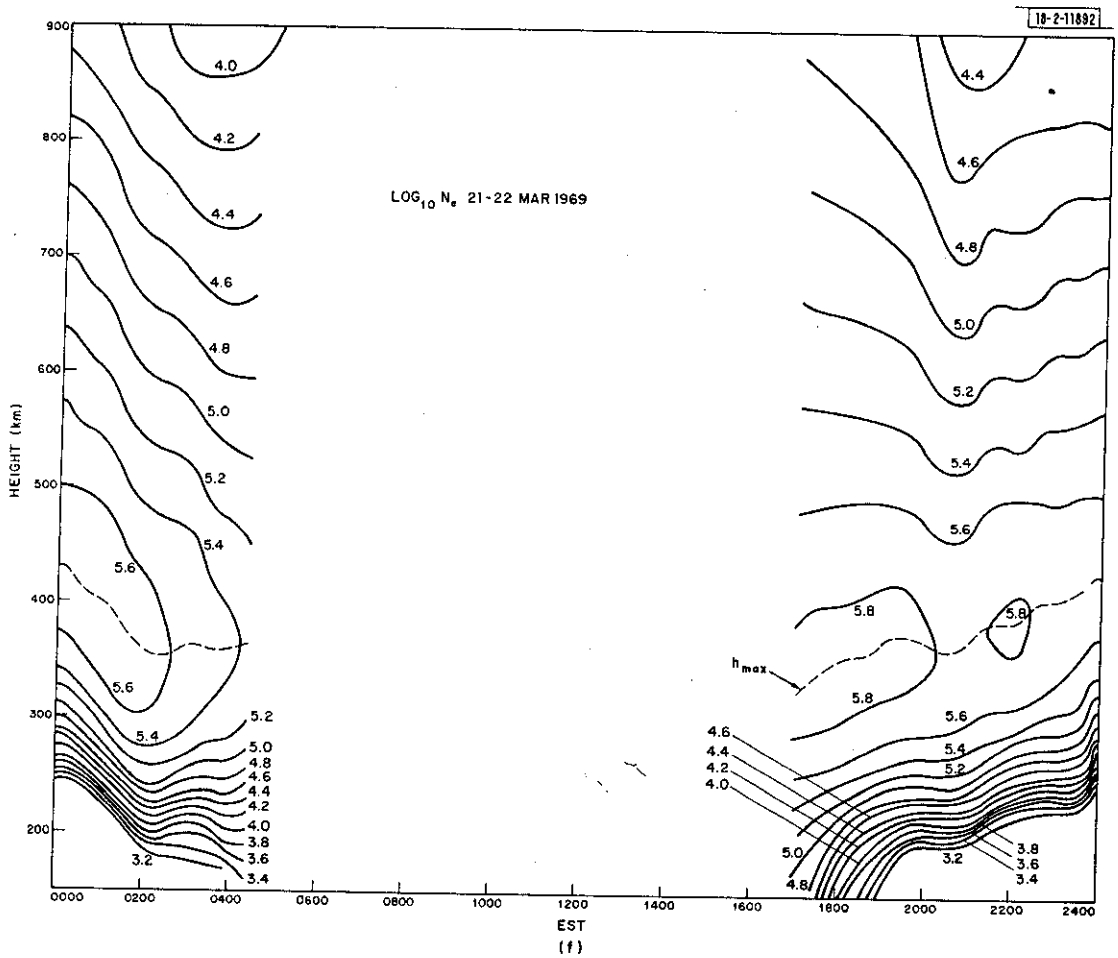

Fig. 3(a-z). Continued.

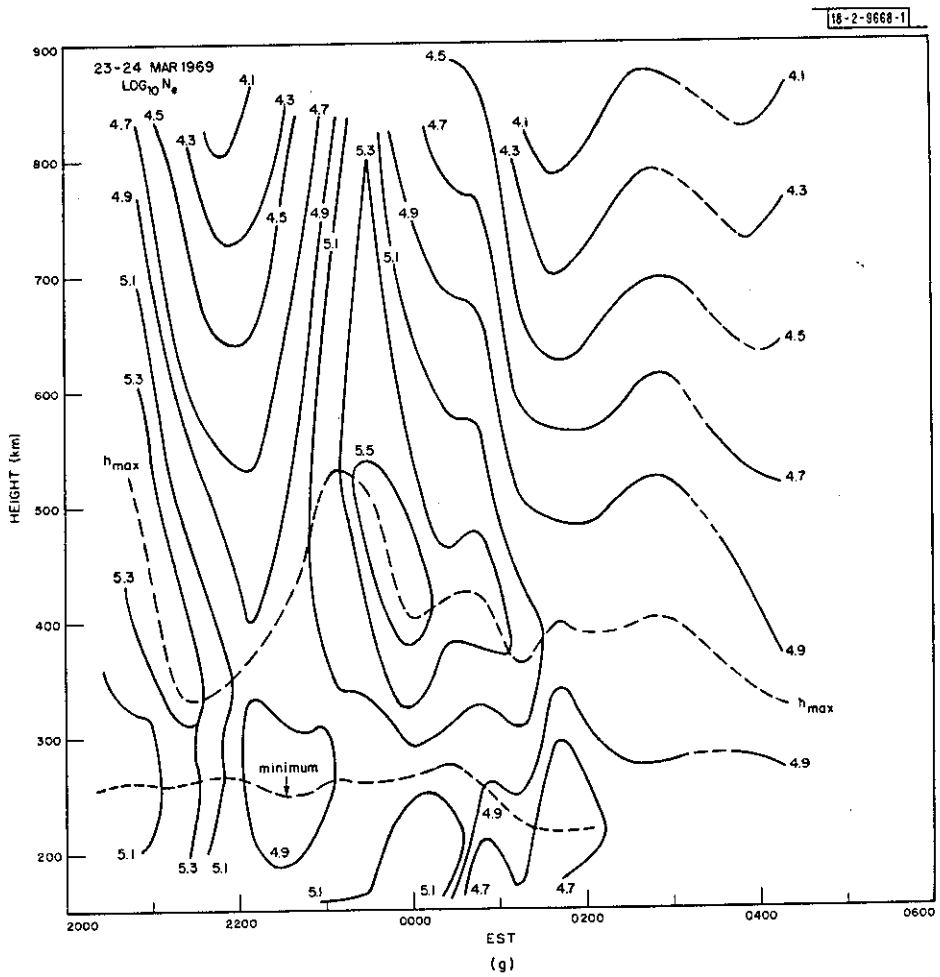

Fig. 3(a-z). Continued.

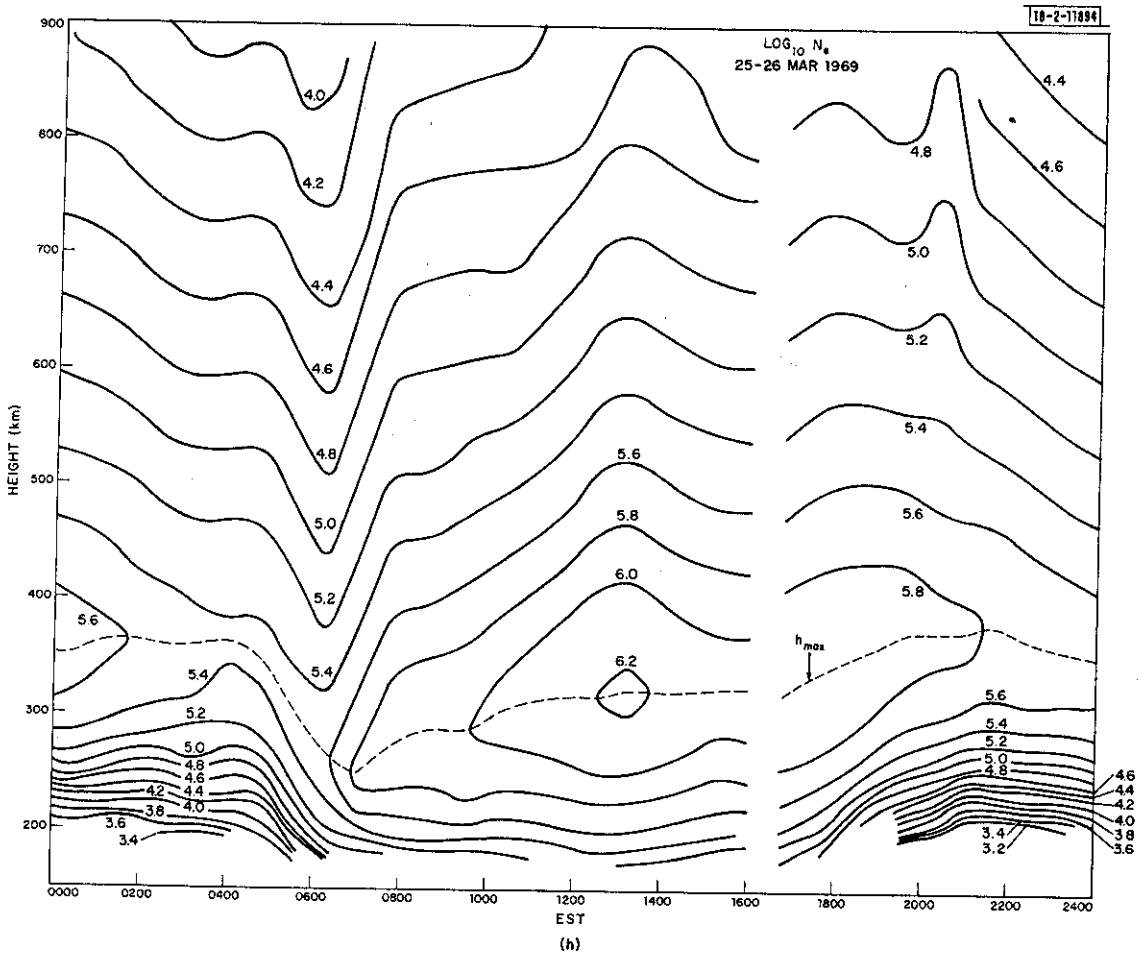

Fig. 3(a-z). Continued.

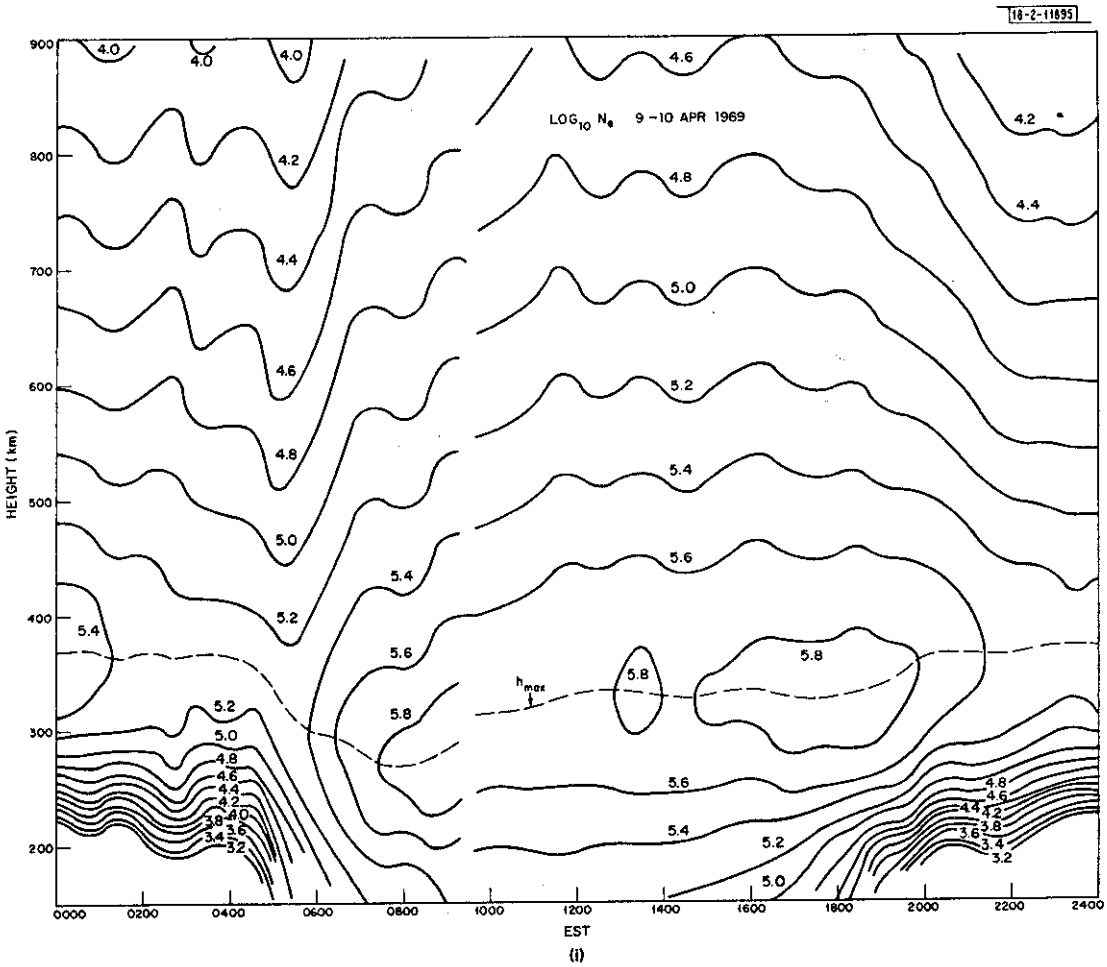

Fig. 3(a-z). Continued.

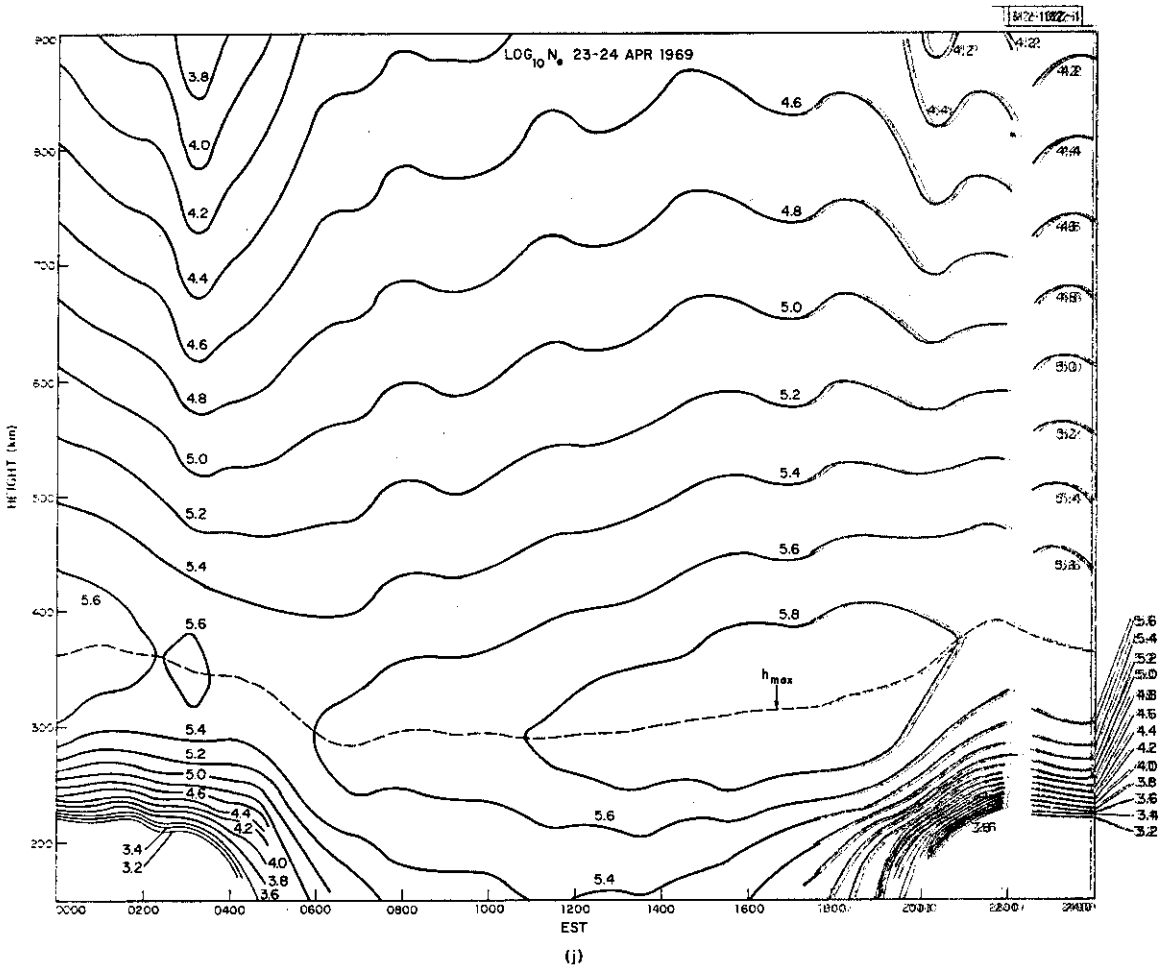

Fig. 3(a-z). Continued.

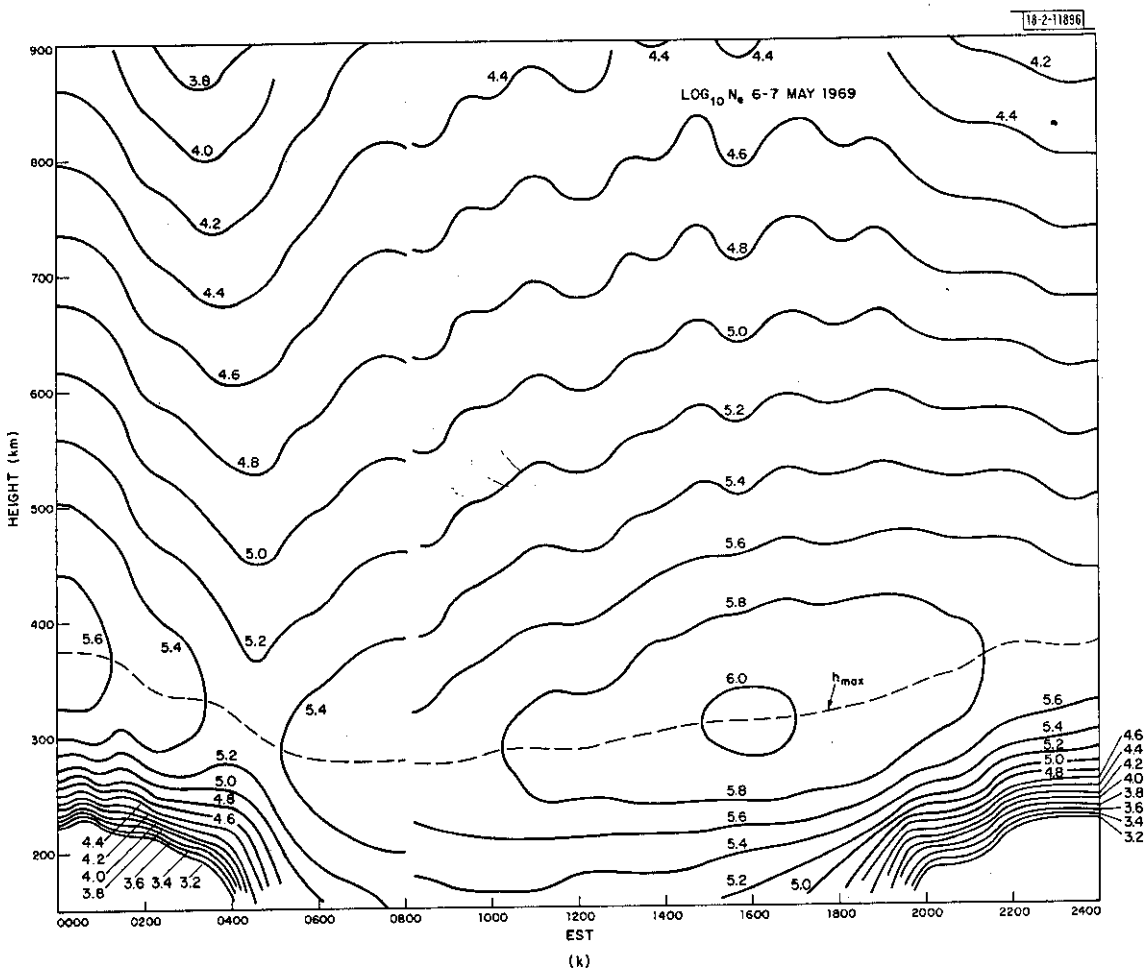

Fig. 3(a-z). Continued.

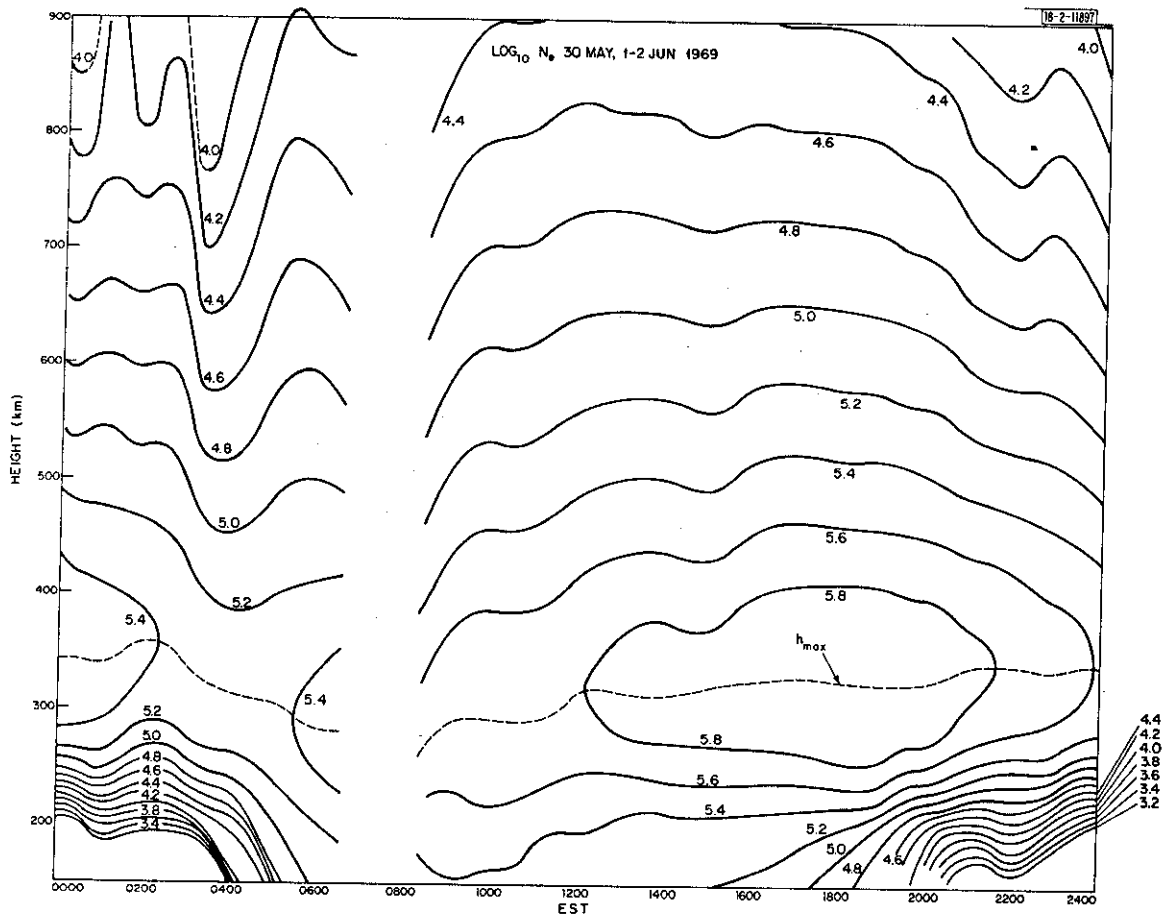

Fig. 3(a-z). Continued.

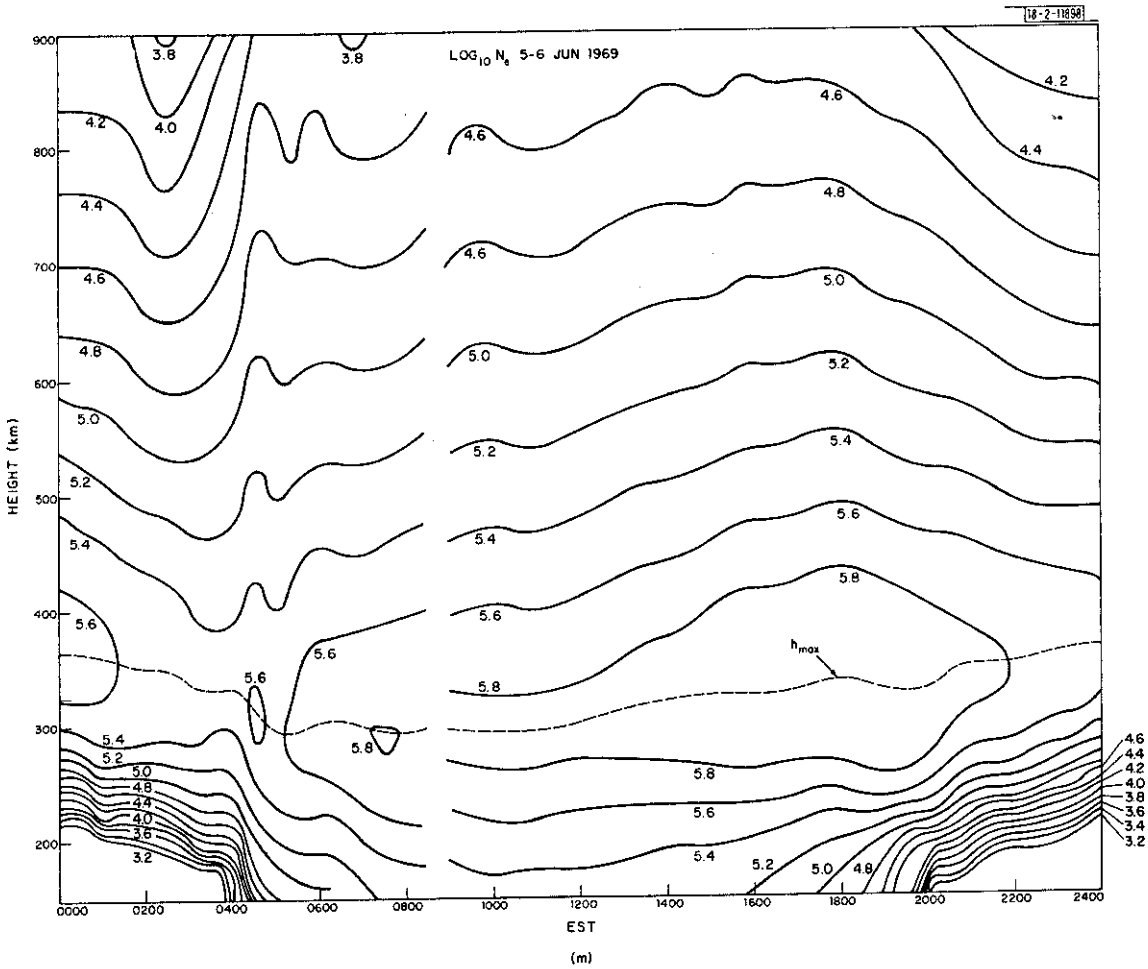

Fig. 3(a-z). Continued.

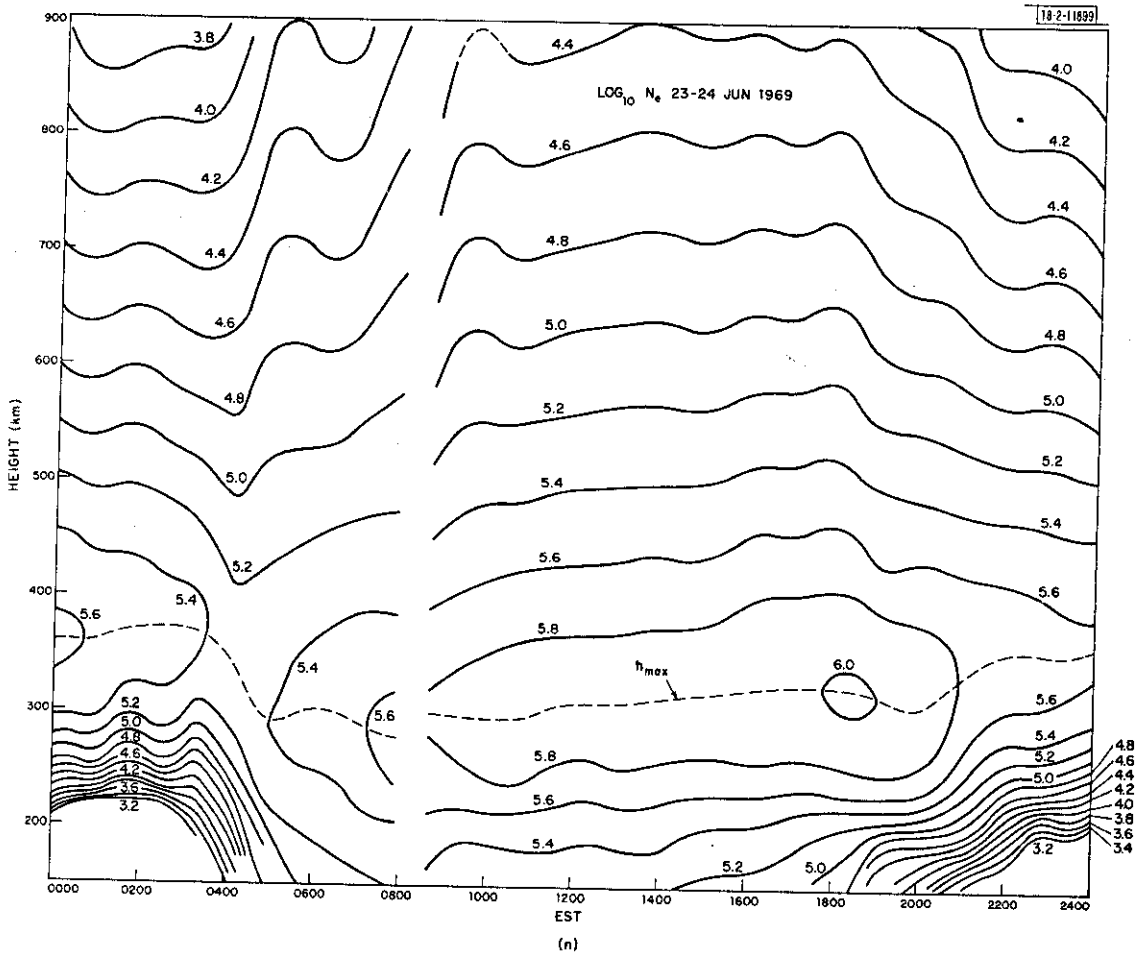

Fig. 3(a-z). Continued.

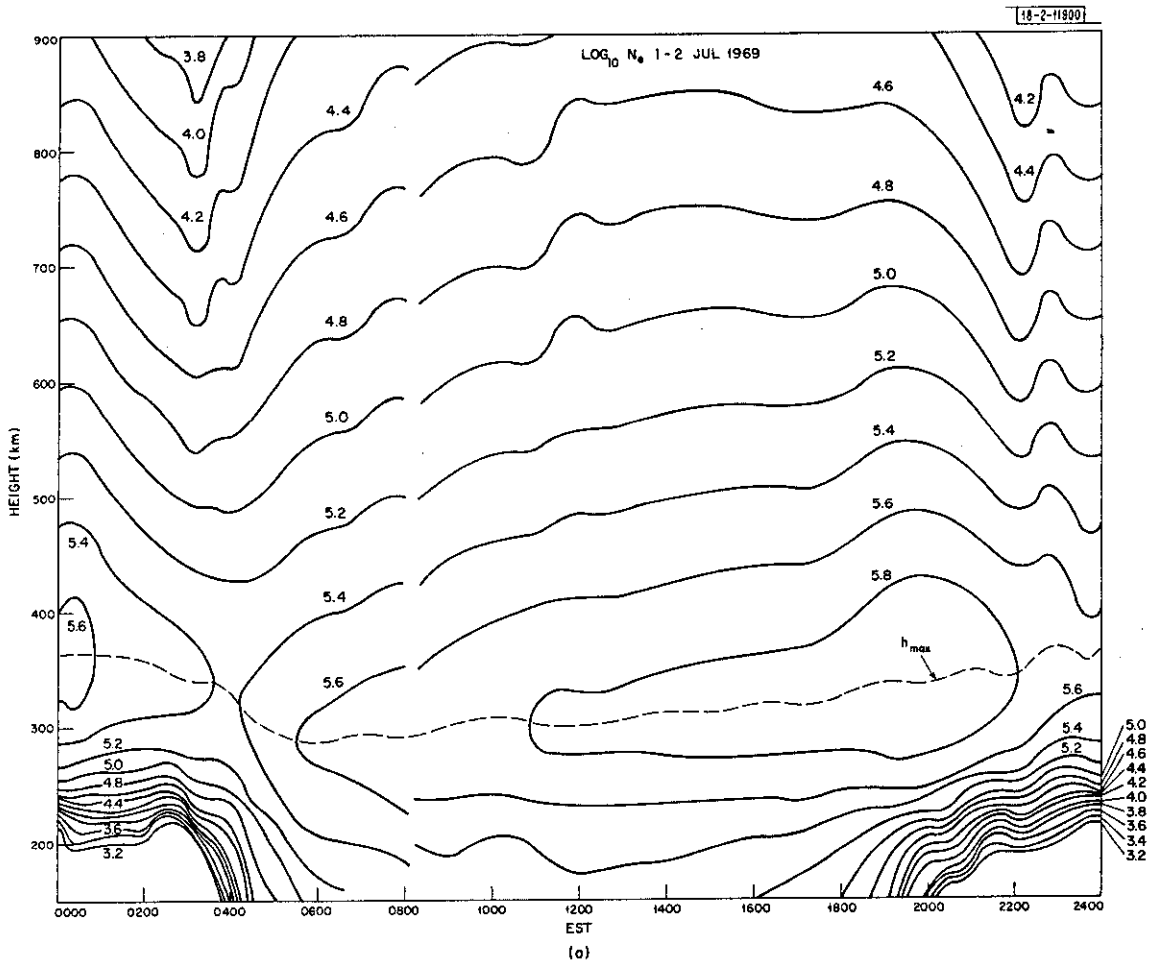

Fig. 3(a-z). Continued.

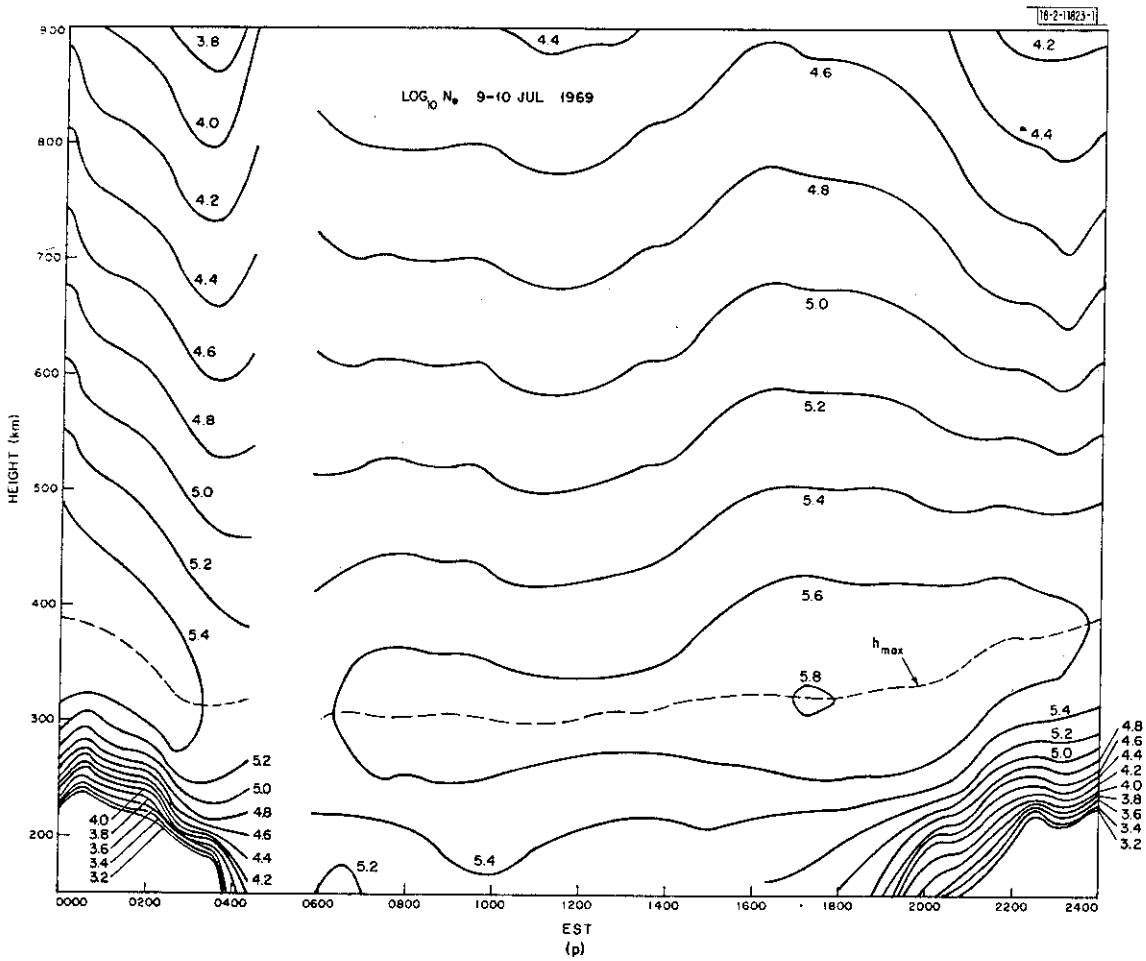

Fig. 3(a-z). Continued.

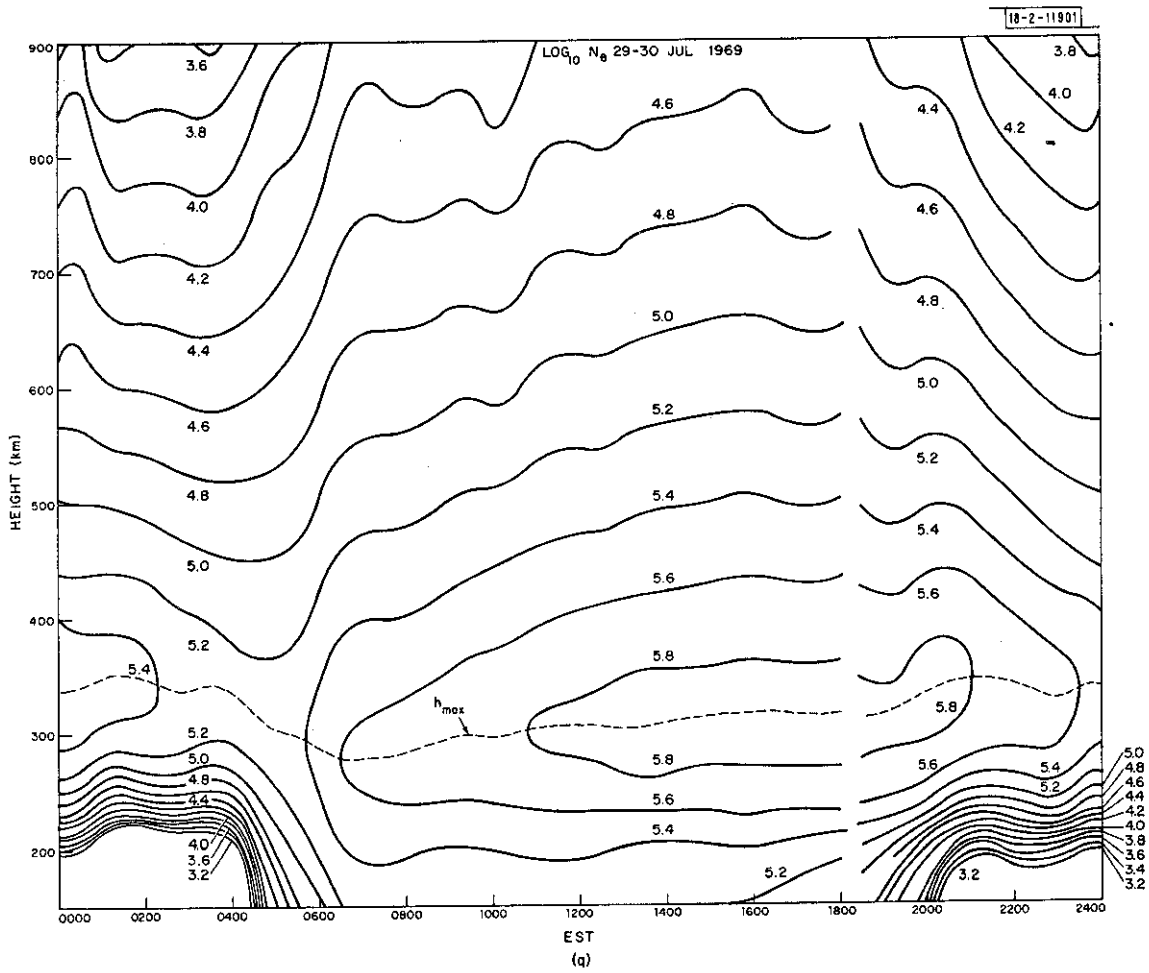

Fig. 3(a-z). Continued.

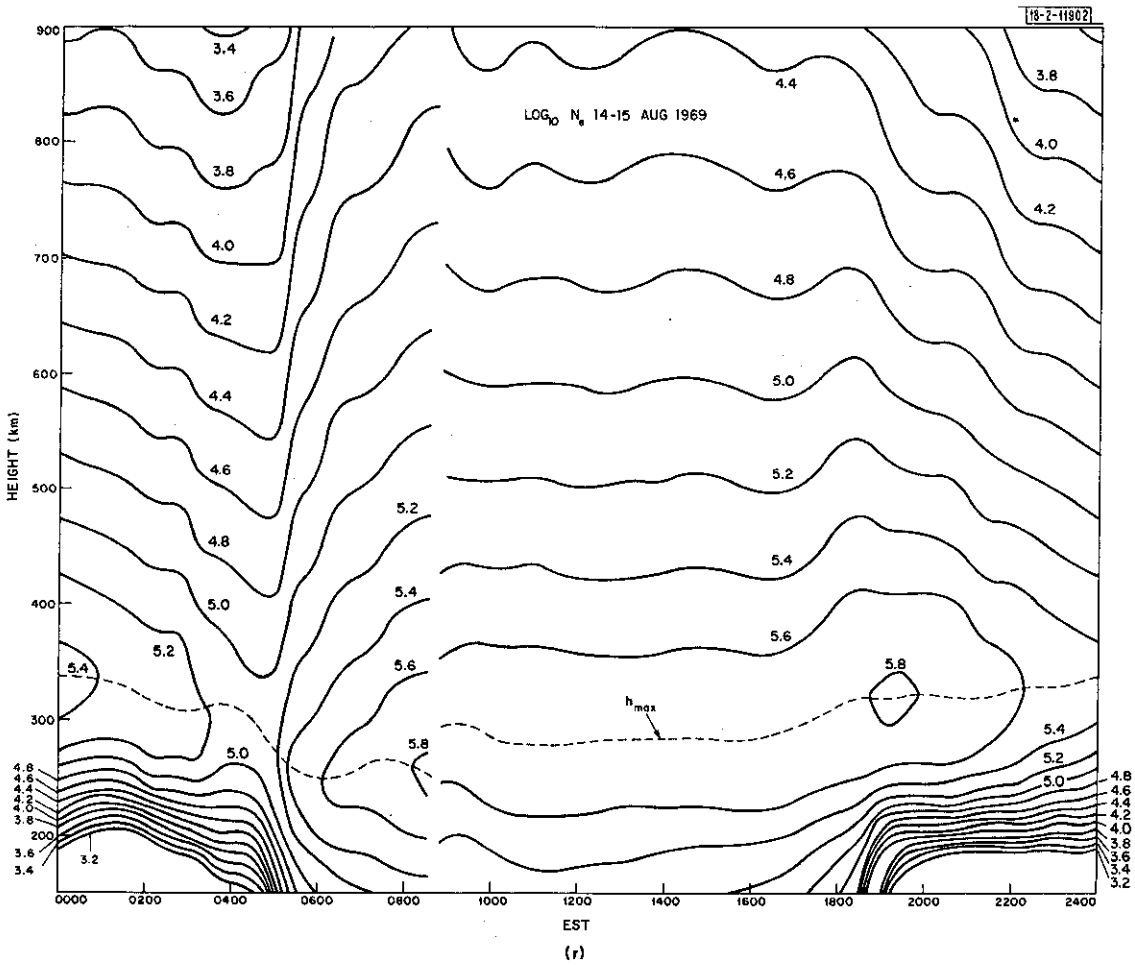

Fig. 3(a-z). Continued.

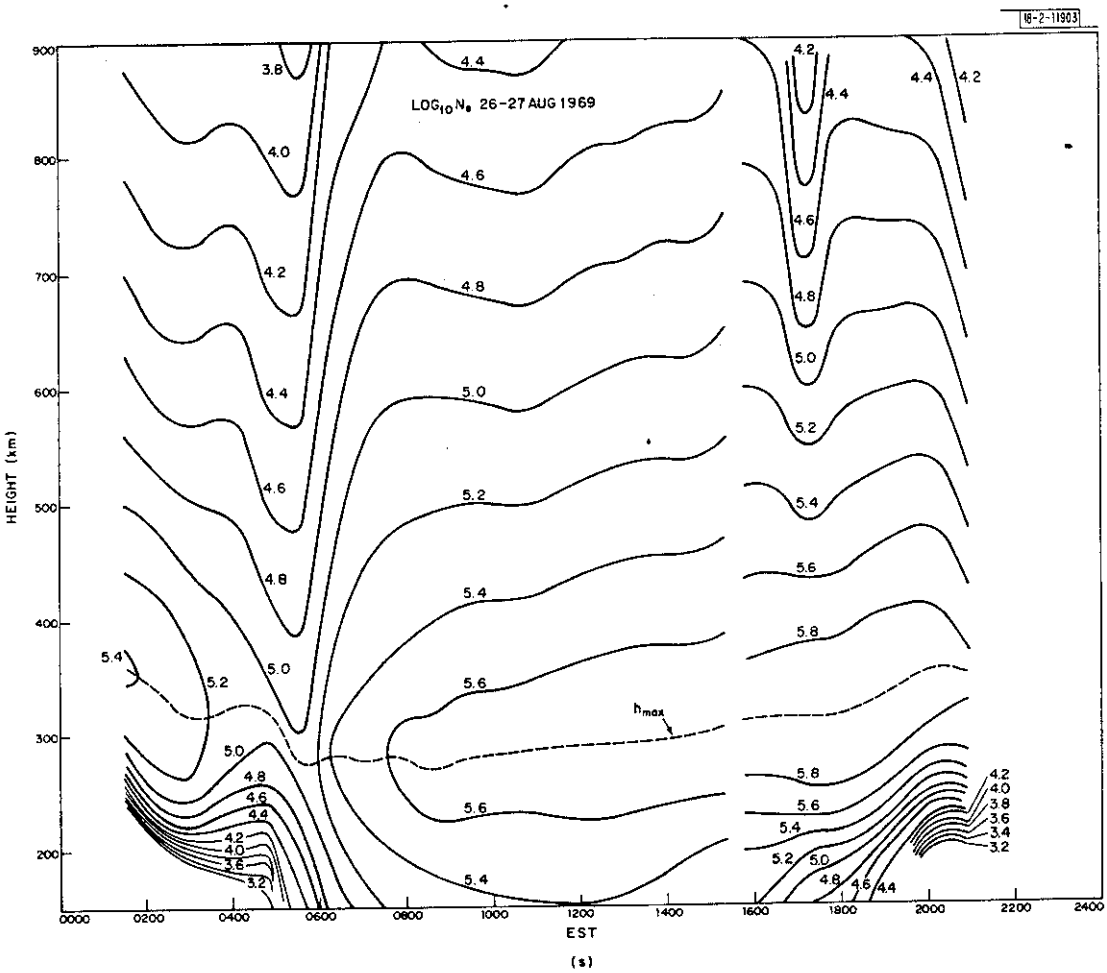

Fig. 3(a-z). Continued.

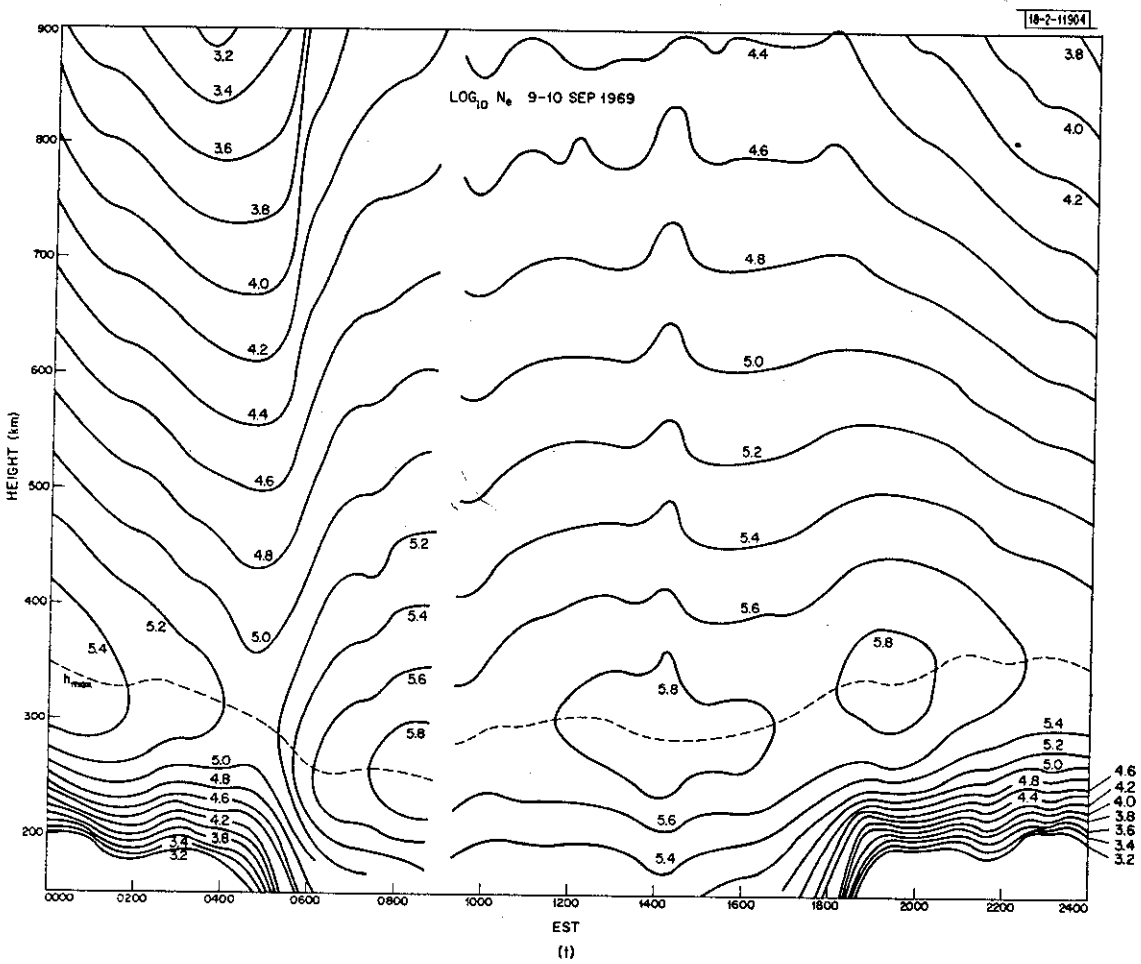

Fig. 3(a-z). Continued.

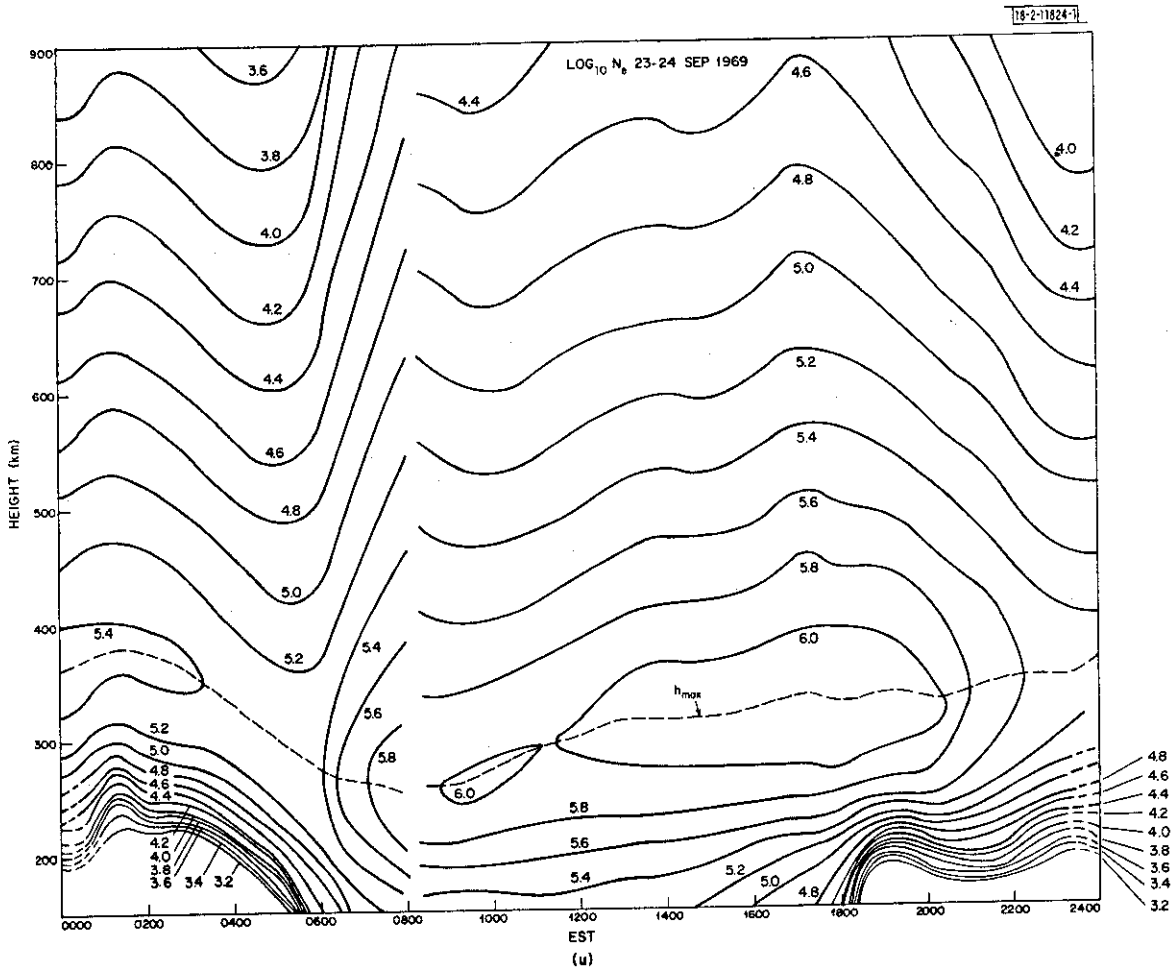

Fig. 3(a-z). Continued.

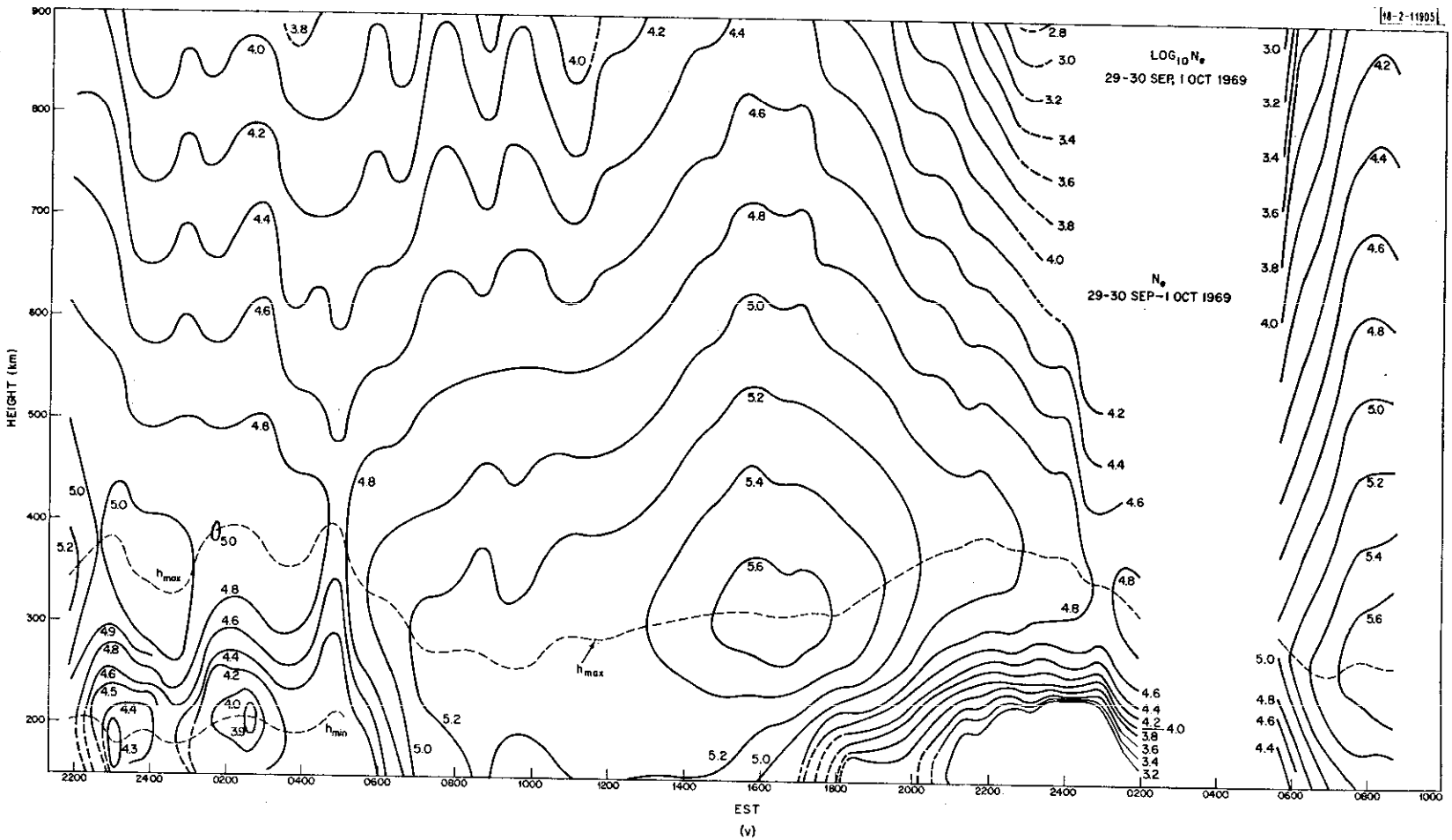

Fig. 3(a-z). Continued.

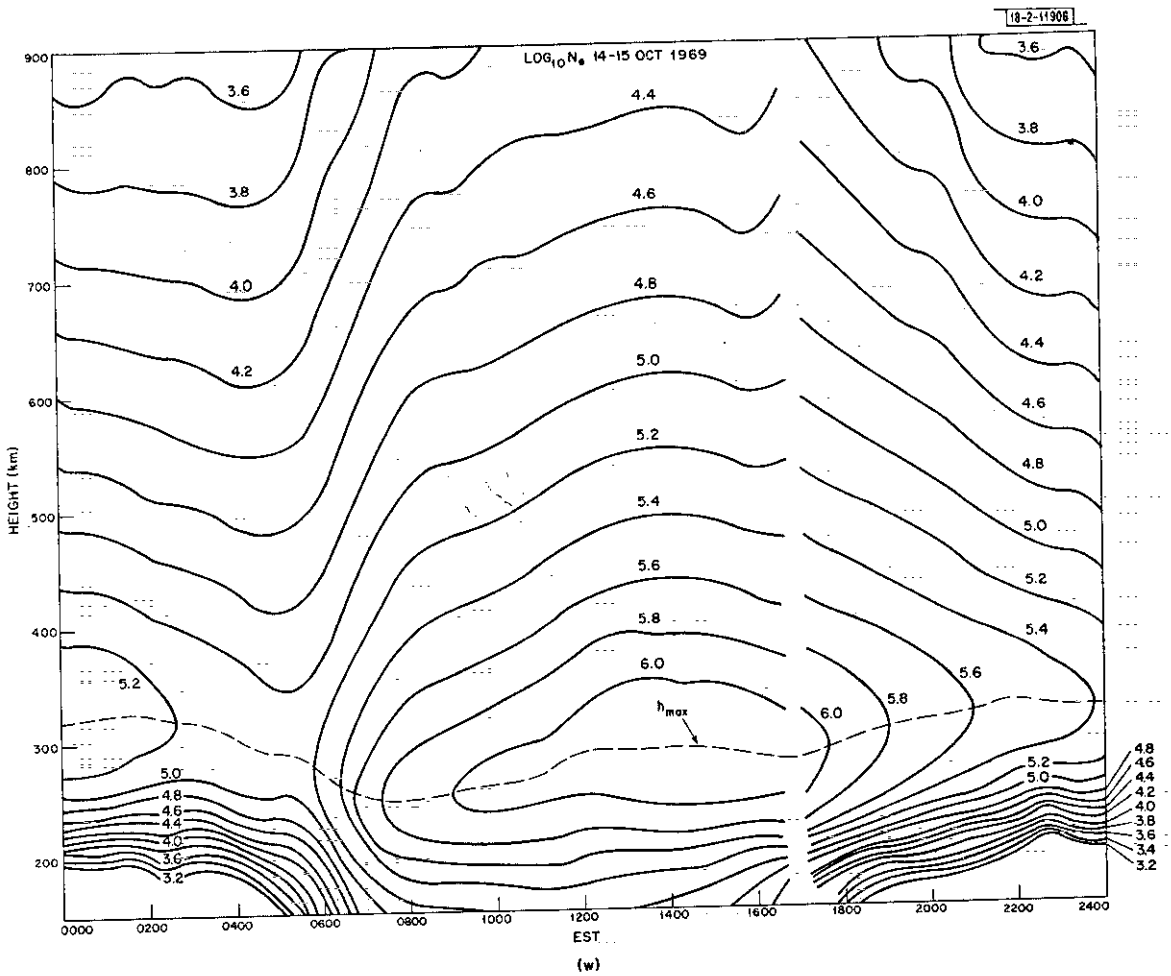

Fig. 3(a-z). Continued.

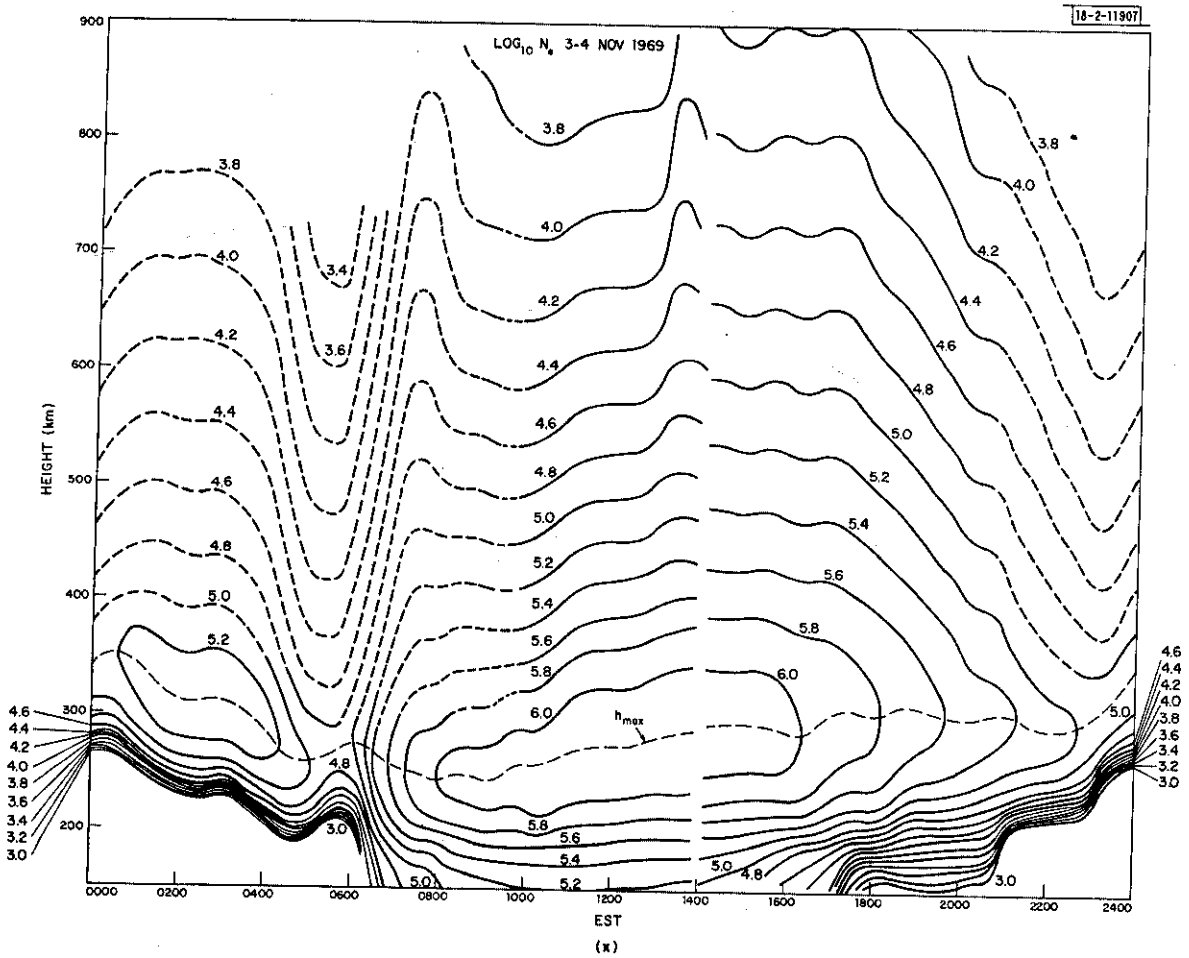

Fig. 3(a-z). Continued.

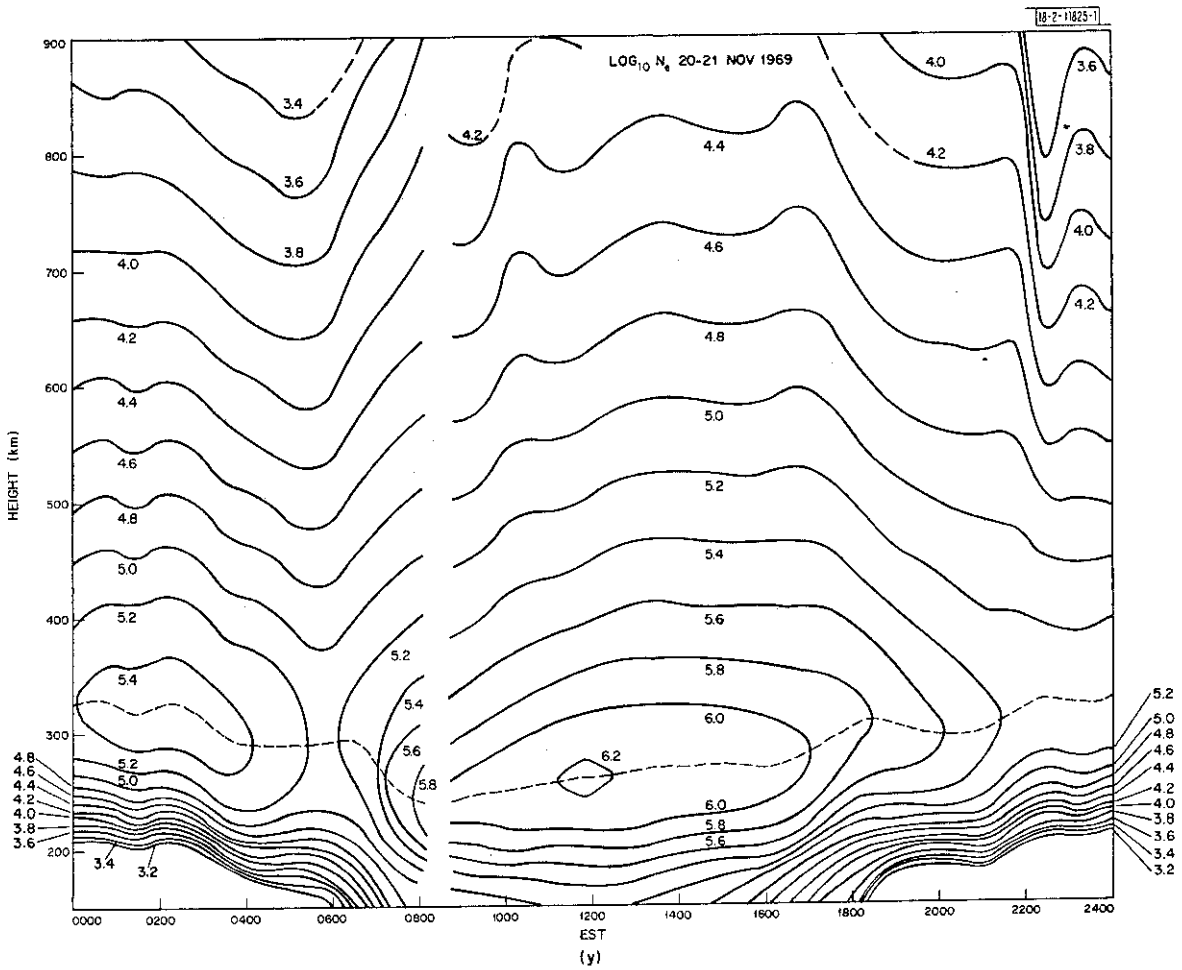

Fig. 3(a-z). Continued.

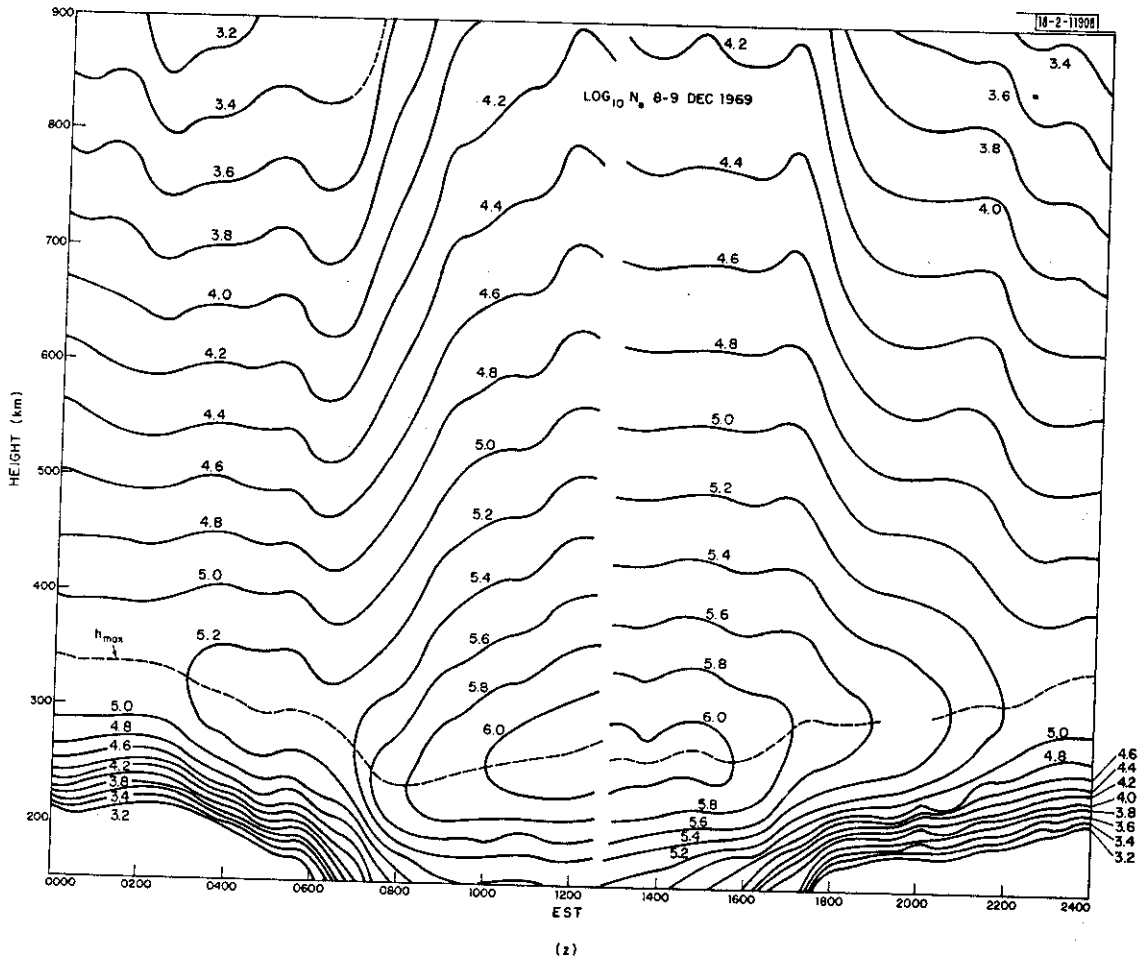

Fig. 3(a-z). Continued.

B. Seasonal Variations

As noted in earlier reports,[1-6] the diurnal variation of the electron density follows one of two characteristic patterns that we have termed "winter" and "summer," respectively. The principal features of the winter behavior are:

(1) There is a large diurnal variation (e.g., 5:1) in peak electron density N_{max}.

(2) The highest values of N_{max} are encountered near 1300 local time.

(3) Following sunrise, the electron density rises to its peak near 1300 and then falls again smoothly.

(4) The peak height h_{max} usually lies in the range 250 to 275 km by day and rises to above 300 km at night.

(5) At night, the electron density decays immediately after sunset to a value that appears to be maintained for the rest of the night.

(6) On many occasions, there is a post-midnight increase in N_{max}. This is usually associated with a downward motion of the layer and a lowering of the plasma temperature.

Figures 3(a), (b), (w), (y), and (z) provide representative examples of the winter-type variation. For the observations reported here, there appears to have been a transition from winter to summer behavior between 25-26 March and 9-10 April [Figs. 3(h) and 3(i)] and a return to winter behavior by 14-15 October [Fig. 3(w)].

The summer behavior may be characterized as follows:

(1) There is only a small diurnal variation in N_{max} (e.g., $\leq$ 2:1).

(2) The highest value of N_{max} is usually encountered near ground sunset (e.g., 1800 to 2000 hours), and is then considerably less than encountered in winter near noon.

(3) Following sunrise, the electron density increases for only 1 to 2 hours, and then changes little throughout the rest of the daytime.

(4) The peak height usually lies between 275 and 300 km by day, i.e., higher than found in winter.

(5) The thickness of the F-layer (e.g., as measured between points of half-peak density) is considerably larger in summer than in winter.

(6) At night, the density decays continuously until sunrise.

Figures 3(j), (k), (m), (n), (p), (q), (t), and (u) appear to be representative examples of this type of behavior.

The transition from summer to winter behavior is fairly rapid, and appears to signal a completely new state for the upper atmosphere. There now appears general agreement that the cause of this change is a seasonal variation in the neutral wind pattern of the upper atmosphere.[10-13] These winds serve to transport atomic oxygen from the summer to the winter hemisphere, thereby altering the ratio of the ionizable constituent (O) to the molecular species (O_2, N_2) responsible for removing O^+ ions. While satellite observations of neutral abundances have been made that are consistent with this hypothesis,[23,24] measurements of the wind system responsible have not been made in sufficient detail to confirm their role. It is also possible that there are

seasonal variations in N_2 and/or O_2 that contribute to the annual variation in F-region behavior.[25] However, measurements made in France and at Millstone of N_2 densities at heights near 110 km appear to rule out the existence of large seasonal changes of N_2 in the lower thermosphere.[25,26]

C. Disturbed Days

We also have described previously variations in these quiet-day patterns encountered during magnetic storms.[4-6,11-14] Three major magnetic storms occurred in 1969 on 24 March, 14 May, and 29 September, and we were fortunate enough to gather data during two of these. The March storm began with a sudden commencement (S.C.) at about 1300 EST on 23 March, which promptly gave rise to K_p values exceeding 5+ for the next 39 hours. Observations began at Millstone at 2040 EST, i.e., 7 hours after the S.C., and were continued until 0500 EST next morning. Additional observations were made on 25-26 March (Table II), by which time the storm largely had subsided. Thus, the 23-24 March observations [Fig. 3(g)] may be contrasted with the behavior two days before the storm [Fig. 3(f)] and a day later [Fig. 3(h)].

During the disturbed period, few reliable readings of f_oF2 were obtained on the ionosonde as a result of increased absorption in the D-layer, and we were obliged to reconstruct the time variation from the intensity of the incoherent scatter echoes in the manner outlined in Ref. 5. Figure 4 presents the results.

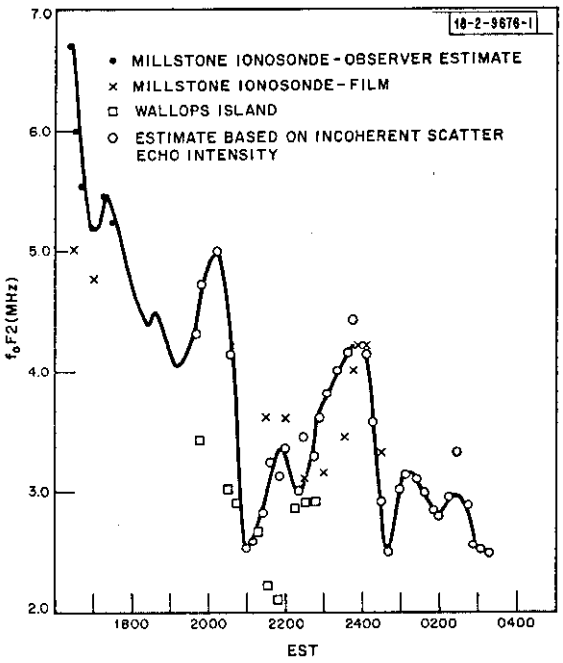

Fig. 4. Variation of f_oF2 MHz obtained for 23-24 March 1969 from variation of incoherent scatter power during period when ionosonde was at times blacked out.

As can be seen in Fig. 3(g), there were large changes in layer shape as well as peak density and height. The F-layer appeared much higher than normal, and the density varied only slowly with altitude. While the interpretation of the results obtained below 170 km altitude is complicated by the presence of ground reflections, it appears that there was a second maximum of ionization located in the E-region, and that the valley between the E- and F-layers was filled with ionization with a density of $\sim 10^5$ el/cm^3. We believe that this behavior, taken together with the elevated electron temperatures observed, is a manifestation of soft ($\geq$100 eV) electron precipitation occurring at the time. More detailed calculations are being performed by Dr. J. F. Noxon (private

communication), but are somewhat hampered by lack of knowledge concerning the state of the neutral atmosphere during the event.

Somewhat similar behavior was observed during the night of 29-30 September in the second storm which commenced at 1050 EST and gave rise to K_p values exceeding 5+ for the following 33 hours. Observations got under way at Millstone at 2200 EST, i.e., some 11 hours after the S.C., and continued until 0900 EST on 1 October, by which time the K_p index had subsided to a level of about 4. Soft precipitation appears to have been present from the time the measurements commenced until about 0400 EST. In this case, however, the density in the valley region was an order-of-magnitude less than encountered on 23-24 March, and the electron temperature was considerably lower also. These findings suggest that the flux of precipitating particles was much lower during this night.

On 30 September, there was an anomalously large evening increase. Elsewhere,[11,14] we proposed that this is a manifestation of substorm electric fields, which appear to penetrate the midlatitude ionosphere around dusk. This explanation has been contested by Jones,[27,28] who claimed that lifting of the layer by electric fields cannot produce ionization increases as large as have been seen (~100 percent). This conclusion was based upon calculations performed using a circuit analog method. More detailed calculations by Tanaka and Hirao,[29] however, appear to support the original explanation.

The observations carried out on the post-storm days, 25-26 March 1969, have been subject to a detailed analysis[30,31] in which they were contrasted with the behavior observed during a quiet day a year later (23-24 March 1970). It appeared that the vertical fluxes of ionization into or from the protonosphere were lower on the disturbed day, and Evans[31] suggested that this arose because of a depletion in the abundance of neutral hydrogen in the upper atmosphere available to charge exchange with O^+. Other explanations are possible, however; for example, the vertical drifts observed on the disturbed day may have been influenced considerably by electric fields, and not caused solely by ambipolar diffusion along the field lines, as was assumed.

D. Winter-Night Behavior

The nighttime behavior of the electron density at Millstone is anomalous. Increases in N_{max} are observed regularly on quiet nights (e.g., 30-31 January, 3-4 November, and 20-21 November), usually commencing near midnight. This phenomenon, which is linked to the more general question of the maintenance of the winter nighttime ionosphere, has been discussed extensively in earlier papers.[4,13,32] The significant features of winter night pre-dawn increases appear to be: (1) They usually commence at about midnight and peak near 0200 EST, but there are variations of up to ±2 hours; (2) the increases in density are always accompanied by a lowering of the plasma temperature (believed to be caused by increased local cooling); (3) the increases are usually accompanied with a lowering of the layer.

This phenomenon is not confined to a small geographical region, but appears to extend in latitude from 30° to 70° according to ITS predictions of f_oF2 (Ref. 33). Figure 5 shows the predictions of the critical frequency for January 1969 at 0600 UT (0100 EST). A ridge of increased values along the east coast of the United States can be seen. While this map is probably inaccurate in auroral latitudes (say north of 50° geographic in this longitude region), increases in f_oF2 are seen regularly in the values reported from Wallops Island (37°N) to the south of Millstone and Ottawa (45°N) to the north, which confirm the general pattern of Fig. 5.

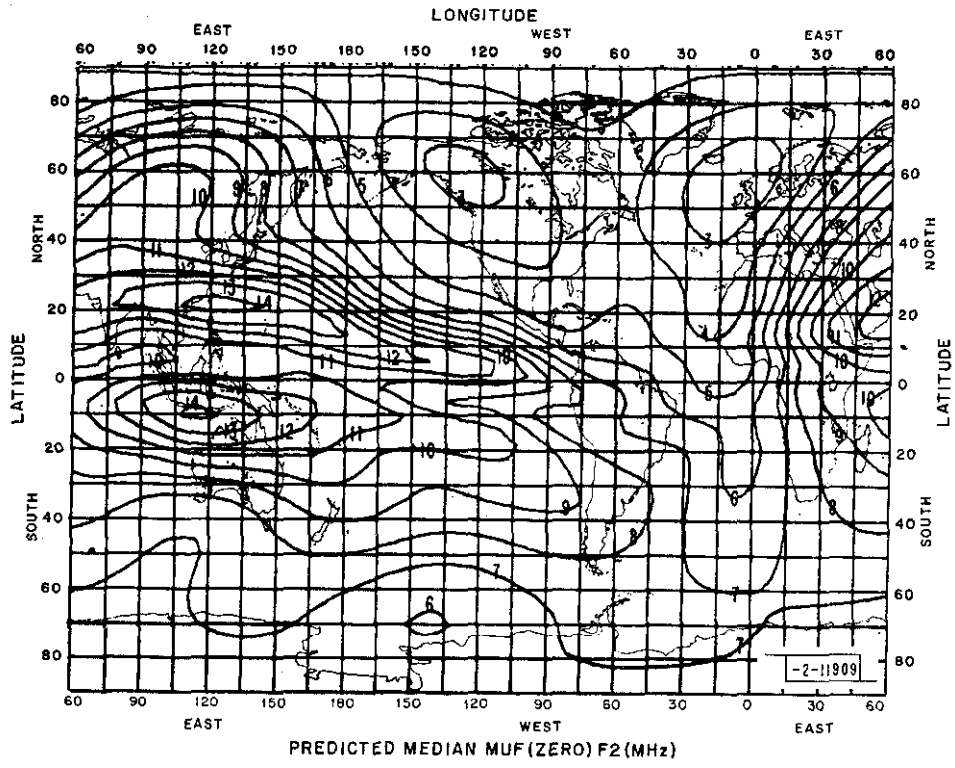

Fig. 5. Contours of f_0F2 at 0100 EST predicted for January 1968.[33]

The increase in N_{max} invariably appears to be accompanied by a lowering of the plasma temperature and consequent redistribution of the electrons in the layer. As a result, the total content increases by a smaller percentage than the peak density. This can be seen in the Millstone profiles, and has been observed directly in measurements of total content conducted using geostationary satellites.[34]

Earlier,[32] we proposed that the density increase was caused by a flux of cool plasma from the magnetosphere. The onset of this flux was supposed to be controlled by the time it takes the field tube to cool following conjugate sunset. Figure 6 shows the time of local and conjugate sunset for Millstone. Owing to the more westerly location of the conjugate point, local midnight occurs 30 minutes later there than at Millstone.

Subsequent studies of the production of photoelectrons arriving from the conjugate ionosphere,[15] and the onset of heating in the local ionosphere following conjugate sunrise[35] showed that the escape of photoelectrons into the magnetosphere should be fully developed whenever the solar zenith distance $\chi \geq 100°$. If this is so, then there is no time during the night at which the conjugate heating should be reduced in the period between mid-October and mid-February (Fig. 6); this finding destroys the earlier hypothesis. Meanwhile, the question of whether a flux of ionization from the magnetosphere could produce an increase in N_{max} has been examined, among others, by Mikhaylov[36] (who, however, neglected the change in the shape of the layer associated with temperature changes). Mikhaylov found that a flux rising to $\sim 5 \times 10^8$ el/cm^2/sec appeared necessary to raise f_0F2 from about 2.5 to 3.5 MHz. As shown in Sec. V, such large fluxes do not appear to exist at Millstone at night.

The more general question of the maintenance of the nighttime ionosphere, by means of a flux of ionization from the magnetosphere, has been discussed by a large number of authors.[37-42]

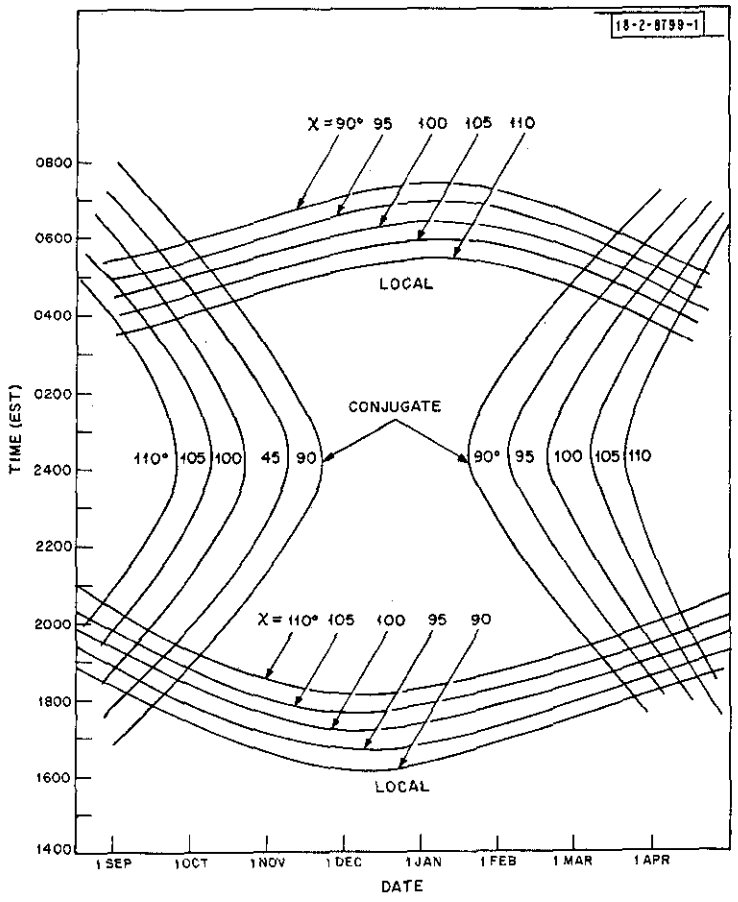

Fig.6. Contours of solar zenith angle X at Millstone and its conjugate point during winter months.

Because it has seemed that the flux available is too small, it has been argued that the principal contributor to the maintenance of the nighttime F-layer at midlatitudes is the existence of thermospheric winds, which blow toward the equator and drive ionization along the field lines to higher levels where the recombination rate is lower. (For review see Rishbeth.[43]) However, direct experimental evidence showing the existence of significant fluxes that would assist in maintaining the nighttime F-layer has recently been obtained at Arecibo,[44] so the question appears far from being settled. We address this topic further in Sec. V.

E. Disturbed-Nighttime Behavior

Millstone lies in what must be termed sub-auroral latitudes, and the local ionosphere may be subject to changes in association with events taking place in the auroral zone to the north. The penetration of substorm electric fields into the midlatitude ionosphere at night has been discussed by Rüster[45]; and, by examining ionosonde records, VanZandt, et al.,[46] Park,[47] and Park and Meng[48] have demonstrated that these fields can penetrate a range of geomagnetic latitude of 20° to 60° during about 9 hours of local time. Prior to midnight, the layer is lifted by an eastward electric field, while after midnight it is usually lowered by westward fields. According to Park and Meng,[48] these effects can be seen most clearly during winter nights when the hours of darkness are longer and the layer normally undergoes only small changes of shape and height with time. These vertical motions of the F2-layer are usually accompanied by changes

in peak density, although there appears to be no simple relationship between N_{max} and $h_{max}F2$. A decrease in the layer height often is accompanied by an initial increase in N_{max}, but a further lowering of the layer will give rise to a rapid decay.[47]

Observations were conducted during magnetically disturbed winter nights on 16-17 January (K_p = 4+ at 0000 hours), 5-6 February (K_p = 4), 12-13 February (K_p = 3+), 26-27 February (K_p = 3), 8-9 December (K_p = 4–). Several of these nights appear to exhibit some of the effects reported by Park and Meng,[48] but at this juncture their association with substorms has not been determined. Particularly striking are the fluctuations in h_{max} observed on 16-17 January, 12-13 February, and 26-27 February, which are associated with variations in N_{max}.

IV. ELECTRON- AND ION-TEMPERATURE RESULTS

A. General

Figures 7(a) through (z) and 8(a) through (z) provide diagrams showing contours of constant electron temperature (at 200°K intervals), and of constant ion temperatures (at 100°K intervals) vs height and time for the periods listed in Table II. These diagrams were prepared from temperature-height profiles drawn by hand through the points plotted by the Calcomp plotter.[5,6]

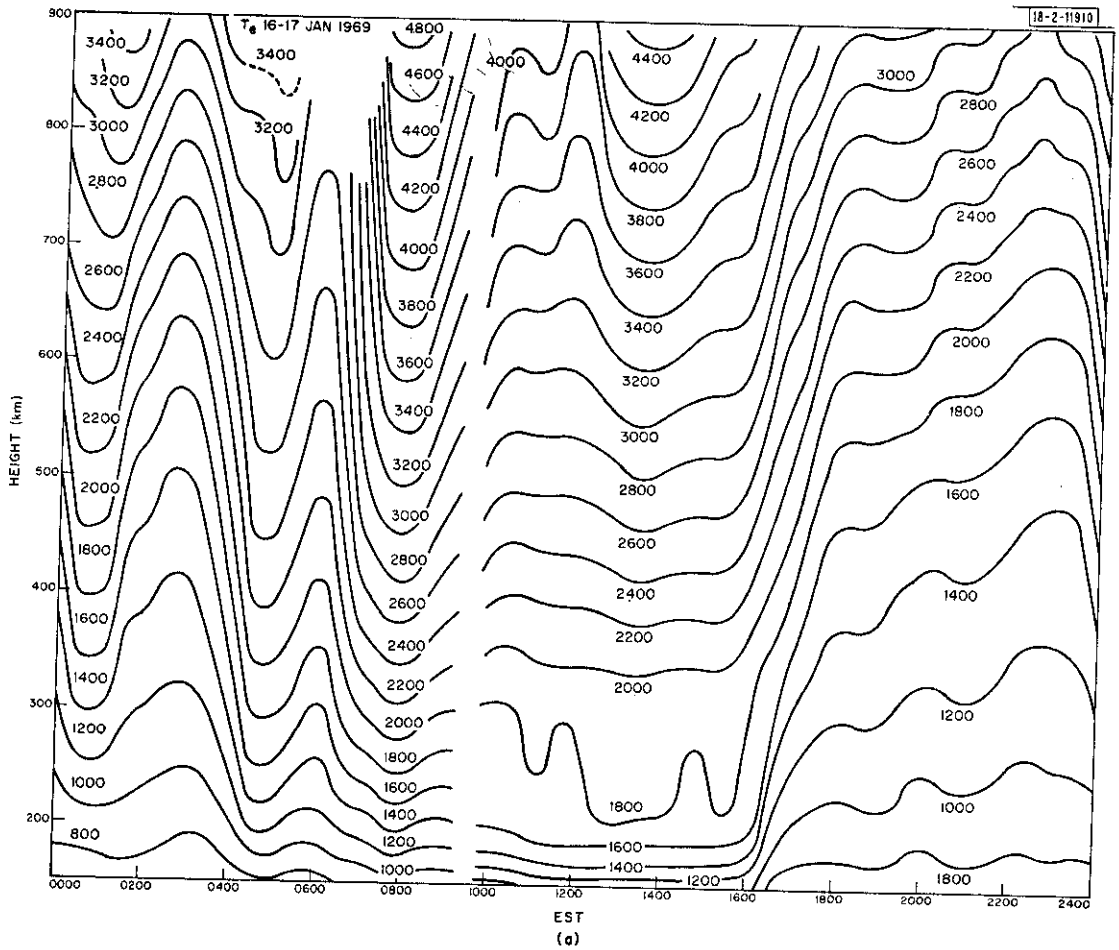

Fig. 7(a-z). Contours of electron temperature T_e observed on days listed in Table II.

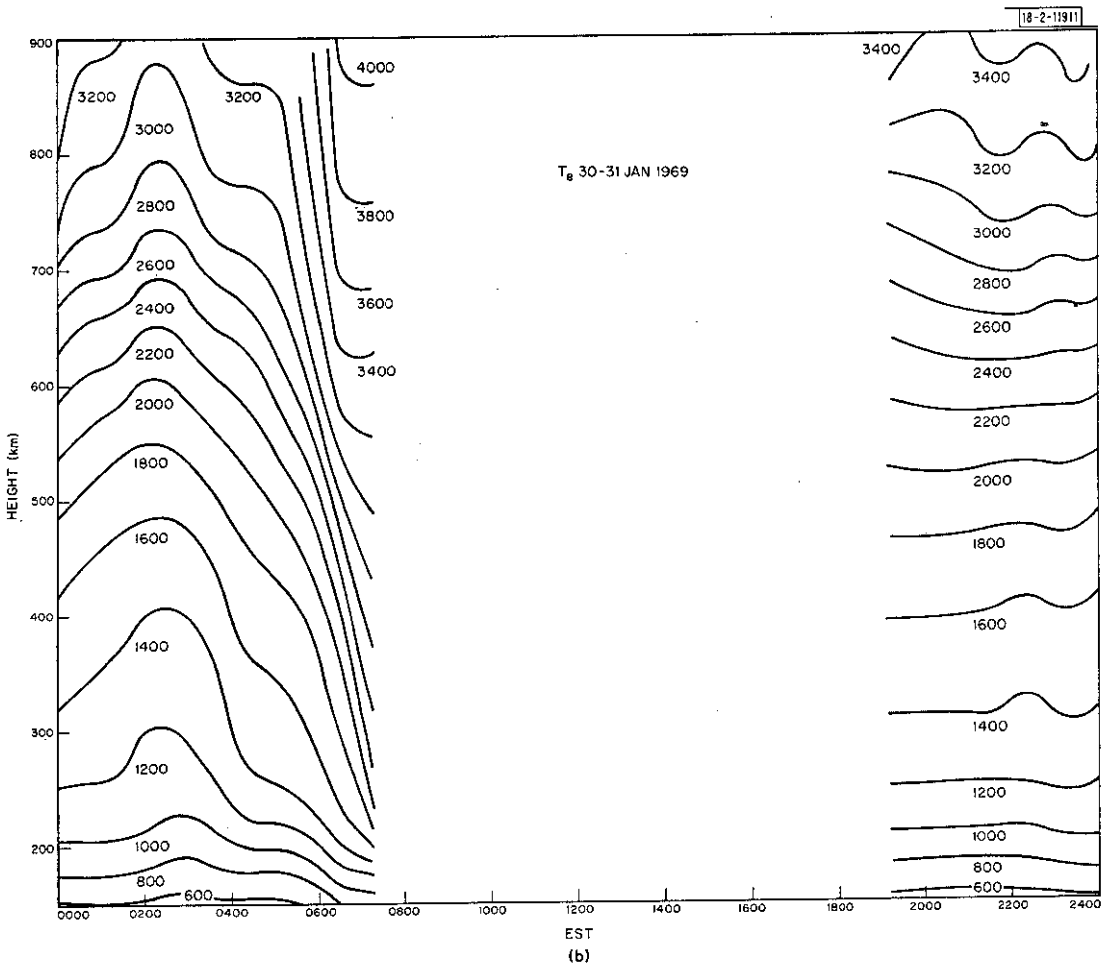

Fig. 7(a-z). Continued.

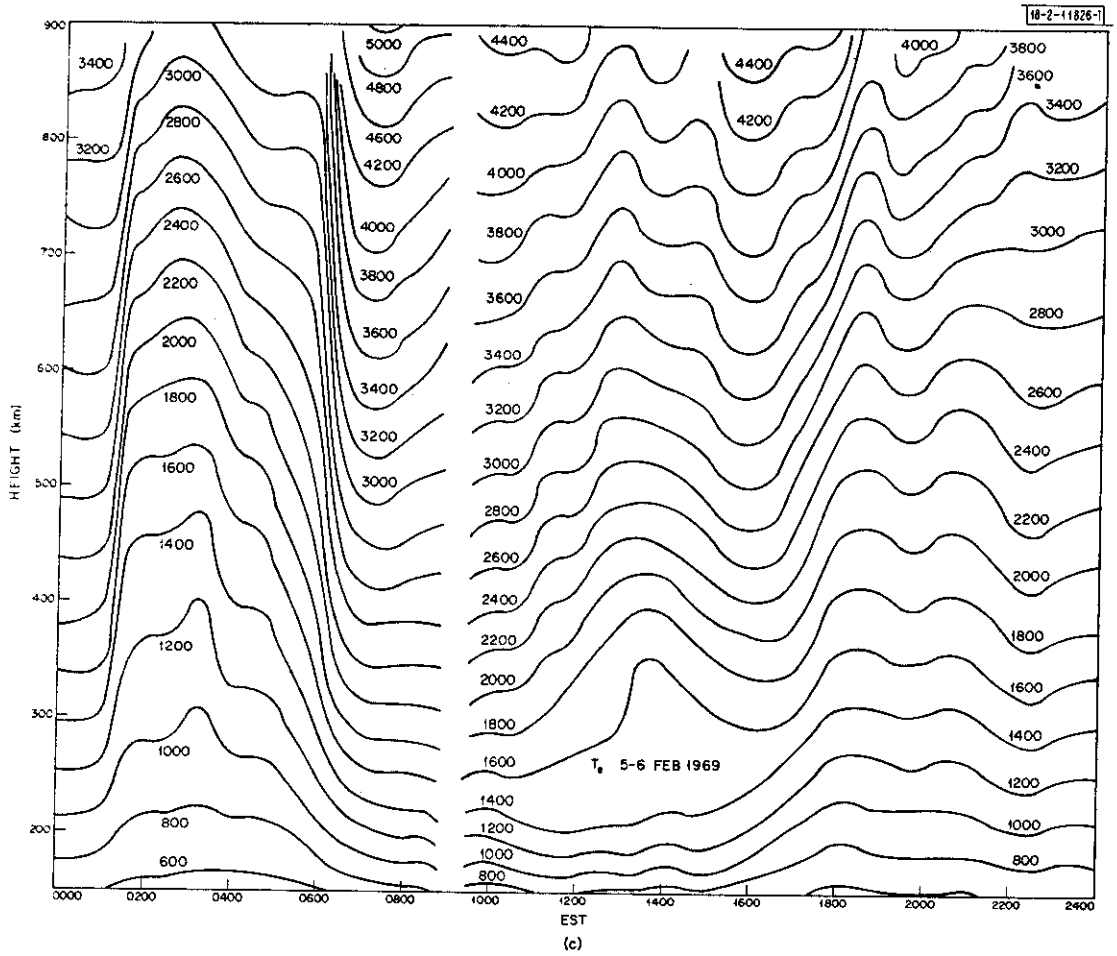

Fig. 7(a-z). Continued.

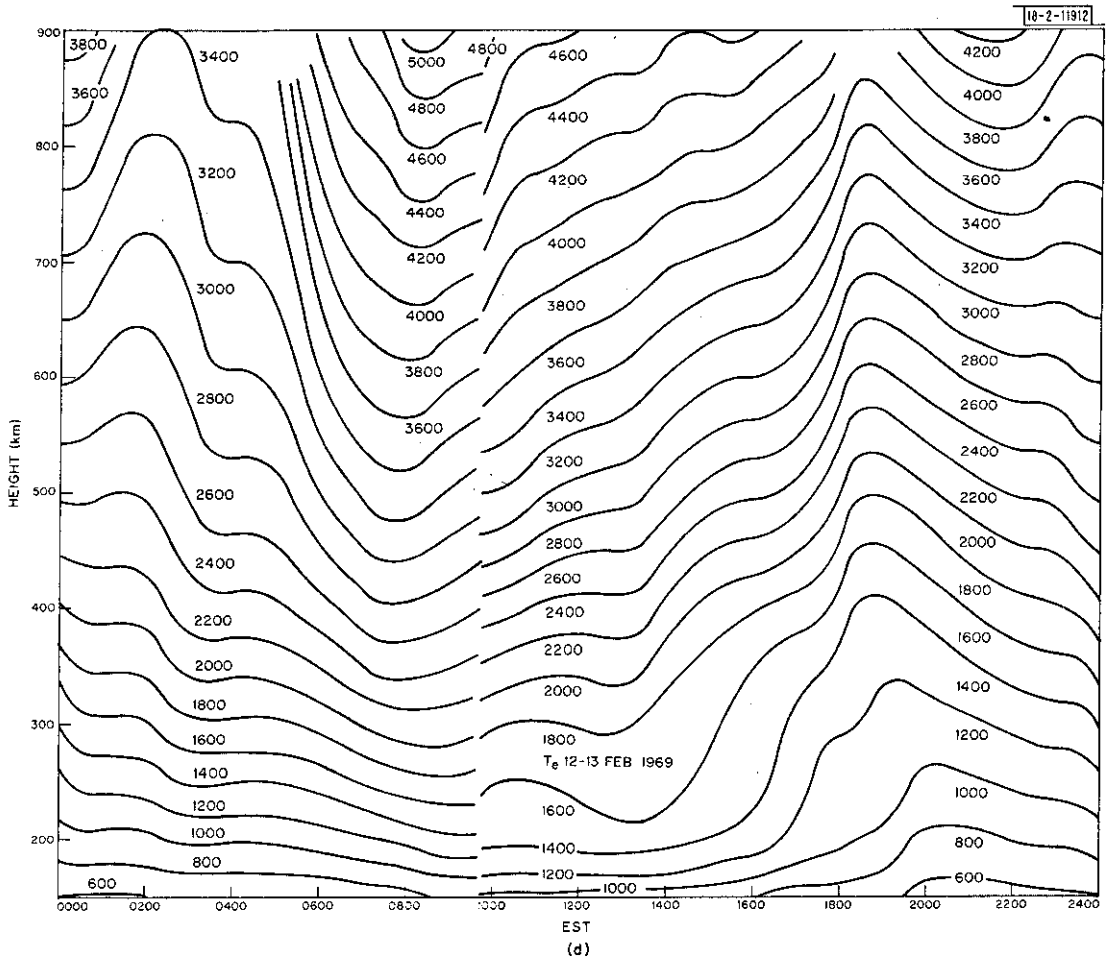

Fig.7(a-z). Continued.

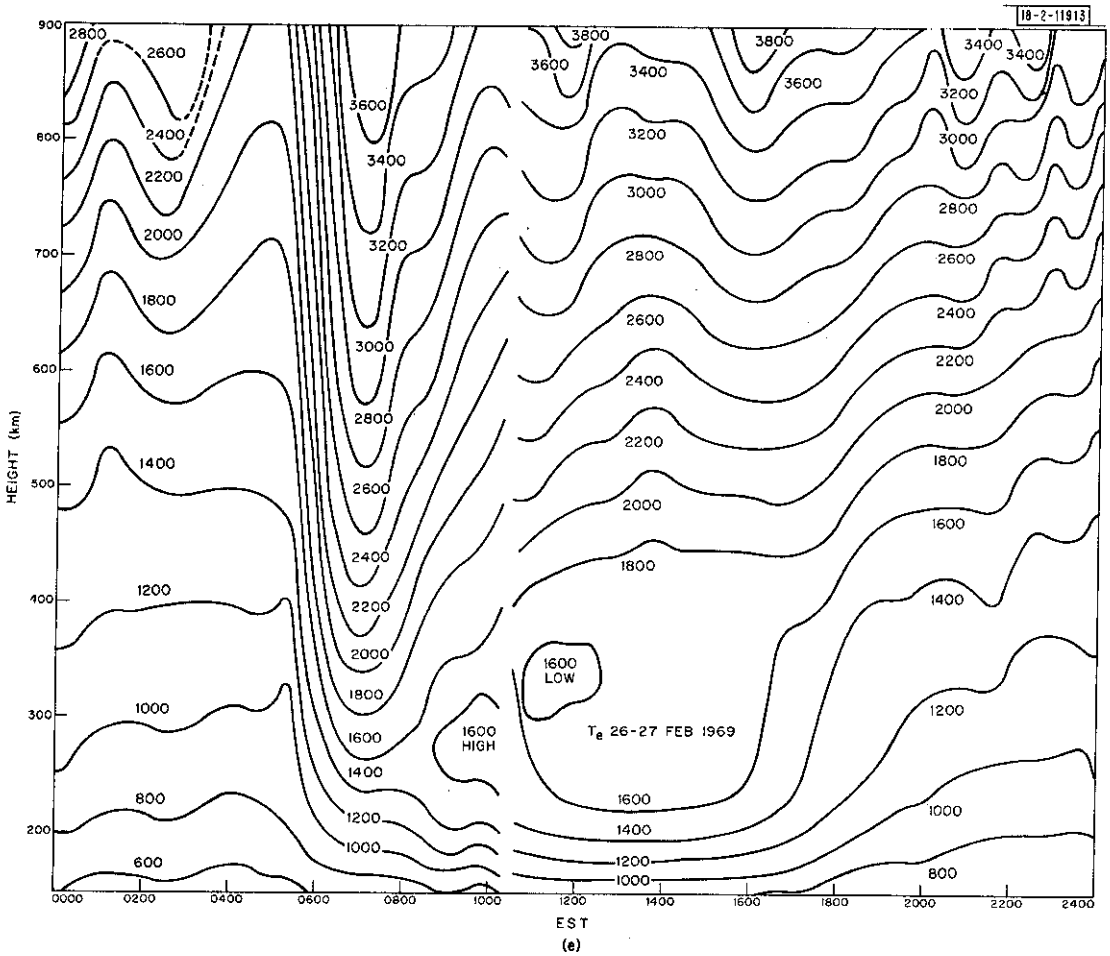

Fig. 7(a-z). Continued.

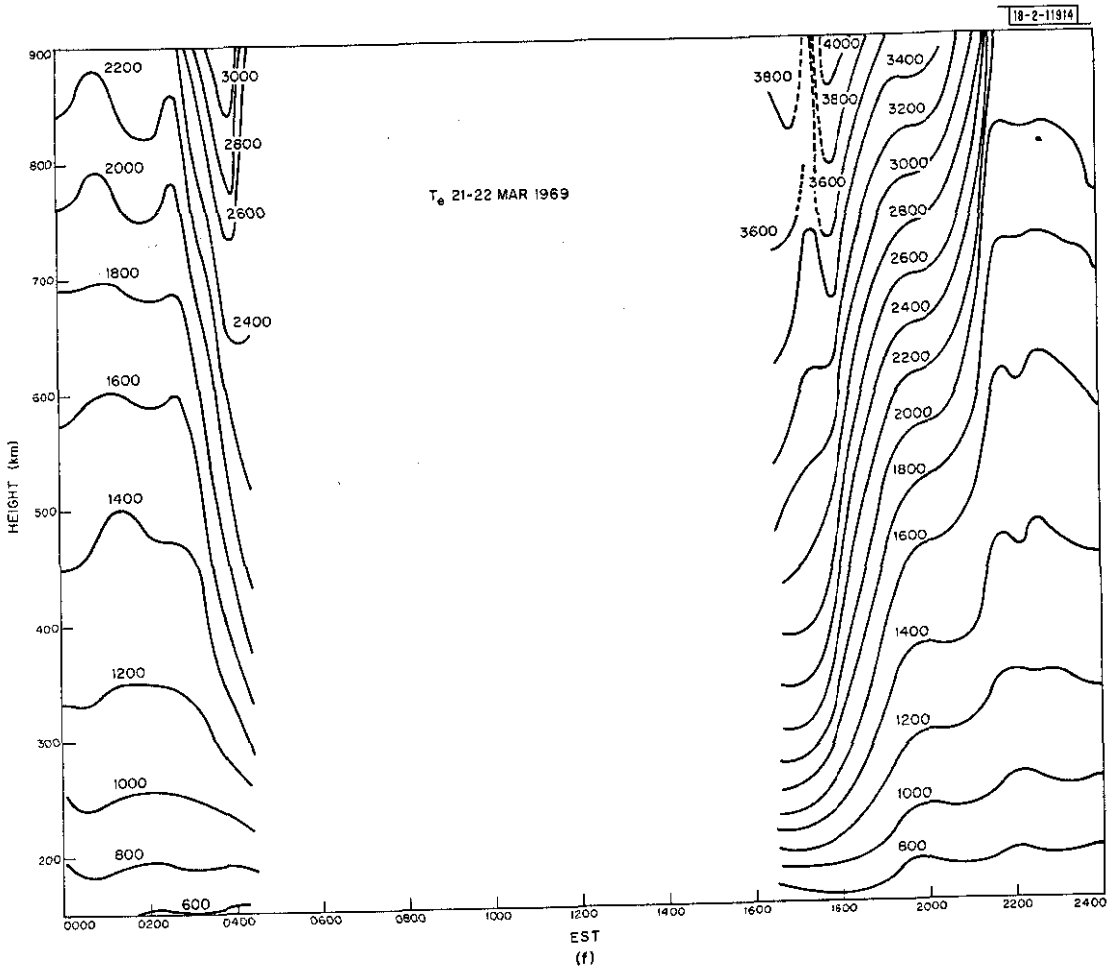

Fig. 7(a-z). Continued.

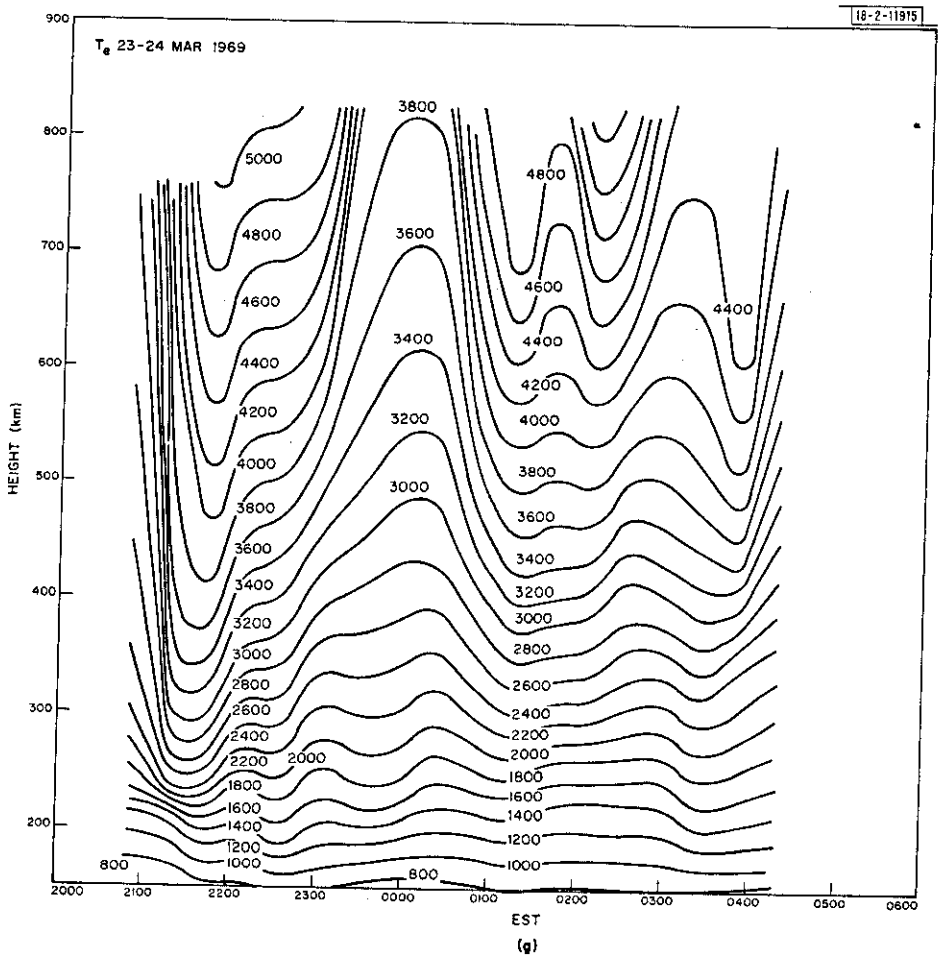

Fig. 7(a-z). Continued.

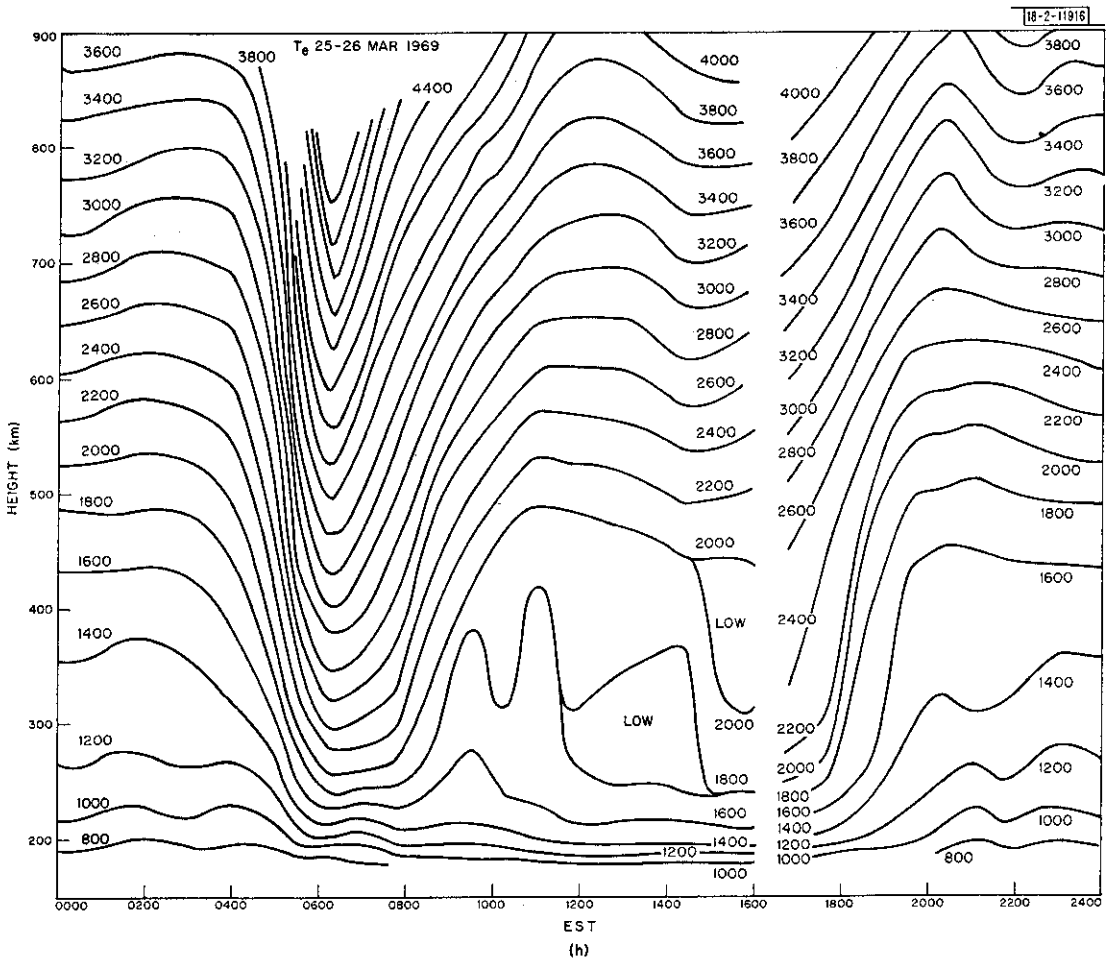

Fig.7(a-z). Continued.

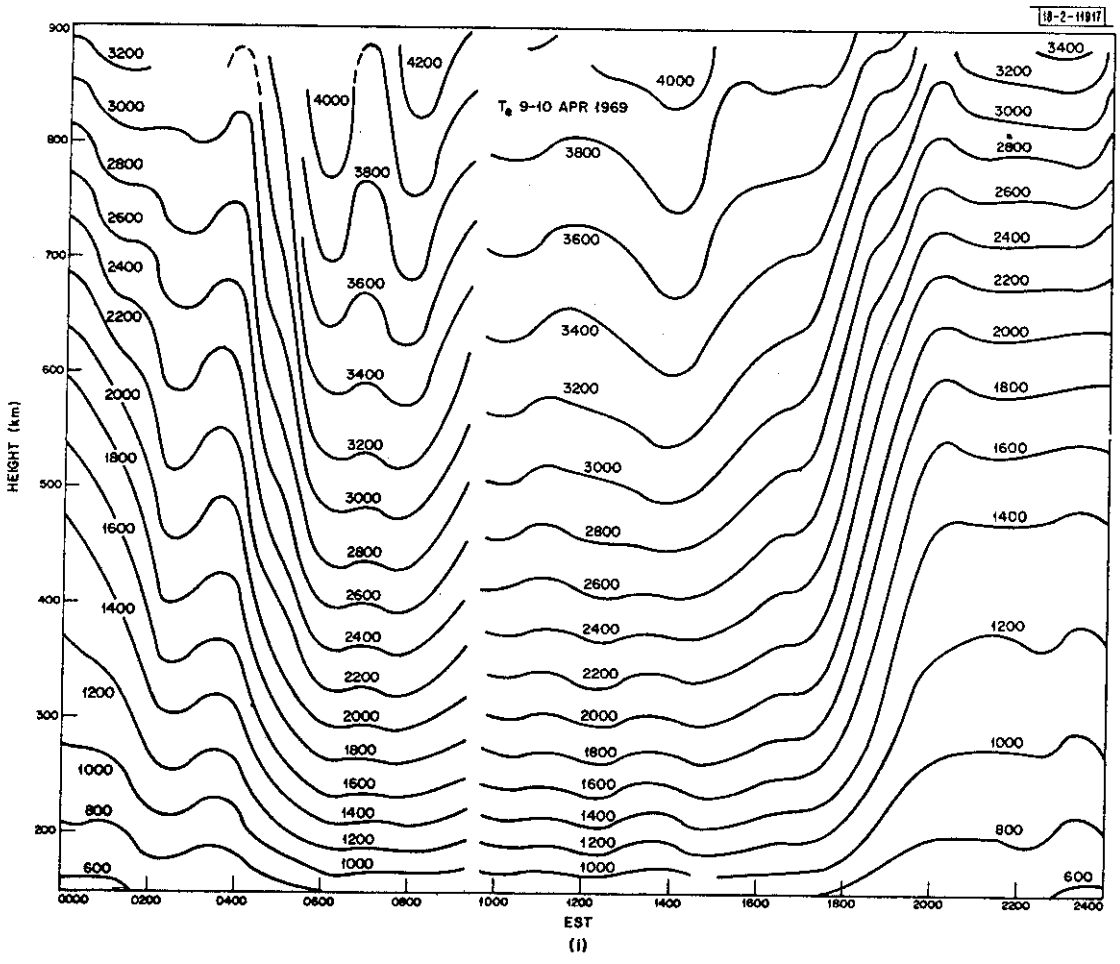

Fig. 7(a-z). Continued.

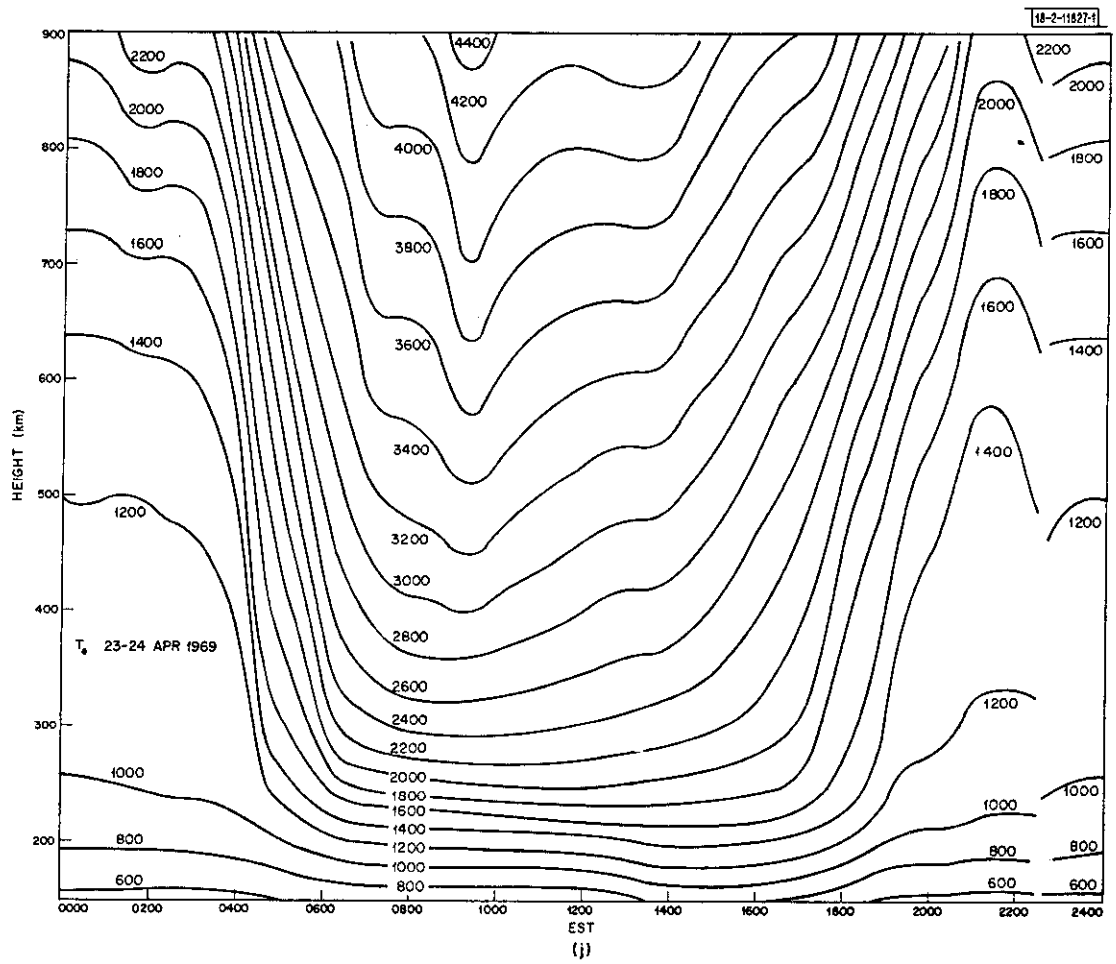

Fig. 7(a-z). Continued.

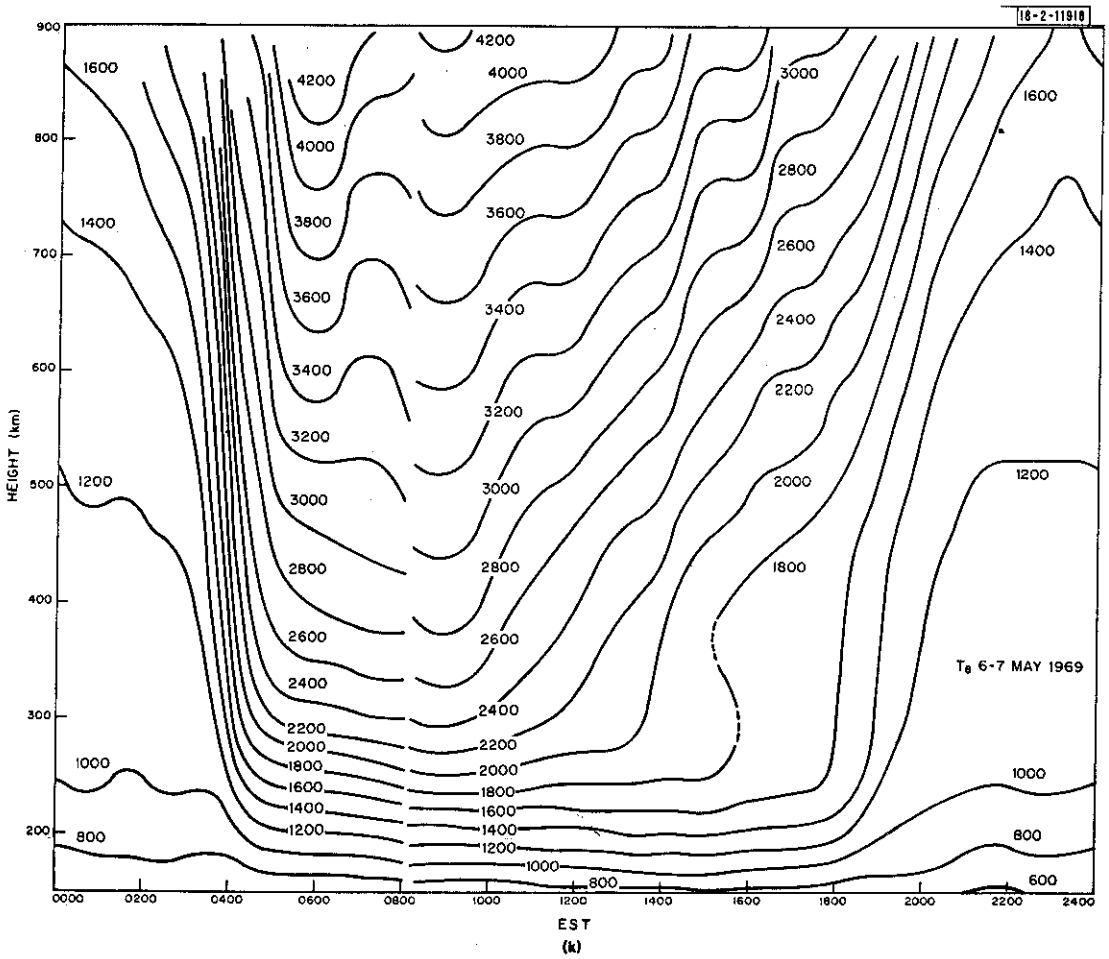

Fig. 7(a-z). Continued.

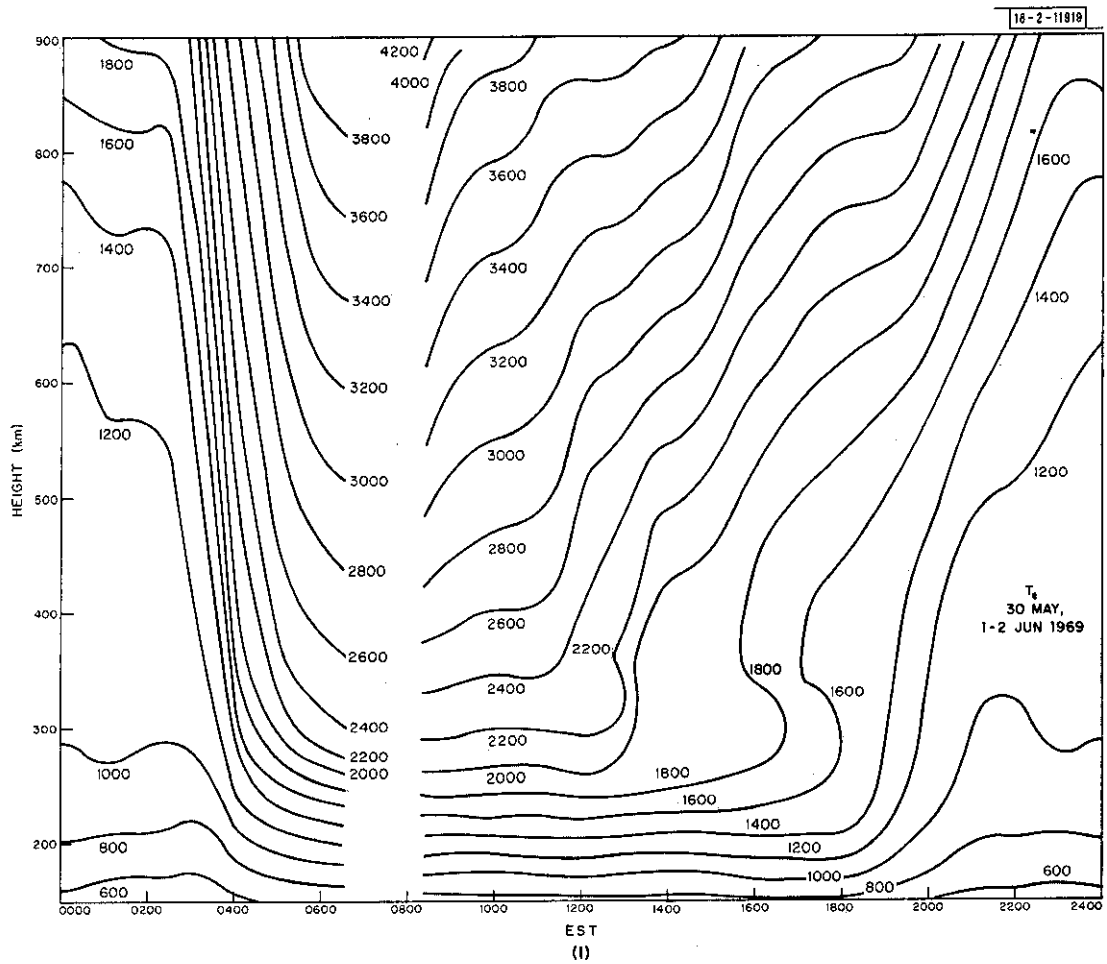

Fig. 7(a-z). Continued.

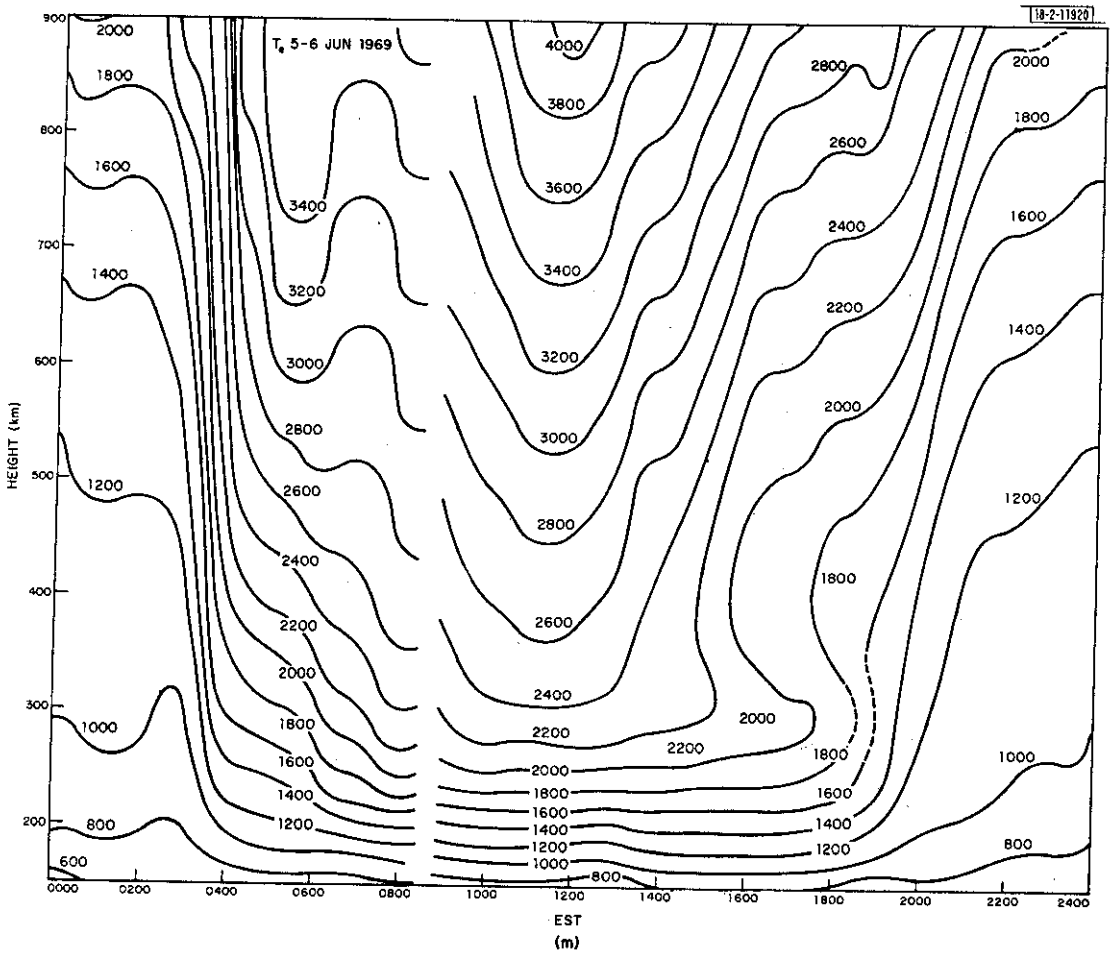

Fig. 7(a-z). Continued.

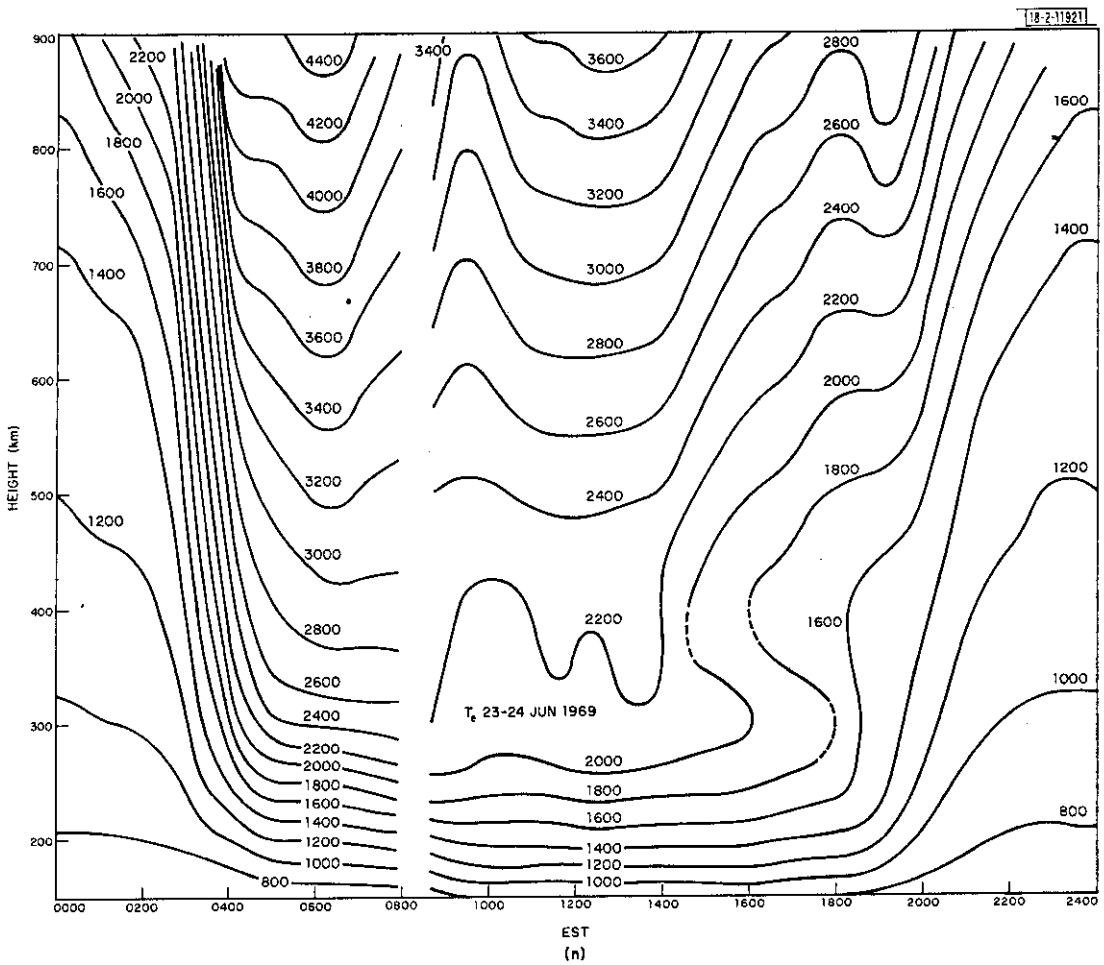

Fig. 7(a-z). Continued.

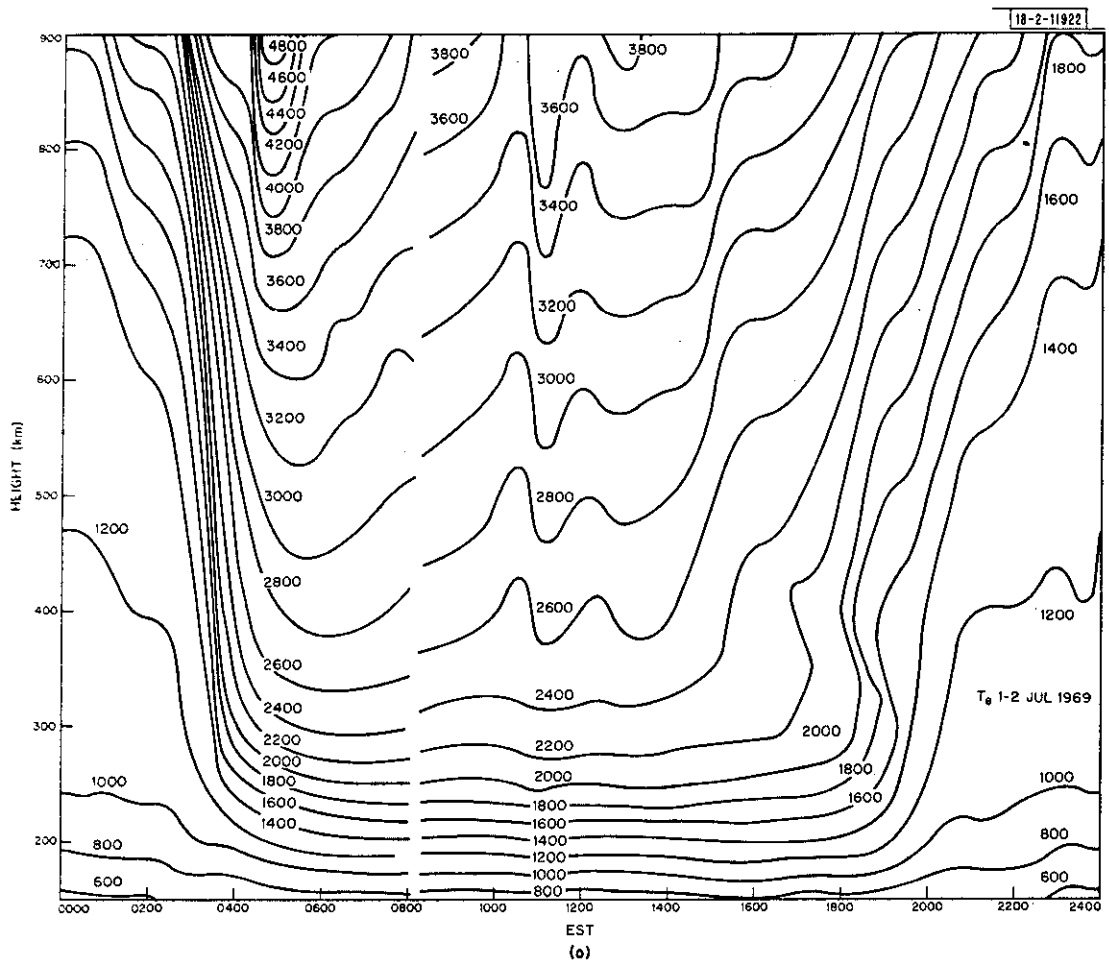

Fig.7(a-z). Continued.

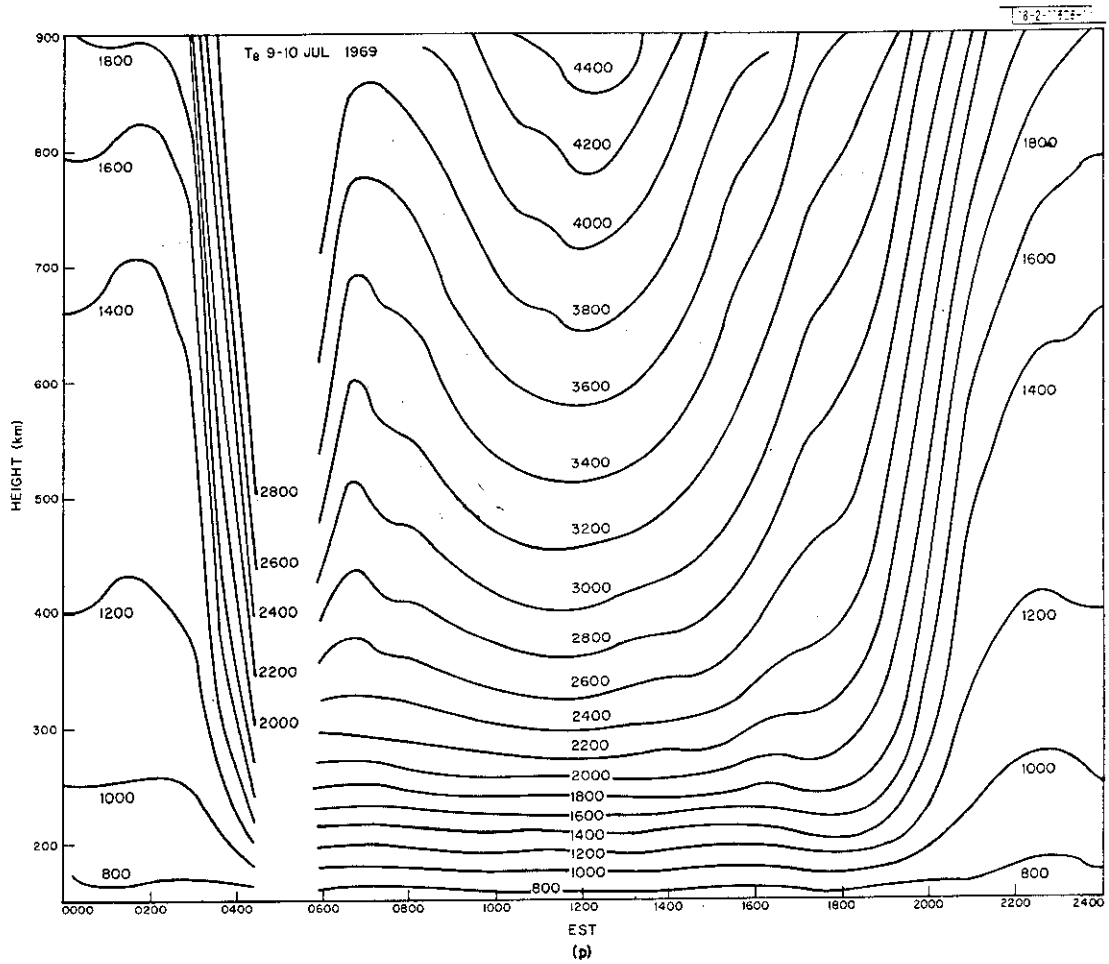

Fig. 7(a-z). Continued.

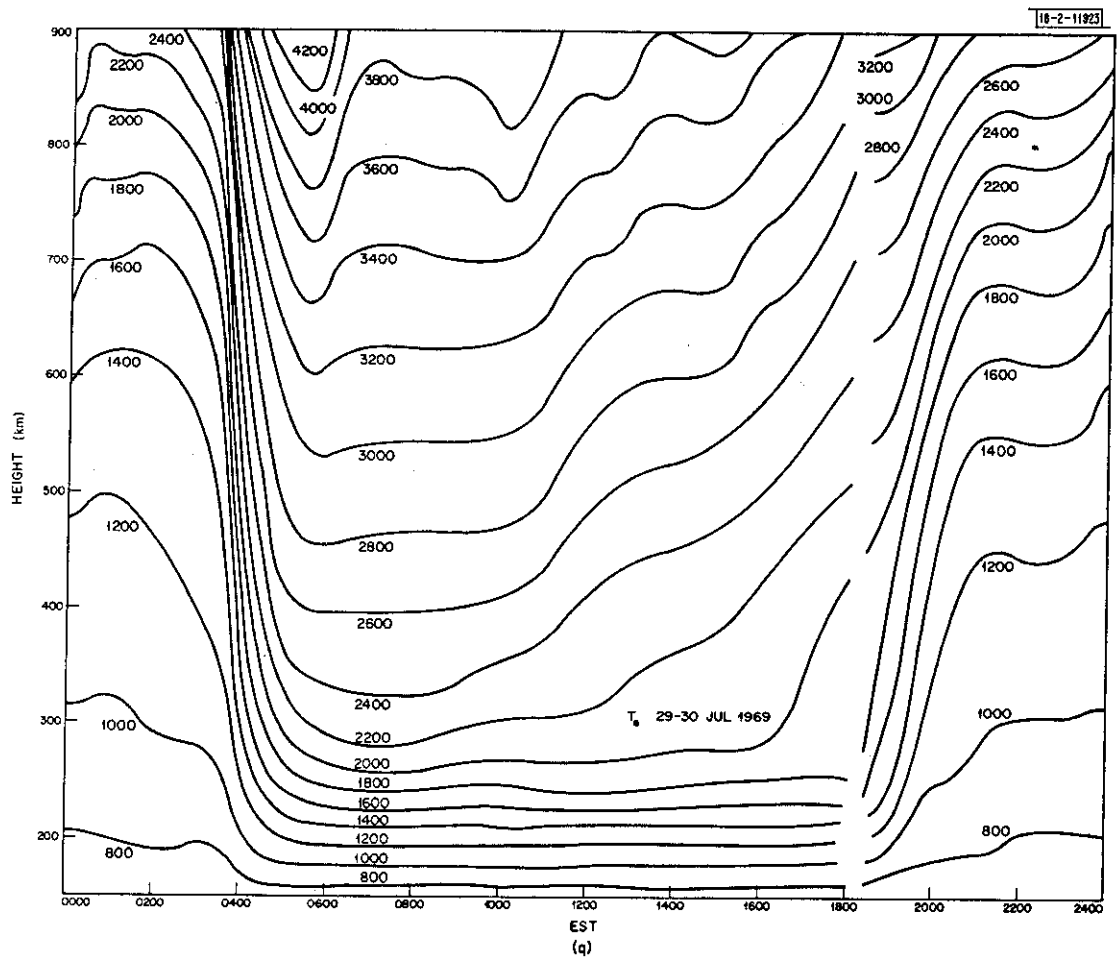

Fig. 7(a-z). Continued.

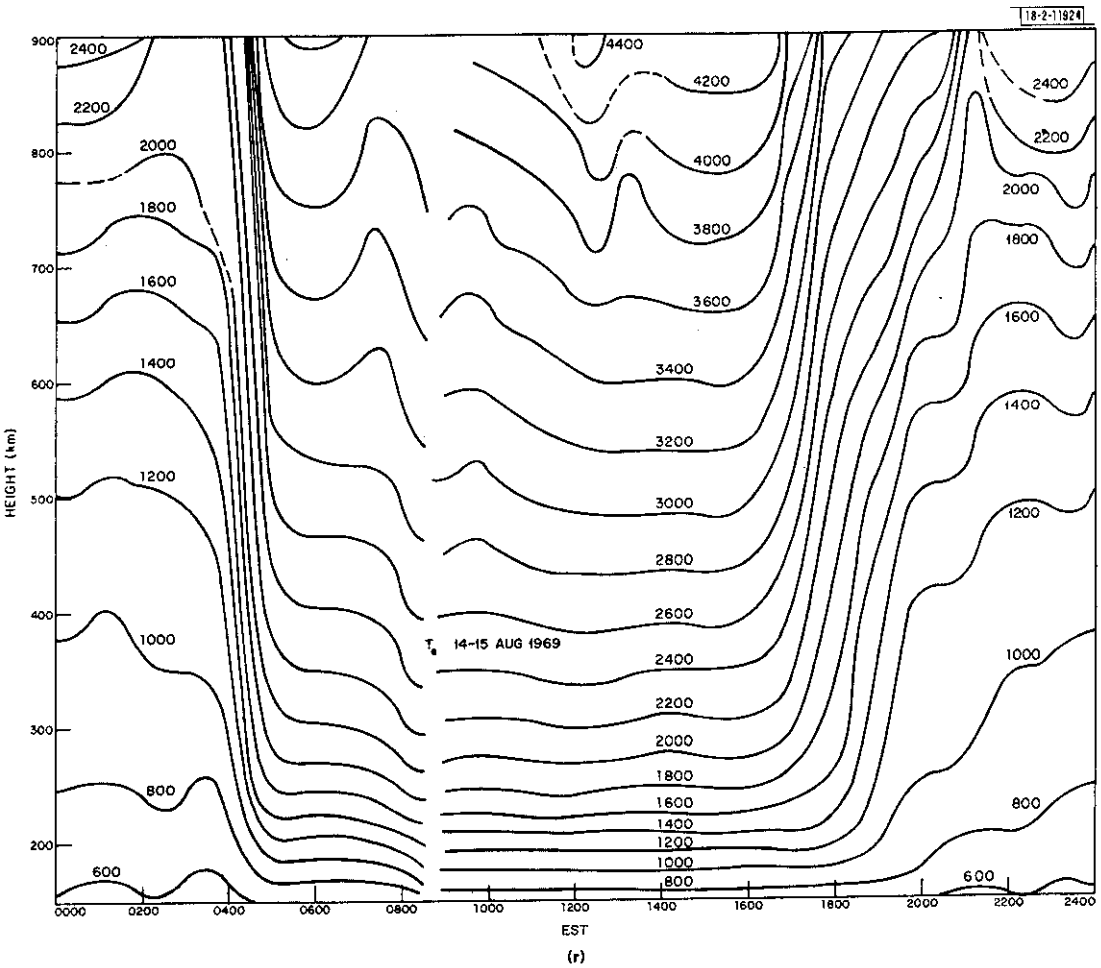

Fig.7(a-z). Continued.

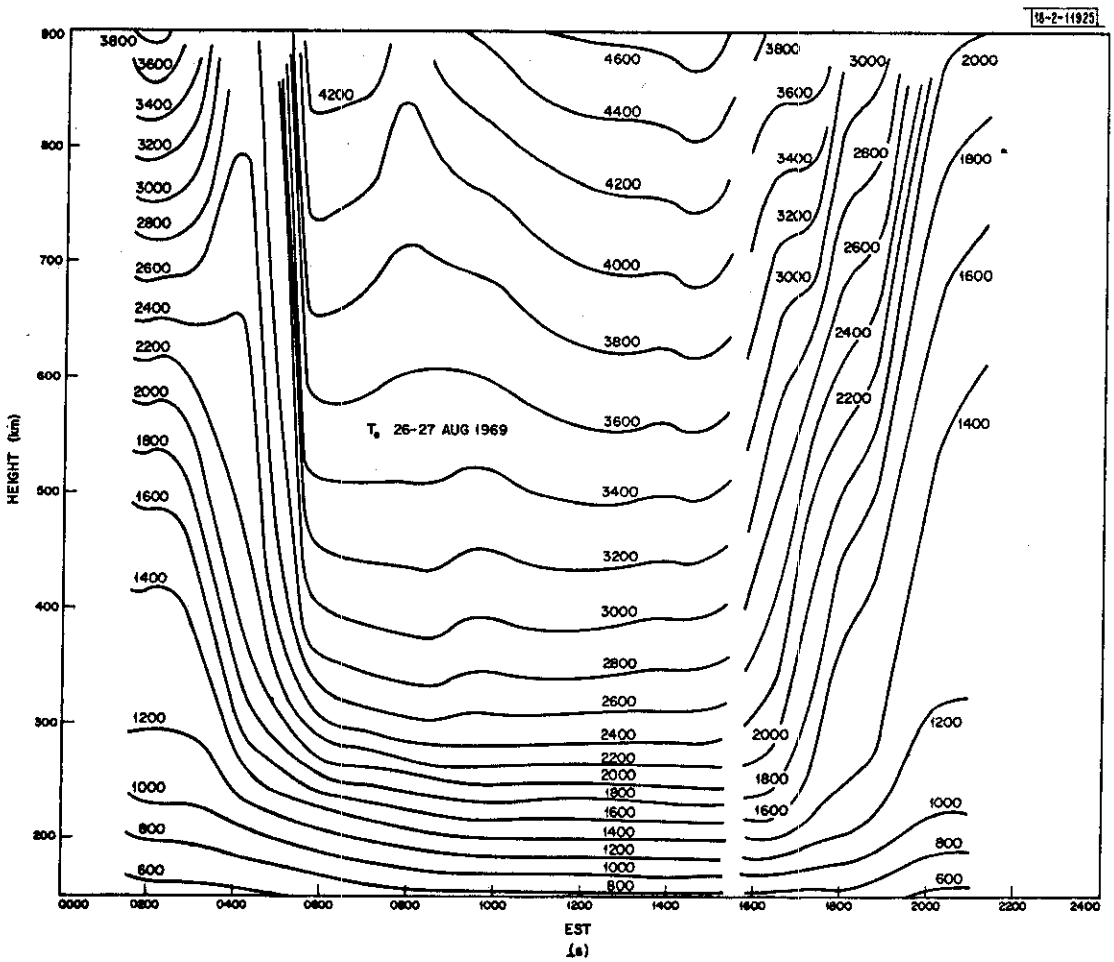

Fig.7(a-z). Continued.

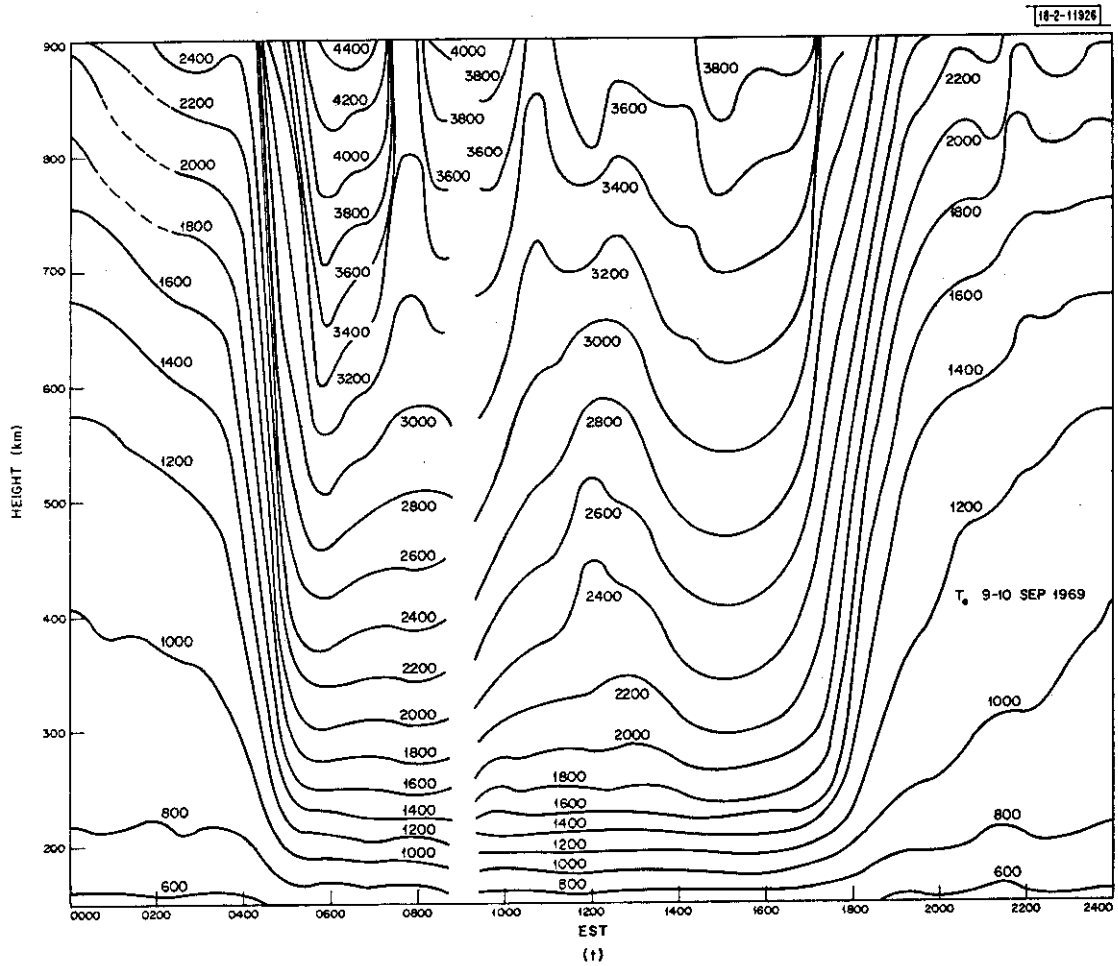

Fig.7(a-z). Continued.

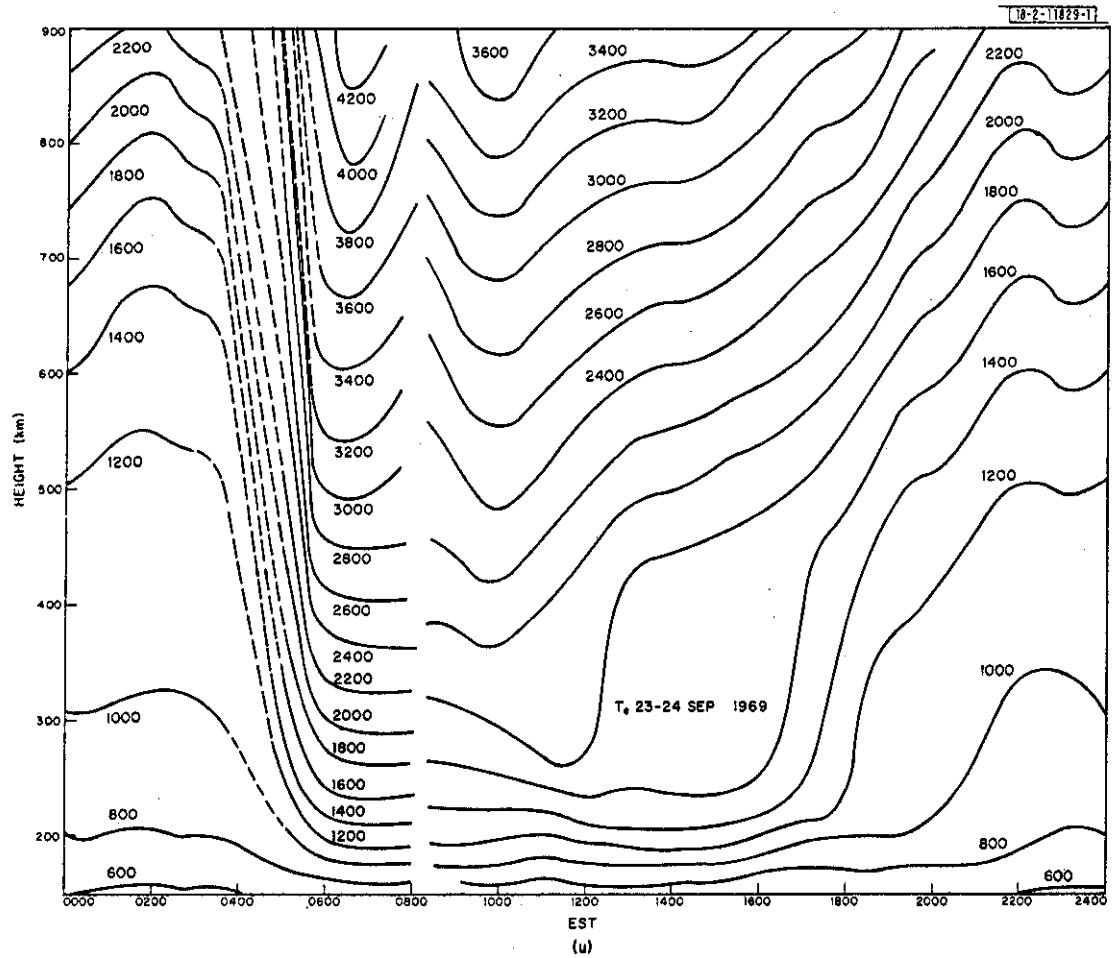

Fig. 7(a-z). Continued.

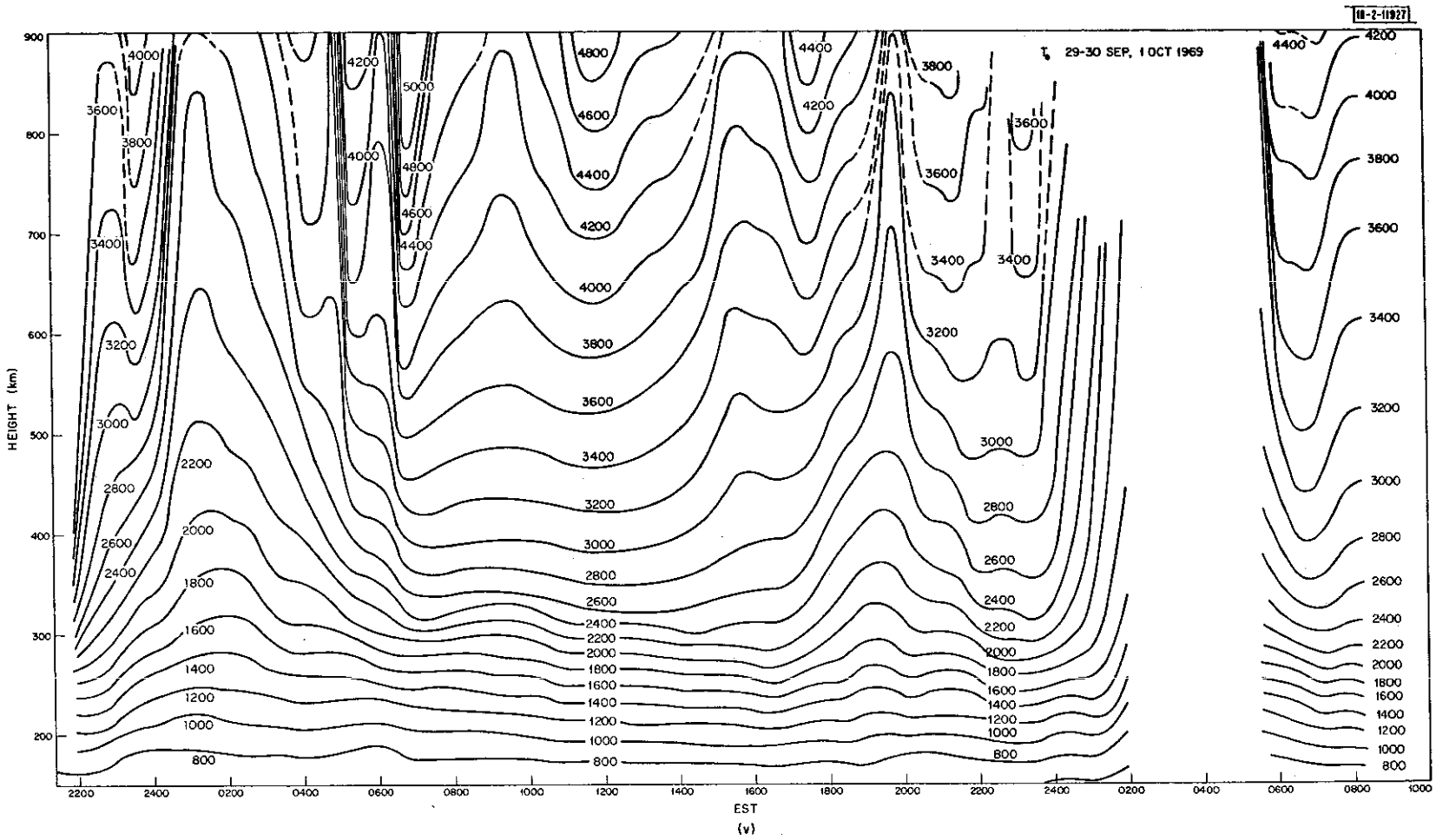

Fig.7(a-z). Continued.

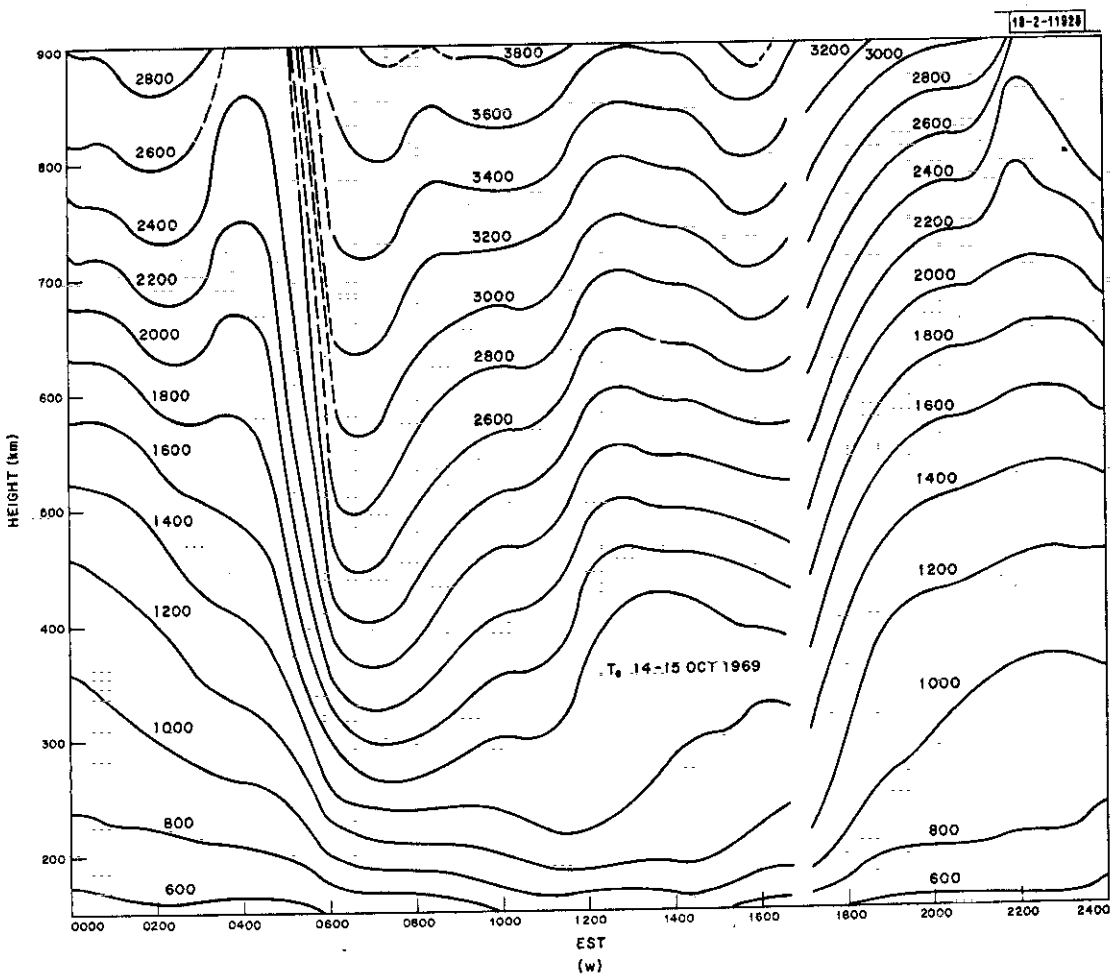

Fig. 7(a-z). Continued.

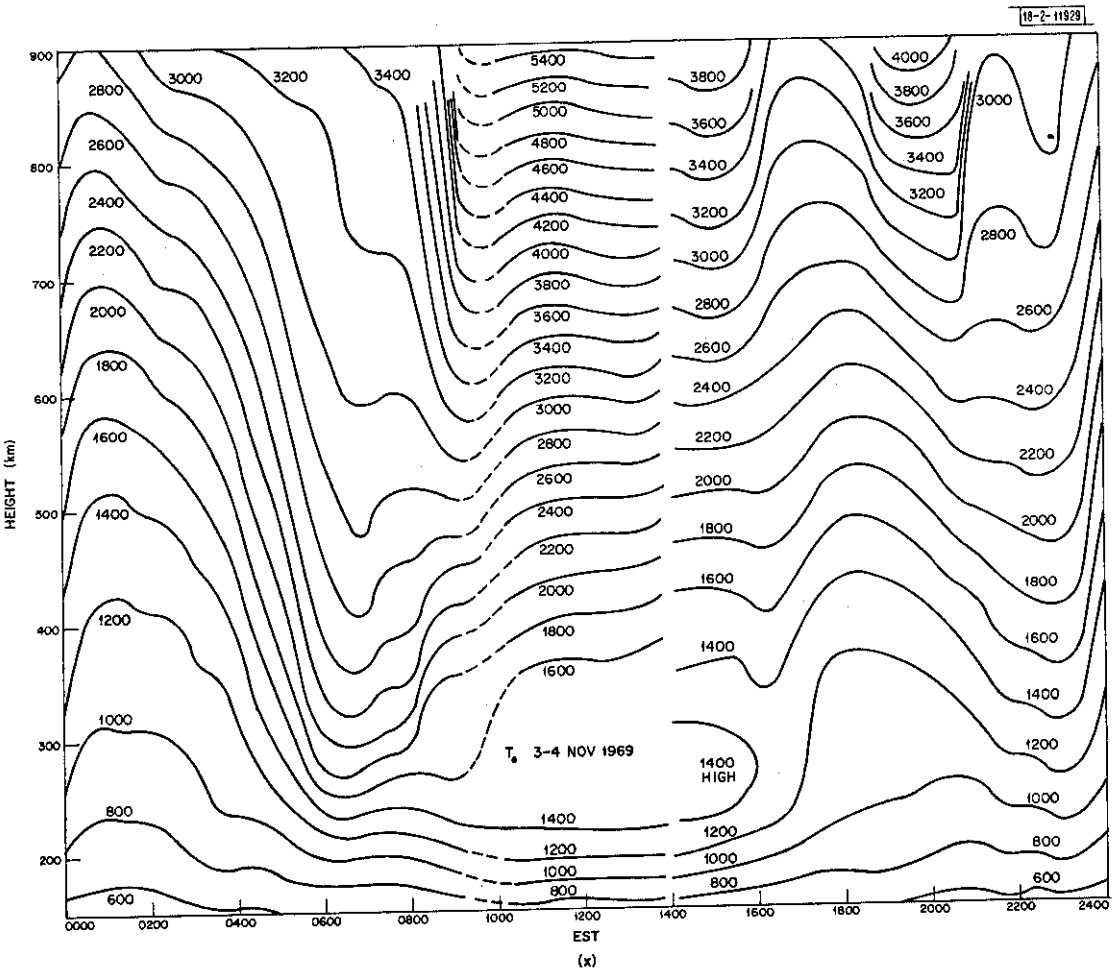

Fig. 7(a-z). Continued.

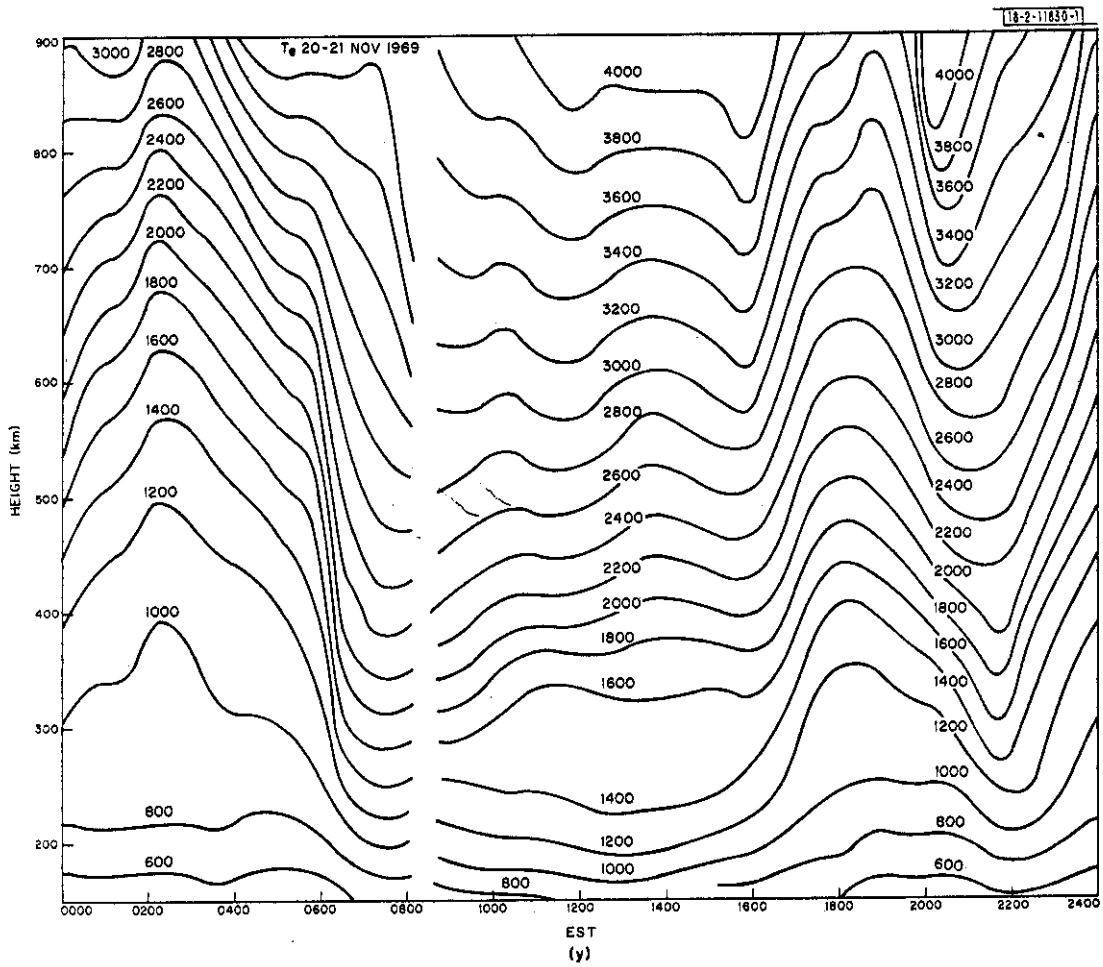

Fig.7(a-z). Continued.

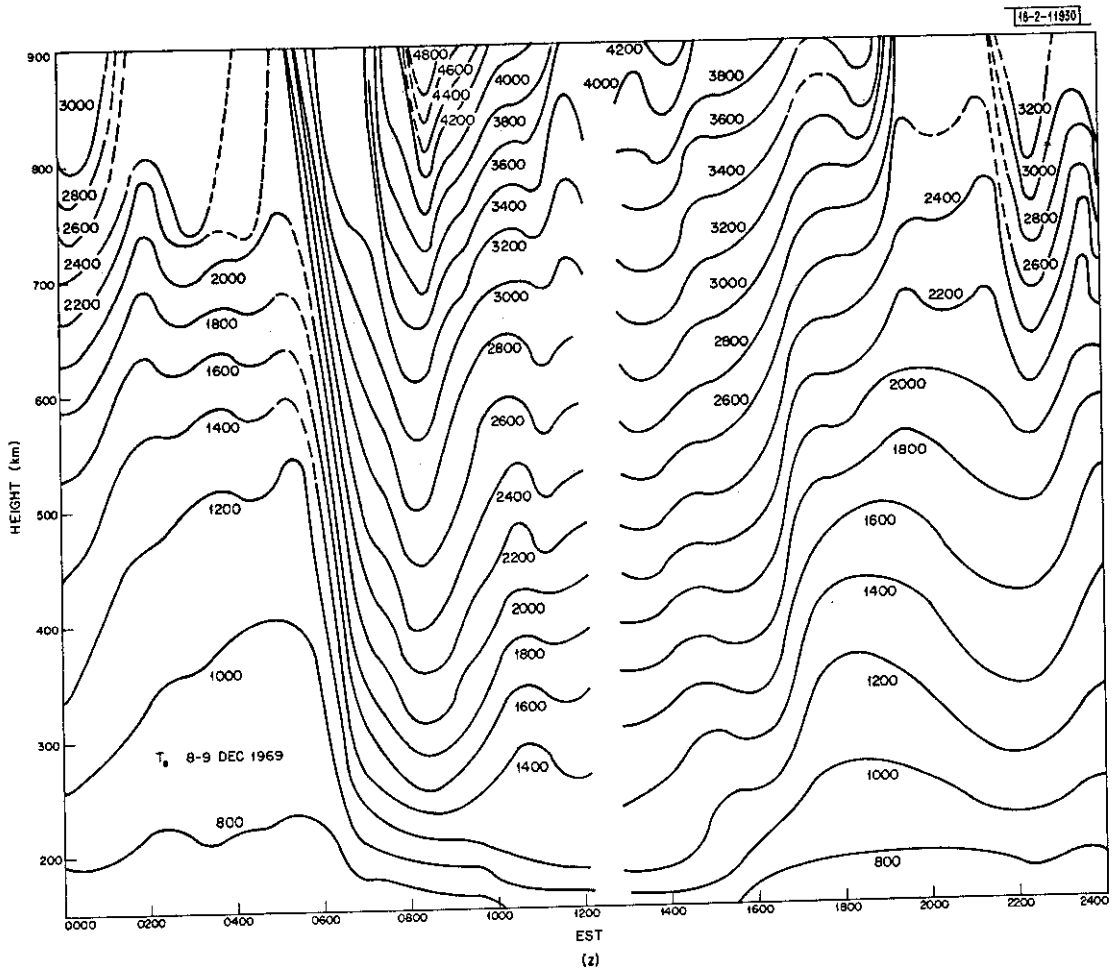

Fig.7(a-z). Continued.

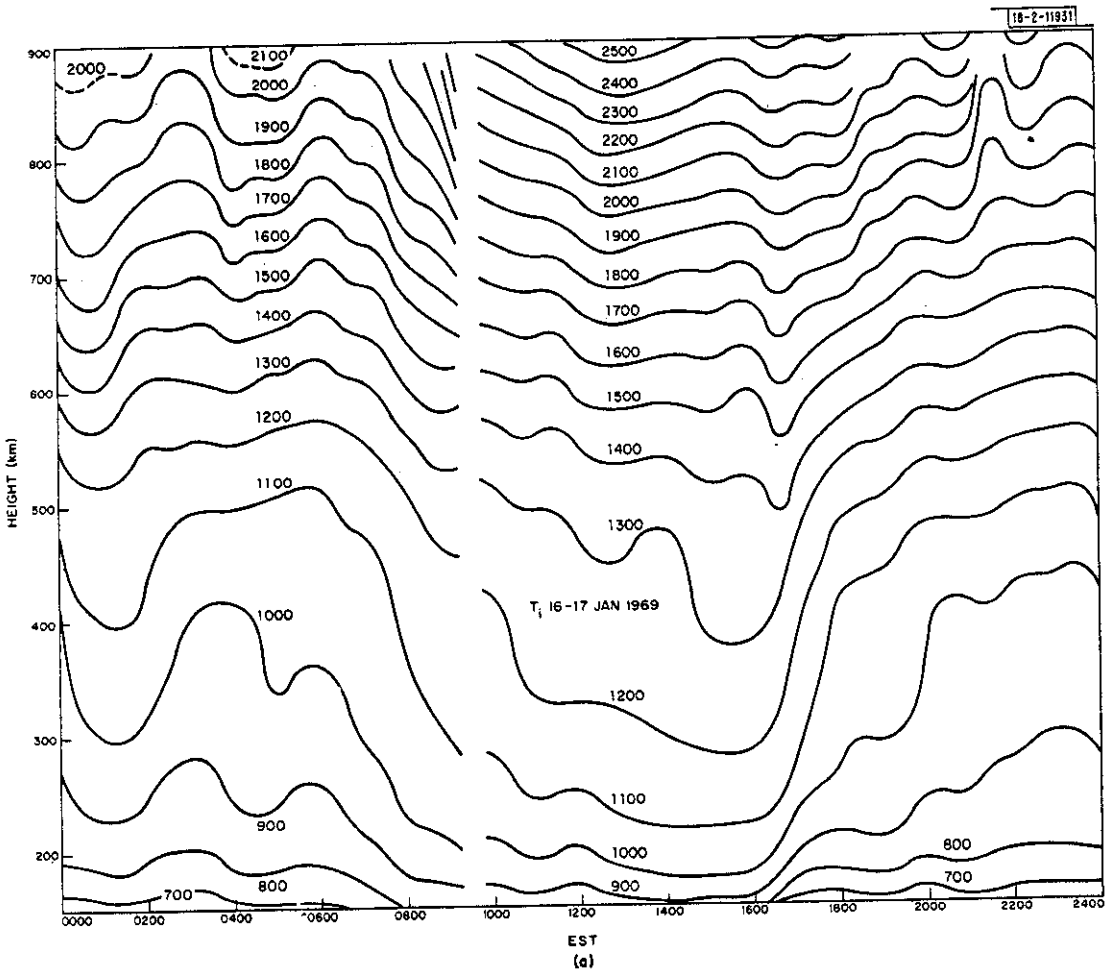

Fig. 8(a-z). Contours of ion temperature T_i observed on days listed in Table II.

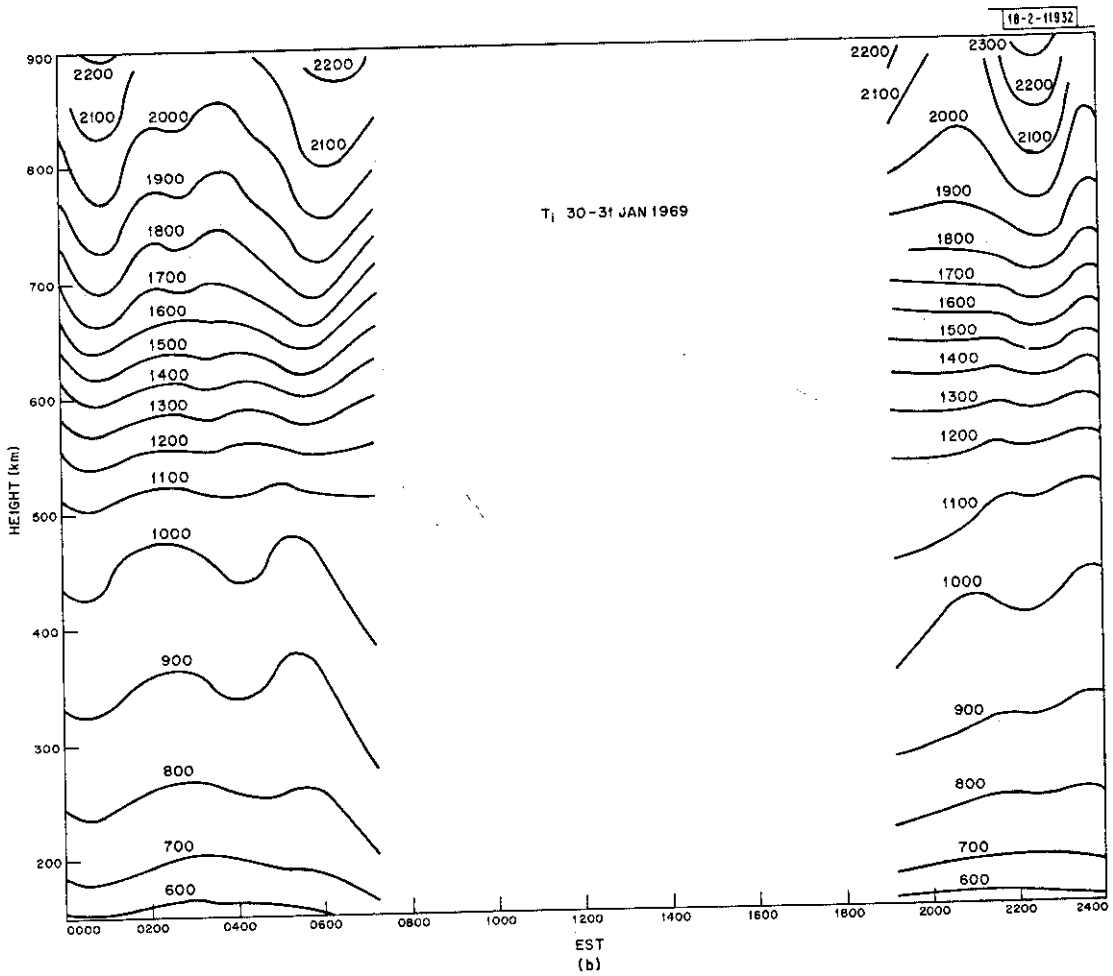

Fig. 8(a-z). Continued.

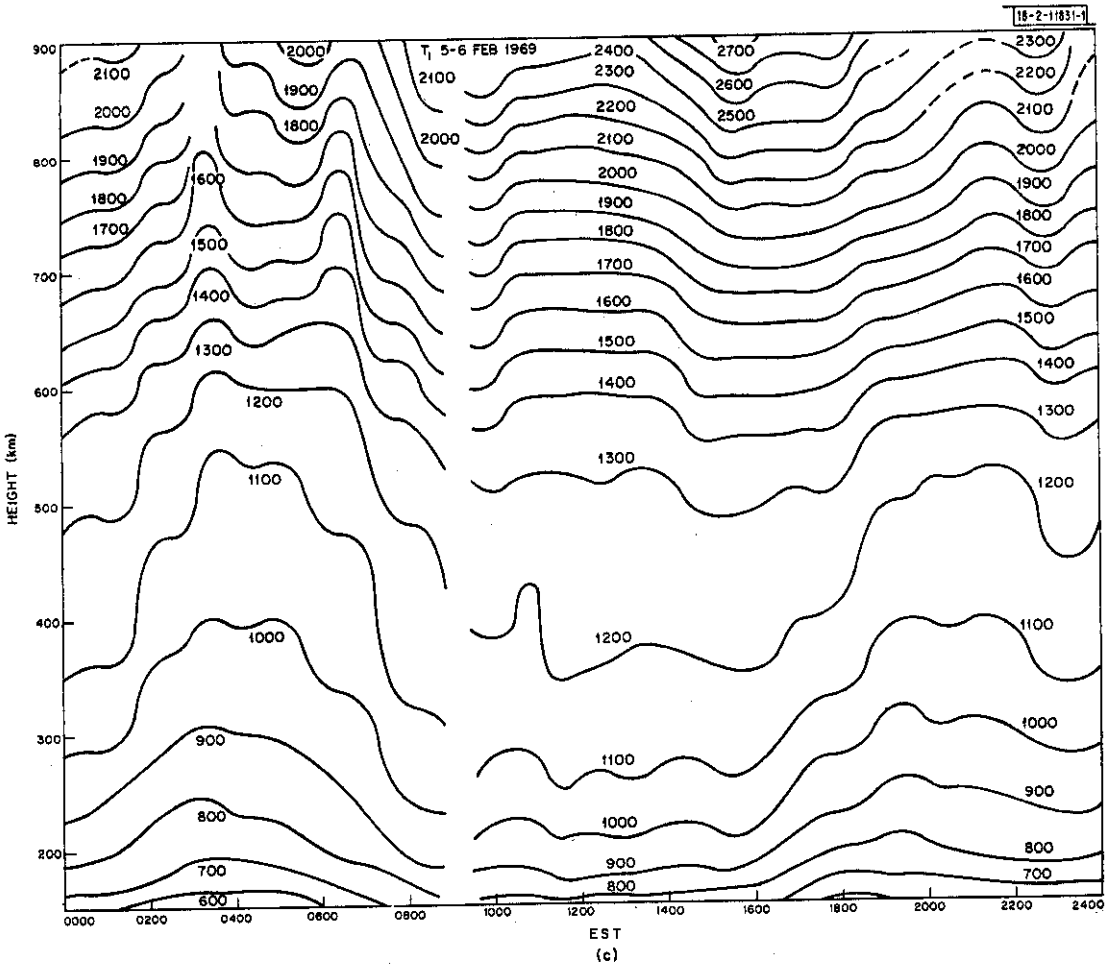

Fig. 8(a-z). Continued.

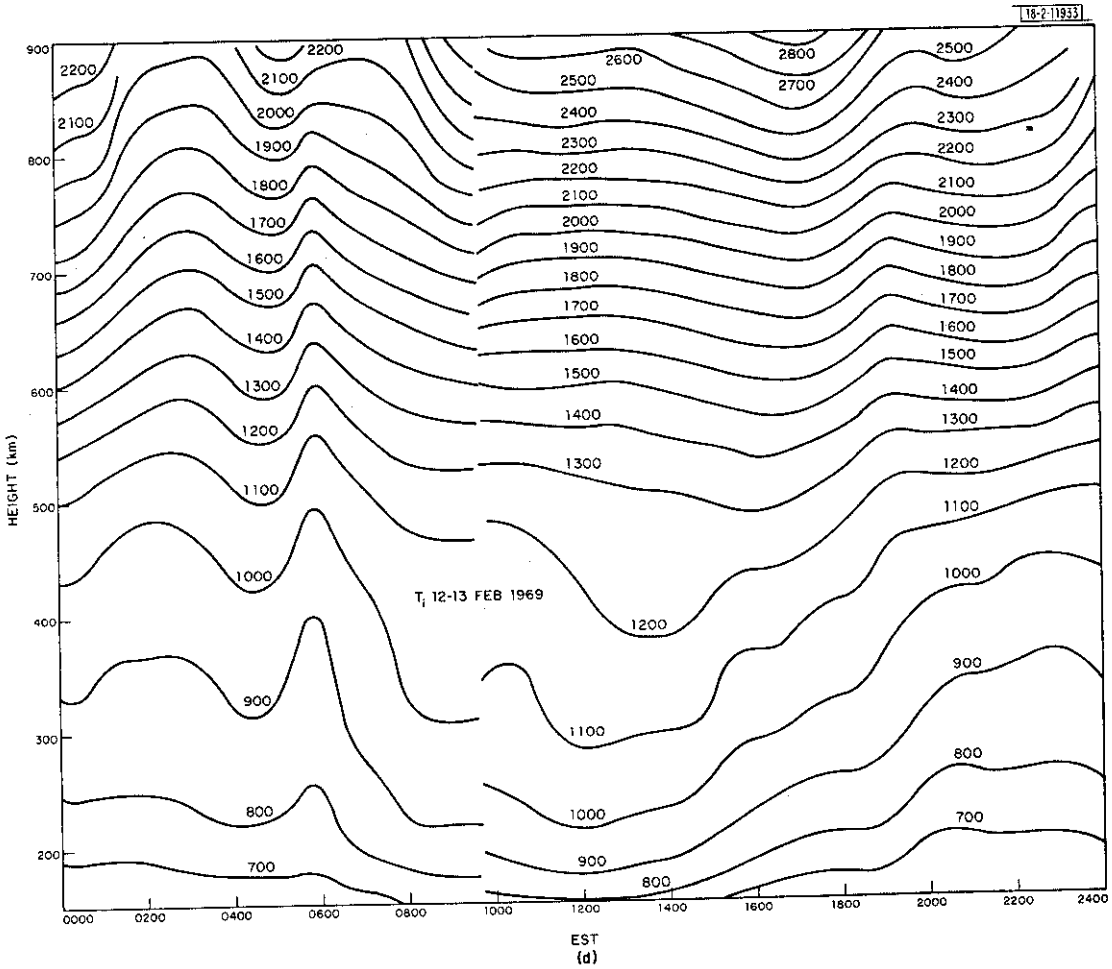

Fig. 8(a-z). Continued.

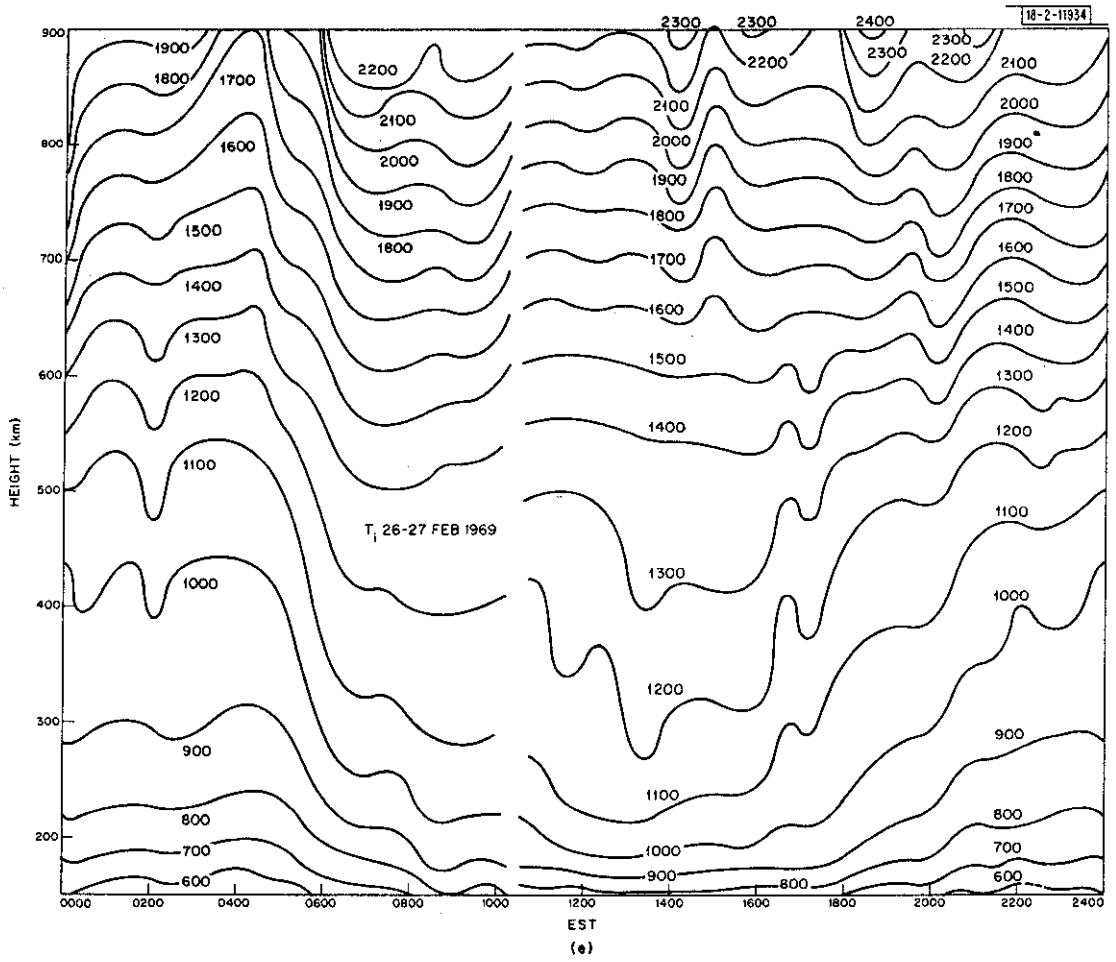

Fig. 8(a-z). Continued.

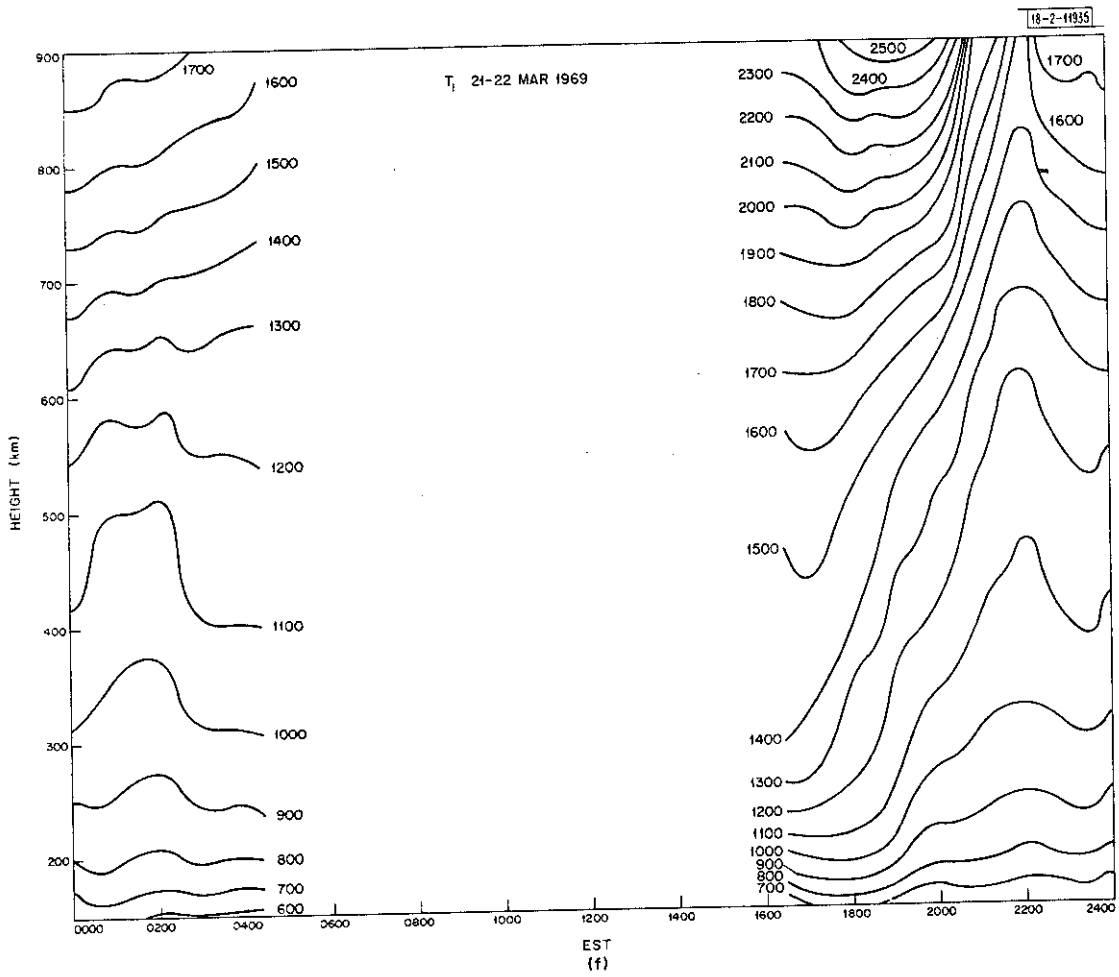

Fig. 8(a-z). Continued.

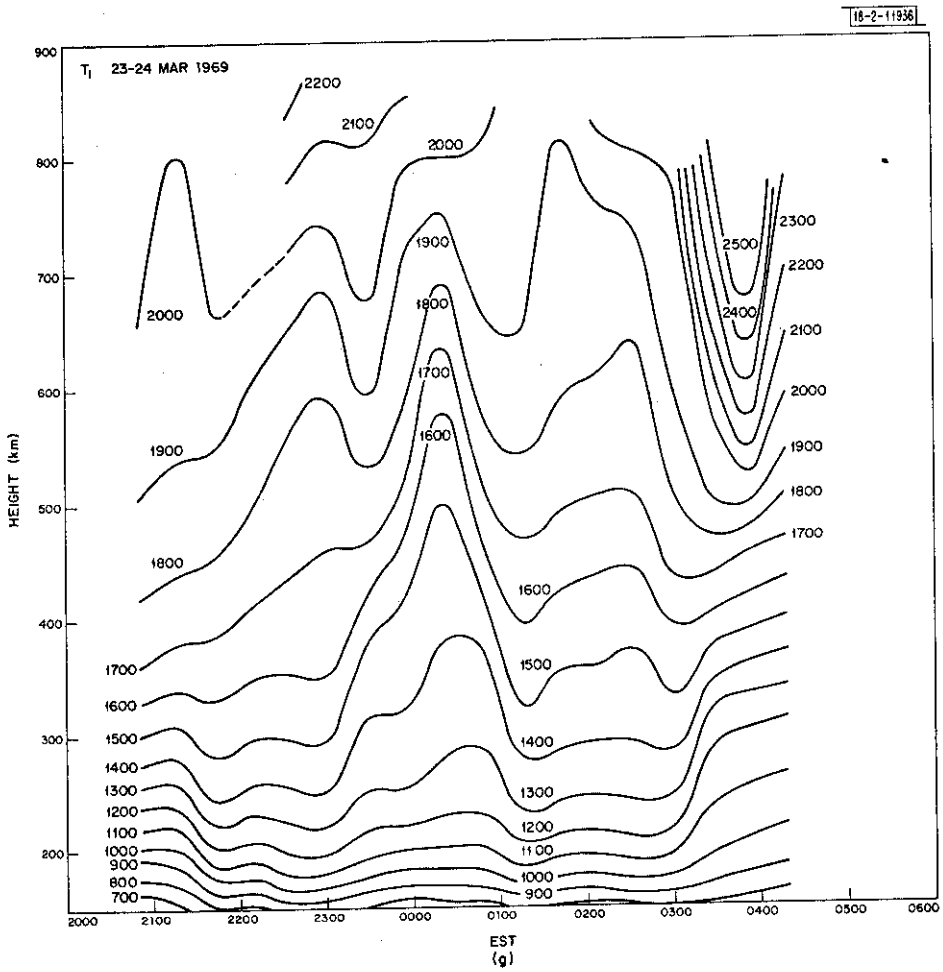

Fig. 8(a-z). Continued.

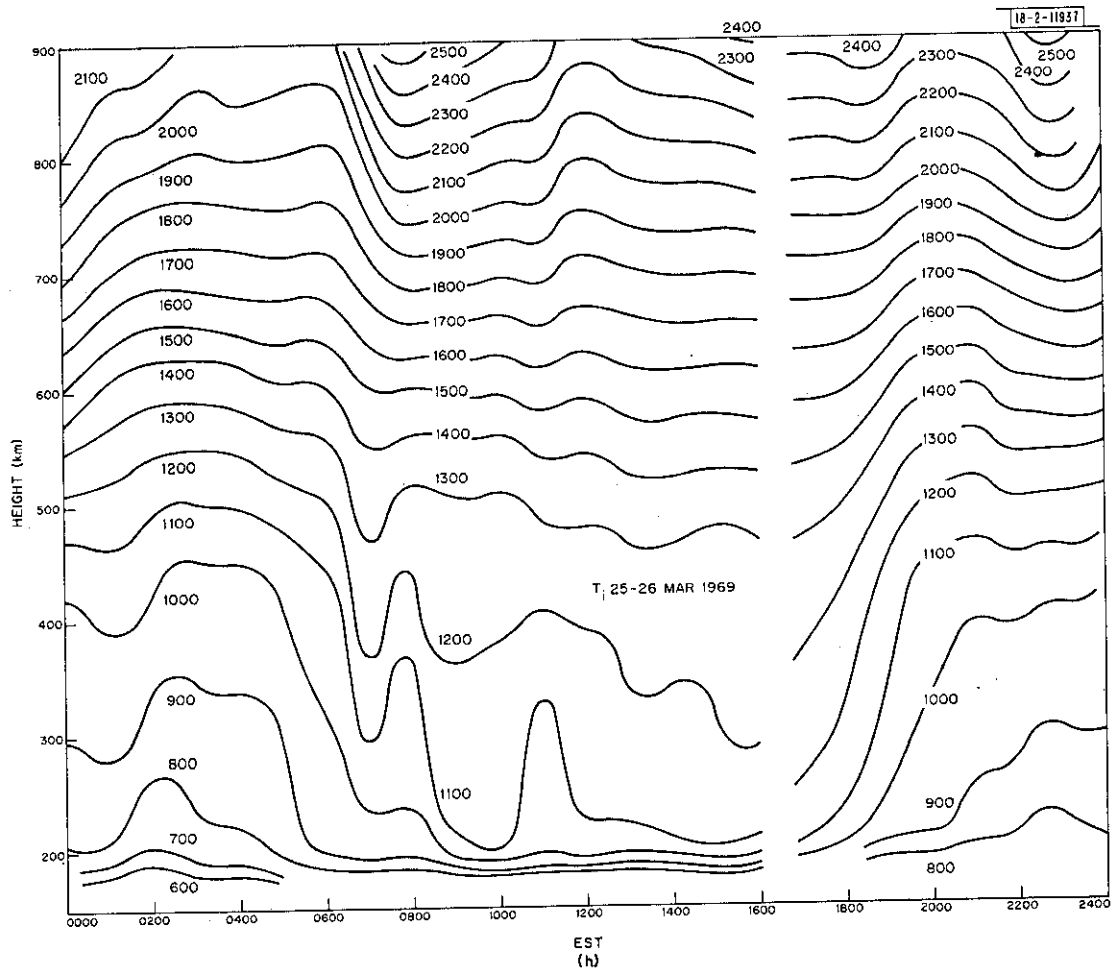

Fig. 8(a-z). Continued.

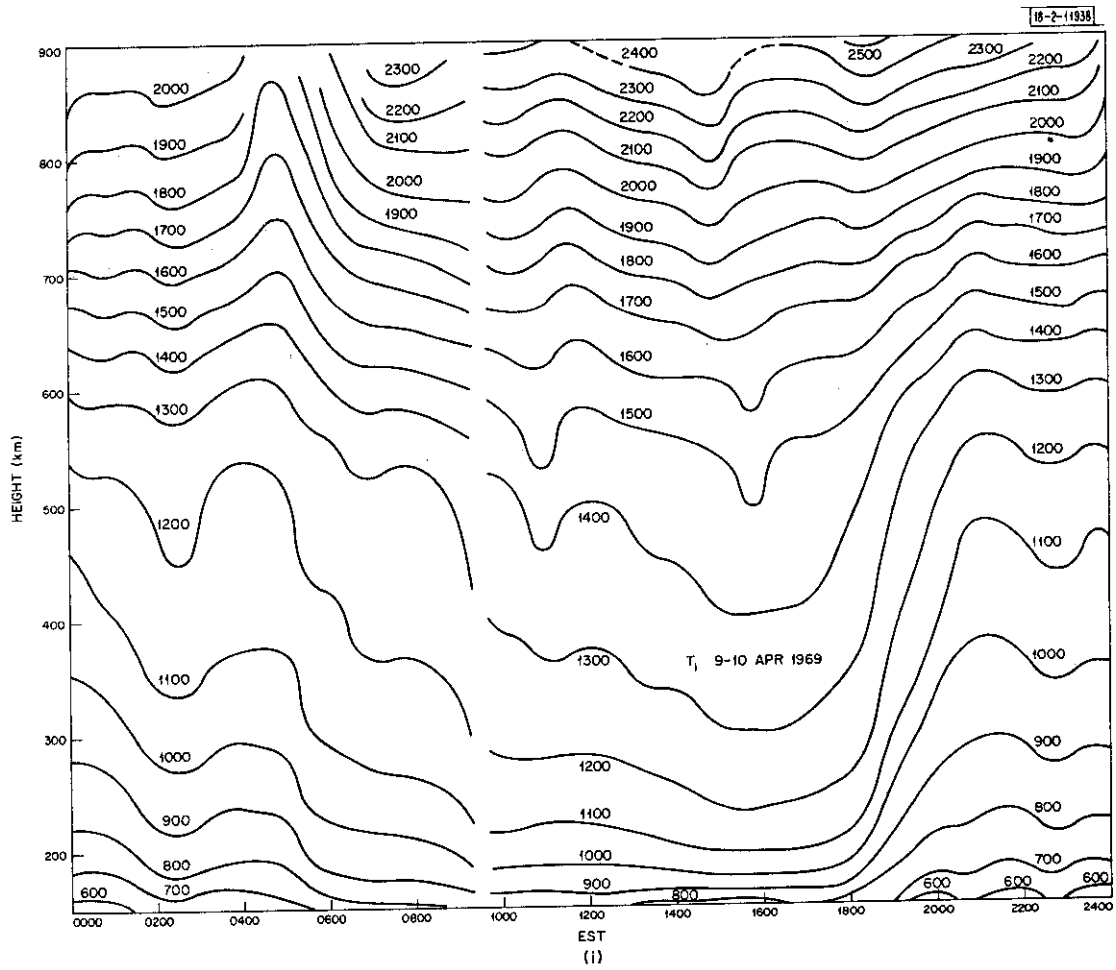

Fig. 8(a-z). Continued.

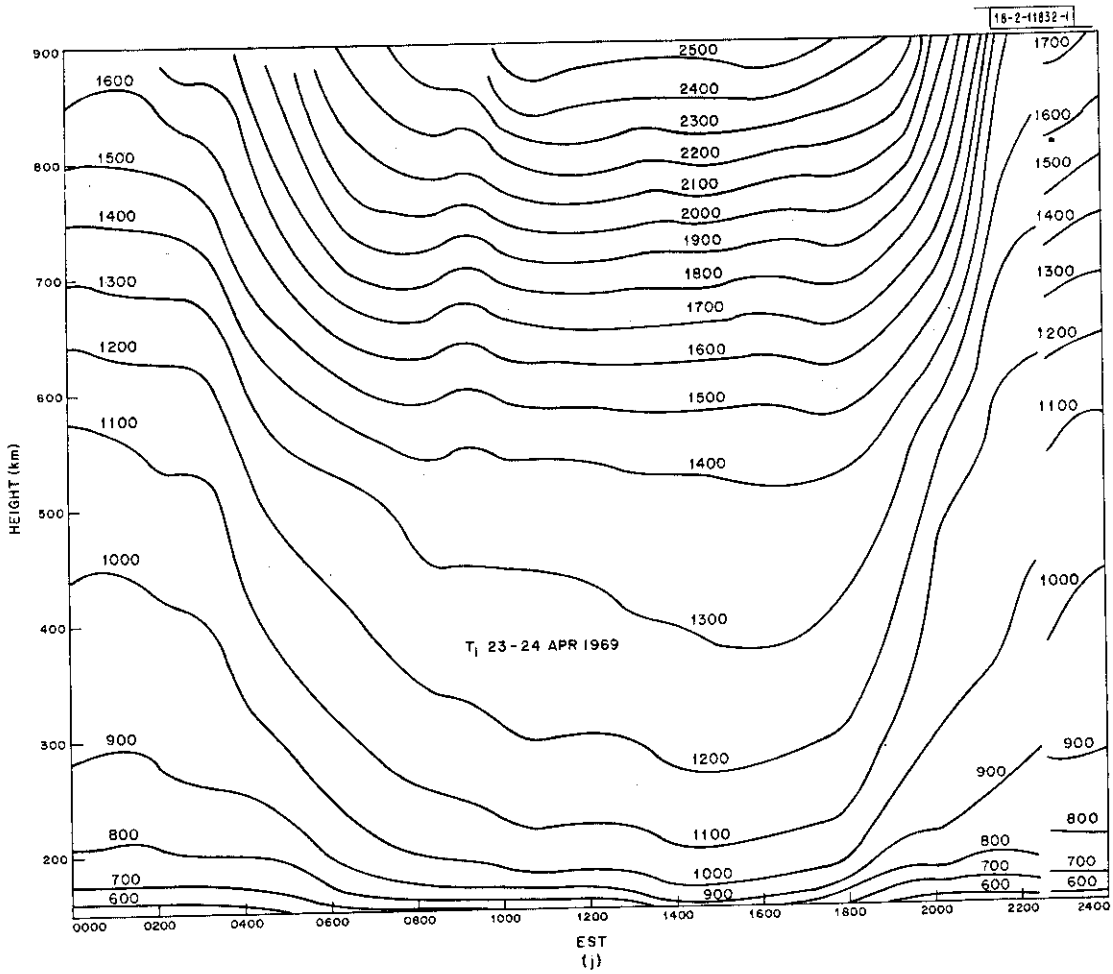

Fig. 8(a-z). Continued.

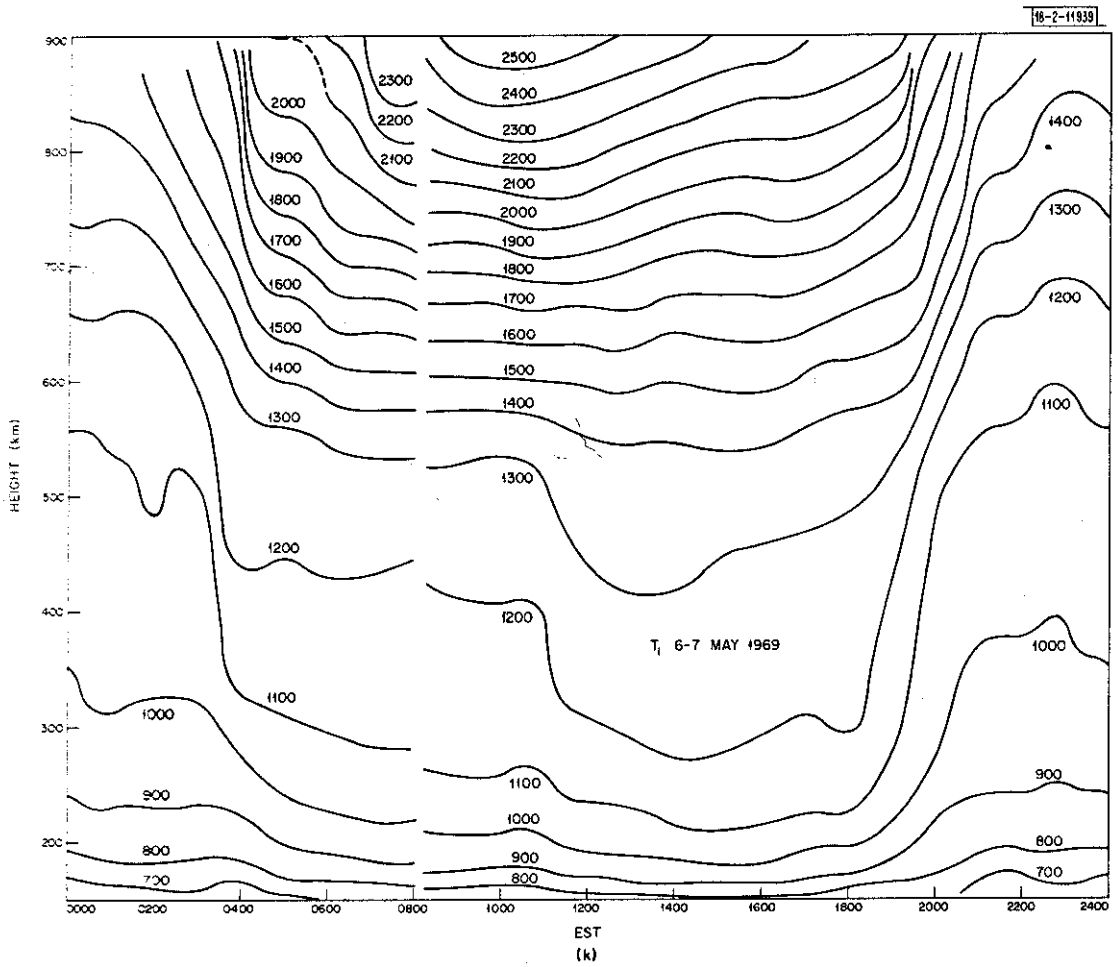

Fig. 8(a-z). Continued.

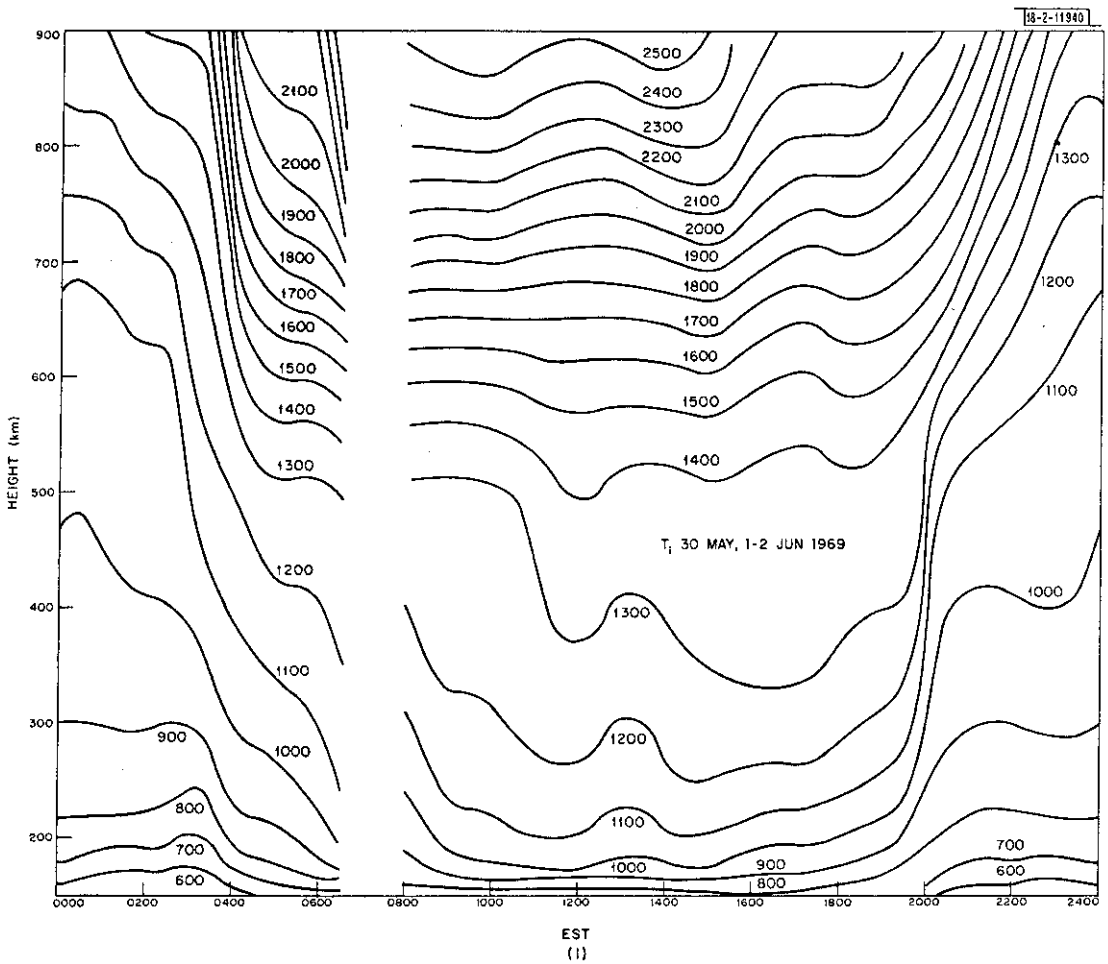

Fig. 8(a-z). Continued.

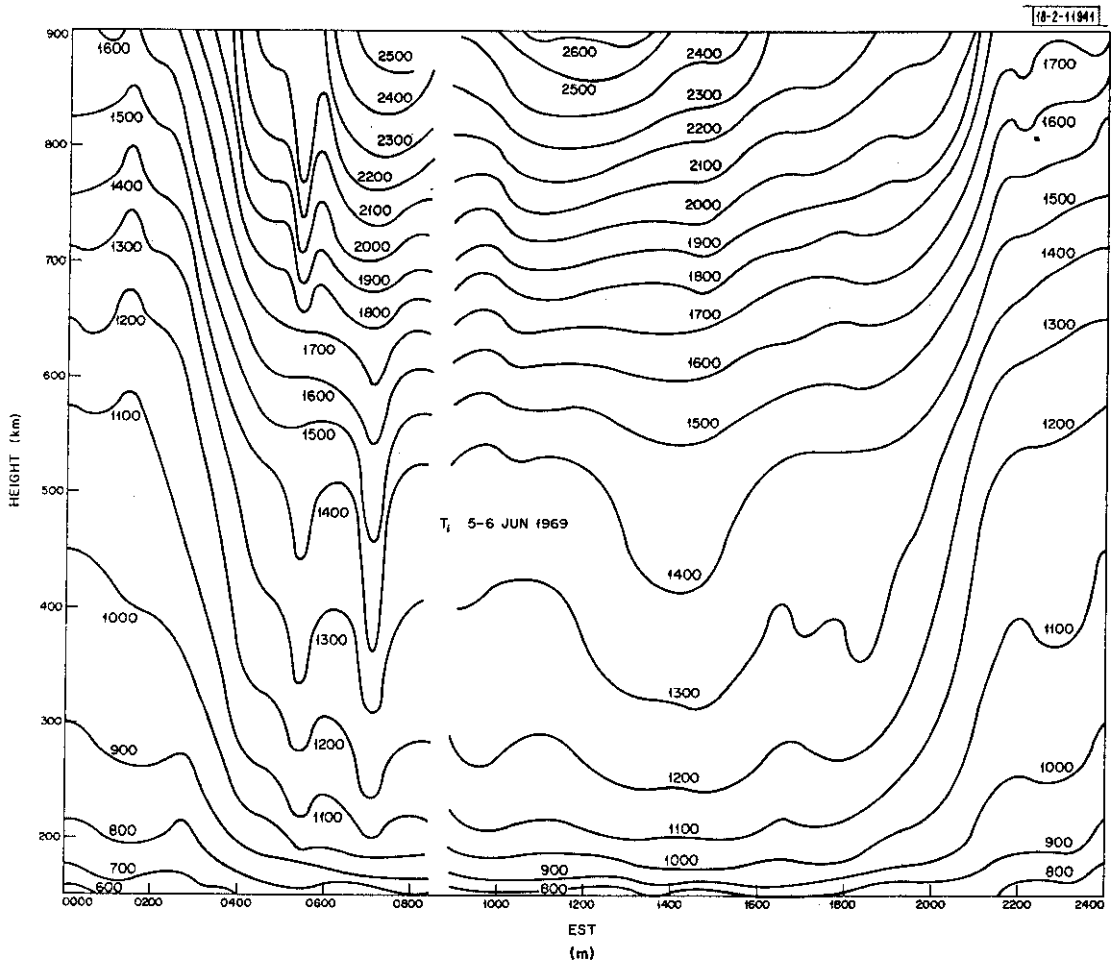

Fig. 8(a-z). Continued.

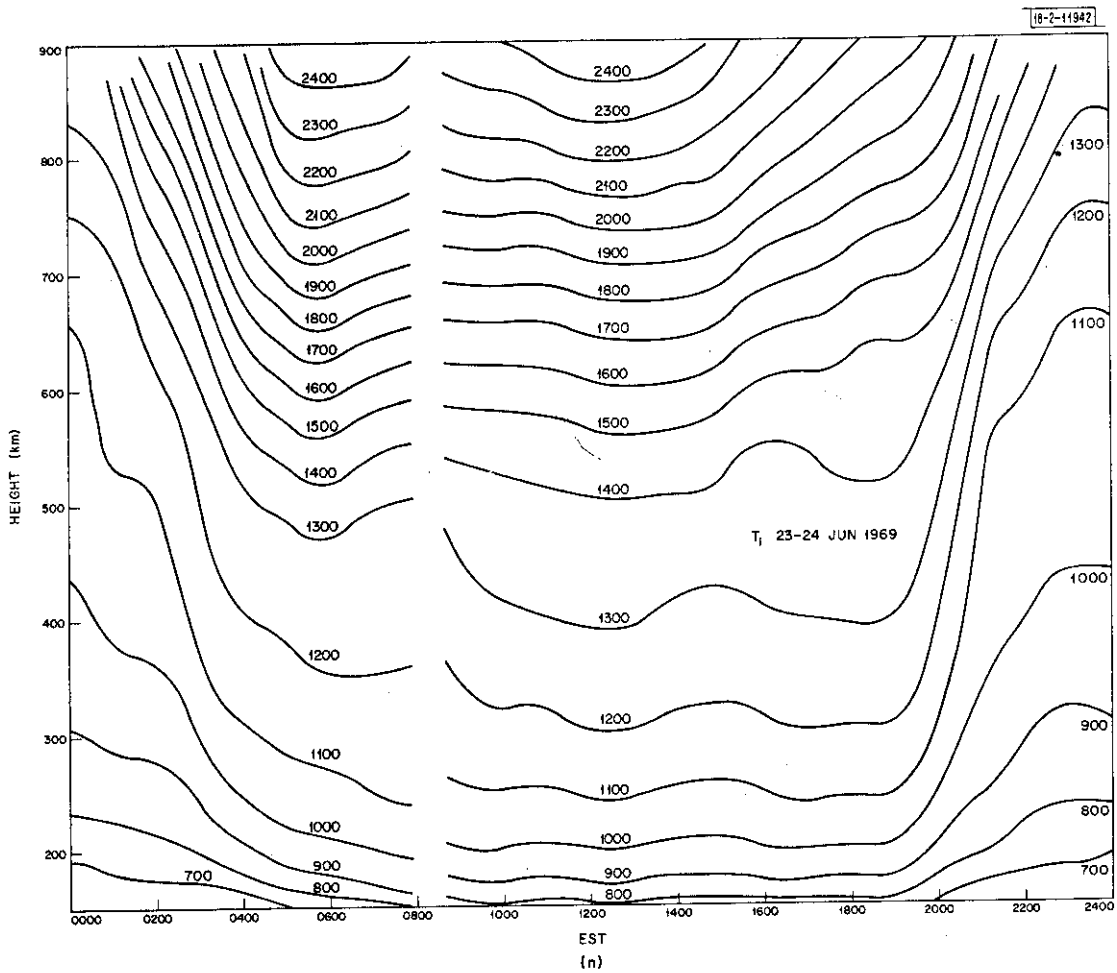

Fig. 8(a-z). Continued.

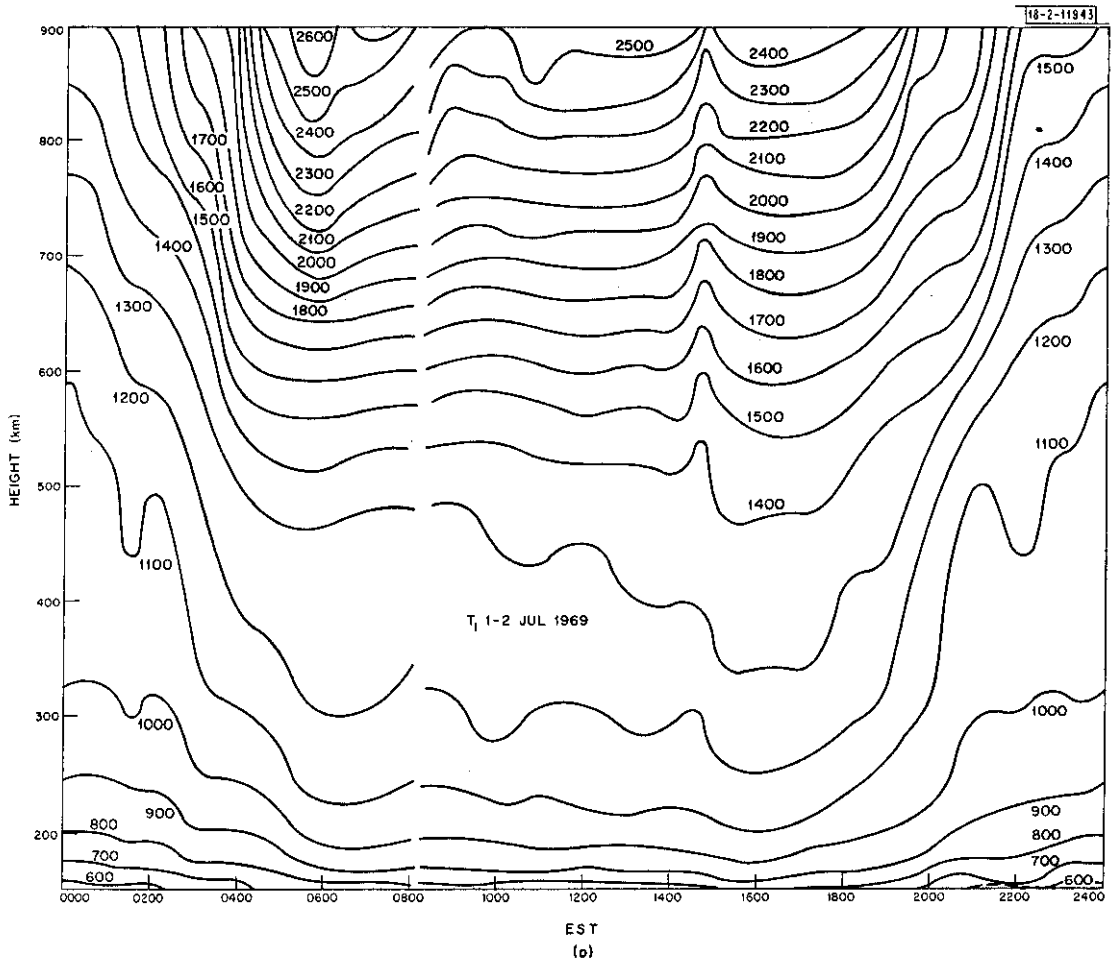

Fig. 8(a-z). Continued.

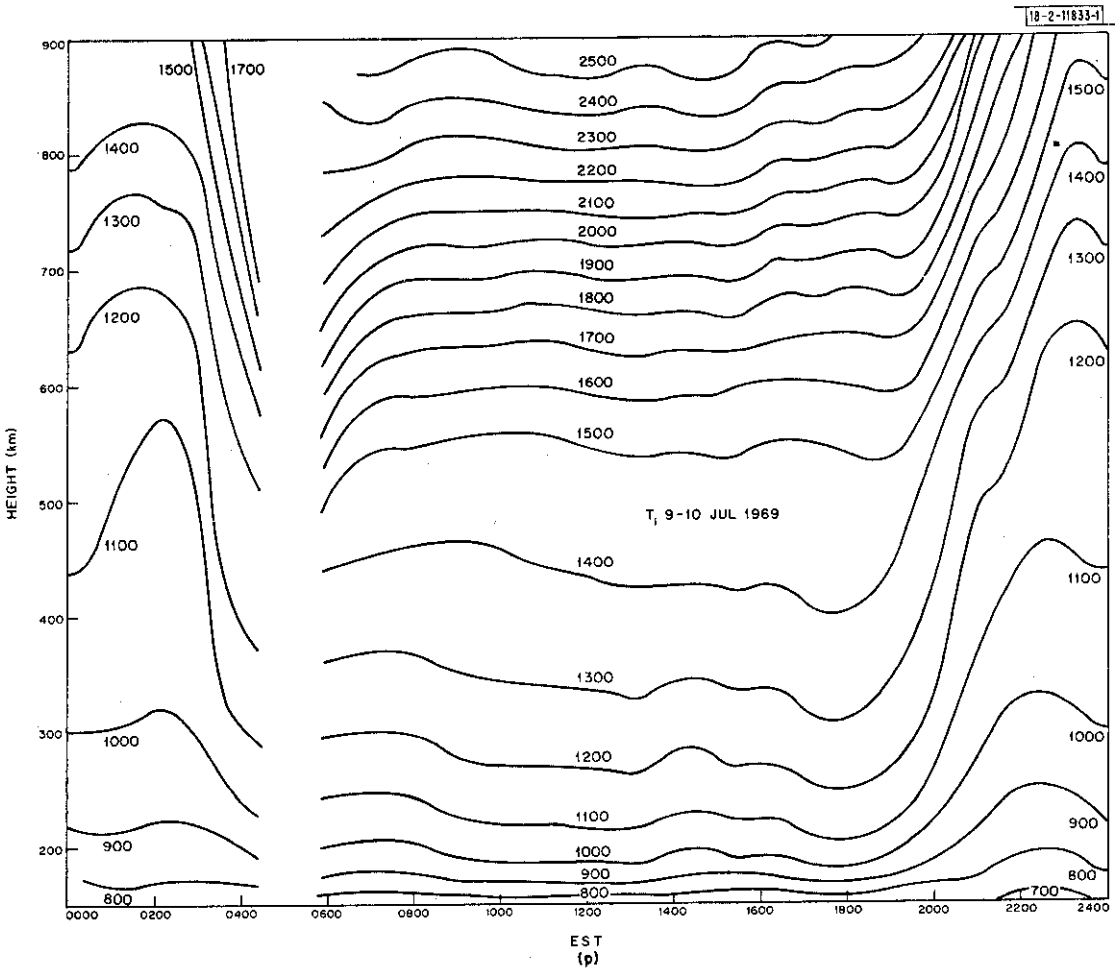

Fig. 8(a-z). Continued.

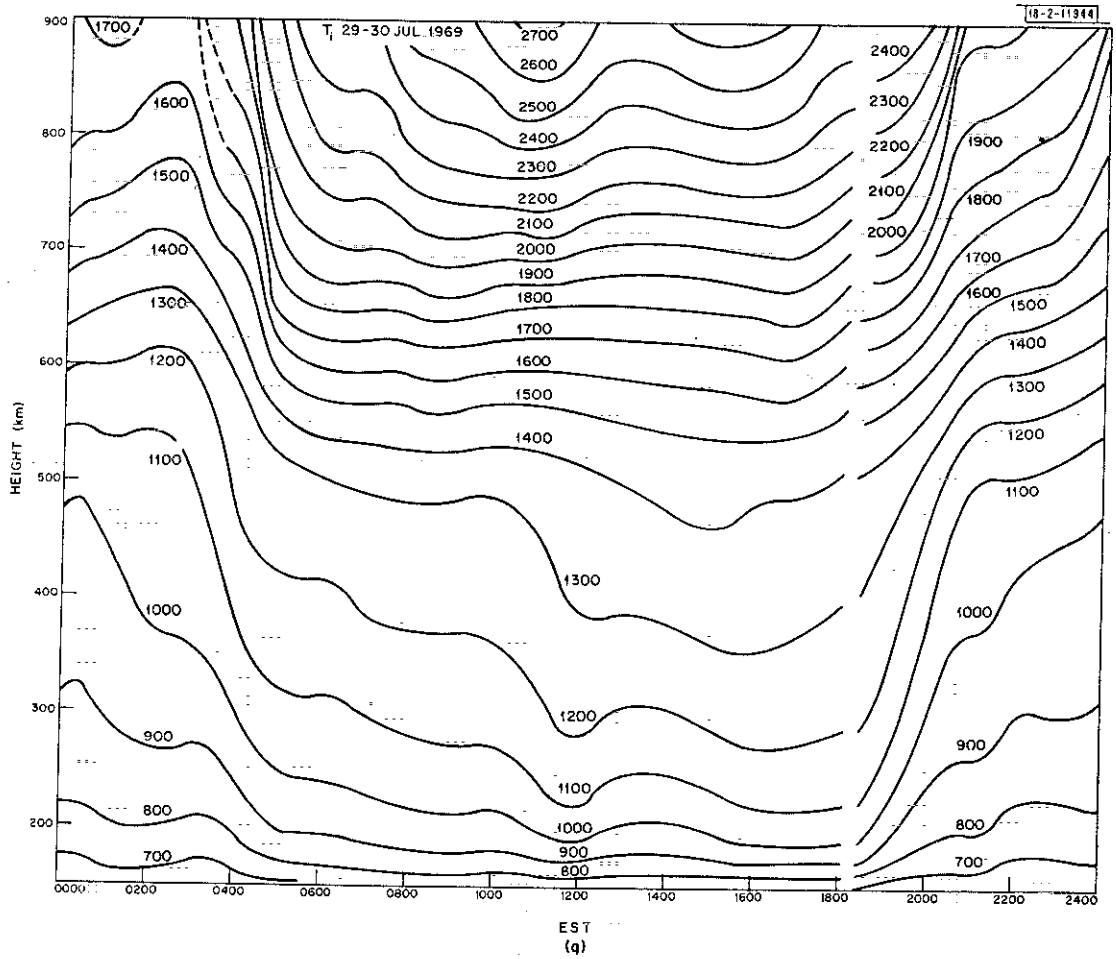

Fig. 8(a-z). Continued.

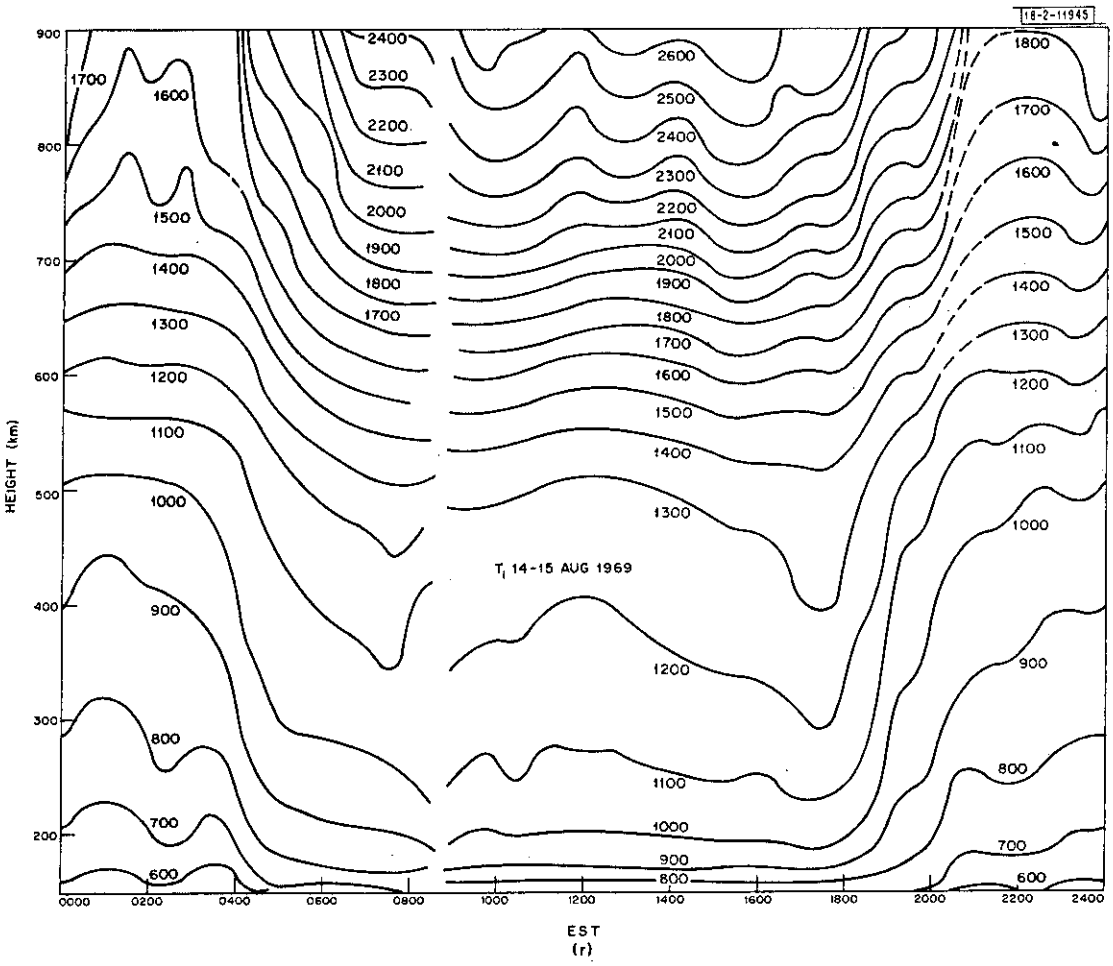

Fig. 8(a-z). Continued.

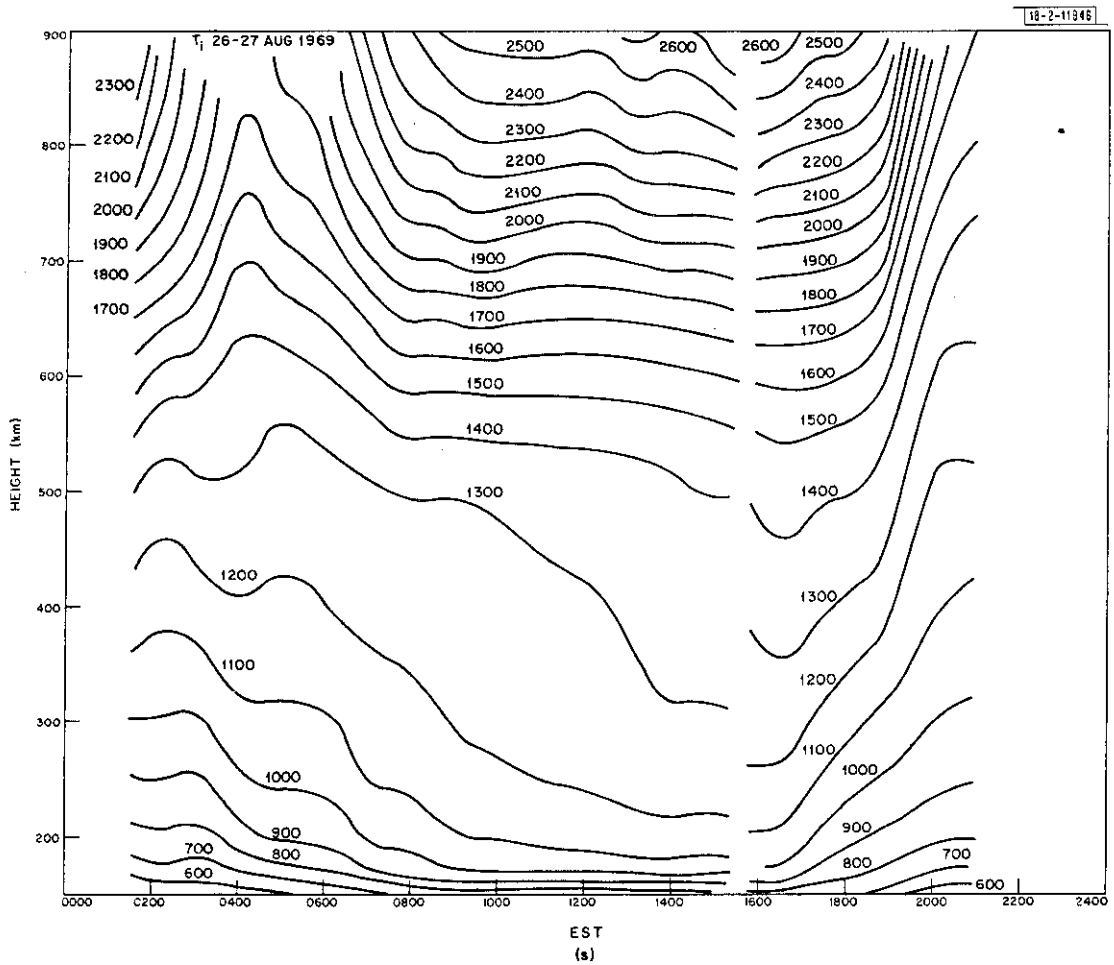

Fig. 8(a-z). Continued.

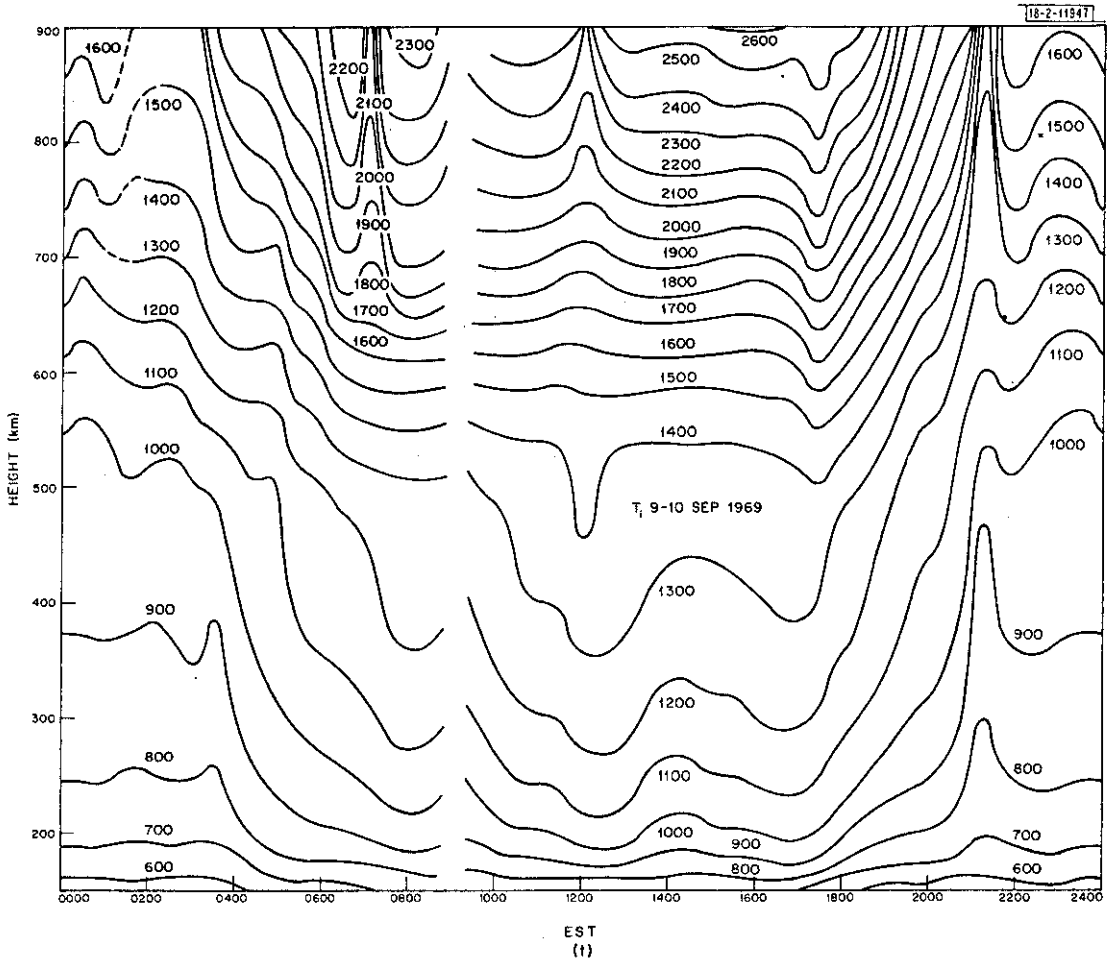

Fig. 8(a-z). Continued.

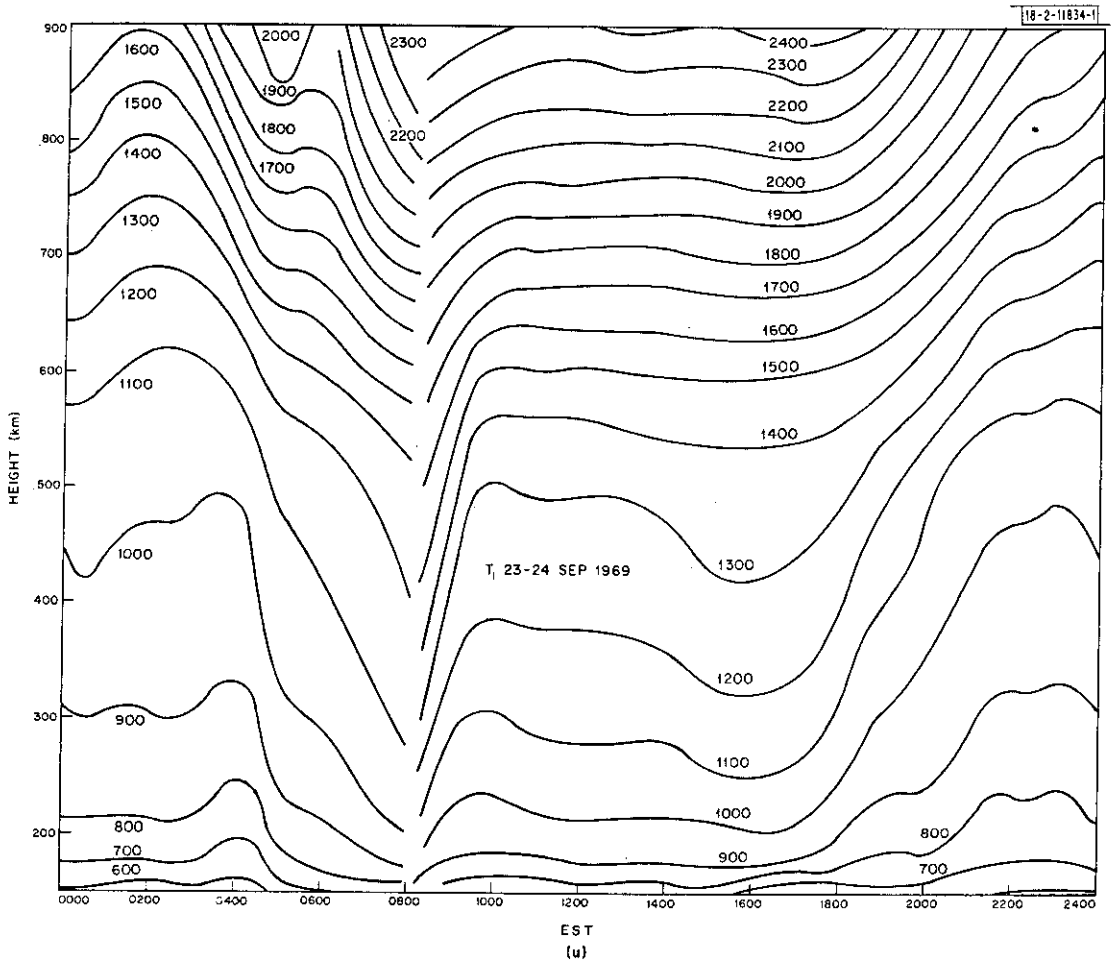

Fig. 8(a-z). Continued.

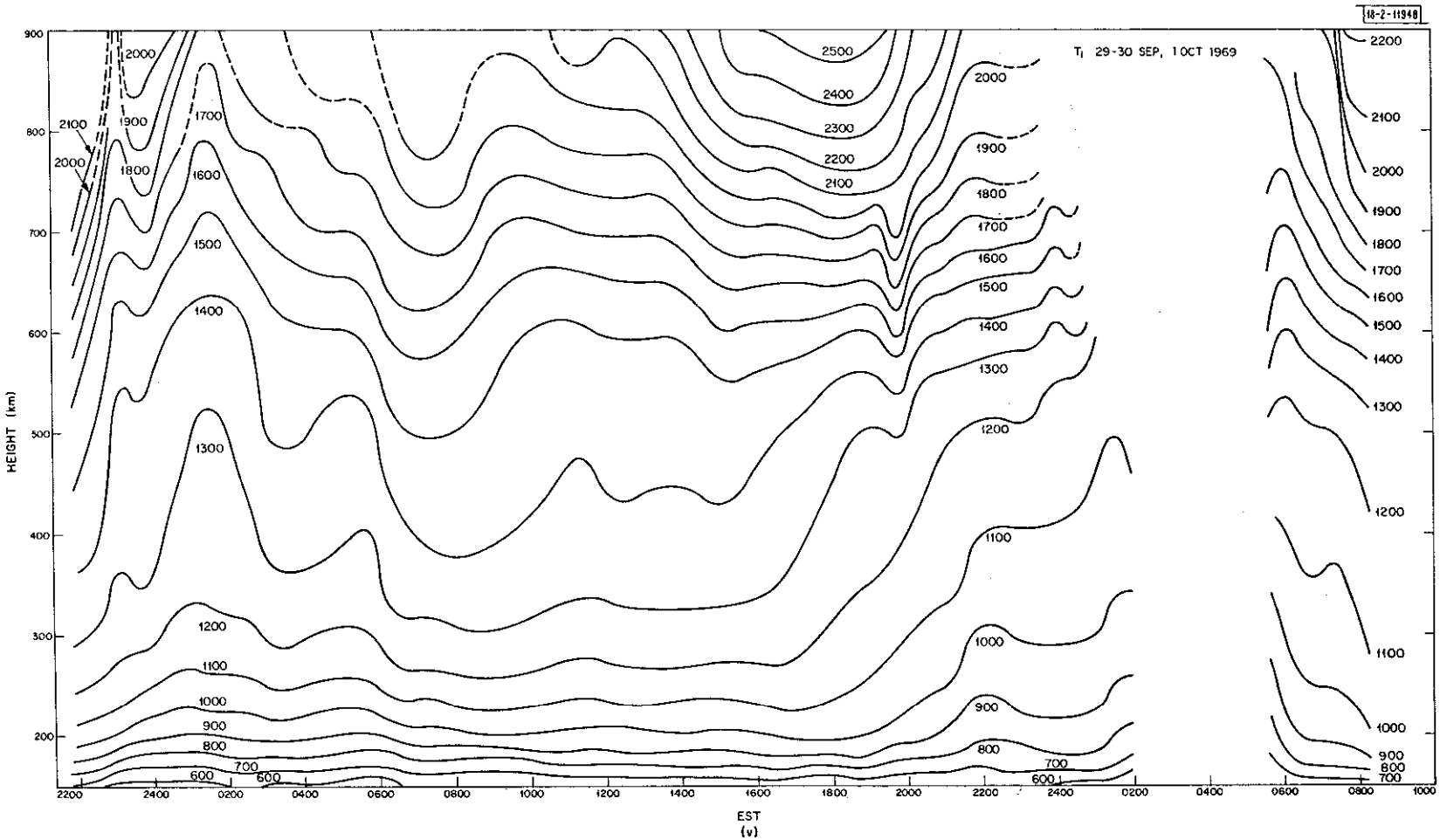

Fig. 8(a-z). Continued.

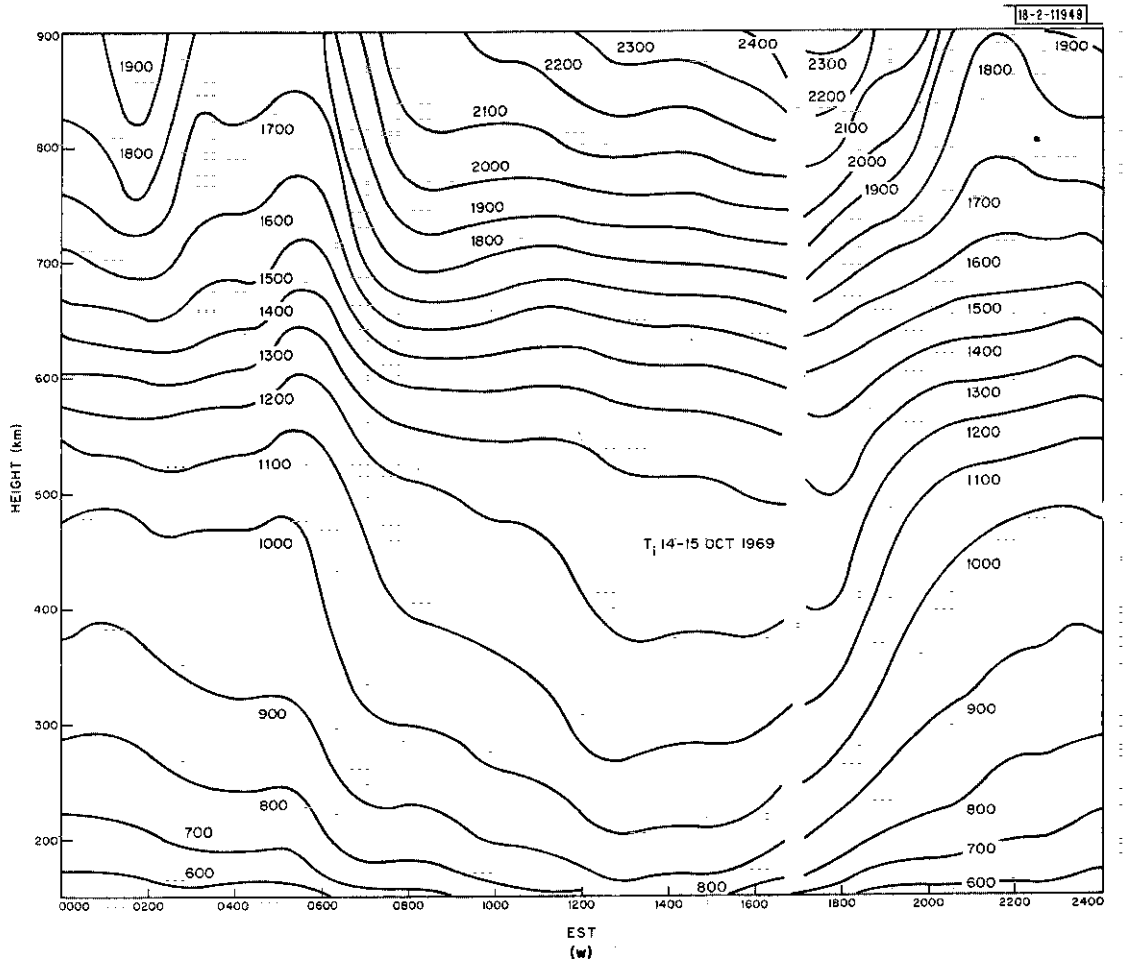

Fig. 8(a-z). Continued.

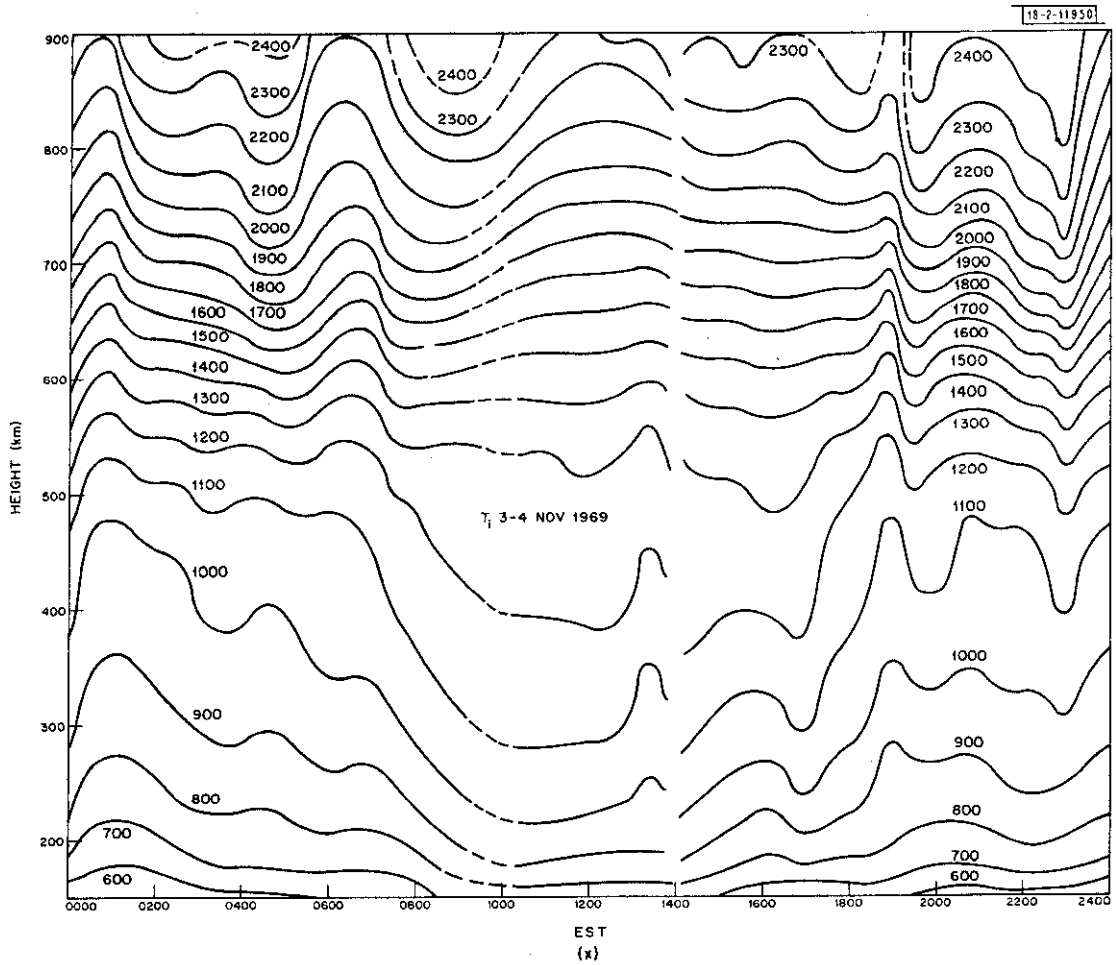

Fig. 8(a-z). Continued.

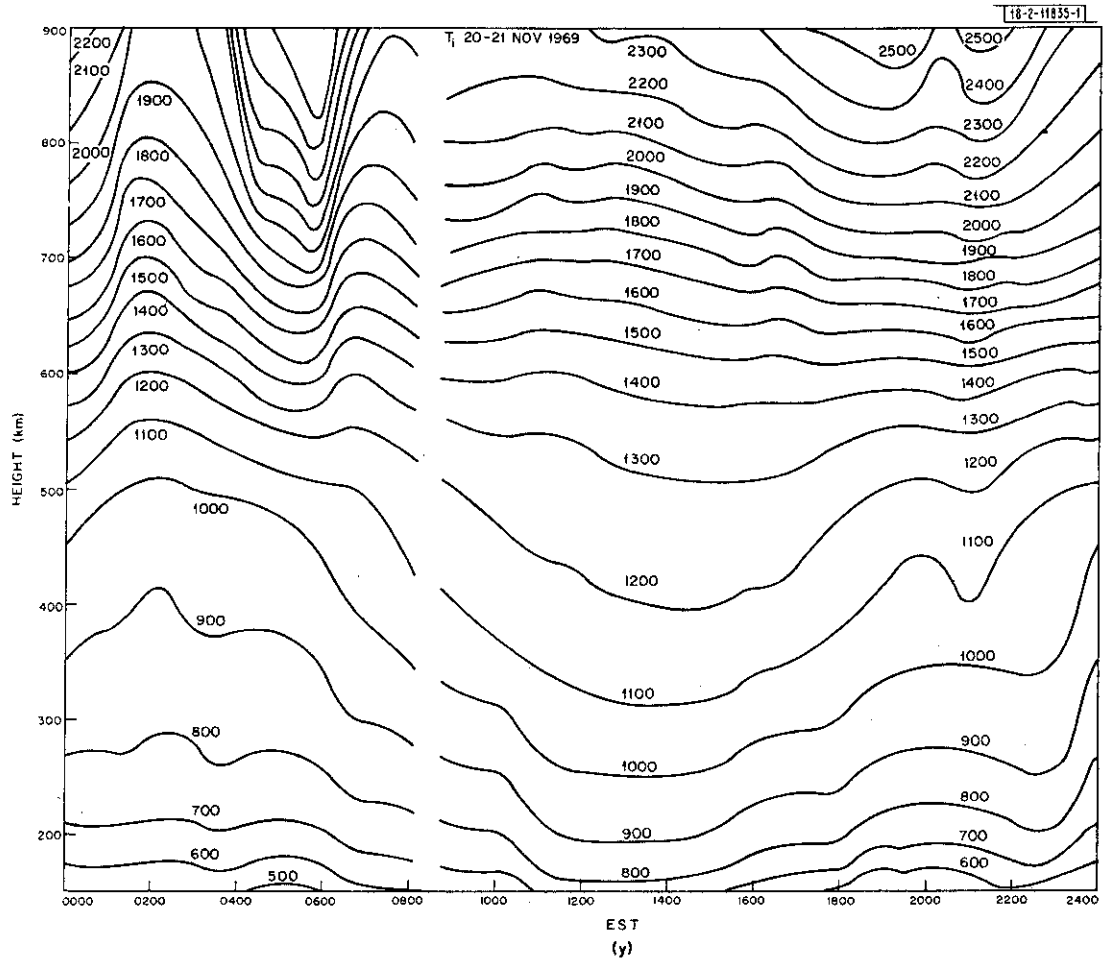

Fig. 8(a-z). Continued.

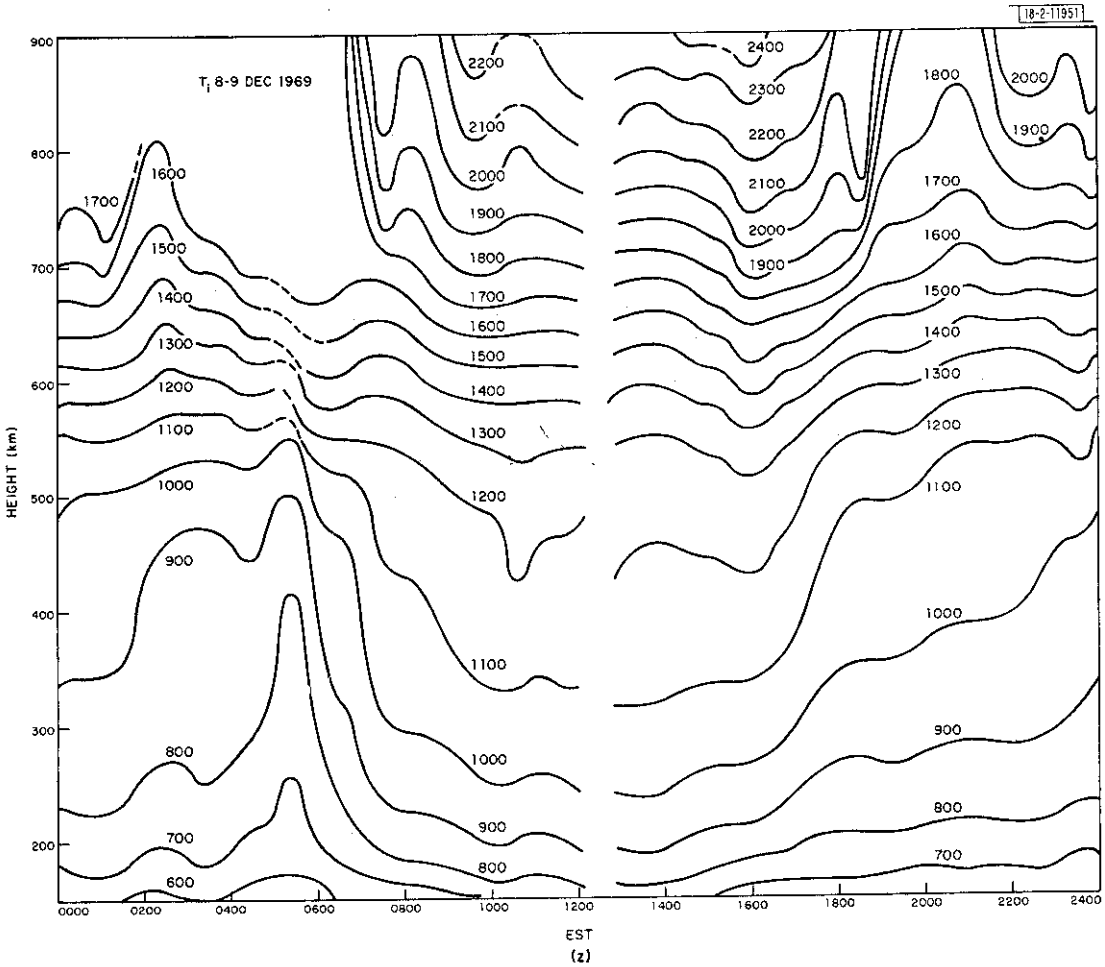

Fig. 8(a-z). Continued.

Since the lowest point available is for 225 km altitude, it was necessary to extend the curves downward, and this was carried out by assuming a fixed value $T_e = T_i = 335°K$ at 120 km altitude.

The results shown in Figs. 3, 7, and 8 have been combined to obtain the diurnal variation of the exospheric neutral temperature via thermal balance arguments, and the results have been reported in Refs. 22 and 49.

B. Quiet-Day Electron Temperatures

The most striking feature of the electron-temperature behavior is that (in contrast to the density) there is little diurnal variation in winter and a large diurnal variation in summer. This is because in winter the conjugate point remains sunlit so that heat is supplied to the protonosphere throughout the night (Fig. 5), and this heat is lost by conduction to the ionosphere through both ends of the field tube. In summer, on the other hand, the length of the day is greater locally than at the conjugate point (Fig. 5).

On some winter nights (e.g., 5-6 February, 12-13 February) local sunset gave rise to only a small decrease in T_e. The winter-night electron temperature was usually seen to decrease at, or shortly after, midnight as the electron density increased. Thus, the temperature change at dawn was more marked. During equinox it is sometimes possible to discern temperature increases associated with conjugate sunrise,[9,35] provided that the local electron density is sufficiently low so that the effect is not masked by the local cooling.[50] As can be seen in Fig. 5, conjugate sunrise ($\chi_{conj} \geq 105°$) precedes local sunrise by a useful margin (1 to 2 hours) only during the period 10-25 March and 15 September – 1 October, approximately. The temperature increase beginning at about 0300 on 22 March [Fig. 7(f)] is an example of conjugate heating. It is possible that the electron-temperature increase beginning somewhat before 0400 on 26 March [Fig. 7(h)] represents another instance, but in this case the temperature increase at local sunrise beginning near 0430 makes it difficult to be certain. Similarly, it appears that there is some indication of a temperature increase beginning before dawn on 24 September [Fig. 7(u)], but the effect is not pronounced.

A consistent feature of the daytime electron temperature is the minimum produced at a level close to or somewhat above $h_{max}F2$ whenever the local cooling becomes large enough. Examples are provided by 26-27 February and 25-26 March which were occasions when $N_{max}F2$ exceeded $\sim 1.5 \times 10^6$ el/cm^3. As we move away from sunspot maximum, instances of electron-temperature inversions become infrequent at Millstone, as the required high electron densities are no longer encountered.[5,6] For the same reason, the probability of encountering a temperature inversion has always been considered to be higher in winter than in summer.[51] During 1969, however, there were several days on which inversions were encountered in summer, particularly during sunset. These include 6 May, 30 May, 5 June, 1 July, and 23 September. It is noteworthy that on these days the electron density at the level of the inversion was typically a little less than 10^6 el/cm^3. However, the peak of the layer was substantially (~25 to 30 km) higher than found in winter, and the local heating from photoproduction would be lowered correspondingly.

During winter nights, the electron temperature varies inversely with the electron density because the local cooling serves to modulate the temperature rise caused by heat conducted from the protonosphere. This is particularly pronounced, for example, on 16-17 January and 4-5 November.

C. Disturbed-Day Electron Temperatures

On the disturbed night of 23-24 March, the electron temperature was initially observed to be increasing, and reached a peak near 2130 EST when it was twice its normal value at most levels. This coincided with the highest electron density encountered in the valley region (near 250 km), suggesting that it was caused by a peak in the precipitating flux. Thereafter, the temperature began to decrease and reached a minimum shortly after midnight that appears to have been caused by the growth of the F2-layer (near 400 km). However, it is possible that conjugate sunset ($\chi_{conj} = 105°$) occurring at 2200 EST contributed to the lowering of the temperature. After midnight, T_e increased again at all levels above 250 km as the F2 density declined. Temperatures in the valley region remained high throughout the night, suggesting that the soft particle flux was present at all times.

During the second geomagnetically disturbed observing period (29 September – 1 October), T_e was already high when the observations began, and declined during the next 2 hours reaching a minimum near 0120 EST that appears to coincide with a peak in the F2-region density. Thereafter, the temperature gradually increased, possibly as a consequence of conjugate sunrise occurring at 0145 EST. The temperature in the valley region beneath the layer peak was substantially less than on 23-24 March. However, it is possible that both sets of temperature measurements are too low owing to the neglect of molecular ions (O_2^+, NO^+) at these levels when interpreting the results (Sec. II-C). Some evidence that molecular ions were abundant at altitudes perhaps as high as 300 km is provided by the large variation of ion temperature below this level at the commencement of the observations on 23 March. This is thought to be unrealistic and to have arisen from assuming that only O^+ ions were present.

D. Ion Temperature

The ion temperature [Figs. 8(a) through (z)] exhibits only a small diurnal change at altitudes below 300 km where the ions and the neutrals are in good thermal contact. At higher altitudes, the ion temperature increases and takes up a value intermediate between the electron temperature and the neutral exospheric temperature. As such, it tends to mirror the changes in the electron temperature.

V. VERTICAL IONIZATION FLUX RESULTS

A. General

The new spectrum analyzer installed in 1968 permitted the first reliable estimates of the vertical velocity of the plasma over Millstone.[20] Preliminary results from this work have been presented.[30,31,52,53] As discussed in Ref. 30, the antenna beam is directed at an angle of 16° to the direction of the magnetic field line. The observed velocity v_{obs} may be considered to be the sum of a component $v_{||}$ parallel to the field and a component $v_{\perp NS}$ perpendicular to the magnetic field oriented in the magnetic NS direction where

$$v_{obs} = 0.96\, v_{||} + 0.28\, v_{\perp NS} \quad . \tag{11}$$

In the F-region the drift velocity $v_{\perp NS}$ will be controlled by the east-west electric field, i.e.,

$$v_{\perp NS} = E_{EW}/B \quad . \tag{12}$$

Separate measurements made using the L-band radar directed obliquely have been made[19,54] which indicate that, except during magnetically disturbed conditions, $v_{\perp NS} \leq 30$ m/sec. Thus, by ignoring the $v_{\perp}$ component, it is possible to regard the observed velocities as providing measurements of $v_{||}$ with errors of up to ±10 m/sec. Since the $v_{\perp}$ component will be height-independent, it is sometimes possible to remove these errors.

The most useful results from the measurements of the vertical velocity are estimates of the N-S component of the thermospheric wind[30] and of the ionization fluxes exchanged with the magnetosphere.[53,55] Since the determination of the winds is currently the subject of a separate study,[56] we confine our attention here to the question of the magnetospheric flux.

A limitation of the drift velocity measurements made at Millstone is that, owing to the great height of the transition altitude between O^+ and H^+ (~2000 km) at this latitude, it is not possible to measure directly the H^+ flux. Instead, the observations yield only the fluxes of the O^+ ions (even when significant H^+ fluxes are present), since O^+ is always the predominant ion.[30] Unfortunately, as shown in Ref. 31, the vertical drift of the ionization at altitudes well above $h_{max}F2$ tends to be controlled by pressure changes occurring in the plasma below. Thus, changes in the height of the layer (e.g., as a result of neutral winds) are reflected in the vertical drift at all altitudes. Similarly, the growth and decay of the layer (under the influence of production and loss) or expansion and contraction (as a result of changes in plasma temperature) also establish vertical fluxes. Thus, in order to obtain information on the exchange of ionization with the protonosphere, it is easiest to study the altitude distribution of the flux when N_e, T_e, and T_i appear to be constant for a period of time.

In practice, it is desirable to average the velocity results obtained over a number of runs, in part, to remove fluctuations of a geophysical nature, e.g., caused by Traveling Ionospheric Disturbances (TIDs), as well as to reduce the uncertainty in the (noisy) estimates. In this connection, it may be noted that the standard deviation in the results varies with signal-to-noise ratio P_s/P_n, and hence on both height and time of day.[52] An empirical result which appears to reproduce the observed variation of the rms deviation with the predetector signal-to-noise P_s/P_n ratio for the results presented in Ref. 52 is

$$\Delta v = \frac{\bar{v}_i}{\sqrt{n}}\left[0.3 + \frac{P_n}{P_s}\right]^{1/2} \text{ m/sec} \qquad (13)$$

where $\bar{v}_i$ is the mean thermal speed of the ions $(2kT_i/m_i)^{1/2}$, and n is the number of independent observations (pulses). For the 8-minute runs conducted at Millstone, Δv typically lies in the range 5 to 20 m/sec, and is comparable to the true drift v. To obtain reliable results, therefore, it is essential to average over several runs, and this requires the existence of a time interval of 1 or 2 hours over which the densities and temperatures appear constant.

B. Steady-State-Velocity-vs-Height Profiles

By examining the contours of density and temperature in Figs. 3(a) through (z) and 7(a) through (z), we have been able to find periods near noon and midnight when the density and temperature appear to be roughly constant with time (Table VI). For these periods, profiles of vertical velocity were computed using three, four, or five cycles of data. Figure 9(a-b) presents examples of the velocities observed by day and by night. Similar diagrams were constructed for all the periods listed in Table VI. In plotting these diagrams, the height assigned to each data point was a

TABLE VI

PERIODS EMPLOYED FOR COMPUTING AVERAGE VERTICAL VELOCITY PROFILES

Date (1969)	Daytime (EST)	Nighttime (EST)	Comments
16-17 January	1200-1400	2200-2330	$\Delta w_B = +7$ m/sec
10-31 January	–	0130-0230	As above
5-6 February	1300-1500	2330-0100	As above
12-13 February	1500-1630	2300-0100	As above
26-27 February	1330-1530	0000-0200	As above
21-22 March	–	2300-0100	As above
25-26 March	1200-1400	–	As above
9-10 April	1200-1400	2300-0100	As above
23-24 April	0800-1000	2230-0030	$\Delta w_B = 0$
6-7 May	–	2230-0030	As above
30-31 May, 1-2 June	0930-1030	–	As above
5-6 June	1000-1200	–	As above
23-24 June	1100-1300	0100-0200	$\Delta w_B = -7$ m/sec
1-2 July	1130-1300	2330-0030	As above
9-10 July	1000-1200	–	As above
29-30 July	–	0000-0130	As above
14-15 August	1000-1200/1200-1400	–	As above
9-10 September	1330-1500	–	As above
23-24 September	0900-1100	0030-0200	As above
14-15 October	1300-1500	–	As above
3-4 November	1400-1530	–	As above
20-21 November	1330-1530	0030-0230	As above
8-9 December	1300-1500	2300-0130	As above

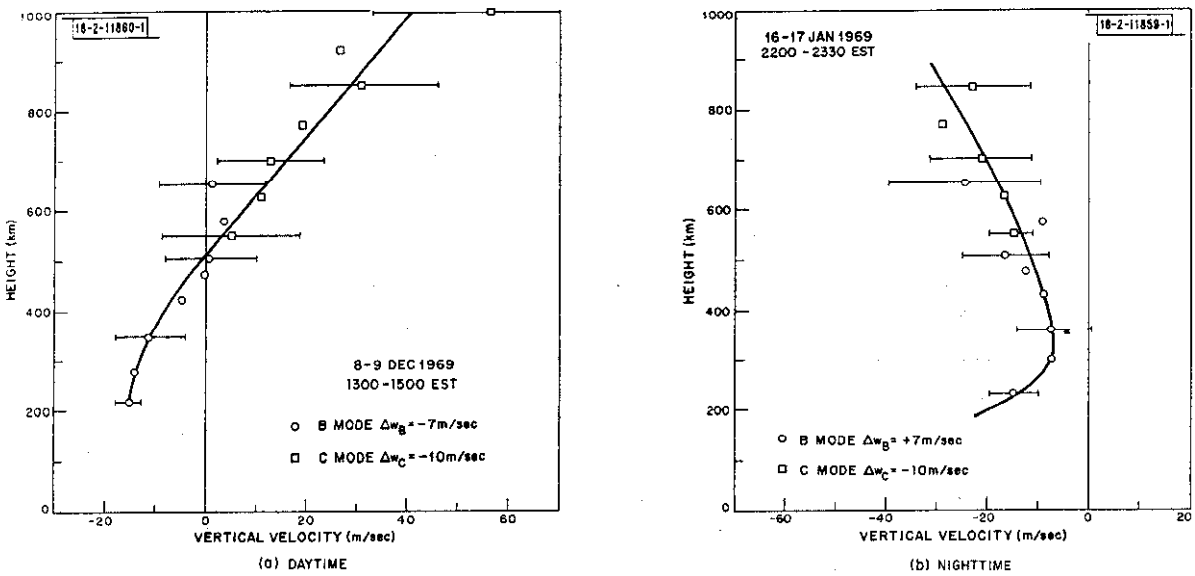

Fig. 9(a-b). Examples of plots of average vertical velocities constructed for periods listed in Table VI.

"weighted height" that takes into account: (1) the triangular weighting imposed by the pulse and matched-filter response (i.e., the radar ambiguity function), and (2) the actual distribution of echo power vs delay. These weighted heights were computed using the echo-power-vs-delay distribution observed in the preceding 100-μsec (A-mode) measurement.

The error bars shown in Fig. 9(a-b) are the rms deviations of the points about their means, and serve to indicate the scatter of the data; these may be taken as typical for the daytime and nighttime curves constructed for 1969. A second source of error encountered in constructing these plots is that introduced by the change in the phase difference between the input and output signals at the transmitter klystron amplifier arising as a result of the fall in the applied voltage during the pulse. The magnitude of this error is discussed in the Appendix where it is shown to be of the order of

$$\Delta w = -\frac{10^8 I_{av}}{(V_m)^{3/2}} \text{ m/sec} \qquad (14)$$

where I_{av} is the average DC current read on the transmitter meter, and V_m is the transmitter voltmeter reading. For typical values, V_m = 100 kV, I_{av} = 3.8 A, $\Delta w \sim -12$ m/sec. Attempts have been made to verify this by means of tests in which the transmitter signal was leaked into the receiver, and the receiver tuning was adjusted to balance the power observed at the center pair of filters. These tests gave an estimate of $\Delta w \sim -10$ m/sec in the C-mode and a somewhat smaller value for the B-mode.

In plotting the velocities [Fig. 9(a-b)], a correction of −10 m/sec was applied to all the points gathered in the C-mode and a correction for the B-mode data was sought by attempting to match the results in the height interval where the results overlap. This procedure seemed justified by the varying condition of the B-mode filter bank during the year.

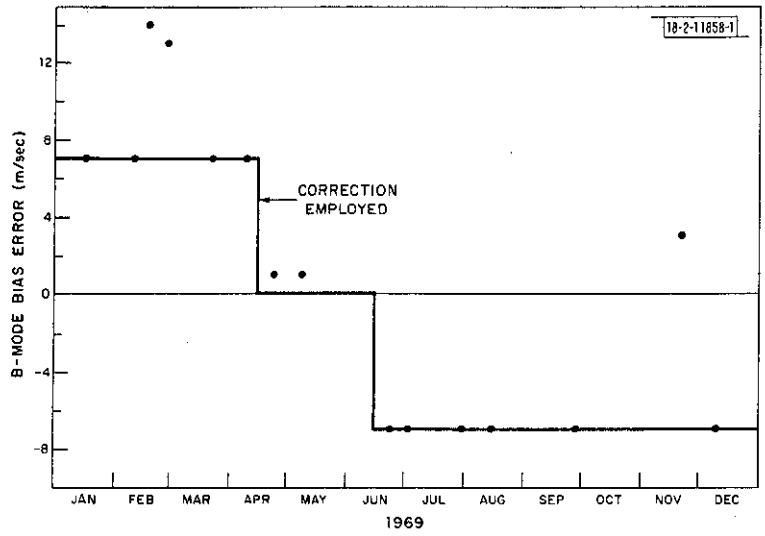

Fig. 10. Estimates of bias errors in B-mode results based on matching velocities to those observed in C-mode in region of overlap. Estimates have been confined to nighttime, as velocity is then less rapidly varying with height. Also shown (solid line) is correction law finally adopted.

Figure 10 shows the values of Δw_B obtained in this manner. The solid line is the correction finally adopted. Unfortunately, this has a systematic variation throughout the year which renders it difficult to detect true seasonal variations in the drifts at low altitudes (unless these happen to be considerably larger).

C. Velocity Results

It can be seen from Fig. 9(a) that during the day the drift below about 500 km is downward. This is because ions created well above the level of peak production (near 180 km) cannot readily be lost there and diffuse downward to lower altitudes where chemical equilibrium holds. Between 500 and 600 km, there is usually a transition to upward drift. Ions created above this transition level diffuse upward and are lost via charge exchange with hydrogen atoms. The protons so created diffuse upward into the magnetosphere.[53,55]

At night [Fig. 9(b)], the drift tends to be downward at all altitudes. There is then a flux of protons from the magnetosphere which charge-exchange with atomic oxygen above $h_{max}F2$. This creates a flux of O^+ ions which diffuse down through the layer peak to levels where the ions are removed at a rate that just balances their rate of arrival (at times when the layer is stationary and stable).

D. Daytime Flux Results

The plots of vertical velocity [e.g., Fig. 9(a-b)] have been employed to construct graphs of vertical flux for daytime and nighttime periods listed in Table VI. In constructing these plots, the velocity was assumed to follow the smooth curve [Fig. 9(a-b)]. This places considerable importance on the interpretation of the velocity results at the highest altitudes, especially during the daytime.

Plots of the daytime fluxes obtained in this manner are shown in Figs. 11(a) through (t). The downward flux appears to reach a maximum close to the F-layer peak that lies in the range

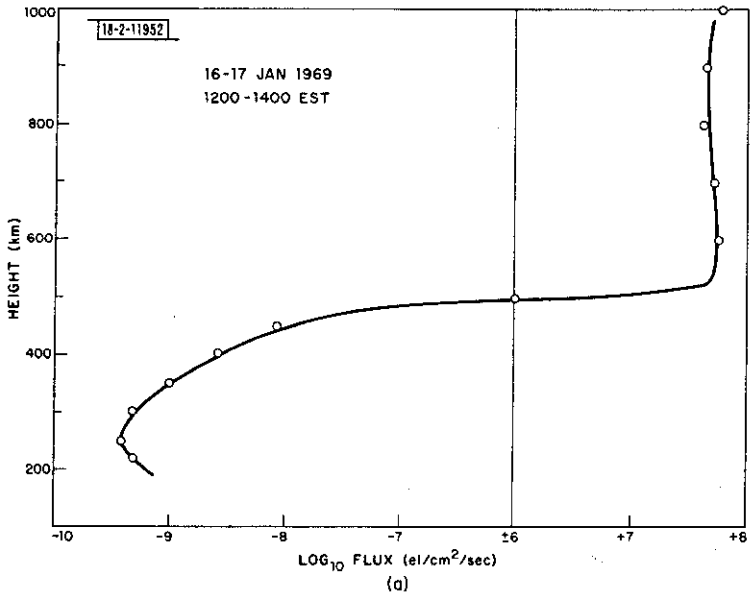

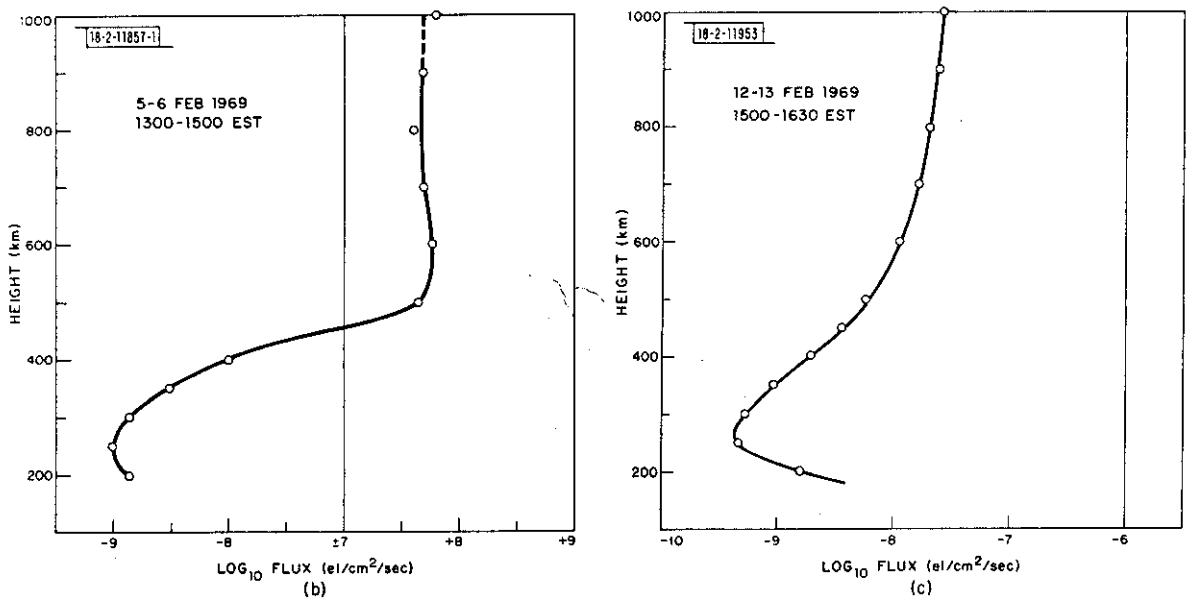

Fig. 11(a-t). Daytime vertical fluxes computed for periods listed in Table VI. Also shown in some cases are "corrected" curves which have been obtained in manner outlined in text (plus signs indicate upward flux; and minus signs indicate downward flux).

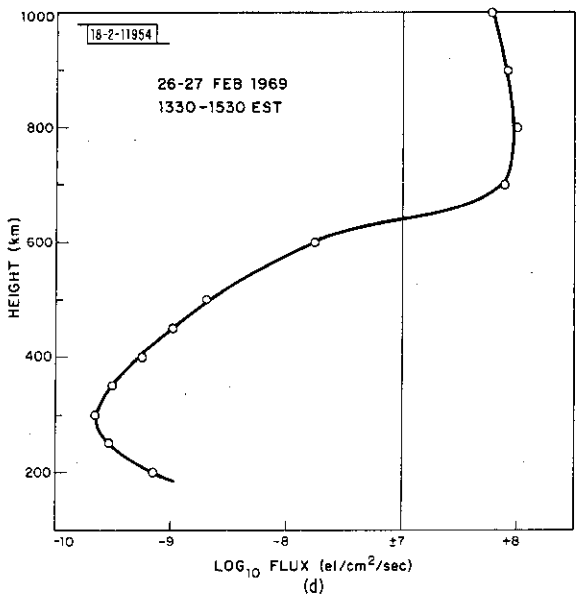

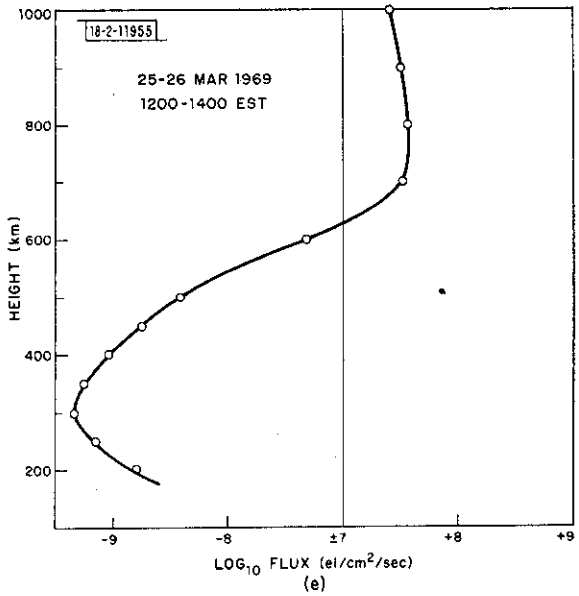

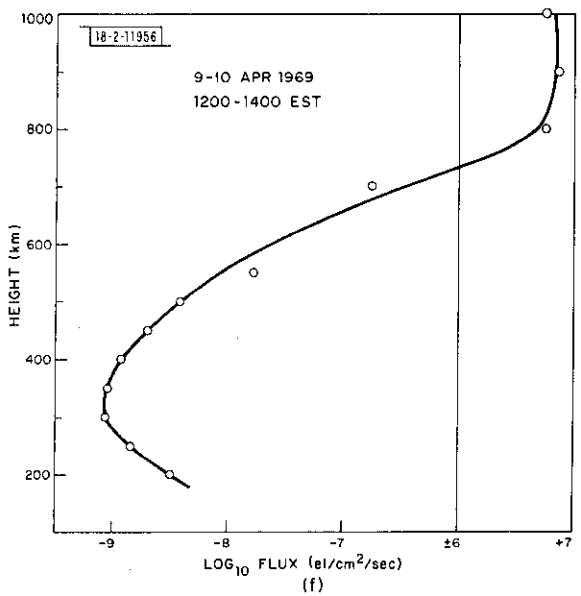

Fig. 11(a-t). Continued.

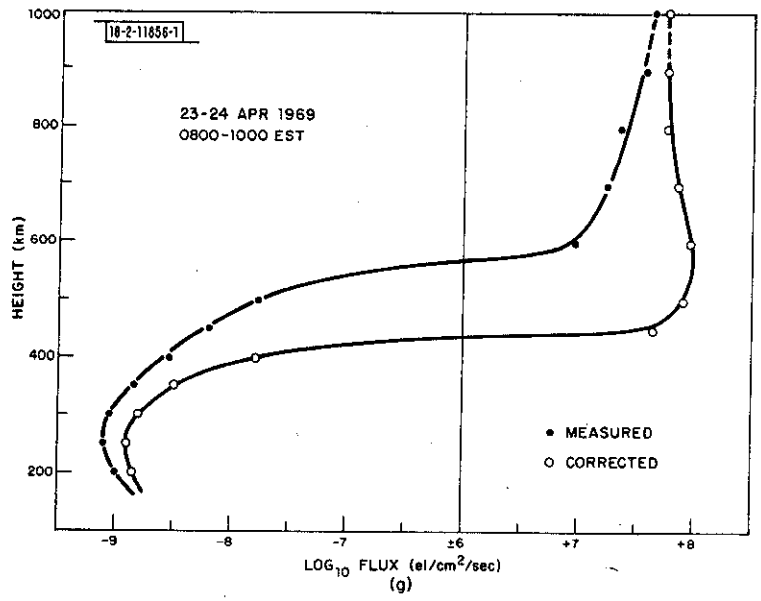

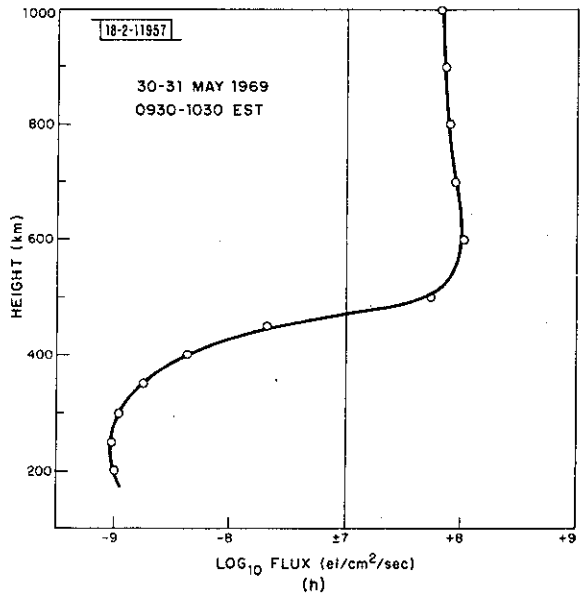

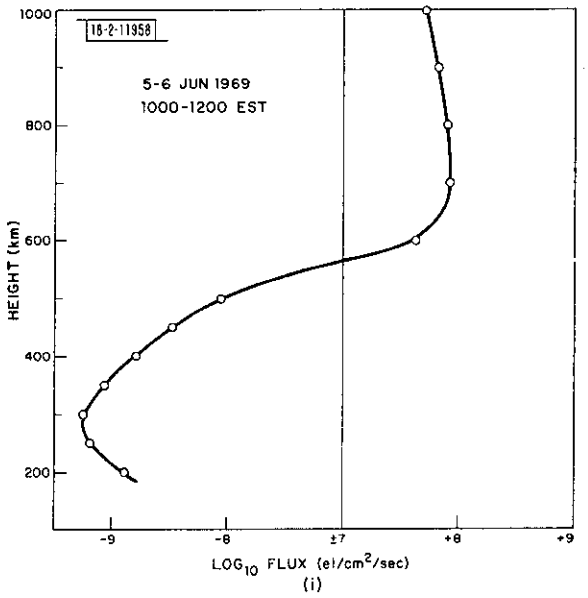

Fig. 11(a-t). Continued.

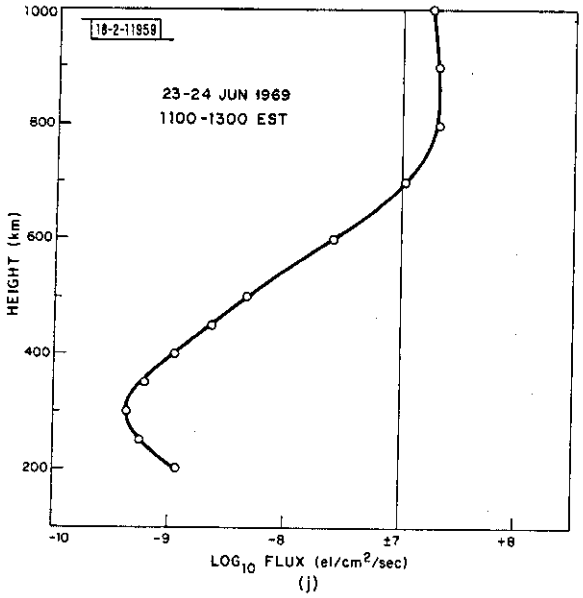

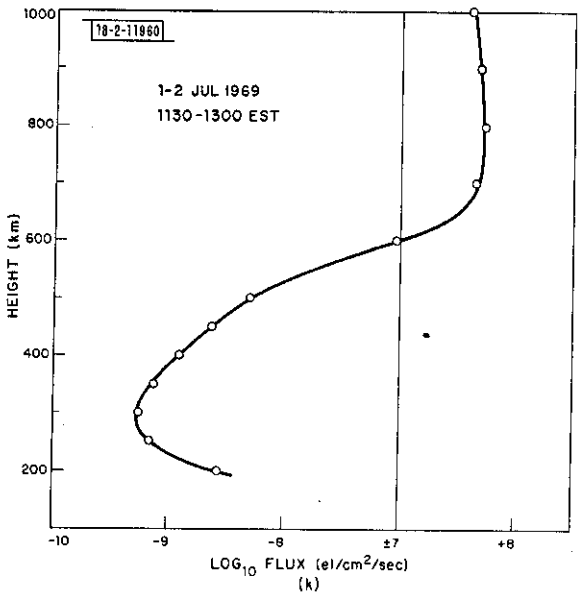

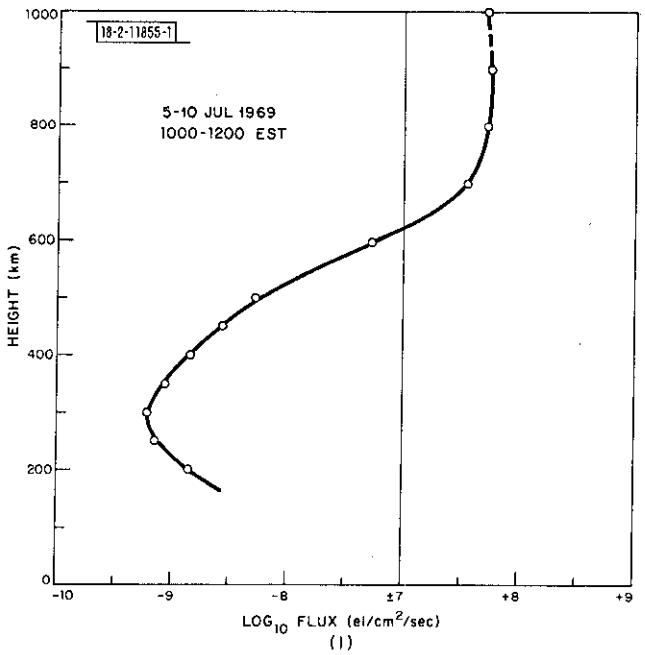

Fig. 11(a-t). Continued.

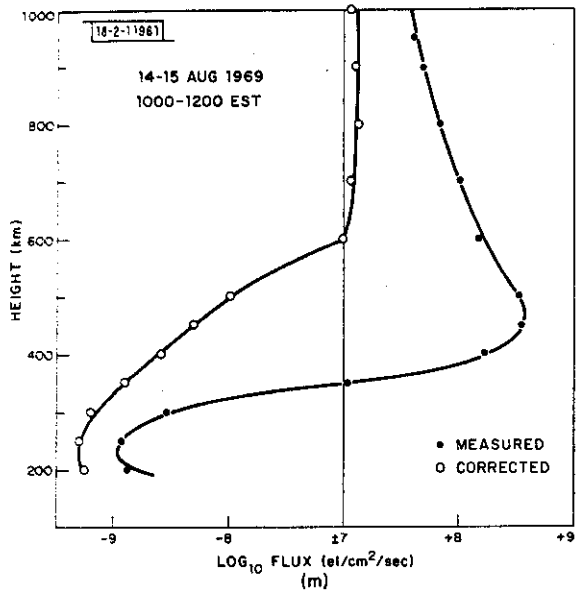

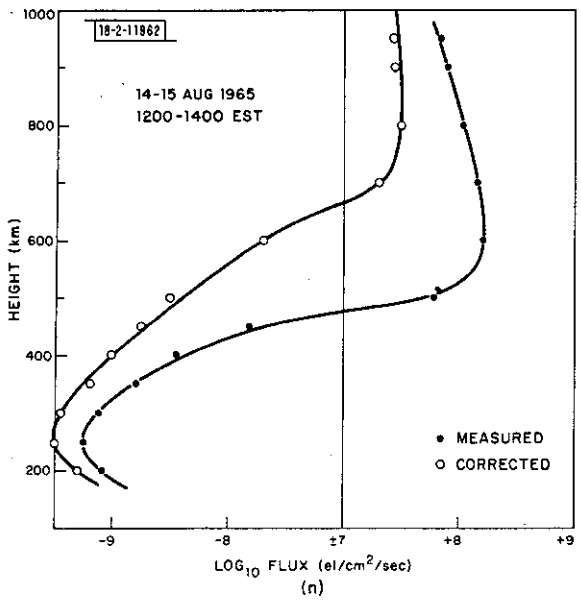

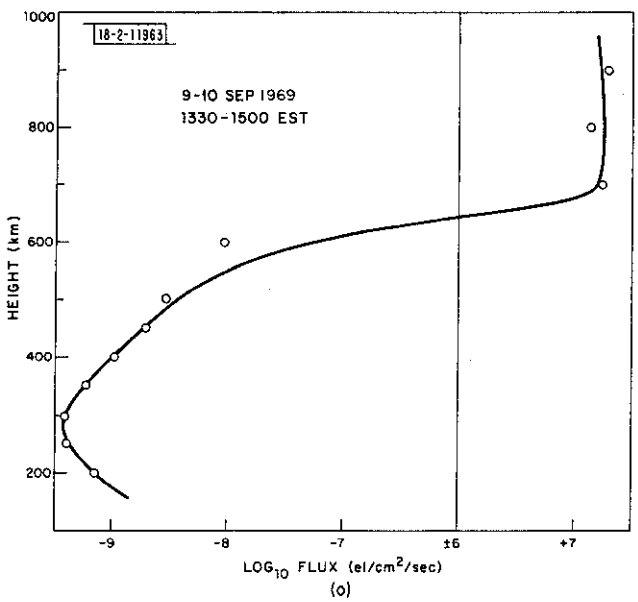

Fig. 11(a-t). Continued.

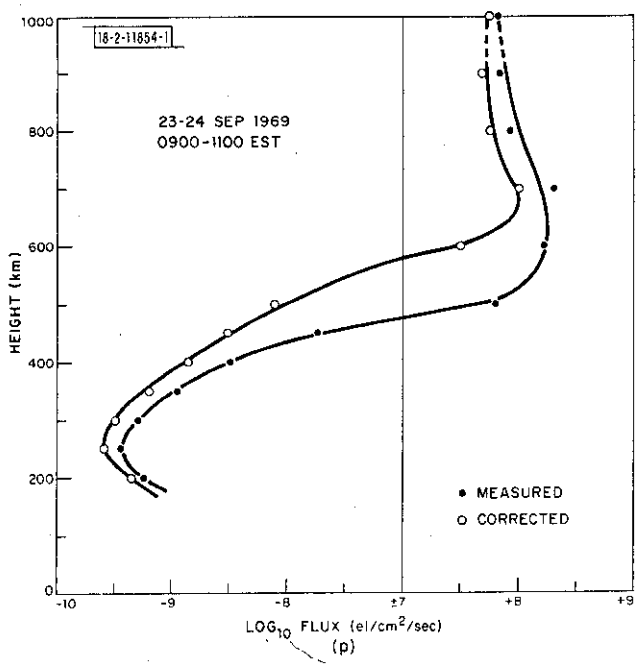

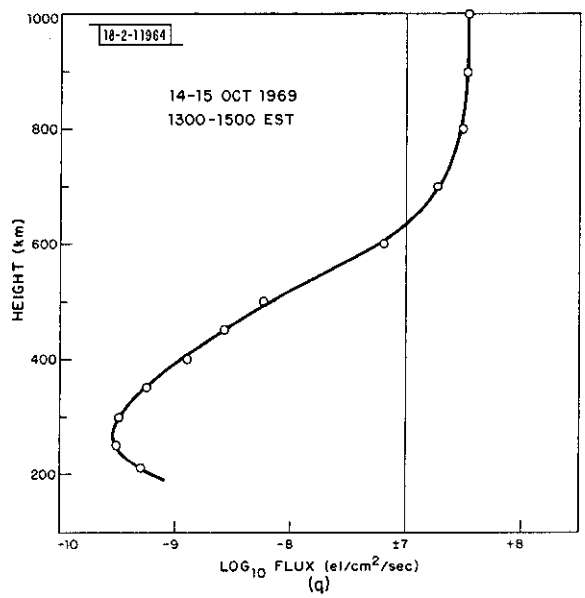

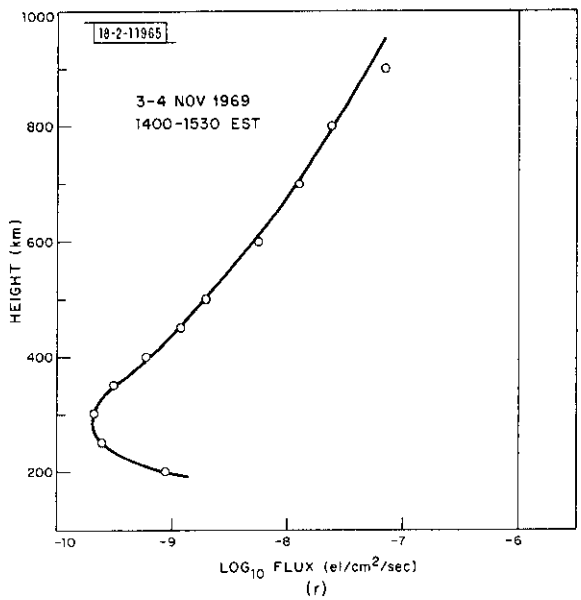

Fig. 11(a-t). Continued.

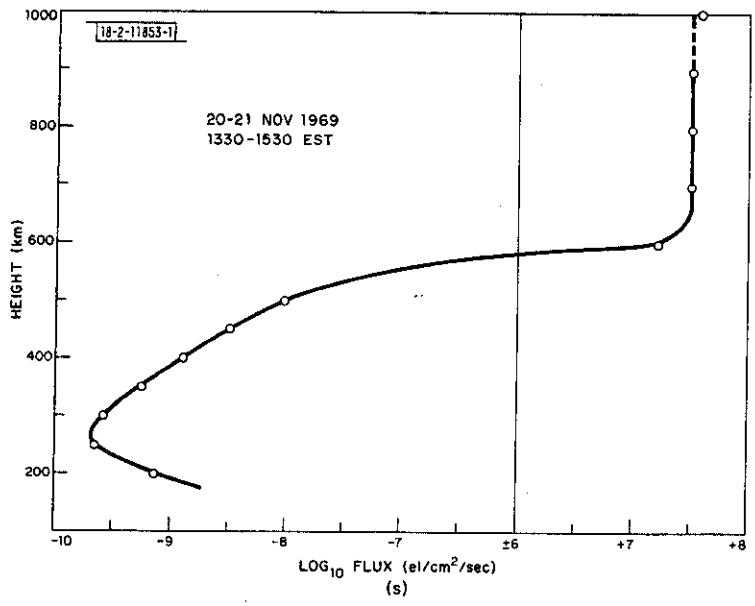

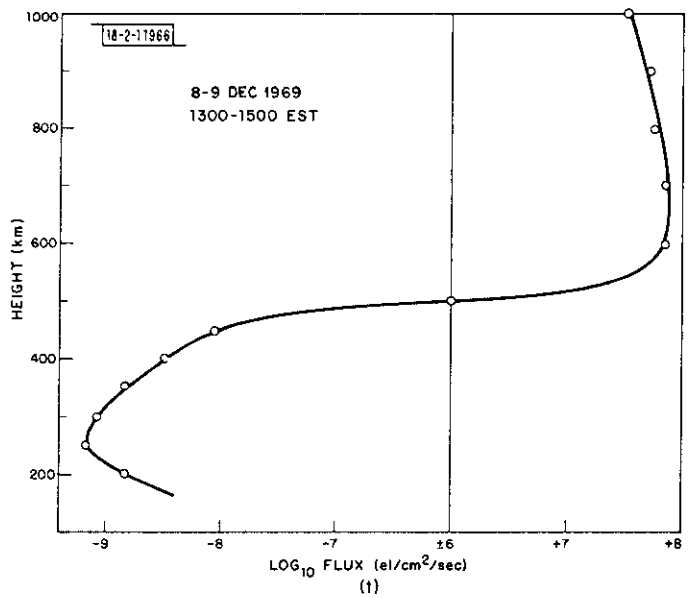

Fig. 11(a-t). Continued.

1 to 6×10^9 el/cm^2/sec. The upward flux is usually found to peak between 600 and 750 km at a value in the range 2×10^7 to 2×10^8 el/cm^2/sec. Above this level, the O^+ flux often is seen to decrease, and this has been attributed to the loss of O^+ through charge exchange with hydrogen atoms.[53] However, in some plots the flux appears independent of altitude, while in others it appears to be increasing. This suggests that the altitude variation may not be well determined. In two cases [Figs. 11(c) and (r)], the flux appears to be downward throughout the altitude range under examination. These appear to be cases in which the velocity profile was computed for a time late in the day when the escape flux was absent. These two cases are not considered representative and have been excluded from further analysis.

The remaining curves of daytime vertical flux [Figs. 11(a), (b), (d) through (q), (s), and (t)] display considerable variation. In order to see if this exhibits any particular regularity, we have plotted (in Fig. 12) the altitude of the transition between upward and downward fluxes and the peak upward flux (against a scale that increases toward bottom). These two quantities appear to vary from day to day in a correlated fashion, suggesting that there are errors in the location of the flux curves with respect to the abscissa. This could be the result of an additional bias

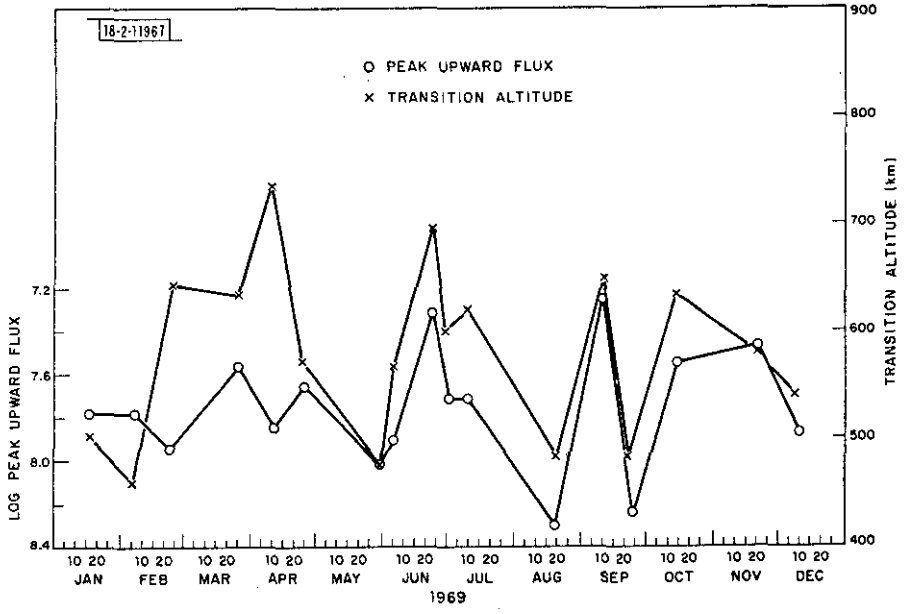

Fig. 12. Values of log peak upward flux observed in plots of Fig. 11, and transition altitude between upward and downward flux regions.

error in the velocity at all altitudes. Such an error could arise as a result of electric fields as outlined above, as an instrumental effect (e.g., improper compensation for frequency chirp), or through vertical motions of the layer (e.g., caused by TIDs) that have not been suppressed through averaging over several cycles of data. This conclusion casts doubt on the accuracy of details such as the decrease in flux above the transition altitude.

Evans and Holt[53] and Schunk and Walker[55] have attempted to compute the H^+ distribution that would be consistent with the observed decrease in O^+ flux for 24 March 1970. In view of the foregoing, it seems that this type of calculation may not be warranted by the accuracy of the results. Indeed, in order to account for a significant decrease in the O^+ flux, one is obliged to postulate an H^+ abundance of the order of 10-percent O^+ at 900 km (Ref. 55). Such a large

percentage abundance could be seen through its effect on the spectrum, but appears to be absent in our results.[57] We conclude that, at Millstone, the O^+/H^+ transition altitude lies well above 1000 km, and hence all escaping positive charges will be carried by atomic oxygen (i.e., as O^+) in the region which we are able to study. That is, we propose that the upward flux above the layer peak should increase with height to a constant value, and the altitude variations seen in Fig. 11 are chiefly introduced by bias errors in the vertical velocity that have not been removed. Accordingly, if F' is the true escape flux and v' is the bias error in the velocity curve, then the observed flux is

$$F_{obs} = F' + N_e v' \qquad (15)$$

where N_e is the electron density. By plotting F_{obs} as a function of N_e, it is possible to determine F' (the intercept) and v' (the slope). This has been attempted in those cases where the upward flux appears to vary markedly with altitude. Figure 13 shows values of the observed flux plotted against the electron density for the case of 14-15 August 1969 when the drift error v' appears to have been extremely large. Curves of "corrected" flux $[N_e(v_{obs} - v')]$ are shown in Figs. 11(g), (m), (n), and (p) where the corrections are largest. It can be seen that the "corrected" curves do exhibit upward flux values that are sensibly constant over the altitude range of interest.

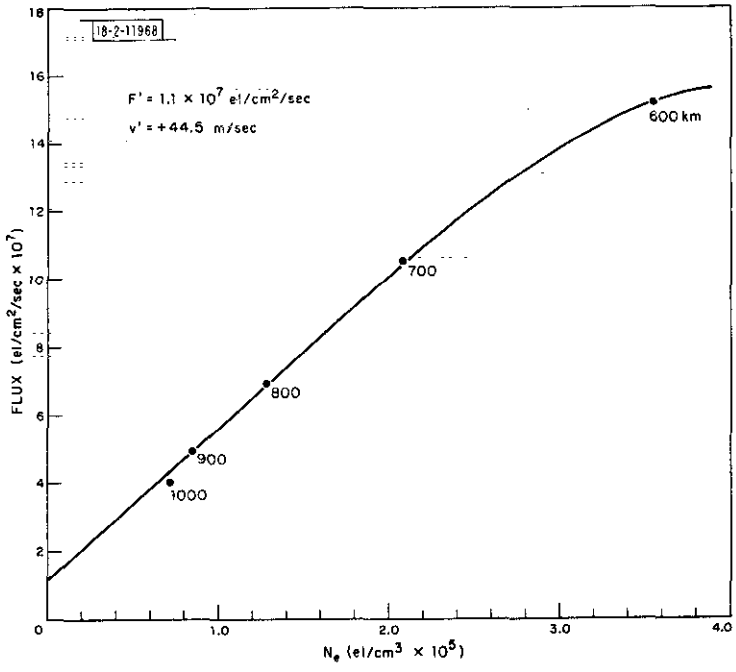

Fig. 13. Plot of observed flux F vs electron density N_e in region of upward flux for 1000-1200 EST on 14-15 August. Slope of line gives magnitude of velocity bias v' required to cause flux to be height-independent over this interval.

Figure 14(a) presents our best estimates of the upward flux after making the above correction in those cases where it was deemed appropriate. It can be seen that the spread in values has been reduced from a factor of 10 (Fig. 12) to a factor of 4. The assumption that the flux should be height-independent may not be strictly correct, in that some loss of O^+ through charge exchange in the region below 1000 km must take place. Thus, it appears that the "corrected" values of Fig. 14(a) are lower limits to the flux. Ignoring the cases in which a corrected flux curve

has been obtained, we get an average value for the escape flux of 5×10^7 el/cm^2/sec, which may be taken as our best estimate of the daytime escape flux during 1969. The average of the transition heights for these cases was 600 km. Adopting a scale height H = 60 km (corresponding approximately to an exospheric temperature of 1000 K), we require the production q at 600 km to be

$$q_{600} = \frac{F'}{H} = 8 \text{ el/cm}^3\text{/sec} \quad . \tag{16}$$

The values of the peak downward flux obtained are shown in Fig. 14(b). Here the scatter remains quite large, but, if the "corrected" points are ignored again, amounts to a factor of 4, and an

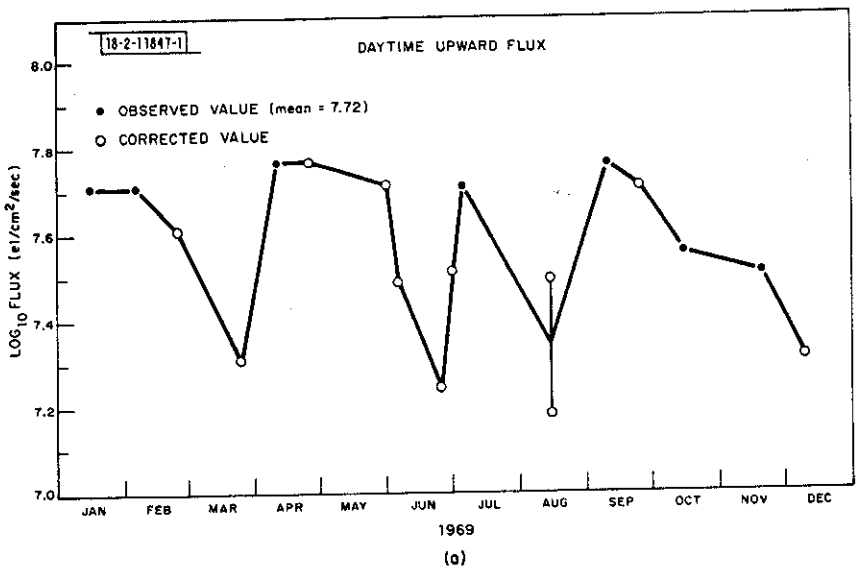

(a)

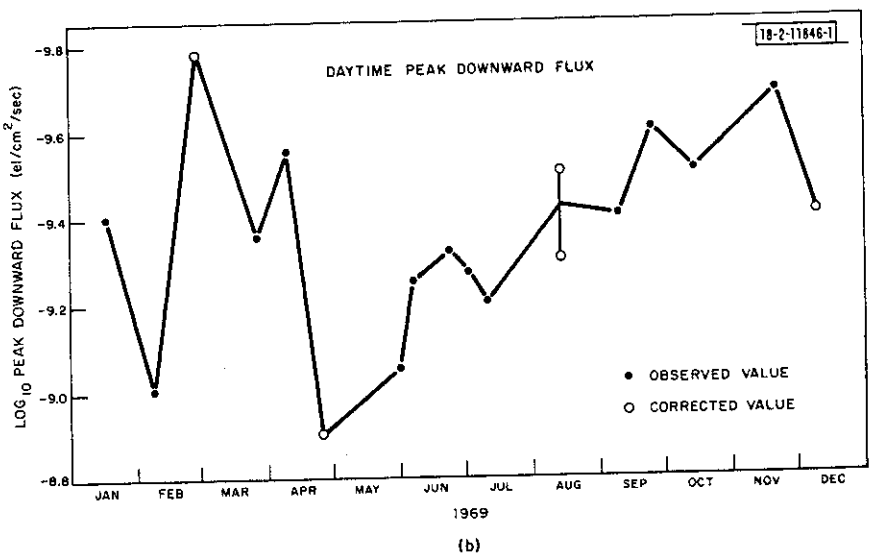

(b)

Fig. 14(a-b). Values of log peak flux obtained from curves of Fig. 11 directly (closed points) or after correction (open points).

TABLE VII

CURVES AVERAGED TO OBTAIN MEAN WINTER AND SUMMER DAYTIME FLUX CURVES

Winter	Summer
16-17 January	23-24 April
5-6 February	30-31 May
14-15 October	5-6 June
20-21 November	1-2 July
8-9 December	9-10 July

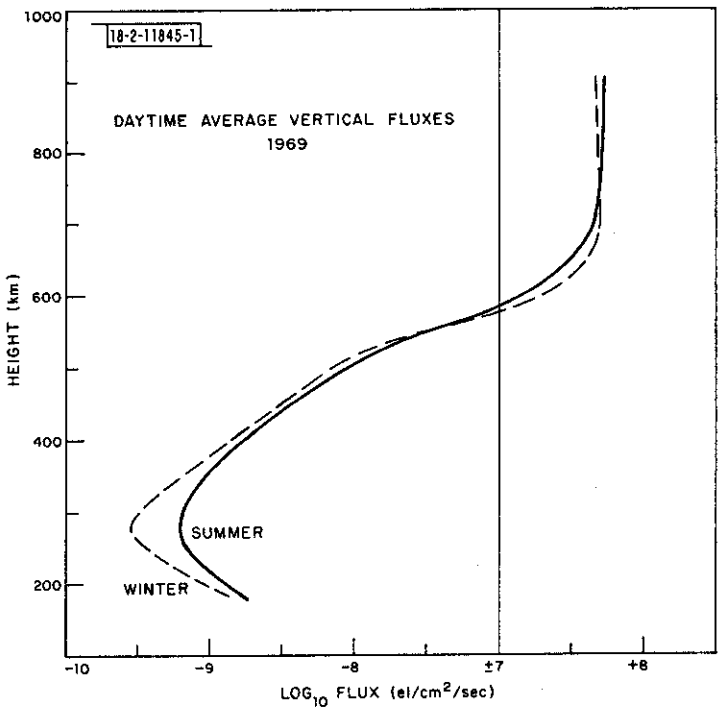

Fig. 15. Average flux curves obtained by taking mean of (uncorrected) curves obtained for five days (Table VII).

average value for the peak downward flux is 2.5×10^9 el/cm^2/sec. The altitude of the peak flux is somewhat variable, but usually lies in the range 250 to 300 km. Above the peak, the log of the flux should decrease linearly over the altitude region of about 350 to 500 km, where production and downward divergence should roughly balance. Extrapolating from this linear region to the 300-km level, we can make an estimate of the flux that would exist there, if loss were negligible (since the peak production lies substantially below this altitude). Adopting this approach, we estimate that the average flux through 300 km in the absence of losses would be 3×10^9 el/cm^2/sec. Employing Eq. (16) and allowing for the escape flux, we obtain

$$q_{300} = 508 \text{ el/cm} \quad . \tag{17}$$

While this appears close to current estimates of F-region production at this level,[58] it is not consistent with the transition altitude of 600 km for the upward flux. Rather, the upward flux must commence in ln(508/8) = 4.15 scale heights above the 300-km level, i.e., at about 550 km. In view of the difficulty in drawing the flux curve through the region where it reverses sign, we do not consider this inconsistency to be serious.

An alternative approach to removing some of the large bias errors in the velocity-vs-altitude curves (Fig. 9) is to average several of the flux curves (Fig. 11). This has been carried out for five "winter" and five "summer" days listed in Table VII, with results that are presented in Fig. 15. The peak upward fluxes appear to be little different from the estimate arrived at above, and the differences between the curves are not considered to be significant. The peak downward flux in winter appears to be twice that observed in summer. This is probably a real effect arising as a result of the greater loss rates during summer. By extrapolating the linear portions of the curves in Fig. 15 between 400 and 500 km down to 300 km we find that in the absence of losses the flux would be $\sim 3 \times 10^9$ el/cm^2/sec in both seasons.

E. Nighttime Flux Results

Vertical flux diagrams similar to those of Fig. 11 were constructed for the nighttime periods listed in Table VI. Except for 29-30 July, when the results appear poor and uncertain, these are shown in Figs. 16(a) through (n). In almost all cases, the flux was found to be downward at all altitudes and resembled the shape of the layer. It is clear from Fig. 9(b) that there can be considerable error in the nighttime fluxes at low altitudes where the drift velocity is small.

Under steady-state conditions, we expect the nighttime F-layer to decay at a rate set by the loss rates pertaining at the altitude of the layer (which, in turn, is governed by the competing processes of downward diffusion under gravity and lifting caused by neutral winds and possibly electric fields). The losses will be offset by O^+ ions created by H^+ diffusing from the protonosphere into the ionosphere. The O^+ ions so created will diffuse downward and should give rise to a flux that is independent of altitude well below the O^+/H^+ transition region. The altitude variation of the flux above 400 to 500 km was observed to be small in only three cases [Figs. 16(b), (m), (n)], and averaging over the interval 600 to 800 km for these three nights we obtain an estimate for this arriving flux of 2×10^7 el/cm^2/sec.

The altitude variation of the flux shown in the remaining plots of Fig. 16 suggests that the layer was descending (as a consequence of loss), i.e., the flux from the magnetosphere was not able to balance the loss at this time (despite the fact that the periods selected for analysis were those when the decay rate appeared small). An alternative explanation is that there was a downward motion due to an eastward electric field. In either case, a large part of the flux observed

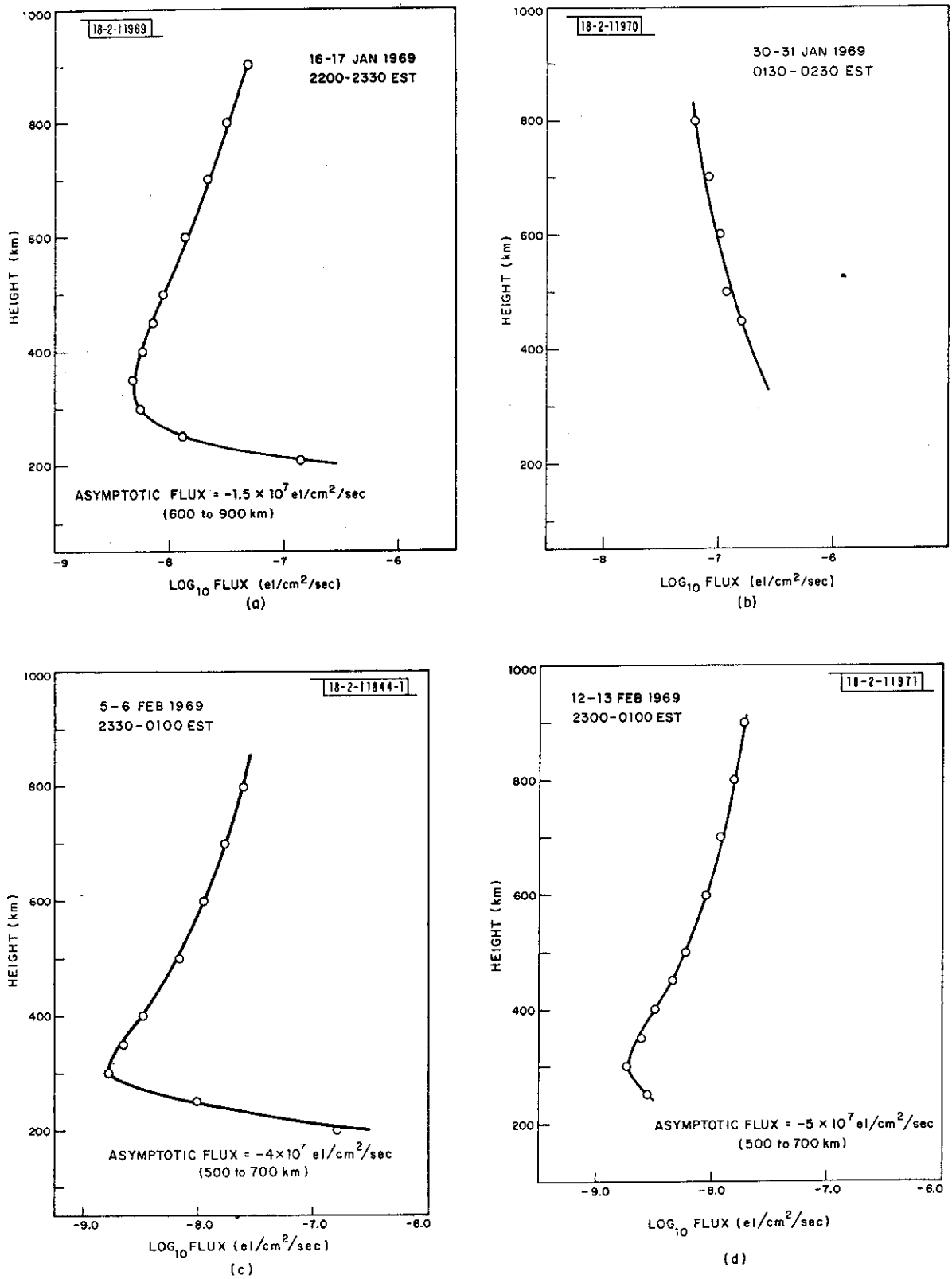

Fig. 16(a-n). Log_{10} vertical flux vs altitude observed for nighttime periods listed in Table VI.

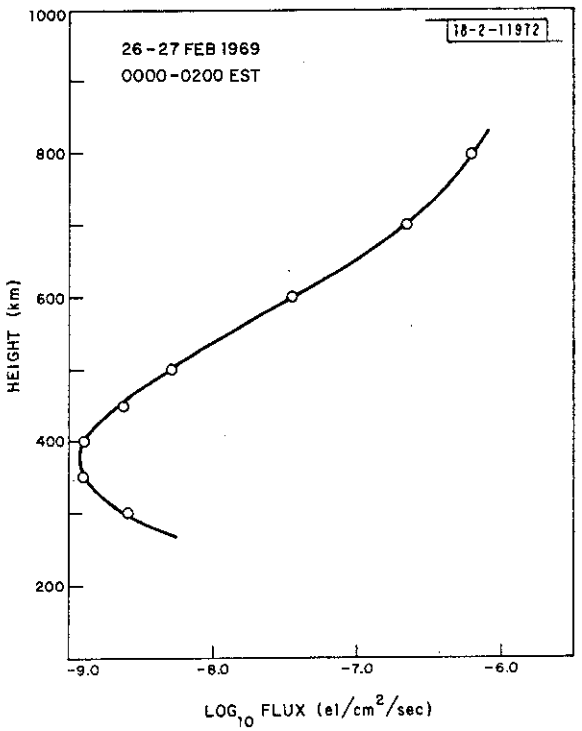

(e)

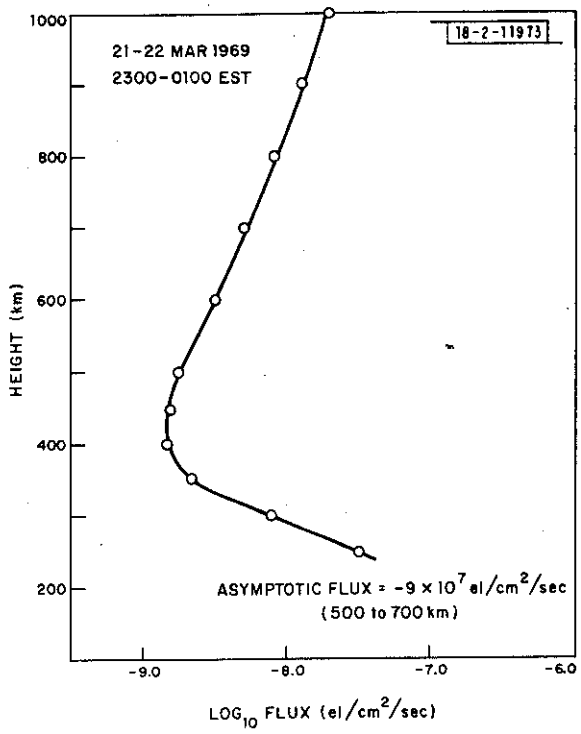

(f)

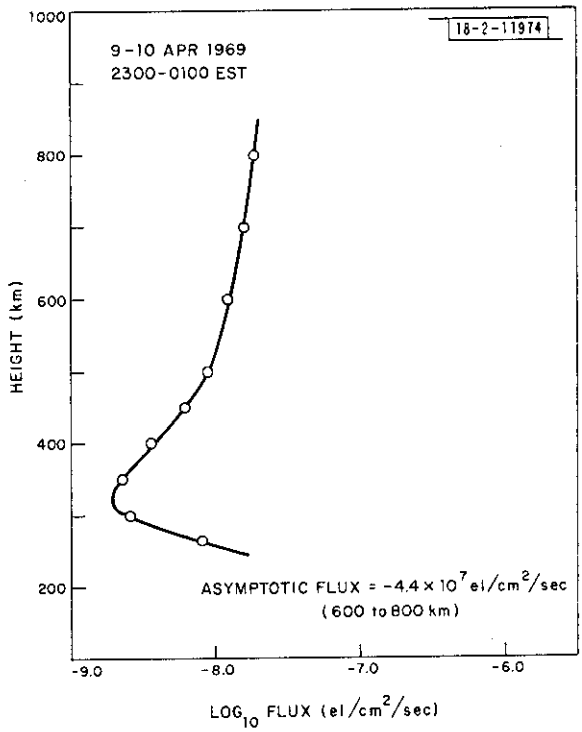

(g)

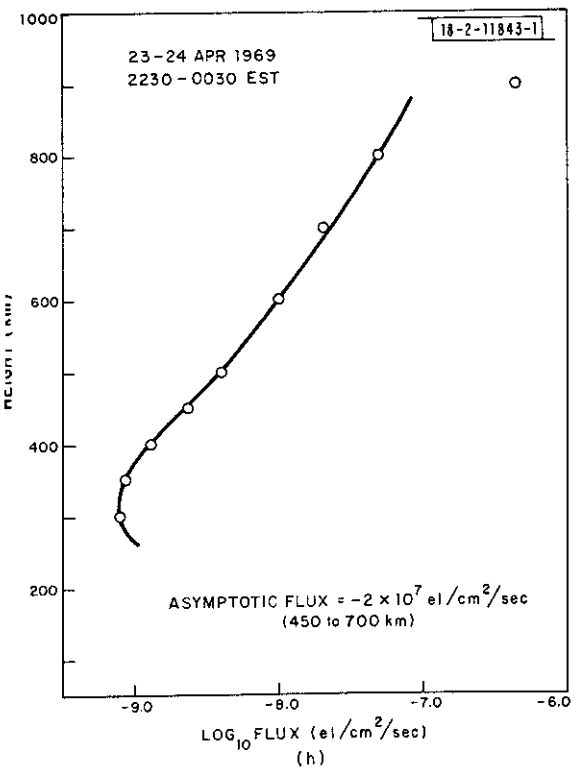

(h)

Fig. 16(a-n). Continued.

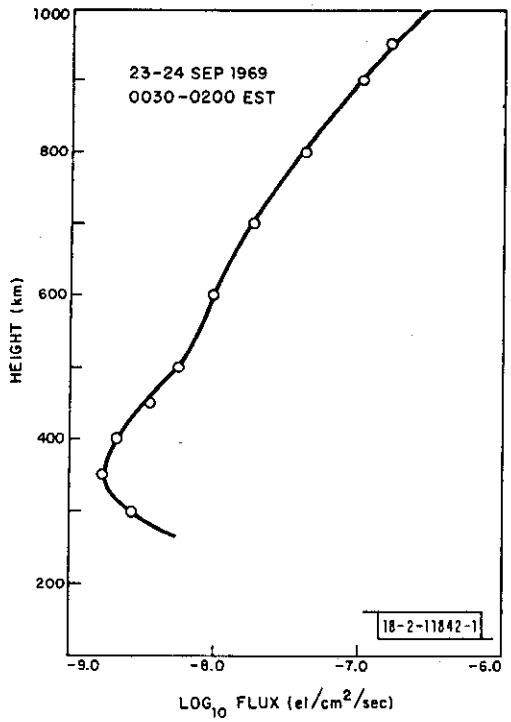

(i)

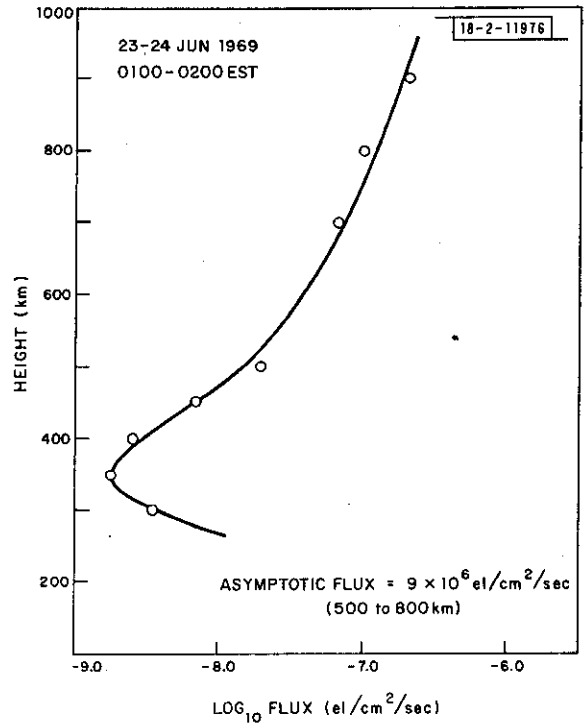

(j)

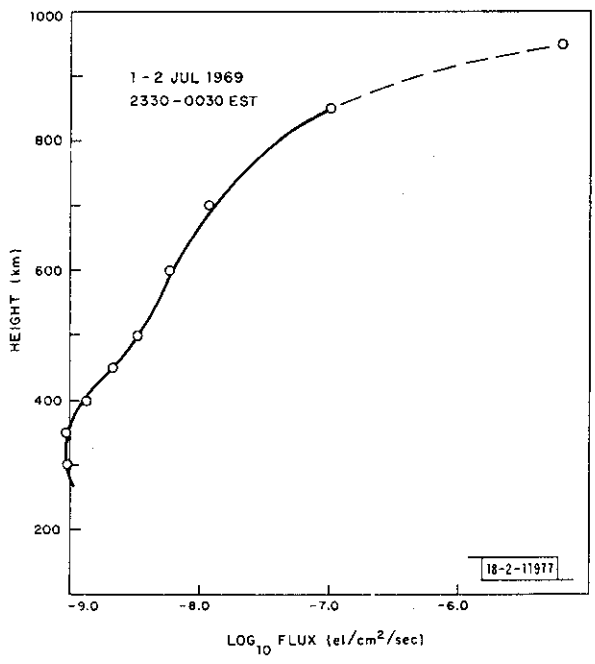

(k)

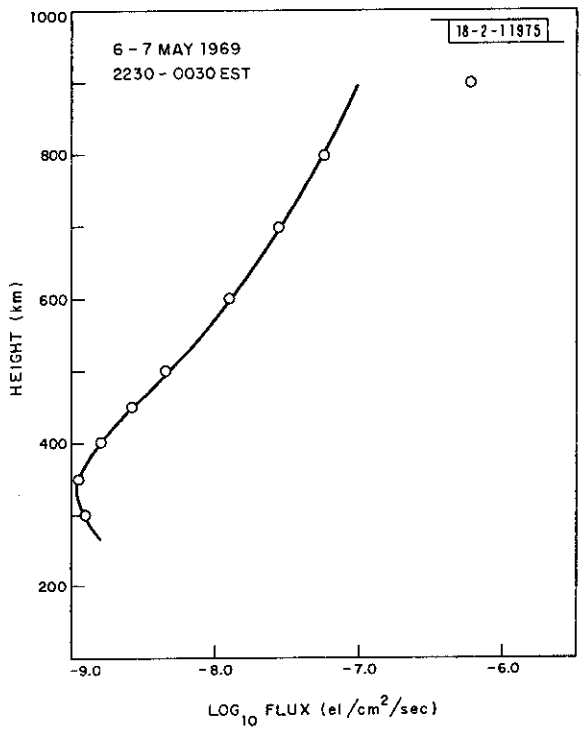

(l)

Fig. 16(a-n). Continued.

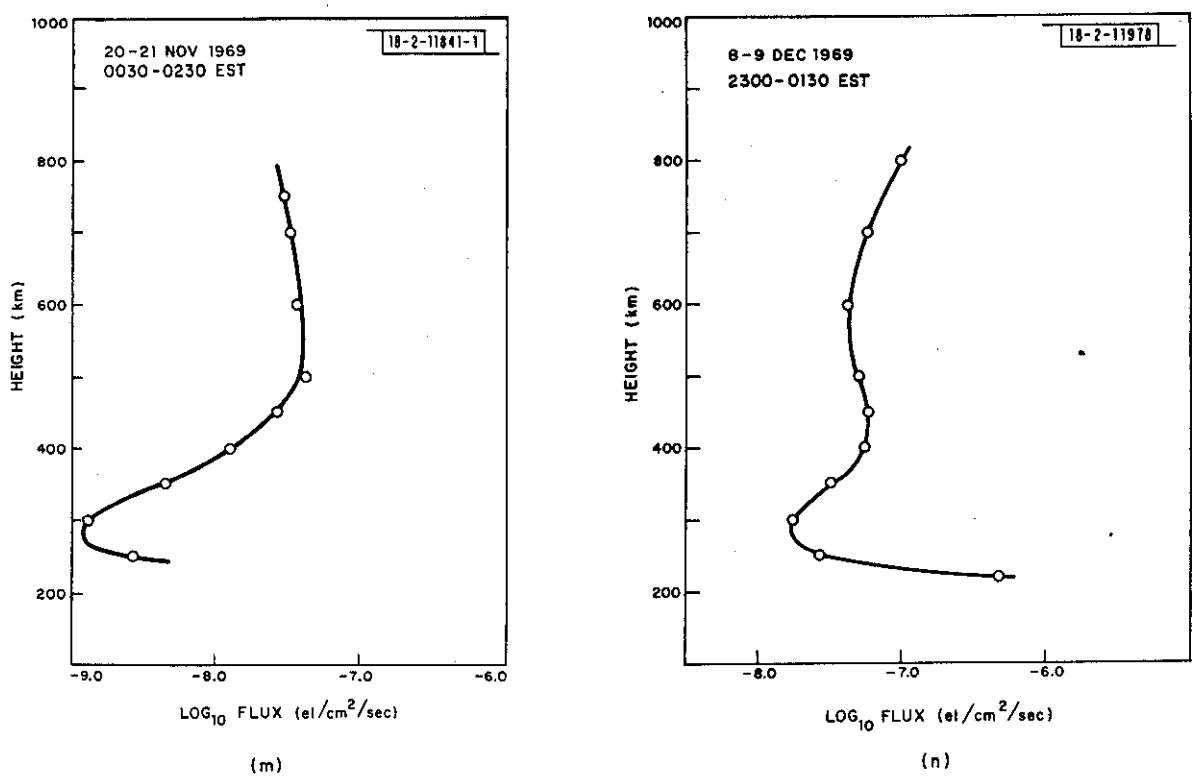

Fig. 16(a-n). Continued.

will be caused by the descent of the layer (with velocity v') so that the observed flux F_{obs} will be given an equation of the form of Eq. (15) where F' is the true flux arriving from the protonosphere. If this is the case, F' can be recovered by plotting F_{obs} vs N_e. However, this must be carried out for the altitude region in which the protonospheric flux is fully established (i.e., below the change-exchange region) and above the region for which losses are important.

Attempts to compute F' from plots of F_{obs} vs N_e for the other nights listed in Table VI lead to sensible values in only six cases (Table VIII). Since the method does not depend upon the layer being stationary, it was applied for a further seven flux diagrams constructed for nights when the layer was clearly descending (Table VIII) and yielded sensible results for five of these. Listed in Table VIII is the height range over which F_{obs} appeared to depend linearly on N_e. In some cases, this was quite restricted, thereby casting some doubt on the validity of the results. An average of the values of F' listed in Table VIII is 3×10^7 el/cm^2/sec. This is close to our other estimate and appears sensible in the light of the escape fluxes found in the daytime. The values for the arriving flux obtained from the two methods are plotted in Fig. 17. We do not believe that the results are sufficiently reliable to permit firm conclusions concerning possible seasonal trends.

The failure of the method of plotting F_{obs} vs N_e to recover a constant flux F' at night in many cases probably stems from a number of causes including: (1) the velocity errors (and hence the flux errors) are larger at night, (2) there is only a limited height interval over which

TABLE VIII

ESTIMATES OF NIGHTTIME PROTONOSPHERIC FLUX

Date (1969)	Nighttime (EST)	F' (el/cm^2/sec)	Linear Range (km)	Comment
16-17 January	2200-2330	-1.5×10^7	600-900	
30-31 January	0130-0230	–	–	
5-6 February	2330-0100	-4×10^7	500-700	
12-13 February	2300-0100	-5×10^7	500-700	
26-27 February	0000-0200	–	–	
21-22 March	2300-0100	-9×10^7	500-700	
25-26 March*	2300-0100	-3.5×10^7	700-900	
9-10 April	2300-0100	-4.4×10^7	600-800	
23-24 April	2230-0030	$+2 \times 10^7$	450-700	Upward flux!
6-7 May	2230-0030	–	–	
30-31 May* 1-2 June*	2300-0100	–	–	Poor velocity profile
5-6 June*	0100-0200	-1.1×10^7	500-900	
23-24 June	0100-0200	-9×10^6	500-800	
1-2 July	2330-0030	–	–	
9-10 July*	2200-0100	-2.4×10^7	500-900	
29-30 July	0000-0130	–	–	Poor velocity profile
14-15 August*	2300-0100	-2.4×10^7	500-700	
9-10 September*	2300-0100	–	–	
23-24 September	0030-0200	–	–	
14-15 October*	2300-0100	1.9×10^7	450-700	
3-4 November	–	–	–	
20-21 November	0030-0230	–	–	
8-9 December	2300-0130	–	–	

* Day added.

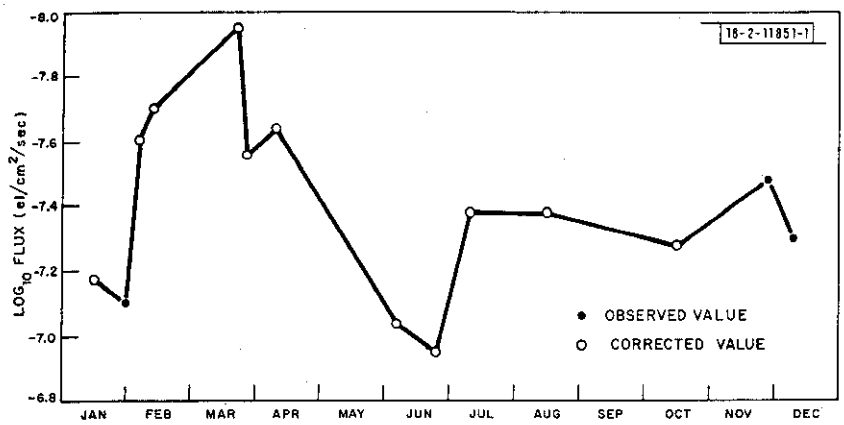

Fig. 17. Plot of nighttime arriving flux vs date for 1969 (Table VIII).

a steady O^+ flux can be expected even when the protonospheric flux is able to balance the loss, and (3) the method depends upon an accurate knowledge of the rate of change of vertical velocity with height, and these changes are smaller by night than by day.

F. Flux Through 650 km

It can be seen in Fig. 11 that the daytime escape flux is usually fully developed by about 650 km altitude, in those cases where the upward flux is height-independent (indicating a stationary layer). Similarly, in Fig. 16 the flux observed near this level is close to the value of the arriving flux when the layer is not moving vertically. Thus, we conclude that under equilibrium conditions the flux through this level provides a useful estimate of the flux being exchanged with the protonosphere. Accordingly, we have computed the flux at this height and plotted this in Figs. 18(a) through (w). The actual estimates were obtained by averaging the velocities observed at 4.5- and 5.0-msec delay and multiplying those by the density at 650 km. The plot for 26-27 February has been omitted from Fig. 18, as the reduced antenna gain brought about by the snow cover (Sec. II-A) appears to have caused the vertical drift velocity estimates to be extremely noisy and unreliable.

The most striking features of Figs. 18(a) through (w) are: (1) the large upward flux established at sunrise by the growth of the layer, (2) the large downward flux set up by the decay of the layer near sunset, and (3) the oscillatory nature of the curves. While many of the fluctuations may be introduced by errors of measurement, it is believed that a significant component is real and a manifestation of the presence of TIDs.[52]

On many days, the transition from upward to downward fluxes appears to occur well before sunset at a time near noon. Thus, the two cases in which the daytime flux was found to go downward at all altitudes [Figs. 11(c) and (r)] appear to be those in which the vertical velocity distribution was computed too late in the day. On some days, the height of the transition from downward to upward flux moved to an altitude above 650 km, e.g., 9-10 April [Fig. 11(f)], 23-24 June [Fig. 11(j)], so that the transition from an upward to a downward flux in Fig. 18 may not mark the exact time at which there ceases to be any escaping flux.

The sunrise onset of the upward flux is usually a readily recognizable feature of the records. These times, adjusted by +14 minutes (to allow for the difference between local and standard time),

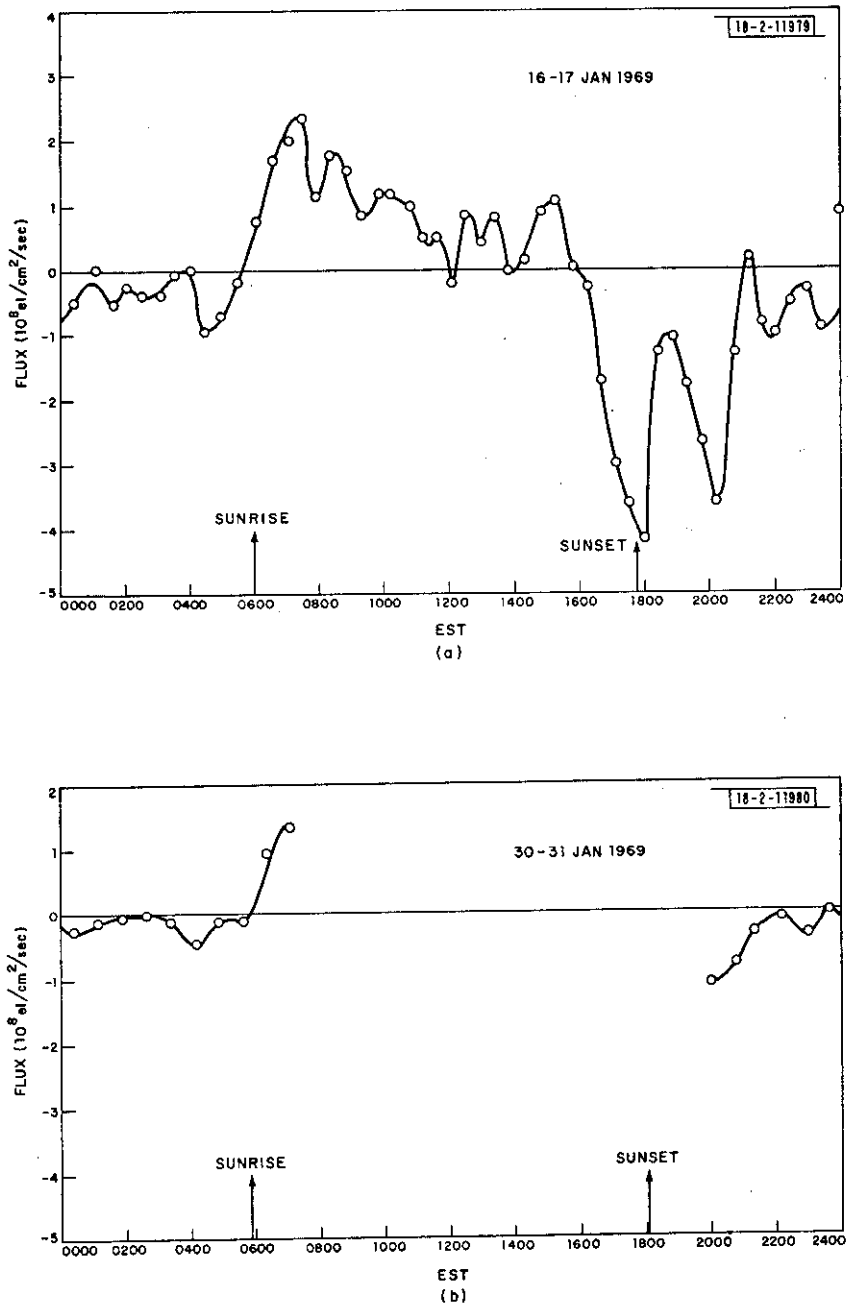

Fig. 18(a-w). Values of $\log_{10}(F)_{650}$, i.e., flux through 650 km for the days listed in Table VI. These are thought to be close to actual protonospheric flux.

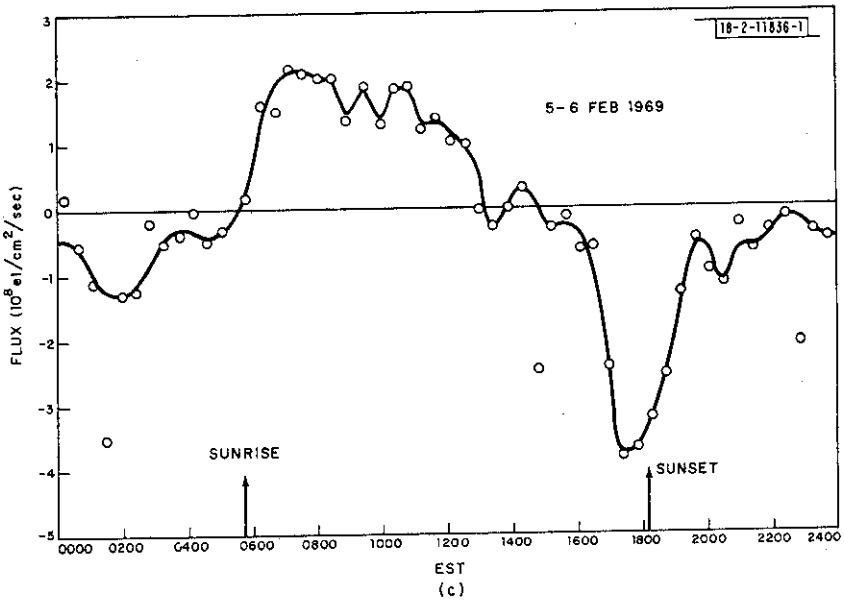

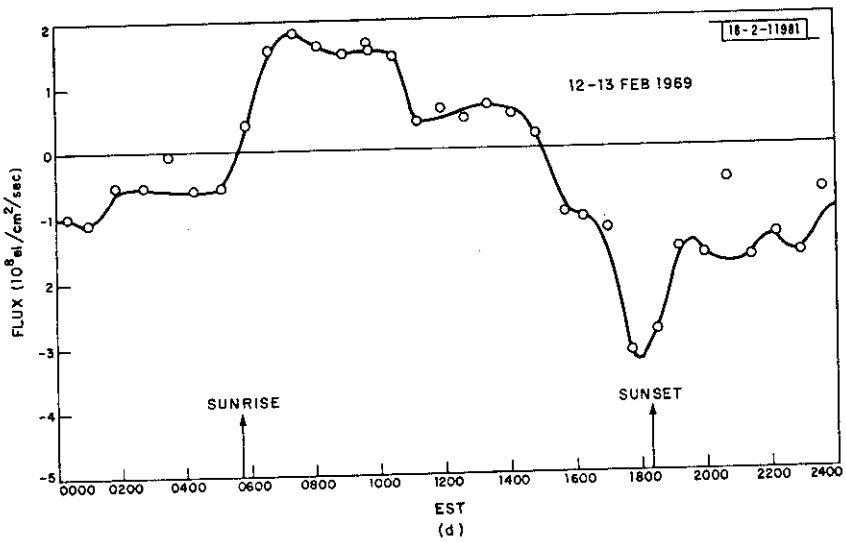

Fig. 18(a-w). Continued.

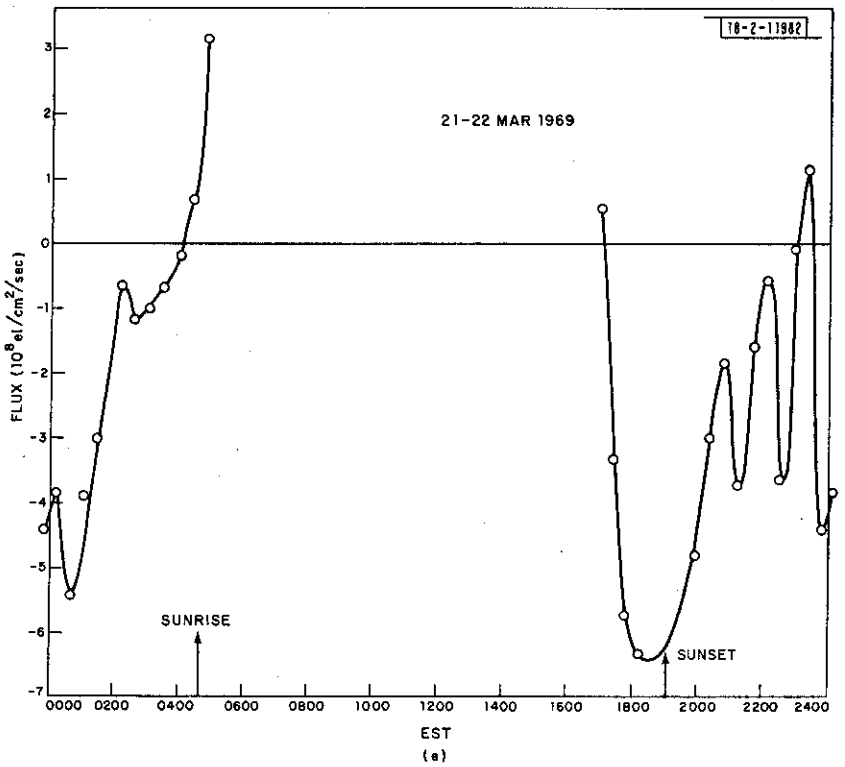

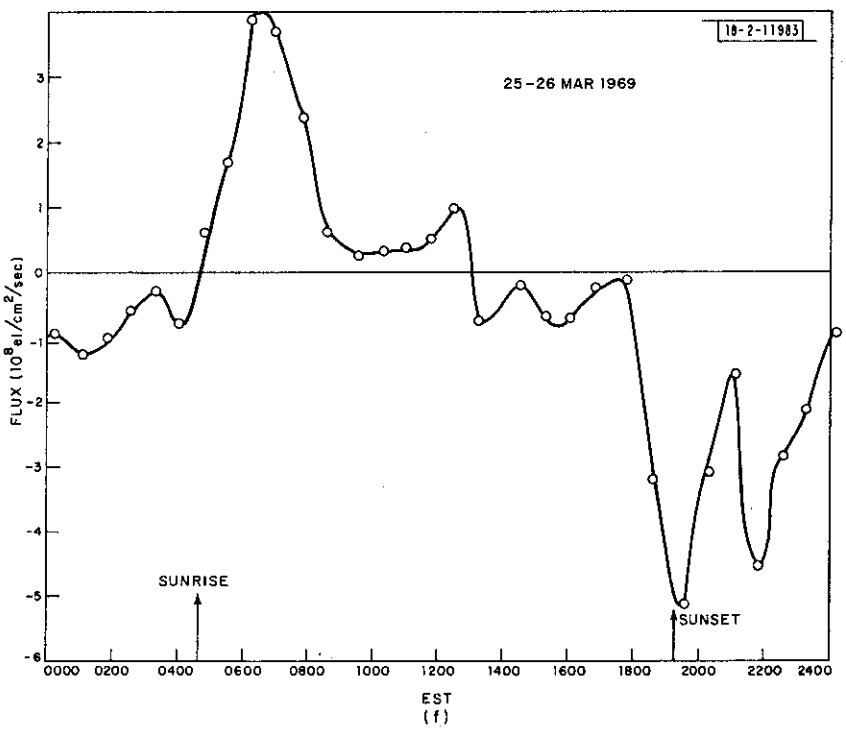

Fig. 18(a-w). Continued.

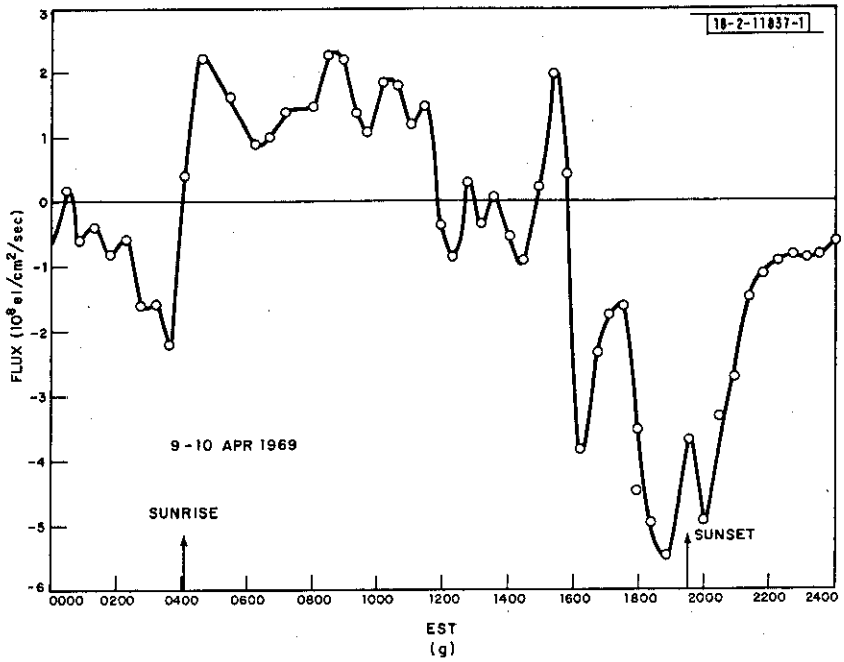

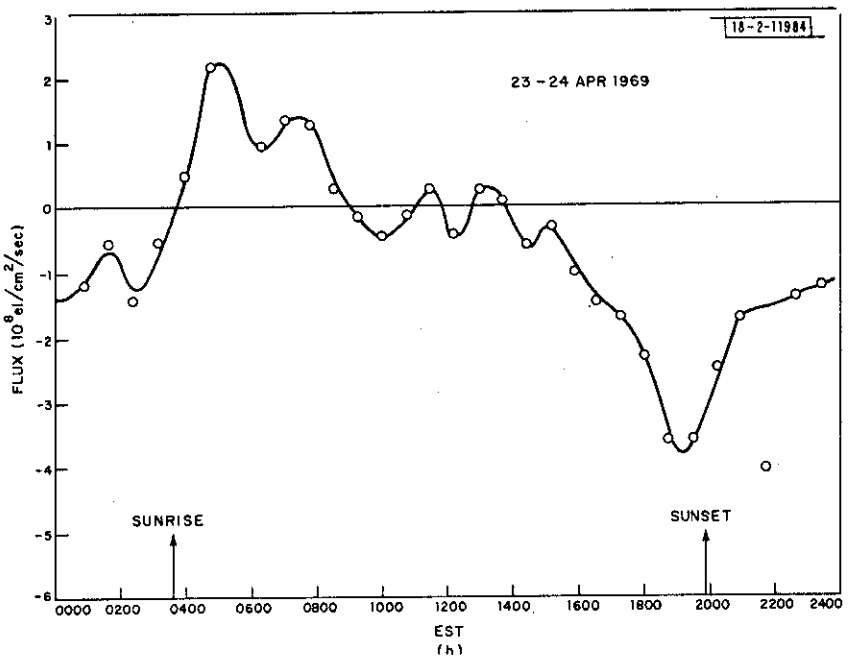

Fig. 18(a-w). Continued.

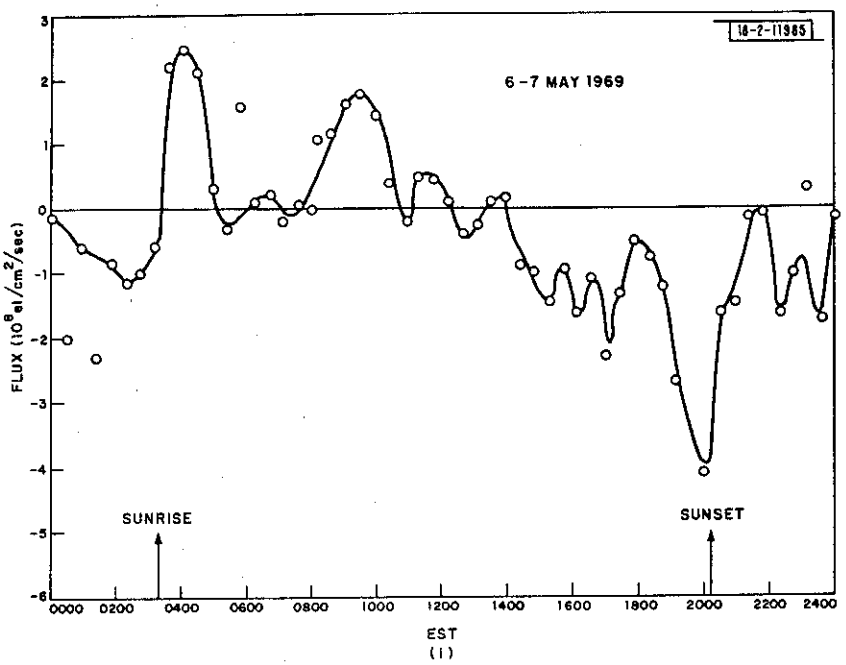

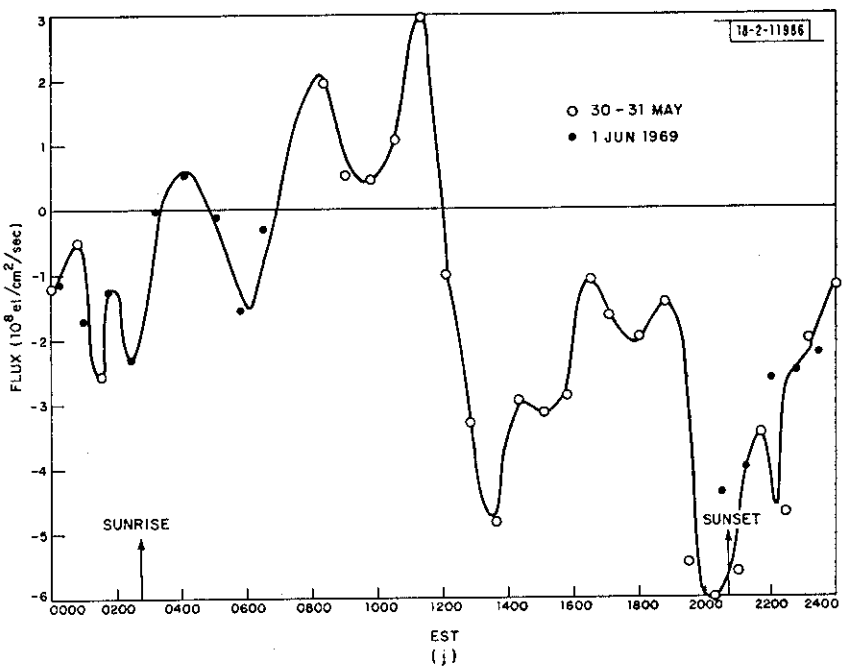

Fig. 18(a-w). Continued.

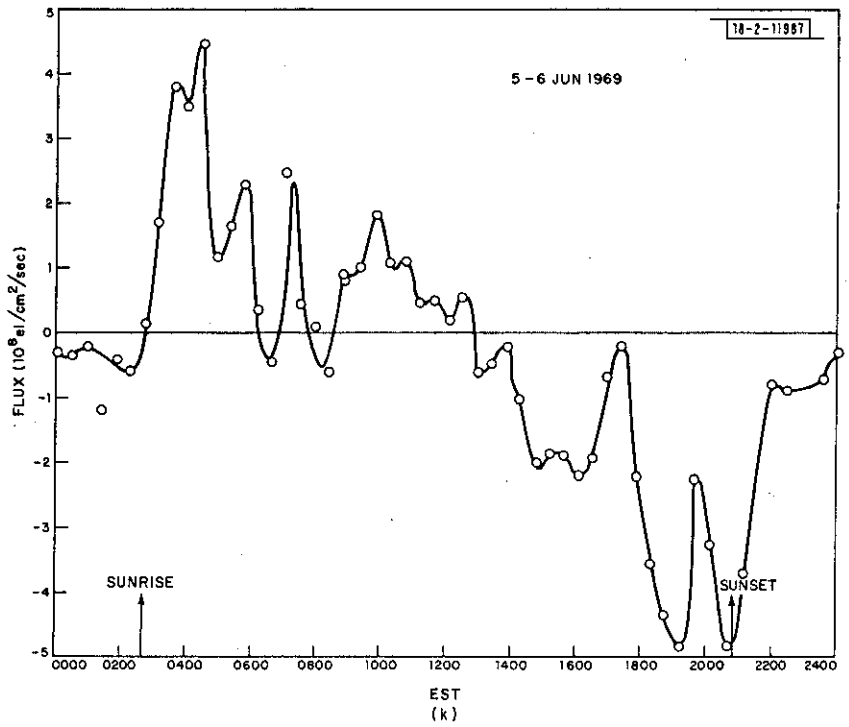

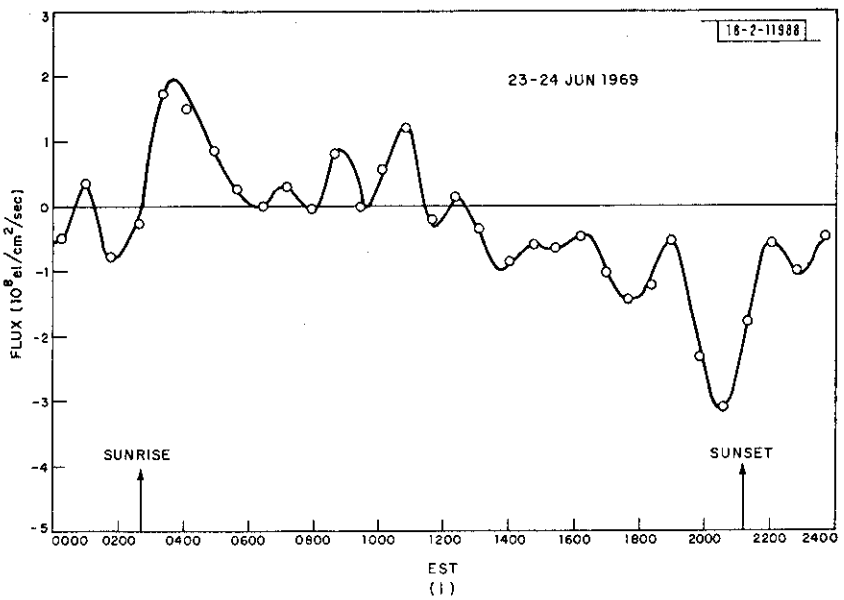

Fig. 18(a-w). Continued.

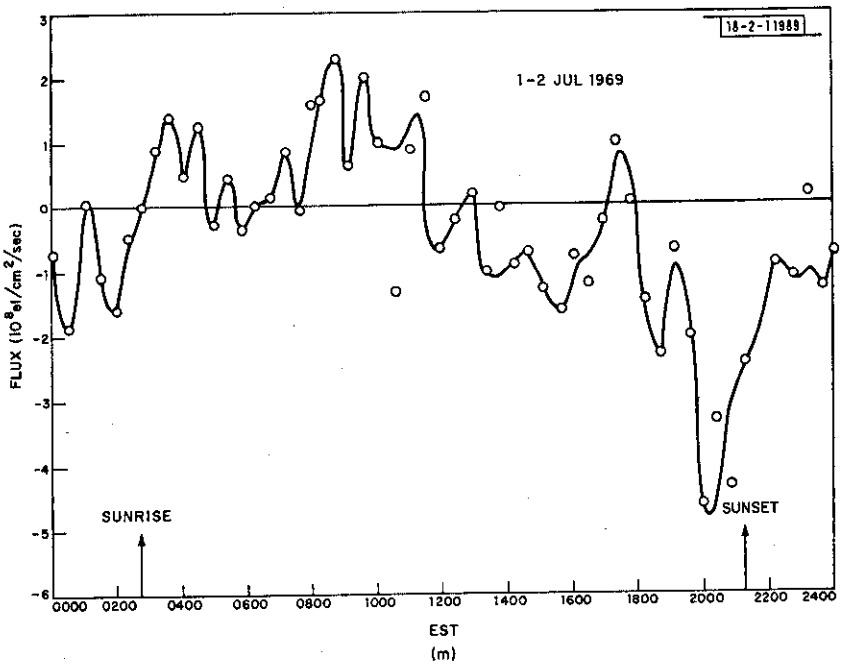

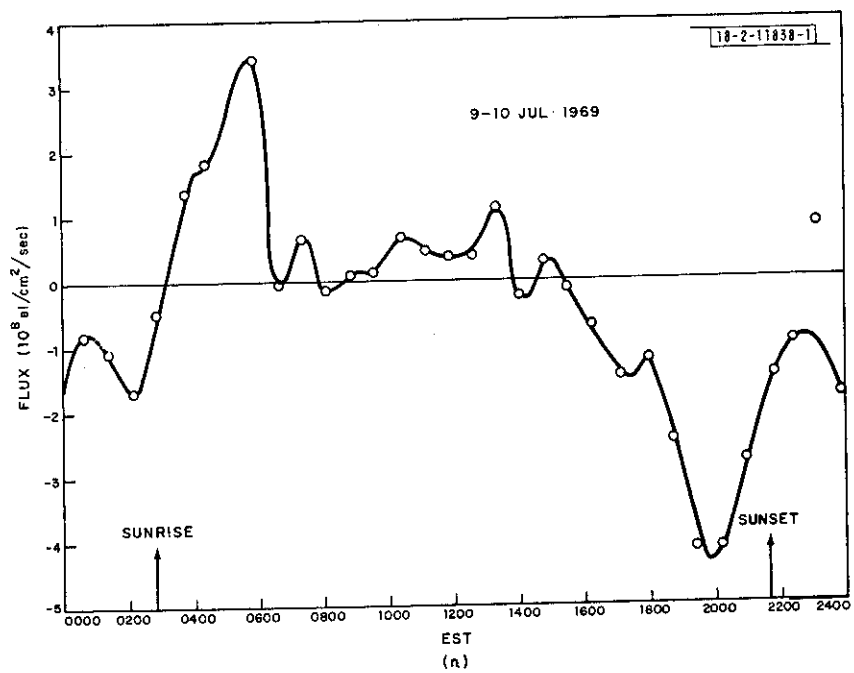

Fig. 18(a-w). Continued.

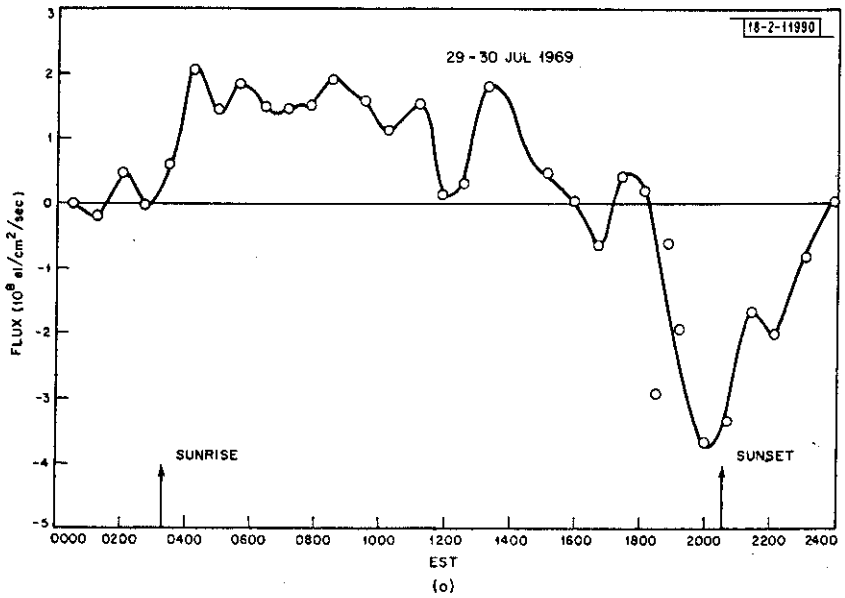

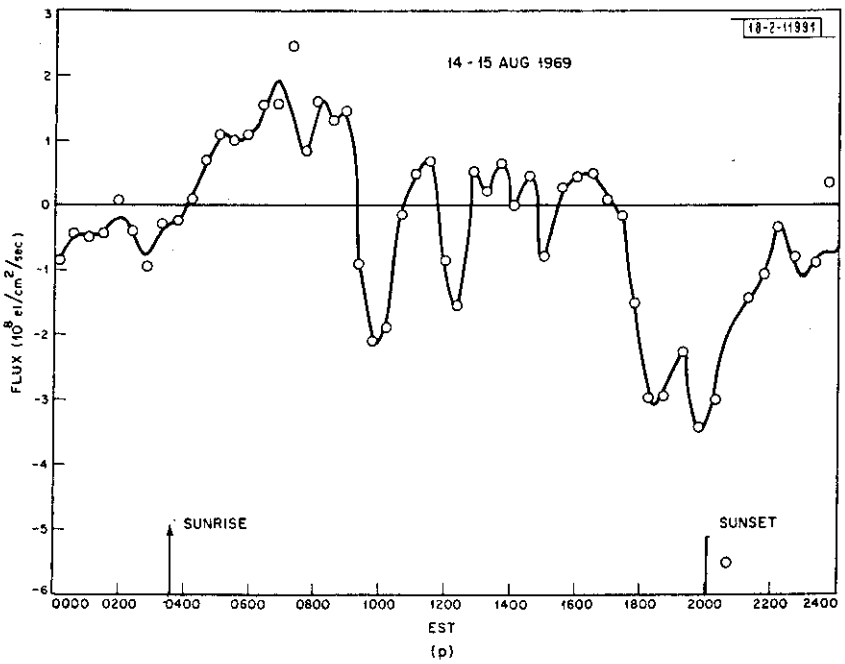

Fig. 18(a-w). Continued.

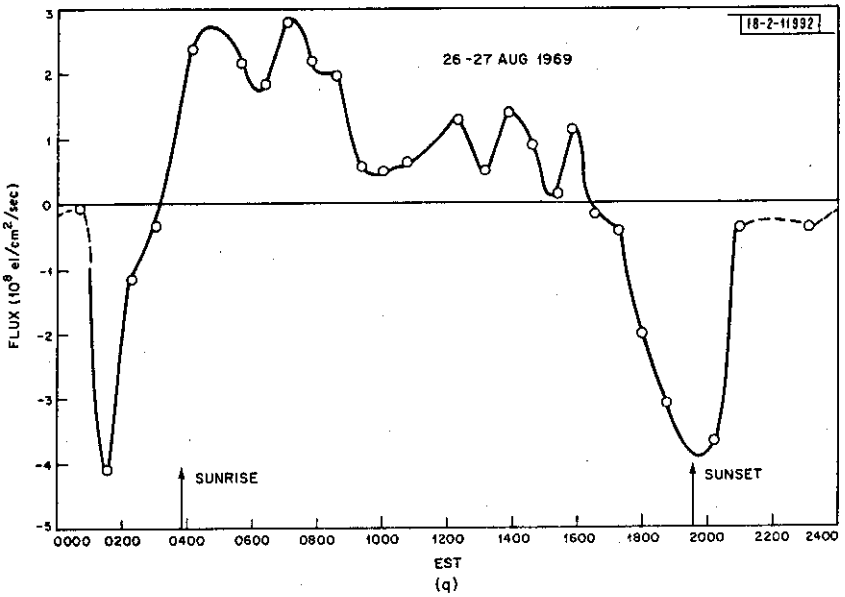

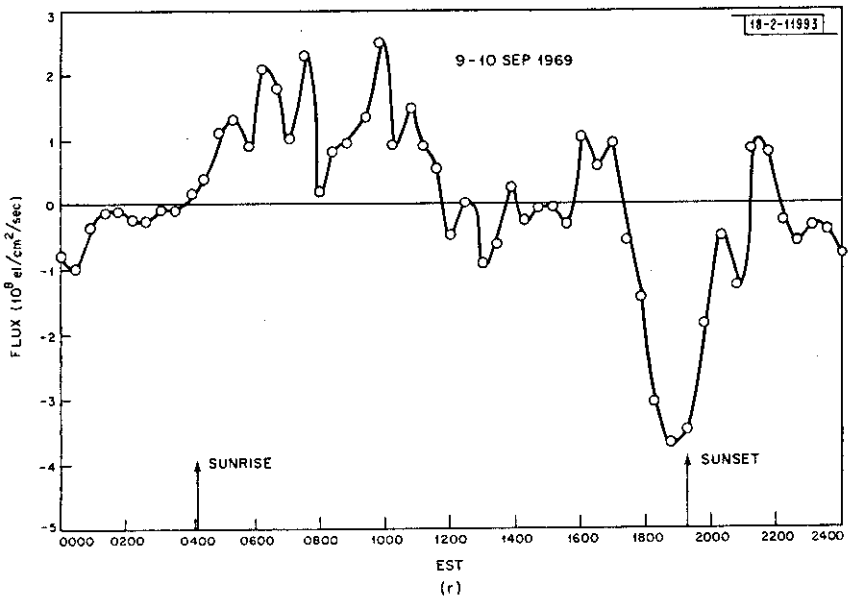

Fig. 18(a-w). Continued.

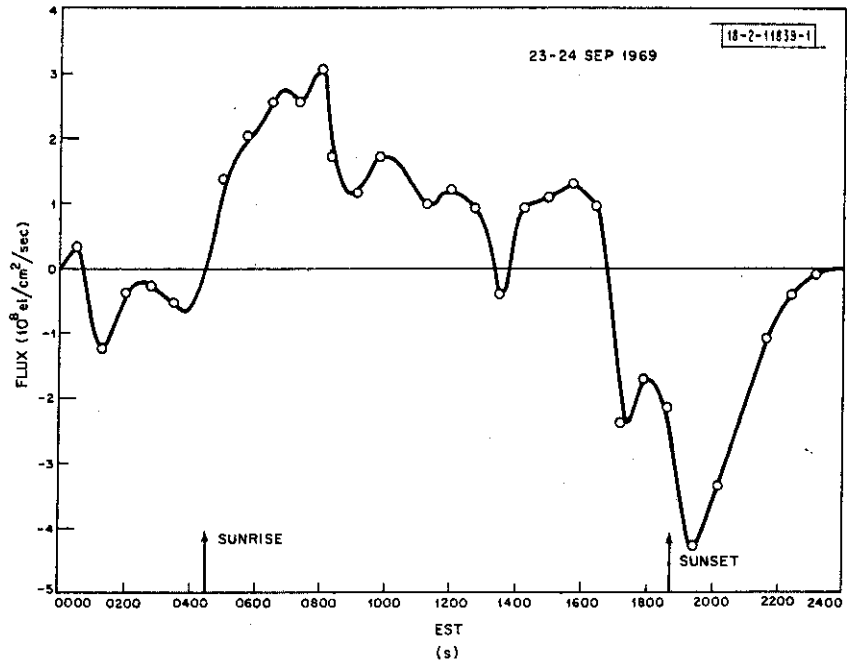

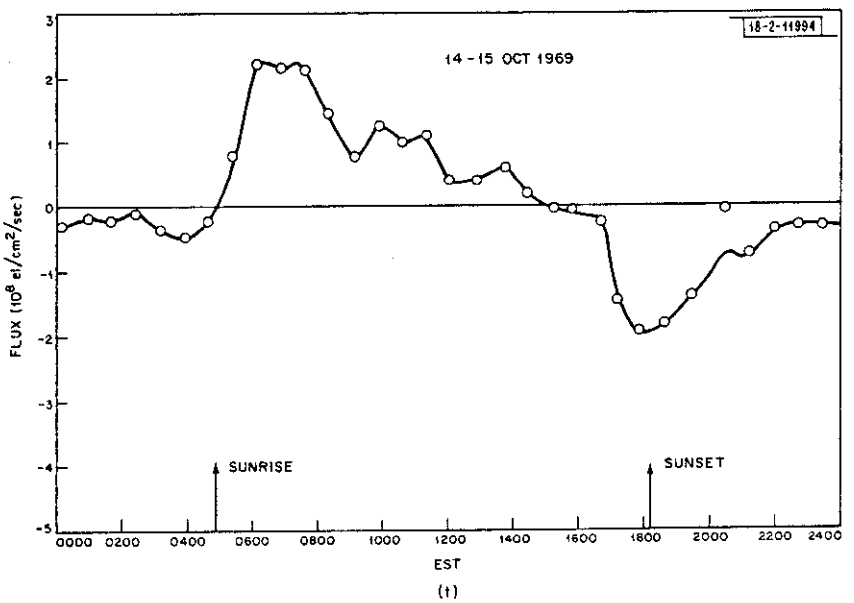

Fig. 18(a-w). Continued.

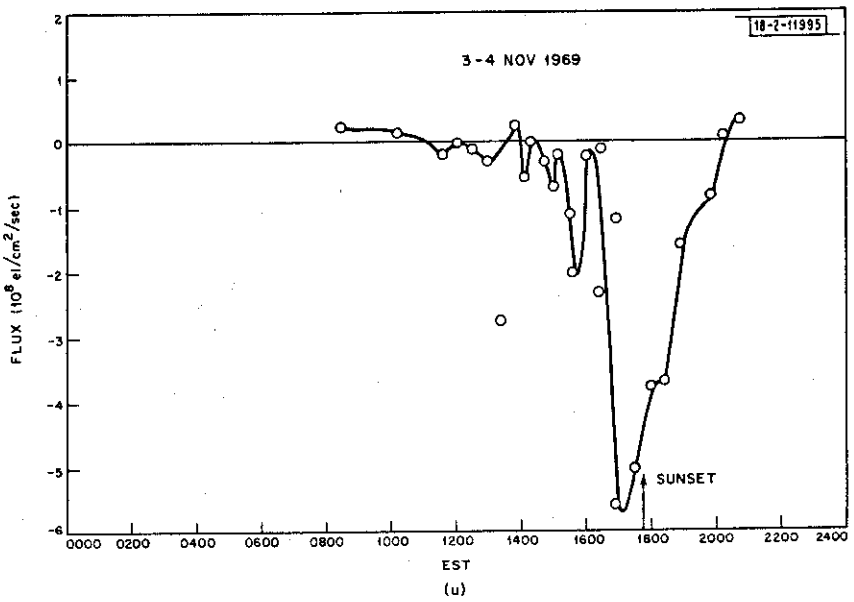

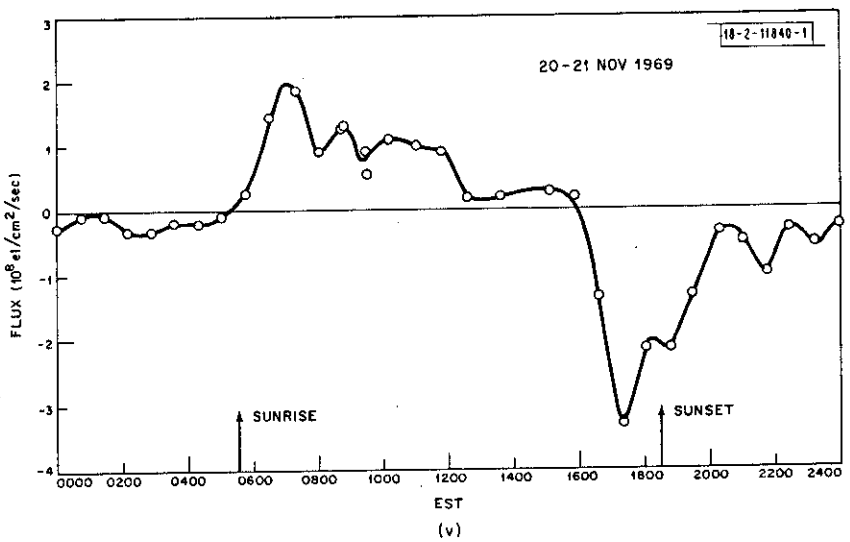

Fig. 18(a-w). Continued.

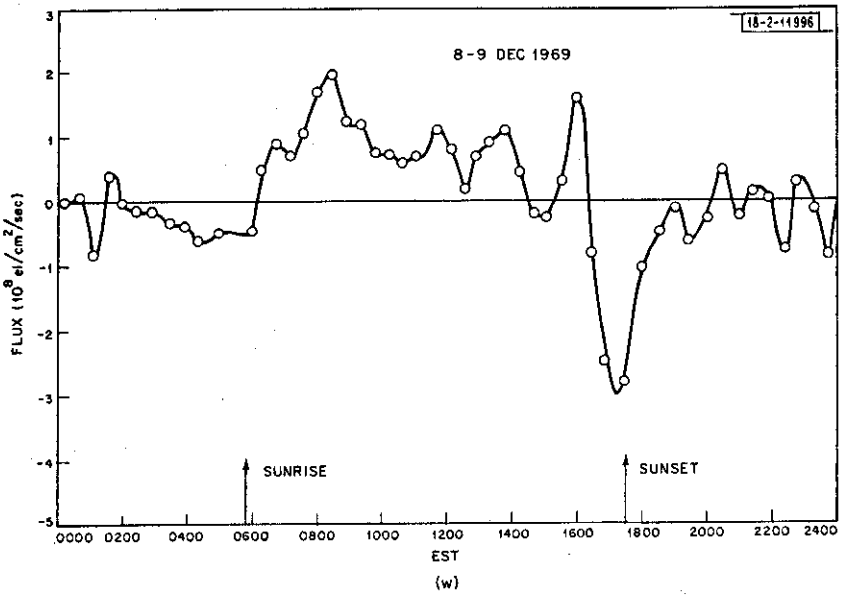

Fig. 18(a-w). Continued.

are plotted in Fig. 19 where they are superimposed on curves indicating the times of sunrise at 0, 100, 200, and 300 km (Ref. 59) for 42° latitude. It is clear from this plot that the onset time coincides closely with the time of sunrise at 200 km altitude. Accordingly, the 200-km sunrise and sunset times have been indicated in Fig. 18. It is striking that the large downward flux observed at sunset usually begins 1 to 3 hours prior to the sunset time and peaks at or slightly before the 200-km sunset. The onset of this downward flux is thought to be caused by the decay of

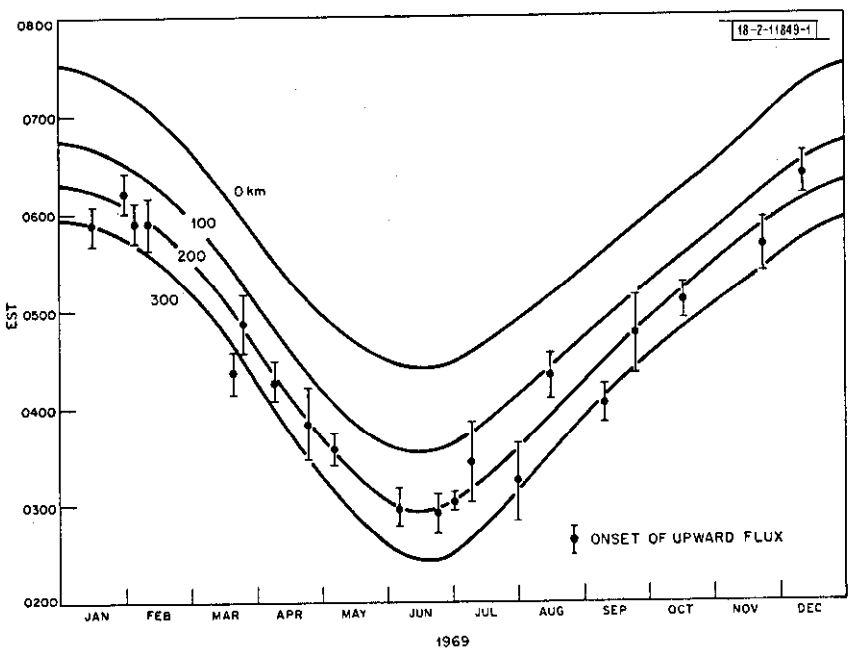

Fig. 19. Times of onset of upward flux (Fig. 18) compared with sunrise in ionosphere at different altitudes.

the F-layer during the afternoon.[30] At sunset, the temperature of the plasma decreases, leading to a thermal collapse of the layer.[30] Sometime the two effects appear to give separate peaks in the downward flux.

Large increases in the downward flux (e.g., rising to 5×10^8 el/cm^2/sec) during winter nights, that could give rise to the observed increases in N_{max},[36] do not appear to occur, thus leaving open the source of this ionization.

VI. SUMMARY

Incoherent scatter data on F-region electron densities, electron and ion temperatures, and vertical velocity have been gathered for periods of 24 hours at a time at the Millstone Hill radar (42.6°N, 71.5°W) approximately twice per month throughout 1969 (Table II). The results span the altitude interval 200 to 900 km, approximately, with a height resolution of 15 km in electron density (near the peak of the layer) and 75 km in the other parameters. The time resolution for a complete altitude profile was either 30 or 45 minutes, depending upon which of two operating modes was employed (Table V). The data-collection and reduction methods have been described in a previous report.[20]

Contour diagrams were constructed showing the variation vs height and time of electron density N_e [Figs. 3(a) through (z)], electron temperature T_e [Figs. 7(a) through (z)], and ion temperature T_i [Figs. 8(a) through (z)]. The electron density exhibits a characteristic winter and summer behavior with a rapid transition between the two (in 1969) around the beginning of the months of April and October. Two cases of auroral precipitation were encountered during the year, when very high F-region electron temperatures were observed and the valley region between the E- and F-regions was filled in.

We have attempted to identify periods near noon and midnight when the F-layer appeared stable and stationary (Table VI), and have constructed curves showing the altitude variation of vertical flux for these times. The character of many of the curves obtained near noon suggests that significant motions of the entire layer and/or instrumental biases in the results were present. By assuming that the escape flux should be altitude-independent above about 700 km, a corrected flux profile could be obtained, and an average value for the escaping flux appears to be 5×10^7 el/cm^2/sec. From the downward-going flux, the production rate at 300 km was deduced to be 500 el/cm^3/sec. The nighttime flux curves show a downward flux at all altitudes with a peak (of very uncertain magnitude) near the peak of the layer. Owing to the greater uncertainties in the data, it is difficult to establish the true protonospheric flux, but the best estimate appears to be half that for the daytime escape flux. The flux through the level 650 km shows that large upward fluxes are established soon after 200 km altitude ionospheric sunrise. Downward fluxes exist for a period after noon when the layer begins to decay until late at night. Large increases of the downward flux that would account for the winter nighttime increases of the F-layer were not seen.

APPENDIX

I. INTRODUCTION

It is possible to calculate from first principles the approximate value of the frequency offset produced in the UHF transmitter. This Appendix outlines the method.

Figure A-1 shows a section through the klystron amplifier. A beam of electrons given off by a cathode is accelerated through a potential V volts and then traverses a drift tube until it impinges on a grounded collector. The beam is kept in focus by an axial magnetic field produced by field coils around the klystron. The velocity of the beam is modulated by the RF field across the gap in the input cavity. The degree of "bunching" of the electrons in the beam increases with distance along the beam so that a much larger RF field can be excited across the gap in the

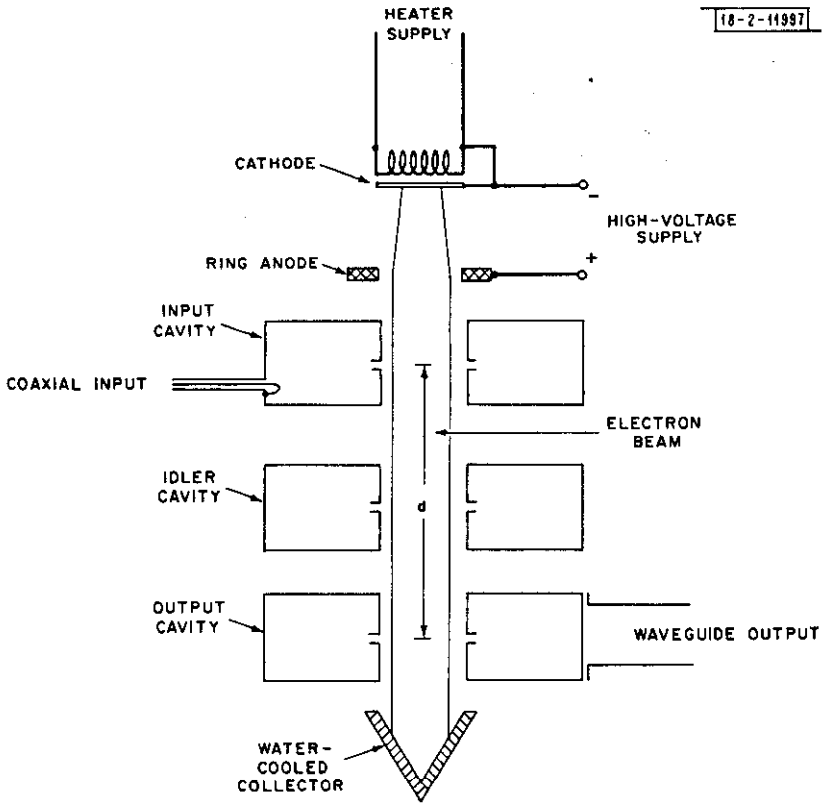

Fig. A-1. Cross section of klystron amplifier tube.

output cavity, the energy being gained at the expense of the energy in the beam. (In the klystrons used at Millstone, only about 30 percent of the beam energy is extracted and the remainder ends up heating the water that cools the collector.) The idler cavity serves to improve the bunching and hence the efficiency of the device.

II. PHASE SHIFT IN THE KLYSTRON

The time interval τ required for the electrons to traverse the distance d between input and output cavities introduces a fixed phase difference φ between the input and output signals.

Hence

$$\varphi = 2\pi f \tau \text{ rad} \tag{A-1}$$

where f is the radar frequency (440 MHz). The time interval τ is given by

$$\tau = d/v_e \text{ sec} \tag{A-2}$$

where v_e is the electron velocity. We can compute v_e knowing that the electron has fallen through a voltage V from

$$\text{electron energy} = 1/2\ m_e(v_e)^2 = eV$$

whence

$$v_e = \left(\frac{2eV}{m_e}\right)^{1/2} . \tag{A-3}$$

Combining Eqs. (A-1), (A-2), and (A-3), we have

$$\varphi = 2\pi f d \sqrt{\frac{m_e}{2eV}} \text{ rad} . \tag{A-4}$$

Scaling the drawing of the X626AC klystron, we find d = 108 cm. Since 1 eV = 1.60×10^{-12} ergs and $m_e = 9.108 \times 10^{-28}$ g, we have

$$\varphi = 2\pi \times \frac{801.7}{\sqrt{V}} \text{ rad} \tag{A-5}$$

where V is the klystron voltage.

III. VOLTAGE DROP DURING THE PULSE

Although the current I through the klystron varies with the applied voltage V, for the small voltage drop occurring during a pulse, we may assume that it is constant. Hence, the rate of change of applied voltage is

$$\frac{dV}{dt} = I/C . \tag{A-6}$$

Here, C is the capacity of the condenser bank (24 μF) and I is the current during a pulse. The fall in voltage during the pulse causes the phase shift φ during the pulse to change at a rate given [from Eq. (A-5)] in

$$\frac{d\varphi}{dt} = -2\pi\ 801.7\ \frac{1}{2V^{3/2}}\ \frac{dV}{dt} \text{ rad/sec} . \tag{A-7}$$

IV. FREQUENCY SHIFT

A constant rate of change of the phase difference corresponds to a frequency shift Δf that is given by

$$\Delta f = \frac{1}{2\pi}\ \frac{d\varphi}{dt} \text{ Hz}$$

$$= \frac{-801.7}{2} \cdot \frac{1}{V^{3/2}} \cdot \frac{dV}{dt} \text{ Hz} . \tag{A-8}$$

Substituting for dV/dt [Eq. (A-6)], we obtain

$$\Delta f = \frac{-400.8\ I}{CV^{3/2}}\ \text{Hz}$$

$$= \frac{-1.67 \times 10^{7}\ I}{V^{3/2}}\ \text{Hz} \qquad \text{(A-9)}$$

V. CURRENT READING

As shown in Fig. A-2, the current through the klystrons is read by a meter which measures only the average current I_{av}. The actual current waveform through the meter is shown in Fig. A-3(a) where t represents the interpulse period (13.0 msec for B-mode, 20.0 msec for

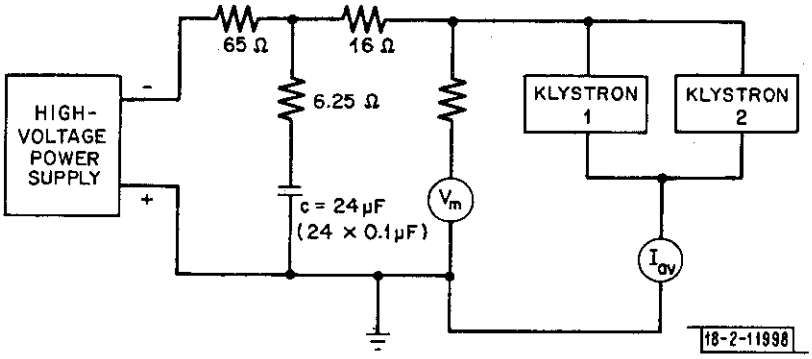

Fig. A-2. Diagram of power supply components.

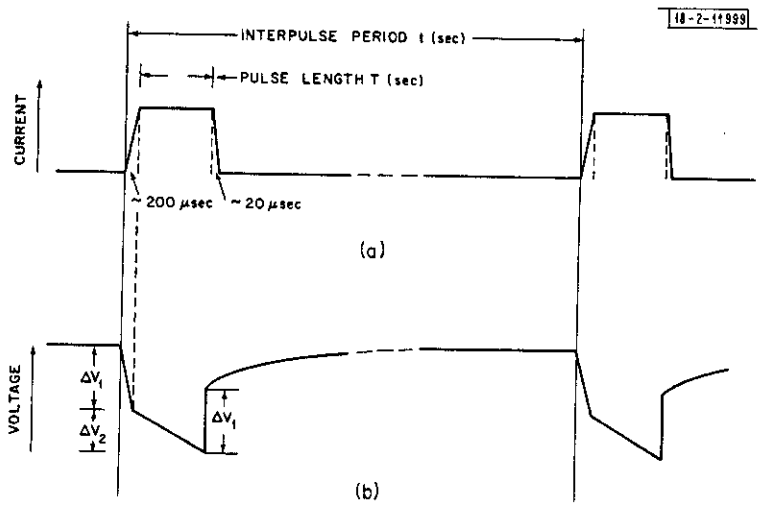

Fig. A-3. Waveforms for current and voltage applied to klystrons: (a) current, (b) voltage.

C-mode) and T is the modulator pulse length (1.0 msec for C-mode). It is clear that the average and peak currents are related through

$$I = FI_{av} \qquad \text{(A-10)}$$

where F is a duty factor equal to 18.0 in the C-mode. The modulator pulse length is adjusted in the B-mode to keep the average current constant. This requires a modulator pulse length T = 0.61 msec. Thus,

$$F = 18.0 \text{ B-, C-mode} \quad . \tag{A-11}$$

Thus, the frequency shift may be written

$$\Delta f = \frac{-1.67 \times 10^{7} \, FI_{av}}{V^{3/2}} \quad . \tag{A-12}$$

VI. VOLTAGE READING

The voltmeter employed to measure the voltage applied to the klystron (Fig. A-2) will have a voltage waveform of the form shown in Fig. A-3(b). As current is drawn through the klystron, there will be a voltage drop through the two resistors that connect the klystrons to the condenser bank of

$$\Delta V_1 = 22.5 \, FI_{av} \text{ volts} \quad . \tag{A-13}$$

There will be a further voltage drop during the pulse of

$$\Delta V_2 = \frac{dV}{dt} \times T \text{ volts}$$

$$= \frac{FI_{av}}{24 \times 10^{-6}} \text{ volts} \quad . \tag{A-14}$$

At the end of the pulse, the voltmeter will again see the full voltage applied to the condenser C. This will recover to its former value as it is charged through the 65- and 6.25-ohm resistors with a time constant

$$\tau = (65 + 6.25) \, C$$

$$= 1.71 \times 10^{-3} \text{ sec} \quad . \tag{A-15}$$

Thus, the voltmeter reads a value V_m which is less than the voltage V' on the condenser bank by an amount

$$V' - V_m = \frac{1}{t} I_{av} F \left[22.5(T + 10^{-4}) + 2.08 \times 10 \, T(T + 1.71 \times 10^{-3})\right] \quad . \tag{A-16}$$

Hence,

$$V' - (V_m)_B = 3.49 \, I_{av} F = 62.9 \, I_{av} \text{ volts} \tag{A-17a}$$

$$V' - (V_m)_C = 4.05 \, I_{av} F = 72.9 \, I_{av} \text{ volts} \quad . \tag{A-17b}$$

The voltage V applied to the klystrons during the pulse is also less than that on the condenser bank V' by an amount

$$V' - V \approx \Delta V_1 + \frac{\Delta V_2}{2} = FI_{av}\,[22.5 + 2.08 \times 10^4 T] \qquad \text{(A-18)}$$

$$V' - V_B = 633\ I_{av} \text{ volts} \qquad \text{(A-19a)}$$

$$V' - V_C = 779\ I_{av} \text{ volts} \quad . \qquad \text{(A-19b)}$$

It follows that, during the pulse, the voltage applied to the klystrons will be the amount given on the meter less ~570 I_{av} volts for the B-mode and ~700 I_{av} volts in C-mode. Thus, Eq. (A-13) may be written

$$\Delta f_B = \frac{3 \times 10^8\ I_{av}}{(V_m - 570\ I_{av})^{3/2}} \text{ Hz} \qquad \text{(A-20a)}$$

$$\Delta f_C = \frac{3 \times 10^8\ I_{av}}{(V_m - 700\ I_{av})^{3/2}} \text{ Hz} \quad . \qquad \text{(A-20b)}$$

The corresponding velocity errors Δw are

$$\Delta w = \frac{\Delta f \lambda}{2}$$

$$\Delta w_B = -\frac{10^8\ I_{av}}{(V_m - 570\ I_{av})^{3/2}} \text{ m/sec} \qquad \text{(A-21a)}$$

$$\Delta w_C = -\frac{10^8\ I_{av}}{(V_m - 700\ I_{av})^{3/2}} \text{ m/sec} \qquad \text{(A-21b)}$$

ACKNOWLEDGMENTS

The author is grateful to W. A. Reid, J. H. McNally, L. B. Hanson, and others of the staff of Millstone Hill who gathered data reported here. R. F. Julian and J. K. Upham were responsible for writing the computer programs required to process the data, while Mrs. A. Freeman and Mrs. J. LaJoie carried out the work of plotting graphs and performing some calculations by hand. During 1969, the incoherent scatter work at Millstone Hill was supported by the U.S. Air Force through its program of general research at Lincoln Laboratory.

REFERENCES

1. J. V. Evans, "Ionospheric Backscatter Observations at Millstone Hill," Technical Report 374, Lincoln Laboratory, M.I.T. (22 January 1965), DDC AD-616607.
2. _____, "Millstone Hill Thomson Scatter Results for 1964," Technical Report 430, Lincoln Laboratory, M.I.T. (15 November 1967), DDC AD-668436.
3. _____, "Millstone Hill Thomson Scatter Results for 1965," Technical Report 474, Lincoln Laboratory, M.I.T. (8 December 1969), DDC AD-707501.
4. _____, "Millstone Hill Thomson Scatter Results for 1966," Technical Report 481, Lincoln Laboratory, M.I.T. ~~(15 December 1970)~~ 19 January 1971, DDC AD-725742.
5. _____, "Millstone Hill Thomson Scatter Results for 1967," Technical Report 482, Lincoln Laboratory, M.I.T. (22 July 1971), DDC AD-735727.
6. _____, "Millstone Hill Thomson Scatter Results for 1968," Technical Report 499, Lincoln Laboratory, M.I.T. (23 January 1973), DDC AD-767251/2.
7. _____, Planet. Space Sci. 13, 1031 (1965), DDC AD-616607.
8. _____, J. Geophys. Res. 70, 1175 (1965), DDC AD-614310.
9. _____, Planet. Space Sci. 15, 1387 (1967).
10. _____, Planet. Space Sci. 18, 1225 (1970), DDC AD-716056.
11. _____, J. Atmos. Terr. Phys. 32, 1629 (1970), DDC AD-716057.
12. _____, J. Geophys. Res. 75, 4803 and 4815 (1970), DDC AD-714447 and AD-714446, respectively.
13. _____, Planet. Space Sci. 21, 763 (1973), DDC AD-772137/6.
14. _____, J. Atmos. Terr. Phys. 35, 593 (1973), DDC AD-771877/8.
15. _____ and I. J. Gastman, J. Geophys. Res. 75, 807 (1970), DDC AD-704626.
16. R. J. Cicerone and S. A. Bowhill, Radio Sci. 6, 957 (1971) [also Aeronomy Report 39, Department of Electrical Engineering, University of Illinois, Urbana (1 September 1970)].
17. J. V. Evans and L. P. Cox, J. Geophys. Res. 75, 159 (1970), DDC AD-703492.
18. L. P. Cox and J. V. Evans, J. Geophys. Res. 75, 6271 (1970), DDC AD-722911.
19. J. V. Evans, J. Geophys. Res. 77, 2341 (1972), DDC AD-752948.
20. _____, R. F. Julian and W. A. Reid, "Incoherent Scatter Measurements of F-Region Density, Temperatures, and Vertical Velocity at Millstone Hill," Technical Report ~~447~~ 477, Lincoln Laboratory, M.I.T. (6 February 1970), DDC AD-706863.
21. J. P. McClure, W. B. Hanson, A. F. Nagy, R. J. Cicerone, L. H. Brace, M. Baron, P. Bauer, H. C. Carlson, J. V. Evans, G. N. Taylor and R. F. Woodman, J. Geophys. Res. 78, 197 (1973).
22. J. E. Salah, "A Study of the Midlatitude Thermosphere by Incoherent Scatter Radar," PhD Thesis, Meteorology Department, M.I.T. (August 1972).
23. A. E. Hedin, H. G. Mayr, C. A. Reber, N. W. Spencer and G. R. Carignan, J. Geophys. Res. 79, 215 (1974).

24. H.G. Mayr and H. Volland, J. Geophys. Res. 77, 6774 (1972).

25. D. Alcayde, P. Bauer and J. Fontanari, J. Geophys. Res. 79, 629 (1974).

26. J.E. Salah, J.V. Evans and R.H. Wand, Radio Sci. 9, 231 (1974), DDC AD-785097/7.

27. K.L. Jones, J. Atmos. Terr. Phys. 33, 1311 (1971).

28. _____, ibid., 35, 1515 (1973).

29. T. Tanaka and K. Hirao, J. Atmos. Terr. Phys. 35, 1443 (1973).

30. J.V. Evans, Radio Sci. 6, 609 (1971), DDC AD-731927.

31. _____, ibid., 6, 843 (1971), DDC AD-737929.

32. _____, J. Geophys. Res. 70, 4331 (1965), DDC AD-623606.

33. U.S. Department of Commerce, Environmental Services Administration, "ITS Ionospheric Predictions for January 1969," TB 11-499-70/TO 31-3-28-2 (October 1968).

34. J.A. Klobuchar, J. Aarons and H.H. Hoseinieh, J. Geophys. Res. 73, 7530 (1968).

35. J.V. Evans, J. Geophys. Res. 73, 3489 (1968), DDC AD-673605.

36. A.V. Mikhaylov, Geomag. and Aeron. 12, 653 (1972).

37. W.B. Hanson and T.N.L. Patterson, Planet. Space Sci. 12, 979 (1964).

38. T. Yonezawa, Space Research V, 49 (1965).

39. J.E. Geisler and S.A. Bowhill, Aeronomy Report 5, Department of Electrical Engineering, University of Illinois, Urbana (1 January 1965).

40. J.E. Geisler, J. Geophys. Res. 72, 81 (1967).

41. V.A. Vasin, L.V. Grishkevich and V.V. Pisareva, Geomag. and Aeron. 10, 473 (1970).

42. G.S. Ivanov-Kholodnyy and A.V. Mikhaylov, Geomag. and Aeron. 13, 39 (1973).

43. H. Rishbeth, J. Atmos. Terr. Phys. 34, 1 (1972).

44. P.Y.S. Hsu and S.F. Chü, "Maintenance of Nighttime F-Region: Observation of Exospheric Electron Flux at Arecibo," J. Atmos. Terr. Phys. (in press, 1975).

45. R. Rüster, J. Atmos. Terr. Phys. 31, 765 (1969).

46. T.E. VanZandt, V.L. Peterson and A.R. Laird, J. Geophys. Res. 76, 278 (1971).

47. C.G. Park, J. Geophys. Res. 76, 4650 (1971).

48. C.G. Park and C.I. Meng, J. Geophys. Res. 76, 8326 (1971); also see 78, 3828 (1973).

49. J.E. Salah and J.V. Evans, Space Research XIII (Akademie-Verlag, Berlin, 1973), p. 267.

50. G. Lejeune and G.N. Taylor, Planet. Space Sci. 20, 1061 (1972).

51. J.V. Evans, J. Geophys. Res. 78, 2344 (1973), DDC AD-772214/3.

52. J.V. Evans, R.A. Brockelman, R.F. Julian, W.A. Reid and L.A. Carpenter, Radio Sci. 5, 27 (1970), DDC AD-704631.

53. J.V. Evans and J.M. Holt, Radio Sci. 6, 855 (1971), DDC AD-738727.

54. V.W.J.H. Kirchoff and L.A. Carpenter, "Dominance of the Diurnal Mode of Horizontal Drift Velocities at F-Region Heights," J. Atmos. Terr. Phys. (in press, 1975).

55. R.W. Schunk and J.C.G. Walker, Planet. Space Sci. 6, 855 (1971).

56. J.E. Salah and J.M. Holt, Radio Sci. 9, 301 (1974), DDC AD-785096.

57. J.L. Massa (private communication).

58. H. Rishbeth and O.K. Garriott, Introduction to Ionospheric Physics (Academic Press, New York, 1969), pp. 170-171.

59. L. Colin and M.A. Myers, "Computed Times of Sunrise and Sunset in the Ionosphere," NASA Technical Memorandum TM X-1233 (April 1966).

UNCLASSIFIED

SECURITY CLASSIFICATION OF THIS PAGE *(When Data Entered)*

REPORT DOCUMENTATION PAGE		READ INSTRUCTIONS BEFORE COMPLETING FORM
1. REPORT NUMBER ESD-TR-74-234	2. GOVT ACCESSION NO.	3. RECIPIENT'S CATALOG NUMBER
4. TITLE *(and Subtitle)* Millstone Hill Thomson Scatter Results for 1969		5. TYPE OF REPORT & PERIOD COVERED Technical Report 6. PERFORMING ORG. REPORT NUMBER Technical Report 513
7. AUTHOR*(s)* Evans, John V.		8. CONTRACT OR GRANT NUMBER*(s)* F19628-73-C-0002
9. PERFORMING ORGANIZATION NAME AND ADDRESS Lincoln Laboratory, M.I.T. P.O. Box 73 Lexington, MA 02173		10. PROGRAM ELEMENT, PROJECT, TASK AREA & WORK UNIT NUMBERS 7X263304D215
11. CONTROLLING OFFICE NAME AND ADDRESS Ballistic Missile Defense Program Office Department of the Army 1320 Wilson Boulevard Arlington, VA 22209		12. REPORT DATE 23 July 1974 13. NUMBER OF PAGES 144
14. MONITORING AGENCY NAME & ADDRESS *(if different from Controlling Office)* Electronic Systems Division Hanscom Air Force Base Bedford, MA 01731		15. SECURITY CLASS. *(of this report)* Unclassified 15a. DECLASSIFICATION DOWNGRADING SCHEDULE

16. DISTRIBUTION STATEMENT *(of this Report)*

Approved for public release; distribution unlimited.

17. DISTRIBUTION STATEMENT *(of the abstract entered in Block 20, if different from Report)*

18. SUPPLEMENTARY NOTES

None

19. KEY WORDS *(Continue on reverse side if necessary and identify by block number)*

Millstone radar	electron density	temperature effects
F-region	ionospheric scatter	spectrum analyzers
diurnal variations	seasonal variations	

20. ABSTRACT *(Continue on reverse side if necessary and identify by block number)*

This report summarizes the results for the electron density distribution, electron and ion temperatures and vertical ionization fluxes in the F-region obtained during 1969 using the Millstone Hill (42.6°N, 71.5°W) Thomson (incoherent) scatter radar system. These data, for the height interval approximately 200 to 900 km, were gathered over 24-hour observing periods, roughly twice per calendar month. The time resolution to obtain results over this entire height interval was either 30 or 45 minutes, depending upon which of two operating modes was employed.

The results for the diurnal variation of the electron density and temperature exhibit the characteristic summer and winter patterns discussed previously. The transition between the two takes place in April and

DD FORM 1 JAN 73 1473 EDITION OF 1 NOV 65 IS OBSOLETE

UNCLASSIFIED

SECURITY CLASSIFICATION OF THIS PAGE *(When Data Entered)*

20. (continued)

October. Two cases of overhead auroral precipitation were observed during the year as a consequence of efforts to observe a stable red arc. Other instances of geomagnetically disturbed behavior were infrequent.

Vertical fluxes of ionization were measured, and the flux escaping to the magnetosphere near midday was found to have an average value of $\sim 5 \times 10^7$ el/cm^2/sec. Near midnight, the magnetosphere appears to supply the local ionosphere with a flux of about half this amount.

☆ U. S. GOVERNMENT PRINTING OFFICE: 1975--600-020--53